University of Alberta

Olefin Activation and Biphosphine-Bridged Bimetallic Complexes

by

Dusan Ristic-Petrovic ©

A thesis
submitted to the Faculty of Graduate Studies and Research
in partial fulfillment of the requirements
for the degree of Doctor of Philosophy

Department of Chemistry

Edmonton, Alberta
Fall, 2002

National Library
of Canada

Acquisitions and
Bibliographic Services

395 Wellington Street
Ottawa ON K1A 0N4
Canada

Bibliothèque nationale
du Canada

Acquisitions et
services bibliographiques

395, rue Wellington
Ottawa ON K1A 0N4
Canada

Your file Votre référence

Our file Notre référence

The author has granted a non-exclusive licence allowing the National Library of Canada to reproduce, loan, distribute or sell copies of this thesis in microform, paper or electronic formats.

The author retains ownership of the copyright in this thesis. Neither the thesis nor substantial extracts from it may be printed or otherwise reproduced without the author's permission.

L'auteur a accordé une licence non exclusive permettant à la Bibliothèque nationale du Canada de reproduire, prêter, distribuer ou vendre des copies de cette thèse sous la forme de microfiche/film, de reproduction sur papier ou sur format électronique.

L'auteur conserve la propriété du droit d'auteur qui protège cette thèse. Ni la thèse ni des extraits substantiels de celle-ci ne doivent être imprimés ou autrement reproduits sans son autorisation.

0-612-81259-6

Canada

University of Alberta

Release Form

Name of Author:	Dusan Ristic-Petrovic
Title of Thesis:	**Olefin Activation and Biphosphine-Bridged Bimetallic Complexes**
Degree:	Doctor of Philosophy
Year this Degree Granted:	2002

Permission is hereby granted to the University of Alberta Library to reproduce single copies of this thesis and to lend or sell such copies for private, scholarly or scientific research purposes only.

The author reserves all other publication rights, and neither the thesis nor extensive extracts from it may be printed or otherwise reproduced without the author's prior written permission.

(signed) ______________________

Dusan Ristic-Petrovic

9816-64 Avenue, Edmonton, Alberta
T6E 0J5
Canada

Date 26 SEPT. 2002

Felix qui potuit rerum cognoscere causus

To my family

Abstract

The reactions of the binuclear complex $[Ir_2(CH_3)(CO)_2(dppm)_2][CF_3SO_3]$ (**1**) (dppm = $Ph_2PCH_2PPh_2$) with a series of olefins in solution have been investigated using multinuclear NMR spectroscopy. The products depend on the temperature and olefin, and fall into three categories: 1) $[Ir_2(H)(CO)_2(\eta^2\text{-}L)(\mu\text{-}CH_2)(dppm)_2][CF_3SO_3]$, 2) $[Ir_2(CH_3)(\eta^2\text{-}L)(CO)_2(dppm)_2][CF_3SO_3]$ and 3) $[Ir_2(CH_3)(\mu\text{-}L)(CO)_2(dppm)_2][CF_3SO_3]$ where L = olefin. The stability order is 3 > 2 > 1, but not all products are observed for all olefins. A proposal is advanced rationalizing the conversion of the s-trans bridged 1,3-butadiene adduct $[Ir_2(CH_3)(CO)_2(\mu\text{-}\eta^2{:}\eta^2\text{-}H_2C{=}CH\text{-}CH{=}CH_2)(dppm)_2][CF_3SO_3]$ (**6A**) to the vinylvinylidene-bridged $[Ir_2(CH_3)(H)(CO)_2(\mu\text{-}H)(\mu\text{-}CC(H)C(H)CH_2)(dppm)_2]\text{-}[CF_3SO_3]$ (**6B**).

The fluoroethenyl complexes, $[Ir_2(CF{=}CF_2)(CH_3)(CO)_2(\mu\text{-}Cl)(dppm)_2][CF_3SO_3]$ (**2**) and $[Ir_2(C(H){=}CF_2)(CH_3)(CO)_2(\mu\text{-}Br)(dppm)_2][CF_3SO_3]$ (**3**) are prepared by the oxidative addition of $ClFC{=}CF_2$ and $BrHC{=}CF_2$, respectively, to (**1**). Protonation of **2** occurs at the Ir-Ir bond giving $[Ir_2(CF{=}CF_2)(CH_3)(CO)_2(\mu\text{-}Cl)\text{-}(\mu\text{-}H)(dppm)_2][CF_3SO_3]_2$ (**4**). Attempts to remove or replace the chloride ligand from **2** failed. Instead, the reaction of **2** with methyl lithium resulted in replacement of one fluoride substituent on the trifluoroethenyl group by a methyl group to give $[Ir_2(CF{=}CFCH_3)(CH_3)(CO)_2(\mu\text{-}Cl)(dppm)_2][CF_3SO_3]$ (**5**). The X-ray structural determination of **5** indicates that replacement of a fluoride trans to the

$Ir-C_2F_3$ bond and migration of the resulting methyldifluoroethenyl group to the metal bearing the methyl ligand have occurred.

Diiridium complexes bridged by dmpm (dmpm = $Me_2PCH_2PMe_2$) were prepared in the course of attempting to develop a rational synthesis of the dmpm analogue of **1**, i.e. $[Ir_2(CH_3)(CO)_2(dmpm)_2][CF_3SO_3]$ (**1-dmpm**). Thus $[Ir_2(CO)_4(dmpm)_2]$ (**15**) reacts with two eq. of methyl trifluoromethanesulfonate to yield $[Ir_2(CH_3)_2(CO)_4(dmpm)_2][CF_3SO_3]_2$ (**16**). The reaction of $[Ir(Cl)(CO)(PPh_3)_2]$ with dmpm affords the triply-bridged complex $[Ir_2Cl(CO)(\mu\text{-}CO)(dmpm)_3][Cl]$ (**17**). The reaction of $[IrCl(COD)]_2$ with excess dmpm followed by CO gives $[Ir(COD)(dmpm)_2]Cl$ (**18**). Methyl trifluoromethanesulfonate addition to the reaction mixture obtained from two equivalents of dmpm forms $[Ir_2(CH_3)Cl_2(CO)_2(dmpm)_2][CF_3SO_3]$ (**19**), which reacts with dichloromethane to yield $[Ir_2Cl_4(CO)_2(dmpm)_2]$ (**20**). Complexes **16**, **17** and **20** have been characterized by X-ray crystallography.

The structures of **1** and **1-dmpm** have been determined using Density Functional Theoretical (DFT) methods. The geometry of the complex is significantly changed when non-hydrogen substituents are present on the phosphorus atoms. The calculated geometry of **1** supports the view that its structure in solution resembles that in the crystal.

Acknowledgements

It is quite certain that I could not have gotten to the point of writing this thesis without a considerable amount of help from my friends. Foremost, I must thank Dr. Robert Hilts, a close friend whom I have known since *he* was in graduate school, for his encouragement and advice. Perhaps most importantly for my future success, Rob suggested that I return to school for a Ph.D. under Professor Martin Cowie. This was very good advice, and I have to thank Marty for being a patient and helpful supervisor, and an all-around swell guy. It is often said that few supervisors teach their students anything about scientific writing. Thankfully, Marty is an exception to this rule; for his generous assistance and guidance in this regard I am most grateful.

In my first crack at graduate school, I had started work with Professor W. A. G. Graham who retired before I returned to complete my studies. To him I owe a debt of gratitude for setting the high standards of professionalism that I continue to strive for today. I must also acknowledge the profound influence upon my career of several of my earlier teachers, notably Mr. John Owen, my first year chemistry instructor, Professor Alexander Kirk, with whom I received my first publication, Dr. Dave Berry, who, as UVIC's inorganic lab coordinator, was unyielding in his insistence upon good chemical technique and Mr. Bill Wilkie, the high school chemistry teacher who got me started down this road in the first place.

Chemistry is stubbornly empirical, in spite of our best efforts at rationalizing its study. Thus the help of other researchers, technicians and support staff is invaluable. The generous help of the X-ray crystallography facility was indispensable, and I must thank Dr. Bob McDonald for going above, and beyond, the call of duty on a regular basis. Also, I am deeply grateful for the generous help of the departmental NMR staff, and especially Mr. Glen Bigam, who is a truly masterful NMR spectroscopist, Mrs. Gertie Aarts who was always supportive and Dr. Tom Nakashima who explained some crucial concepts to me. As well, I must thank Ms. Jeanette Loiselle, the departmental secretary, for helping me navigate the otherwise unfathomable arcania of the University's bureaucratic structure.

On a day-to-day basis, one's labmates set the tone for the grad school experience. Early on I was inspired by Dr. George Richter-Addo and Dr. Jim Hoyano, who taught me many of the techniques I employ in the lab every day. In recent years I have enjoyed the companionship of many fine colleagues, including Dr. Todd Graham and Mr. Christopher Lee among many others. I should also mention the current crop of students in our research group, Bryan Rowsell (thanks for the port!), Amala Choksii, Jason Anderson and Steve Trepanier. To you, and all the others who will follow, I remind you of this ancient truism: *Assiduus usus uni rei deditus et ingenium et artem saepe vincit (!)*

Lastly, I thank my wife, Carol, for her immense patience and unfailing support.

Table of Contents

Chapter 1 Introduction 1

Objectives of this thesis 15

References 16

Chapter 2 Olefin coordination to $[Ir_2(CH_3)(CO)_2(dppm)_2][CF_3SO_3]$ 29

Introduction 29

Experimental 33

General Comments 33

Preparation of Compounds 34

Results

2.1. Reaction of ethene with $[Ir_2(CH_3)(CO)_2(dppm)_2]$ $[CF_3SO_3]$ (**1**) 41

2.2. Reactions of 1,2-dienes with $[Ir_2(CH_3)(CO)_2(dppm)_2][CF_3SO_3]$ (**1**) 41

2.2.1. Reaction of allene with $[Ir_2(CH_3)(CO)_2(dppm)_2][CF_3SO_3]$ (**1**) 41

2.2.2. Reaction of methylallene with $[Ir_2(CH_3)(CO)_2(dppm)_2][CF_3SO_3]$(**1**) 51

2.2.3. Reaction of 1,1-dimethylallene with $[Ir_2(CH_3)(CO)_2(dppm)_2][CF_3SO_3]$ (**1**) 60

2.3. Reactions of 1,3-dienes with $[Ir_2(CH_3)(CO)_2(dppm)_2][CF_3SO_3]$ (**1**) 62

Discussion 66

Conclusions 77

References and Footnotes 78

Chapter 3 Fluoroethene Complexes 80

Introduction 80

Experimental 81

General Comments 81

Preparation of Compounds 82

Results 86

3.1. Reaction of fluoroethene with $[Ir_2(CH_3)(CO)_2(dppm)_2][CF_3SO_3]$ (**1**) 86

3.2 Reaction of Z-1,2-difluoroethene with $[Ir_2(CH_3)(CO)_2(dppm)_2][CF_3SO_3]$ (**1**) 91

3.3. Reaction of 1,1-difluoroethene with $[Ir_2(CH_3)(CO)_2(dppm)_2][CF_3SO_3]$ (**1**) 92

3.4 Reaction of trifluoroethene with $[Ir_2(CH_3)(CO)_2(dppm)_2][CF_3SO_3]$ (**1**) 97

Discussion 103

Conclusions 113

References 114

Chapter 4 Fluoroethenyl Complexes 116
  Introduction 116
  Experimental 118
    General Comments 118
    Preparation of Compounds 119
    X-Ray Data Collection 125
    Structure Solution and Refinement 129
  Results and Compound Characterization 130
  Discussion 150
  Conclusions 154
  References and Footnotes 155

Chapter 5 Complexes Containing the dmpm Ligand 160
  Introduction 160
  Experimental 161
    General Comments 161
    Preparation of Compounds 163
  Results and Discussion 171
  Conclusions 194
  References and Footnotes 196

Chapter 6 Conclusions 198

References and Footnotes 211

Appendix Calculated Structures of 1 and 1-dmpm 213

Introduction 213

Theoretical Methods and Software 214

Results 214

References 223

List of Tables

Chapter 2

Table 2.1. NMR Data for the Compounds. 35

Chapter 3

Table 3.1 NMR data for reactions of **1** with fluoroolefins. 83

Table 3.2. Crystallographic Experimental Details. 87

Table 3.3. Selected Interatomic Distances (Å) and Angles (deg) 101

Table 3.4. Chemical shift change upon coordination for partially fluorinated ethenes. 108

Chapter 4

Table 4.1. Spectroscopic Data for the Compounds. 120

Table 4.2. Crystallographic Experimental Details for Compounds **11, 13** and **14.** 126

Table 4.3. Selected Interatomic Distances and Angles for Compound **11**. 135

Table 4.4. Selected Interatomic Distances and Angles for Compound **13.** 142

Table 4.5. Selected Interatomic Distances and Angles for Compound **14.** 148

Chapter 5

Table 5.1. Spectroscopic data for the compounds. 164

Table 5.2. Crystallographic Experimental Details for compounds **16**, **17** and **20.** 167

Table 5.3. Selected interatomic distances (Å) and angles (deg) within the complex cation of **16**. 176

Table 5.4. Selected interatomic distances (Å) and angles (deg) within the complex cation of **17**. 181

Table 5.5. Selected interatomic distances (Å) and angles (deg) for compound **20**. 190

Appendix

Table A.1. Selected distances for the calculated and experimentally determined structures of **1**. 218

Table A.2. Selected angles for the calculated and experimentally determined structures of **1**. 218

List of Figures

Chapter 1

Figure 1.1. Coordination geometries of dppm-bridged binuclear complexes. 4

Figure 1.2. Typical trans bridged (type **A**) structure with phenyls included and equatorial ligands not shown. 6

Figure 1.3. Typical trans bridged (type **A**) structure of a dmpm complex with methyls included and equatorial ligands not shown. 8

Figure 1.4. Activation of vinylic bonds by an adjacent metal. 9

Figure 1.5. A dipeptide **I** and a fluoroolefin isostere **II**. 11

Figure 1.6. Synergic components of metal-olefin bonding according to the Dewar-Chatt-Duncanson model. 12

Figure 1.7. Bonding extremes of the metal-olefin interaction. 13

Chapter 2

Figure 2.1. $^{31}P\{^1H\}$ spectrum of the reaction mixture of ethene and **1** at -80 °C in CD_2Cl_2. 38

Figure 2.2.1. $^{31}P\{^1H\}$ NMR of the reaction of allene with **1** in CD_2Cl_2, -90 to -70 °C. 42

Figure 2.2.2. $^{31}P\{^1H\}$ NMR of the reaction of allene with **1** in CD_2Cl_2, -60 to -40 °C. 43

Figure 2.2.3. $^{31}P\{^1H\}$ NMR of the reaction of allene with **1** in CD_2Cl_2, -40 to -10 °C. 44

Figure 2.2.4. $^{31}P\{^1H\}$ NMR of the reaction of allene with **1** in CD_2Cl_2, -5 to 5 °C. 45

Figure 2.3. Hydride region of the ^1H spectrum of **3A** and **3B** at -90 °C. 47

Figure 2.4.1. ^{31}P NMR spectra of the mixture of **1** and methylallene in CD_2Cl_2 from -80 °C to -60 °C. 52

Figure 2.4.2. ^{31}P NMR spectra of the mixture of **1** and methylallene in CD_2Cl_2 from -40 °C to -20 °C. 53

Figure 2.4.3. ^{31}P NMR spectra of the mixture of **1** and methylallene in CD_2Cl_2 from -10 °C to 27 °C. 54

Figure 2.5. $^{31}P\{^1H\}$ spectrum of a mixture of $[Ir_2(CH_3)(CO)_2(\mu\text{-}\eta^2\text{:}\eta^2\text{-}H_2C{=}CH\text{-}CH{=}CH_2)(dppm)_2][CF_3SO_3]$ (**6A**) and **1** in CD_2Cl_2 at -55 °C. 63

Figure 2.6. Schematic drawing of the complex cation of **6A** showing ^1H and ^{13}C chemical shifts in ppm. 64

Figure 2.7. Portion of the ROESY spectrum of **6A** in CD_2Cl_2 at -55 °C. 65

Figure 2.8. *Endo* and *exo* isomers of $[Ir_2(H)(CO)_2(syn\text{-}\eta^2\text{-}H_2C{=}C{=}CH(CH_3))(\mu\text{-}CH_2)(dppm)_2][CF_3SO_3]$ (**4B**). 68

Chapter 3

Figure 3.1. Orientations of the 1,1-difluoroethene ligand in **9A.** 94

Figure 3.2. Representation of the X-ray structure of the cation of **11.** 100

Figure 3.3. Potential energy diagram showing the proposed relationship of the bridged and terminal olefin adducts of **1**. 106

Chapter 4

Figure 4.1. Perspective view of the $[Ir_2(CF{=}CF_2)(CH_3)(CO)_2(\mu\text{-}Cl)(dppm)_2]^+$ cation of complex **11** showing the atom-labeling scheme. 134

Figure 4.2. Perspective view of the $[Ir_2(CF{=}CF_2)(CH_3)(CO)_2(\mu\text{-}H)(\mu\text{-}Cl)(dppm)_2]^{2+}$ cation of complex **13** showing the atom-labeling scheme. 141

Figure 4.3. Perspective view of the $[Ir_2(CF{=}C(F)CH_3)(CH_3)(CO)_2(\mu\text{-}Cl)(dppm)_2]^+$ cation of complex **14** showing the atom-labeling scheme. 147

Chapter 5

Figure 5.1. Perspective view of the $[Ir_2(CO)_4(Me)_2(dmpm)_2]^{2+}$ ion of **16** showing the atom-labeling scheme. 175

Figure 5.2. Perspective view of the $[Ir_2Cl(CO)(\mu\text{-}CO)(dmpm)_3]^+$ ion of **17** showing the atom labeling scheme. 180

Figure 5.3. Alternate view of the complex cation of **17**. 184

Figure 5.5. Perspective view of $[Ir_2Cl_4(CO)_2(dmpm)_2]$, **20**, showing the atom labeling scheme. 192

Figure 5.6. Alternate view of the molecule, **20**, illustrating the torsion of the trans biphosphine groups about the Ir(1)-Ir(2) bond. 193

Figure 6.1. Fluxional process connecting the two terminal methyl forms of **1** and the interception of an agostic intermediate by an olefin ligand L to give the observed methylene-hydride product. 201

Appendix

Figure A.1. Comparison of calculated and X-ray core geometries of dhpm, dmpm and dppm analogues of **1**. 217

Figure A.2. DFT-calculated structure of $[Ir_2(CH_3)(CO)_2(dppm)_2]^+$ (**1**). 219

Figure A.3. DFT-calculated structure of $[Ir_2(CH_3)(CO)_2(dppm)_2]^+$ **(1)** shown in a space filling representation. 220

Figure A.4. DFT-calculated structure of $[Ir_2(CH_3)(CO)_2(dmpm)_2]^+$ (**1-dmpm**). 221

Figure A.5. DFT-calculated structure of $[Ir_2(CH_3)(CO)_2(dmpm)_2]^+$ (**1-dmpm**) shown in a space filling representation. 222

List of Schemes

Chapter 1

Scheme 1.1. Comparison of α-hydrogen elimination on a metal surface or in a bimetallic complex and β-hydrogen elimination with a monometallic complex. 933 3

Scheme 1.2. Iridium-methyl C-H activation upon ligand addition to $[Ir_2(CH_3)(CO)_2(dppm)_2][CF_3SO]$ (**1**). 9

Chapter 2

Scheme 2.1. Products obtained at ambient temperature from the reaction of ethene, carbon monoxide and phosphines with **1** in CH_2Cl_2. 30

Scheme 2.2. Reaction of allene, methylallene and 1,1-dimethylallene with **1** in CH_2Cl_2 solution. 31

Scheme 2.3. Reaction of butadiene with **1** in CH_2Cl_2 forming $[Ir_2(CH_3)(H)(CO)(\mu\text{-}H)(\mu\text{-}CC(H)C(H)(CH_2)(dppm)_2][CF_3SO_3]$ (**6B**). 32

Scheme 2.4 Reaction of **1** with ethene to form **2A**. 37

Scheme 2.5. Products of the reaction of allene with **1**. 48

Scheme 2.6 Products of the reaction of methylallene with **1**. 58

Scheme 2.7. Products obtained from the reaction of 1,1-dimethylallene with **1**. 61

Scheme 2.8. Isomerization of μ-η^2-bridging allenyl complexes and conversion to η^1-η^3 allenyl bridged complexes. 71

Scheme 2.9. Formation of the vinyl carbene **3F** product from the allenyl bridged complex **3E** via a trimethylenemethane intermediate. 74

Scheme 2.10. Proposed route for the double olefinic C-H activation of **6A** to form **6B**. 76

Chapter 3

Scheme 3.1. Comparison of bonding modes of tetrafluoroethene and ethane. 81

Scheme 3.2. Reactions of mono- and di- fluoroolefins with $[Ir_2(CH_3)(CO)_2(dppm)_2][CF_3SO_3]$ (**1**), in CD_2Cl_2. 91

Scheme 3.3. Reactions of trifluoroethene with $[Ir_2(CH_3)(CO)_2(dppm)_2][CF_3SO_3]$ (**1**), in CD_2Cl_2. 98

Scheme 3.4 Possible sites of attack of olefin ligands on **1** to form a dimetallacyclobutane complex. 110

Scheme 3.4. Proposed route for the transformation of $[Ir_2(CH_3)(CO)_2(\mu\text{-}CHF{=}CF_2)(dppm)_2][CF_3SO_3]$ (**10**) to $[Ir_2CH_3(H)(CO)_2(\mu\text{-}X)(\mu\text{-}CHF{=}CF_2)(dppm)_2][CF_3SO_3]$ (**11**) , X = F or H. 112

Chapter 4

Scheme 4.1. Reaction of **1** with chlorotrifluoroethene, 1-bromo-2,2-difluoroethene and iodotrifluoroethene. 132

Scheme 4.2. Reaction of **1** with H^+ or methyl lithium. 139

Scheme 4.3. Reaction of [$Ir_2(CF{=}CF_2)(CH_3)(CO)_2(\mu\text{-}Cl)(dppm)_2$] [$CF_3SO_3$] with methyl lithium forming [$Ir_2(CF{=}CFMe)(CH_3)(CO)(\mu\text{-}Cl)(\mu\text{-}CO)(dppm)_2$] [$CF_3SO_3$] (**14**). 153

Chapter 5

Scheme 5.1. Preparation of **1-dmpm** according to Reinking *et al.* 172

Scheme 5.2. Preparation of [$Ir_2(CH_3)Cl_2(CO)_2(dmpm)_2$][$CF_3SO_3$], **19** and its subsequent conversion to [$Ir_2Cl_4(CO)_2(dmpm)_2$], **20**, upon standing in CH_2Cl_2. 188

Chapter 1

Introduction

Hydrocarbons are important chemical feedstocks, constituting one of the mainstays of the chemical industry,[1] and the catalytic transformation of commodity chemicals such as olefins and other hydrocarbons is an area of increasing current interest.[2] Because a preponderance of industrial catalytic processes are heterogeneous in nature,[3] much work has been done in an attempt to understand the intimate nature of substrate-surface interactions.[4] Owing to the difficulty in studying adsorbed species on heterogeneous catalysts, chemists have often resorted to the use of discrete transition metal complexes as homogeneous solution phase models of these surface processes.[5,6]

Metal complexes having a single metal centre are among the simplest homogeneous phase models for chemical transformations on metal surfaces. However they cannot model processes requiring the participation of more than one metal atom. This limitation may be overcome by employing metal cluster compounds, containing several metal atoms in close proximity along with supporting ligands.[7] The "cluster/surface" analogy, described by Muetterties, views the metal atoms in the cluster as representing a portion of the metal surface, while the supporting ligands are considered to resemble chemisorbed species in the vicinity of a particular site on the surface.[8-11]

Insofar as the interactions of small molecules with metal catalyst surfaces may require the involvement of more than one metal atom, the smallest cluster that could serve as a model for metal-metal cooperativity is a bimetallic complex. One example of a process occurring on a metal surface that can be modeled by a bimetallic complex is cleavage of C-H bonds of adsorbed hydrocarbons on such surfaces. Although mononuclear late-metal alkyl complexes are prone to β-hydrogen elimination when β-hydrogens are present,[12] they do not usually undergo α-hydrogen elimination.[13, 14] However the presence of a second, adjacent metal can lead to α-hydrogen elimination through the involvement of an adjacent metal atom as shown in Scheme 1.1. The products formed are a metal hydride and a carbene, which in Scheme 1.1 is shown in a bridging mode. This is an example of a reactivity pathway that is more common in polynuclear complexes, since in mononuclear complexes geometric constraints predispose metal alkyls towards β-hydrogen elimination, forming an olefin ligand and a metal hydride.[15]

For a soluble bimetallic complex to be a useful model system for bimetallic reactivity, the bimetallic framework should persist as the reaction proceeds. Ligands that prevent the fragmentation of the bimetallic core, while permitting reaction to occur, are required. An effective strategy involves the use of bridging ligands which hold the two metals in close proximity, and inhibit fragmentation

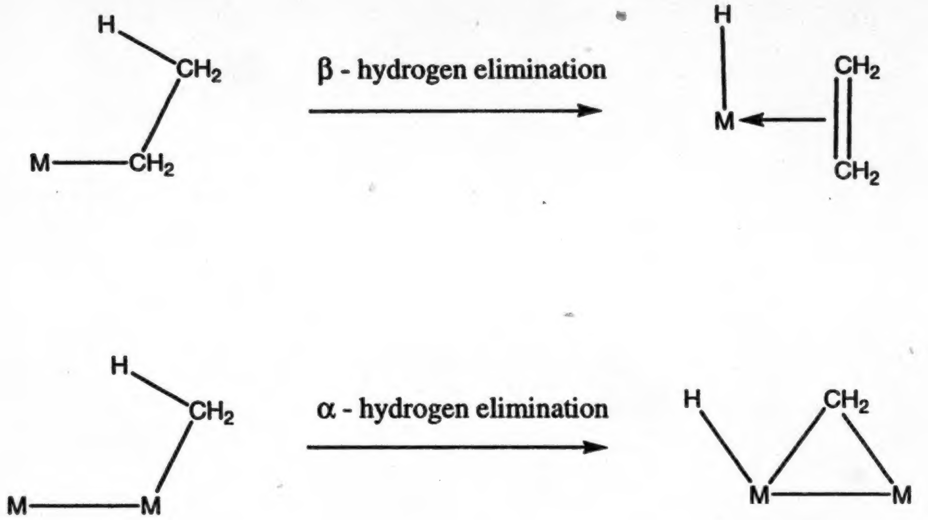

Scheme 1.1. Comparison of α-hydrogen elimination on a metal surface or in a bimetallic complex and β-hydrogen elimination with a monometallic complex.

into mononuclear species. This has the advantage of maintaining the binuclear framework even in the absence of a metal-metal bond. In late-metal complexes, which display an extensive chemistry involving phosphine ligands, the ligand bis(diphenylphosphino)methane (dppm) mimics the ubiquitous triphenylphosphine ligand and has been used extensively to bridge two metals.[16] This ligand can accommodate a wide range of M-M distances and complexes have been prepared for many metals. Frequently the stoichiometry of dppm-bridged binuclear complexes has one ligand per metal (i.e. $M_2(dppm)_2$) and for this stoichiometry a variety of structural types are known. These can be grouped into four classes based on the orientation of the dppm ligands with respect to each other, as shown in Figure 1.1.

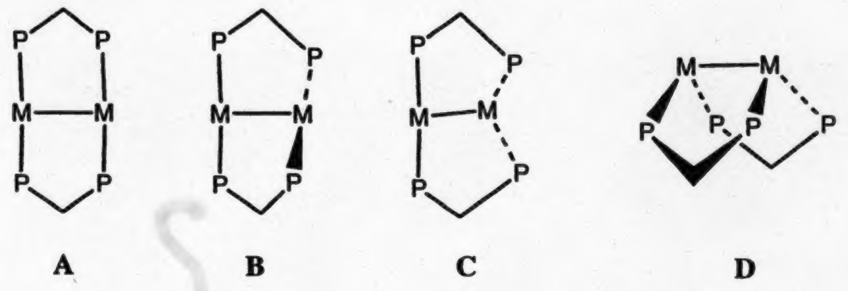

Figure 1.1. Coordination geometries of dppm-bridged binuclear complexes. Only the inner M_2P_4 core is shown. Phenyl groups have been omitted for clarity. Dashed lines (---) are used to represent bonds going into the page.

The typical geometries of bis dppm-bridged bimetallic complexes are trans-bridged (**A**), twisted trans-bridged (**B**), mixed cis/trans-bridged (**C**) and cis-bridged (**D**). In the trans-bridged type **A**, the P-M-P angles approximate 180 degrees on both metals and the P-M-P vectors on both metals are close to parallel, while in the cis-bridged type **D** the P-M-P angles at each metal are substantially less than 180 degrees. In the mixed form **C** one P-M-P angle approximates 180 degrees, while the other has a cis arrangement of phosphines. In the twisted trans-bridged form **B**, both metals have a trans phosphine arrangement, however the P-M-P vector at one metal is twisted with respect to the other, yielding a staggered phosphine arrangement when viewed down the metal-metal bond.

If, in trans-bridged complexes (types **A**, **B** and **C**), the sites on the metal occupied by the phosphorus atoms of dppm are viewed as axial, then the other ligands, including the organic substrates of interest to us, occupy equatorial positions. The steric requirements about the equator of the complex are determined in large part by the dppm phenyl groups, which shield the metals to some extent, potentially inhibiting ligand attachment at the metals and certainly influencing the ligand arrangement in the equatorial plane. Because of the steric bulk imposed by the phenyl groups the optimal arrangement, sterically, is **A**, trans/trans-bridged (see Figure 1.2). The other structural types all involve bringing the phenyl rings closer together. Twisted complexes (**B**) occur where there are strong eclipsing interactions of the equatorial ligands, which can be minimized by rotation about the metal-metal axis. Cis-orientation of the dppm ligands is most demanding sterically, and occurs when the strain thus induced is compensated for by the additional bonding interactions of the ligands occupying the former equatorial plane.

Nuclear magnetic resonance spectroscopy is useful in elucidating the structural type of these complexes. The use of biphosphine ligands makes ^{31}P NMR spectroscopy particularly valuable. If the metals are chemically equivalent, as in *trans*-$[IrCl(CO)(dppm)]_2$, all four phosphorus nuclei can also be chemically equivalent, in which case the $^{31}P\{^1H\}$ NMR spectrum appears as a singlet. However, if the metal environments are chemically inequivalent then the pairs of

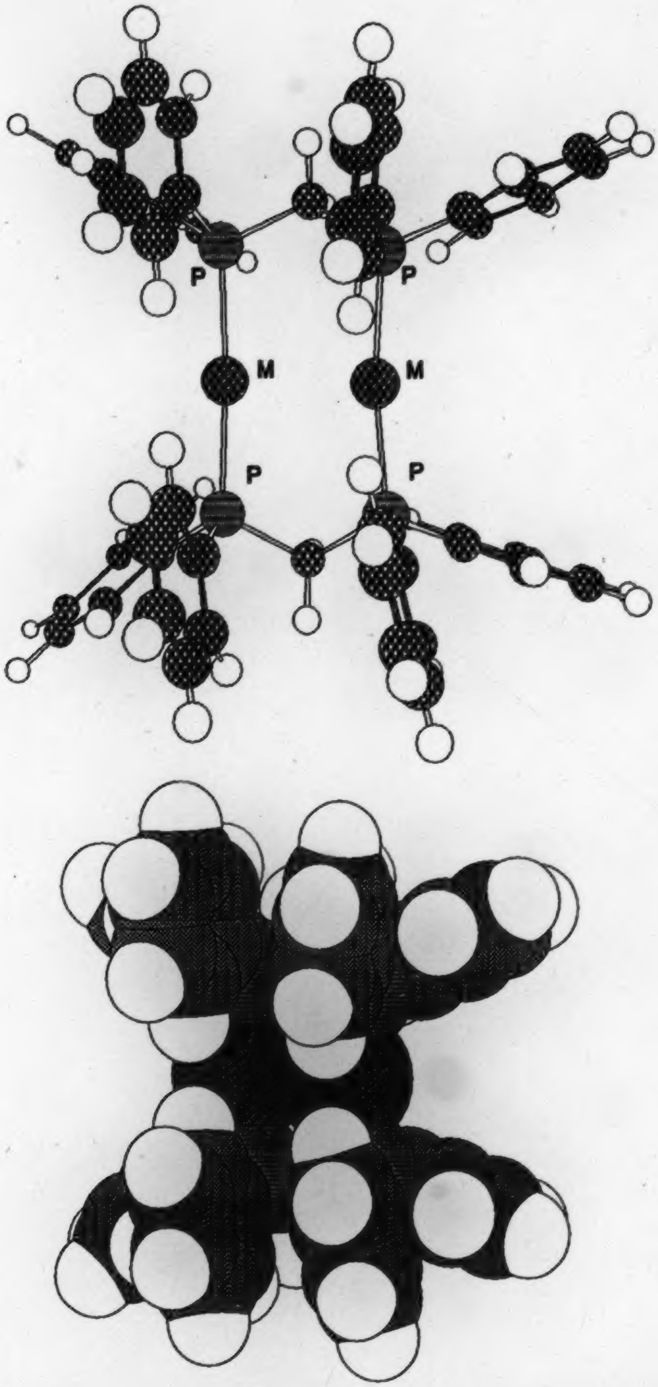

Figure 1.2. Typical trans bridged (type **A**) structure with phenyls included and equatorial ligands not shown. The lower illustration shows the approximate van der Waals surfaces for the atoms.

phosphines on one metal are inequivalent to those on the other, and an AA'BB' spin system results. Clearly if additional factors arise that remove the equivalence of the ^{31}P nuclei on a given metal, all four ^{31}P nuclei become chemically inequivalent and a more complex ^{31}P spectrum results that is characteristic of an ABCD spin system.

Other, less sterically demanding ligands of the biphosphine type have been used to prepare bimetallic complexes. Ligands of the type drpm (r = alkyl, aryl)[20] may be used to adjust the steric *and* electronic properties of the ligand by changing the "r" groups of the biphosphine. One such ligand that has been shown to form stable bridged complexes, but often of greater reactivity than similar dppm complexes, is the ligand dmpm (r = methyl; dmpm = bis(dimethylphosphino)methane).[19, 21-62] This ligand has a smaller Tolman cone angle than dppm (dmpm, 102°; dppm, 121°),[63, 64] resulting in less crowding of the equatorial region of trans-bridged complexes than is the case for dppm, as may be realized from a comparison of Figure 1.3 to that shown for dppm in Figure 1.2. Also, dmpm is a better σ - donor than dppm, so that it confers greater basicity on the metal centres than does dppm.[19] In addition to singly and doubly bridged complexes, a few triply dmpm-bridged bimetallics have also been prepared.[38, 60, 65, 66-74] Triple-bridging of the bimetallic core occurs because of the relatively small steric requirements of dmpm (as opposed to dppm, where triple bridges are less common[75-78]).

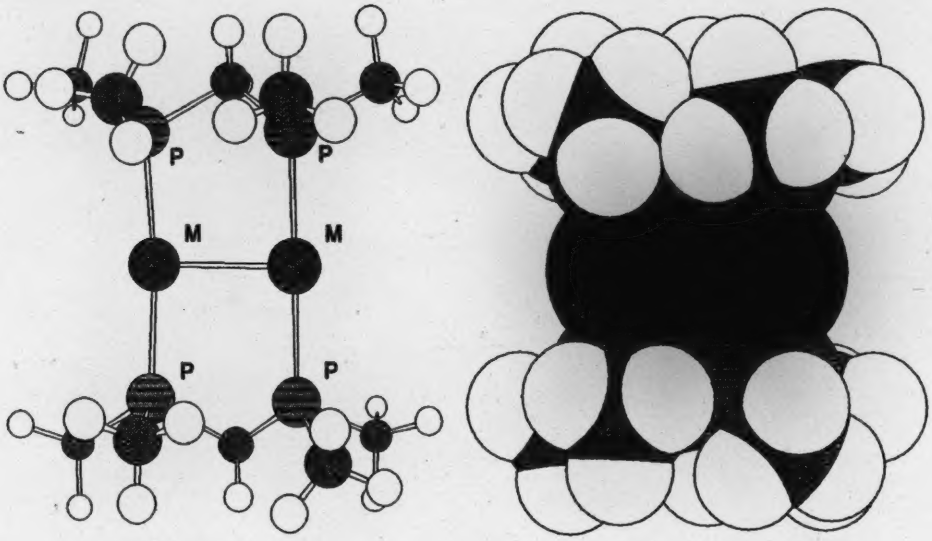

Figure 1.3. Typical trans bridged (type **A**) structure of a dmpm complex with methyls included and equatorial ligands not shown. The right-hand illustration shows the approximate van der Waals surfaces for the atoms.

In addition to forming bridged complexes, there are a number of chelated dmpm complexes known possessing from one to three dmpm ligands; most of these are mononuclear.[64 - 66, 79 - 86] In a few instances, mononuclear dmpm complexes have been used to prepare heterobinuclear dmpm-bridged complexes.[87]

The discovery that ligand addition to the methyl complex $[Ir_2(CH_3)(CO)_2(dppm)_2][CF_3SO_3]$ (**1**) could result in C-H activation of the methyl group by the adjacent metal,[88] as shown in Scheme 1.2, led to an investigation of the reactivity of **1** with unsaturated organic substrates. It was reasoned that the resulting methylene and hydride fragments might be more reactive towards insertion reactions than the original methyl group, leading to new carbon-carbon bond-formation pathways for methyl groups. Initial studies with alkynes led to a variety of reaction pathways, however, the reactivity of **1** with olefins had not been extensively investigated.[89] We therefore sought to extend studies of the reactivity of **1** with olefin molecules.

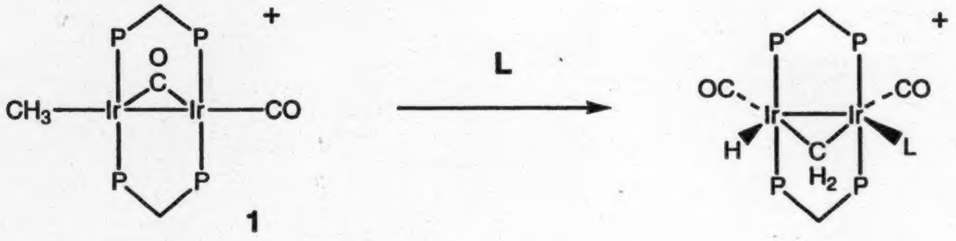

Scheme 1.2. Methyl group C-H activation upon ligand addition to $[Ir_2(CH_3)(CO)_2(dppm)_2][CF_3SO]$ (**1**).

Of additional interest is the potential ability of binuclear complexes to activate vinylic bonds. When coordinated to one metal, the vinylic bonds of the coordinated olefin can be close to the adjacent metal which might promote the activation of these bonds, leading to vinyl ligands, as shown in Figure 1.4.

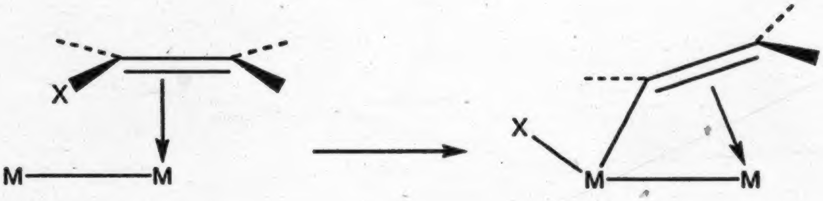

Figure 1.4. Activation of vinylic bonds by an adjacent metal.

While changing the bridging ligand framework may be used to alter the reactivity of bimetallic complexes, the interactions with hydrocarbon substrates may also be affected by the partial or complete substitution of hydrogen by fluorine. The effect of fluorine substitution on the reactivity of hydrocarbons with transition-metal complexes is an area of increasing interest. Particularly important is the ability of some transition metal complexes to activate normally inert C-F linkages and the potential for novel synthetic transformations involving both replacement of fluorine and incorporation of fluorine into organic compounds.[90-92] There is considerable economic interest in fluorine substitution of hydrogen in pharmaceuticals, where the similarities and differences between the C-F and C-H linkages are exploited to achieve improved selectivity and to modify other physiological properties.[93 - 95, 90] Fluorine is intermediate in size between hydrogen and an hydroxyl group, but has a greater inductive electron withdrawing ability.[90] Thus replacement of a hydroxyl (or as discussed below, a carbonyl oxygen) with fluorine can affect the properties of biological molecules, without greatly changing the size or shape of the molecule.[94] In this way, fluorinated analogues of biologically active molecules may bind to the same receptors (often active sites of enzymes) as the non-fluorinated analogues, but with different effects. Thus, fluoroolefin isosteres of peptides, an example of which is shown in Figure 1.5, are used as isoelectronic and isosteric replacements (peptidomimetics) for the peptide amide bond.[96] Such fluoroolefin isosteres possess similar steric properties, bond lengths and bond angles to those of the amide bond, permitting binding with the active site of a target enzyme, but, unlike the peptide, have a fixed conformation, effectively inhibiting subsequent reaction.[96]

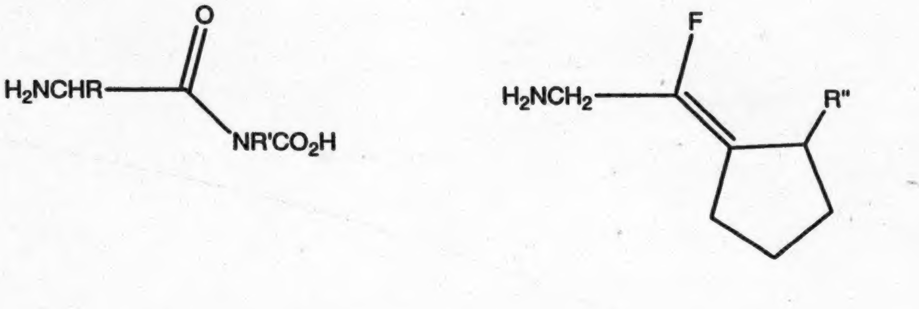

I II

Figure 1.5. A dipeptide **I** and a fluoroolefin isostere **II**.

The metal-fluorocarbon bond is generally stronger than an equivalent metal-hydrocarbon bond, but, apart from this there are several differences in the bonding of fluorine-substituted organic ligands to metals.[97] These arise because of the high electronegativity of the fluorine atom and because of steric repulsions between the lone pairs on fluorine and other groups, including other fluorine atoms.[98]

In the Dewar-Chatt-Duncanson model the bonding of an olefin to a transition metal centre is described in terms of the synergic contributions of two effects, as illustrated schematically in Figure 1.5.[99-101] These may be described respectively as the donation of electron density from filled olefin orbitals to the metal, and the acceptance of electron density by virtual antibonding orbitals on the olefin.

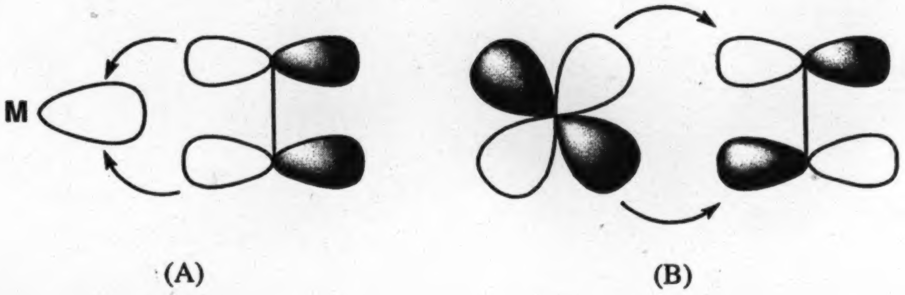

Figure 1.6. Synergic components of metal-olefin bonding according to the Dewar-Chatt-Duncanson model: (A) shows the σ-donor interaction and (B) the π-acceptor interaction.

The antibonding π^* orbital of a monoolefin is of suitable symmetry for interaction with a filled d-character orbital on the metal. As the degree of back-donation increases (or the acceptor ability of the olefin increases) the geometry of the ligated olefin is increasingly perturbed from the ground state (free) geometry. Thus the bonding orbitals of the ligated carbon atoms develop greater p character and so approach a limiting tetrahedral sp^3 geometry as the acceptor ability of the π^* orbital increases.

Thus, in tetrafluoroethene complexes the geometry at the ligated carbon atom is approximately tetrahedral,[102-105] whereas in non-fluorinated olefin complexes, the loss of planarity of the olefin upon coordination is less if there are no electron-withdrawing substituents on the olefin. All of the monometallic tetrafluoroethene complexes that have been structurally characterized may be described as metallacyclopropanes due to the tetrahedral geometry at carbon which is consistent with the above-mentioned rehybridization at carbon.[106 - 142]

Figure 1.7 (A) shows the π-olefin extreme of bonding where the interaction is mainly a σ-donor one and corresponds to the diagram showing orbital overlap in Figure 1.6 (A). Figure 1.7 (B) shows the extreme valence bond representation of the extensive π-acceptor interaction, diagrammed in Figure 1.6 (B) where the structure is best described as that of a metallacyclopropane.

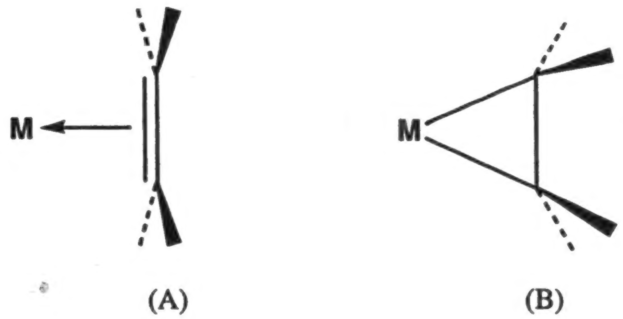

Figure 1.7. Bonding extremes of the metal-olefin interaction.

Because of the high electronegativity of fluorine, there is a substantial ionic contribution to the metal-fluorocarbon bond and an increase in s-character of the bond, which results in a marked decrease in the bond length.[97] Thus, while a fluoroolefin ligand approximates the steric requirement of a non-fluorinated olefin, the bonding interaction with the metal and the geometry of the ligated olefin are changed. Also, coordination of fluoroolefins to metal centres renders fluorine α to the metal centre susceptible to removal by Lewis acids, including protons.[104, 143-159] This is generally regarded as being due to the metal-fluorocarbon σ-bonding orbital having some antibonding character with respect to the α C-F bond.[97, 160] An alternative explanation involves π back donation from the metal into C-F σ^* orbitals, thereby weakening the bond. This requires that a trifluoromethyl group should be a better π acceptor than a methyl group. This view has been deprecated on the basis of calculations involving Mn-CF_3 complexes which have indicated that the trifluoromethyl group is no better a π acceptor than a methyl group, and that the C-F σ^* orbital is too high in energy for this type of interaction.[97, 160] This explanation is still, however, favoured by some authors.[143]

Relatively few fluoroolefin complexes have been prepared, compared to the number of olefin complexes, which are legion. The vast majority have been tetrafluoroethene complexes; only a few partially-fluorinated ethene complexes having been reported.[106-127, 161-162] The relative stability of hydrocarbyl olefin complexes and fluorinated ones has been explored briefly, with the conclusion that partially fluorinated olefins are more labile than non-fluorinated olefins, and that tetrafluoroethene complexes are as, or more stable than ethene complexes, although the exact order of trifluoroethene in this series probably depends on the particular system in question.[102, 161] This trend has been attributed to a combination of the effect of increasing fluorination on the electron accepting ability of the fluoroolefin and the deformation energy cost for changing the planar (sp^2 hybridized carbon) geometry of the free olefin towards the geometry of the coordinated ligand (approaching sp^3 hybridized carbon).[162] Thus, while the presence of electron-withdrawing substituents confers better π-acceptor properties on the olefin, it also comes with an increased deformation energy cost.[161-162] Apart from steric interactions with the metal-containing fragment, the energy of the olefin-metal interaction may be partitioned into two major contributions: the "bond-snap" energy, which is the energy required to break the metal-olefin bond (the olefin being in the coordinated geometry), and the deformation energy.[162] The sum of these two components is the overall bond energy for the metal-olefin interaction.[162]

Objectives of this thesis

The first goal of this thesis was to extend the reactivity studies of $[Ir_2(CH_3)(CO)_2(dppm)_2][CF_3SO_3]$ (**1**) to include olefin coordination. To that end, the bonding modes of some simple olefins and fluoroolefins in homobimetallic biphosphine-bridged complexes of iridium, and the steric and electronic effects that give rise to these bonding modes, were investigated. Since both terminal (η^2) and bridged (μ^2) bonding modes for unsaturated ligands had been previously encountered in this system,[88, 89, 163, 164] it was hoped that the reasons for the different bonding modes could be explained. As well, it was hoped that a better understanding of these factors might allow the rationalization of some of the transformations, in particular olefin C-H activation, that have been previously been reported in these systems.[88, 89] The effect of varying the degree of fluorine substitution in an olefin upon the bonding mode, as well as the possibility of C-F activation was to be considered.

The chemistry of related dmpm complexes was investigated in the hope of stabilizing, by virtue of the lesser steric requirements and enhanced basicity conferred by the dmpm ligand, some of the intermediates that occur for the dppm complexes. In particular, it was hoped that the dmpm analogue of $[Ir_2(CH_3)(CO)_2(dppm)_2][CF_3SO_3]$ (**1**) (i.e. **1-dmpm**)[47] could be investigated for its reactions with olefins.

References

1. Mears, D.; Eastman, A. D. in *Kirk-Othmer Encyclopedia of Chemical Technology, 4th. Ed.*, Wiley-Interscience: New York, 1995; http://www.mrw.interscience.wiley.com/kirk/articles/survmear.a01; accessed 14 July, 2002.
2. See, for example: (a) Shilov, A. E.; Shul'pin, G. B. *Catalysis by Metal Complexes, Vol. 21. Activation and Catalytic Reactions of Saturated Hydrocarbons in the Presence of Metal Complexes*, Kluwer: Dordrecht, 2000. (b) Torrent, M.; Sola, M.; Frenking, G.; *Chem. Rev.* **2000**, *100*, 439. (c) Aresta, M.; Armor, J. N.; Barteau, M. A.; Beckman, E. J.; Bell, A. T.; Bercaw, J. E.; Creutz, C.; Dinjus, E.; Dixon, D. A.; Domen, K.; Dubois, D. L.; Eckert, J.; Fujita, E.; Gibson, D. H.; Goddard, W. A.; Goodman, D. W.; Keller, J.; Kubas, G. J.; Kung, H. H.; Lyons, J. E.; Manzer, L. E.; Marks, T. J.; Morokuma, K.; Nicholas, K. M.; Periana, R.; Que, L.; Rostrup-Nielson, J.; Sachtler, W. M. H.; Schmidt, L. D.; Sen, A.; Somorjai, G. A.; Stair, P. C.; Stults, B. R.; Tumas, W.; *Chem. Rev.* **2001**, *101*, 953.

3. (a) Satterfield, C. N. *Heterogeneous Catalysis in Practice;* McGraw-Hill: New York, 1980. (b) Bond, G. C. *Heterogeneous Catalysis;* Clarendon: Oxford, 1987. (c) Davis, B. H.; Hettinger, W. P. Jr., eds., *Heterogeneous Catalysis;* American Chemical Society: Washington, DC, 1983.
4. (a) Niemantsverdriet, J. W. in *Catalysis;* Moulijin, J. A.; van Leeuwen, P. W. N. M.; Santen, R. A., eds.; Elsevier: Netherlands, 1993, Chapter 10. (b) Campbell, I. M. *Catalysis at Surfaces;* Chapman and Hall: New York, 1988, Chapter 4.
5. a) Atwood, J. D. *Coord. Chem. Rev.* **1988**, *83*, 93. b) Marks, T. J. *Acc. Chem. Res.* **1992**, *25*, 57.
6. Suss-Fink, G.; Meister, G. *Adv. Organomet. Chem.* **1993**, *35*,41.
7. Cotton, F. A. *Quart. Rev.* **1966**, *20*, 389.
8. Muetterties, E. L. *Science* **1977**, *196*, 839.
9. Muetterties, E. L.; Rhodin, T. N.; Bans, E.; Brucker, C. F.; Pretzer, W. R. *Chem. Rev.* **1979**, *79*, 91.
10. Muetterties, E. L. *Pure. Appl. Chem.* **1982**, *54*, 83.
11. Muetterties, E. L *Chem. Soc. Rev.* **1982**, *11*, 283.
12. Collman, J. P.; Hegedus, L. S.; Finke, R. G. *Principles and Applications of Organotransition Metal Chemistry;* University Science Books: Mill Valley, CA. p. 383.
13. Crabtree, R. H. *The Organometallic Chemistry of the Transition Metals;* John Wiley and Sons: New York, 1988. p. 327
14. Calvert, R. B.; Shapley, J. R. *J. Am. Chem. Soc.* **1977**, *99*, 5225.

15. Zaera, F. *Chem. Rev.* **1995**, *95*, 2651.

16. Chaudret, B.; Delavaux, B.; Poilblanc, R. *Coord. Chem. Rev.* **1988**, *86*, 191.

17. Haiduc, I.; Silaghi-Dimitrescu, I. *Coord. Chem. Rev*. **1986**, *74*, 127.

18. Puddephatt, R. J. *Chem. Soc. Rev*. **1983**, 12, 99.

19. Jenkins, J. A.; Ennett, J. P.; Cowie, M. *Organometallics* **1988**, *7*, 1845.

20. Cronin, L.; Nicasio, M. C.; Perutz, R. N.; Peters, R. G.; Roddick, D. M.; Whittlesey, M. K. *J. Am. Chem. Soc.* **1995**, *117*, 10047.

21. Karsch, H. H.; Milewski-Mahrla, B. *Angew. Chem., Int. Ed. Engl.* **1981**, *20*, 814.

22. Karsch, H. H.; Schubert, U. *Z. Naturforsch.* **1982**, *B37*, 186

23. Ling, S. S. M.; Puddephatt, R. J.; Manojlovic-Muir, L.; Muir, K. W. *J. Organomet. Chem.* **1983**, *255*, C11.

24. Ling, S. S. M.; Puddephatt, R. J.; Manojlovic-Muir, L.; Muir, K. *W. Inorg. Chim. Acta*. **1983**, *77*, L95.

25. Kullberg, M. L.; Kubiak, C. P. *Organometallics* **1984**, *3*, 632.

26. Manojlovic-Muir, L.; Muir, K. W.; Frew, A. A.; Ling, S. S. M.; Thomson, M. A.; Puddephatt, R. J. *Organometallics* **1984**, *3*, 1637.

27. De Leeuw, G.; Field, J. S.; Haines, R. J.; McCulloch, B.; Meintjies, E.; Monberg, C.; Oliver, G. M.; Ramdial, P.; Sampson, C. N.; Sigwarth, B.; Steen, N. D.; Moodley, K. G. *J. Organomet. Chem* **1984**, *275,* 99.

28. McLennan, A. J.; Puddephatt, R. J. *Organometallics* **1985**, *4*, 485.

29. Ling, S. S. M.; Jobe, I. R.; Manojlovic-Muir, L.; Muir, K. W.; Puddephatt, R. J. *Organometallics* **1985**, *4*, 1198.

30. Ling, S. S. M.; Payne, N. C.; Puddephatt, R. J. *Organometallics* **1985**, *4*, 1546.

31. Azam, K. A.; Ferguson, G.; Ling, S. S. M.; Parvez, M.; Puddephatt, R. J.; Srokowski, D. *Inorg. Chem.* **1985**, *24*, 2799.

32. Kullberg, M. L.; Lemke, F. R.; Powell, D. R.; Kubiak, C. P. *Inorg. Chem.* **1985**, *24*, 3589.

33. Lemke, F. R.; Kubiak, C. P. *J. Chem. Soc., Chem. Commun.* **1985**, 1729

34. Karsch, H. H.; Milewski-Mahrla, B.; Besenhard, J. O.; Hofmann, P.; Stauffert, P.; Albright, T. A. *Inorg. Chem.* **1986**, *25*, 3811.

35. Anderson, L. B.; Cotton, F.A.; Falvello, L. R.; Harwood, W.S.; Lewis, D.; Walton, R. A. *Inorg. Chem.* **1986**, *25*, 3637.

36. Cotton, F. A.; Falvello, L. R.; Harwood, W. S.; Powell, G. L.; Walton, R. A. *Inorg. Chem.* **1986**, *25*, 3949.

37. Manojlovic-Muir, L.; Jobe, I. R.; Maya, B. J.; Puddephatt, R. J. *J. Chem. Soc., Dalton Trans.* **1987**, 2117.

38. Price, A. C.; Walton, R. A. *Polyhedron* **1987**, *6*, 729.

39. Ni, J.; Kubiak, C. P. *Inorg. Chim. Acta*, **1987**, *127*, L37.

40. Wu, J.; Fanwick, P. E.; Kubiak, C. P. *Organometallics* **1987**, *6*, 1805.

41. Wu, J.; Fanwick, P. E.; Kubiak, C. P. *J. Am. Chem. Soc.* **1988**, *110*, 1319

42. a) Richmond, M. K.; Scott, S. L.; Yap, G. P. A.; Alper, H.; *Organometallics* **2002**, *in press*. Retrieved from http://pubs.acs.org 14 July 2002. b) Xia,

B.-H.; Che, C.-M.; Phillips, D. L.; Leung, K.-H.; Cheung, K.-K.; *Inorg. Chem.* **2002**, *in press.* Retrieved from http://pubs.acs.org 14 July 2002.

43. Johnson, K. A.; Gladfelter, W. L. *Organometallics* **1989**, *8*, 2866.

44. Jaw, H. C.; Savas, M. M.; Rodgers, R. D.; Mason, W. R. *Inorg. Chem.* **1989**, *28*, 1028.

45. Reinking, M. K.; Ni, J.; Fanwick, P. E.; Kubiak, C. P. *J. Am. Chem. Soc.* **1989**, *111*, 6459.

46. Wu, J.; Fanwick, P. E.; Kubiak, C. P. *J. Am. Chem. Soc.* **1989**, *111*, 7812

47. Reinking, M. K.; Fanwick, P. E.; Kubiak, C. P. *Angew. Chem. Intl. Ed. Eng.*, **1989**, *28*, 1377.

48. Johnson, K. A.; Gladfelter, W. L. *Organometallics* **1991**, *10*, 376.

49. Davies, J. A.; Dutremez, S.; Pinkerton, A. A.; Vilmer, M. *Organometallics* **1991**, *10*, 2956.

50. Ara, I.; Fanwick, P. E.; Walton, R. A. *Inorg. Chem.* **1991**, *30*, 1973.

51. Perreault, D.; Drouin, M.; Michel, A.; Miskowski, V. M.; Schaefer, W. P.; Harvey, P. D. *Inorg. Chem.* **1992**, *31*, 695.

52. Jenkins, J. A.; Cowie, M. *Organometallics* **1992**, *11*, 2767.

53. Doherty, N. M.; Hogarth, G.; Knox, S. A. R.; Macpherson, H. A.; Melchior, F.; Morton, D. A. V.; Orpen, A. G. *Inorg. Chim. Acta* **1992**, *198*, 257.

54. Keim, W.; Kraneburg, P.; Dahmen, G.; Deckers, G.; Englert, U.; Linn, K.; Spaniol, T. P.; Raabe, G.; Kruger, C *Organometallics* **1994**, *13*, 3085.

55. Davies, J. A.; Kirschbaum, K.; Kluwe, C. *Organometallics* **1994**, *13*, 3664.

56. Blau, R. J.; Chisholm, M. H.; Eichhorn, B. W.; Huffman, J. C.; Kramer, K. S.; Lobkovsky, E. B.; Streib, W. E. *Organometallics* **1995**, *14*, 1855.

57. Alvarez, M. A.; Garcia, M. E.; Riera, V.; Ruis, M. A.; Falvello, L. R.; Bois, C. *Organometallics* **1997**, *16*, 354

58. Lin, W.; Wilson, S. R.; Girolami, G. S. *Organometallics* **1997**, *16*, 2987.

59. Chisholm, M. H.; Folting, K.; Kramer, K. S.; Streib, W. E. *Organometallics*, **1997**, *119*, 5528.

60. Alvarez, M. A.; Garcia, M. E.; Riera, V.; Ruis, M. A *Organometallics* **1999**, *18*, 634.

61. Reid, S. M.; Mague, J. T.; Fink, M. J. *J. Am.Chem. Soc.* **2001**, *123*, 4081.

62. Hartwig, J. F.; Andersen, R. A.; Bergman, R. G. *Organometallics* **1991**, *10*, 1710.

63. Tolman, C. A. *Chem. Rev.* **1977**, *77*, 313.

64. Karsch, H. H. *Chem. Ber.* **1984**, *117*, 3123.

65. King, R. B.; Raghuveer, K. *S. Inorg. Chem.* **1984**, 23, 2482.

66. Payne, N. C.; Puddephatt, R. J.; Ravindranath, R.; Treurnicht, I. *Can. J. Chem.* **1988**, *66*, 3176.

67. Ling, S. S. M.; Jobe, I. R.; McLennan, A. J.; Manojlovic-Muir, L.; Muir, K. W.; Puddephatt, R. J. *J. Chem. Soc., Chem. Commun.* **1985**, 566.

68. Bensch, W.; Prelati, M.; Ludwig, W. *J. Chem. Soc., Chem. Commun.* **1986**,1762.

69. Anderson, L. B.; Cotton, F. A.; Falvello, L. R.; Harwood, W. S.; Lewis, D.; Walton, R. A. *Inorg. Chem.* 1986, 25, 3637.

70. Manojlovic-Muir, L.; Jobe, I. R.; Ling, S. S. M.; McLennan, A. J.; Puddephatt, R. J. *J. Chem. Soc., Chem. Commun.* **1985**, 1725.

71. Meyer, K. E.; Fanwick, P. E.; Walton, R. A. *J. Am. Chem. Soc.* **1990**, *112*, 8586.

72. Meyer, K. E.; Root, D. R.; Fanwick, P. E.; Walton, R. A. *Inorg. Chem.* **1992**, *31*, 3067.

73. Meyer, K. E.; Fanwick, P. E.; Walton, R. A. *Inorg. Chem.* **1992**, *31*, 4486.

74. Cotton, F. A.; Murillo, C. A.; Wang, X. *J. Am. Chem. Soc.* **1998**, *120*, 9594.

75 Stern, E. W.; Maples, P. K. *J. Catal.* **1972**, *27*, 120.

76. Brown, M. P.; Puddephatt, R. J.; Rashidi, M.; Seddon, K. R. Inorg. *Chim. Acta* **1977**, *23,* L27.

77. Hunt, C.; Balch, A. L. *Inorg. Chem.* **1981**, *20*, 2267.

78. Kirss, R. U.; Eisenberg, R. *Inorg. Chem.* **1989**, *28*, 3372.

79. Tilley, T. D.; Andersen, R. A.; Zalkin, A. *Inorg. Chem.* **1983**, 22, 856. 51.

80. Wong, W. K.; Chiu, K. W.; Wilkinson, G.; Howes, A. J.; Motevalli, M.; Hursthouse, M. B. *Polyhedron* **1985**, *4,* 603

81. Wong, W. K.; Chiu, K. W.; Wilkinson, G.; Motevalli, M.; Hursthouse, M. B. *Polyhedron* **1985**, *4,* 1231.

82. Hadj-Bagheri, N.; Puddephatt, R. J. *Polyhedron* **1988**, 7, 2695. 37.

83. Palma-Ramirez, P.; Cole-Hamilton, D. J.; Pogorzelec, P.; Campora, J. *Polyhedron* **1990**, *9*, 1107.

84. Gross, C. L.; Girolami, G. S. *Organometallics* **1996**, *15*, 5359.

85. Gross, C. L.; Girolami, G. S. *J. Am. Chem. Soc.* **1998**, *120*, 6605.

86. Martin, R. L. *J. Am. Chem. Soc.* **1999**, *121*, 9459.

87. a) Cotton, F. A.; Dunbar, K. R.; Hong, B.; James, C. A.; Matonic, J. H.; Thomas, J. L. C. *Inorg. Chem.* **1993**, *32*, 5183. b) Mague, J. T. *Inorg. Chem.* **1994**, *33*, 4261. c) Hsu, T. C.; Helvoigt, S. A.; Partigianoni, C. M.; Turro, C.; Nocera, D. *Inorg. Chem.* **1995**, *34*, 6186.

88. Torkelson, J.R.; Antwi-Nsiah, F.H.; McDonald, R.; Cowie, M.; J.G. Prius, J.G.; Jalkanen, K.J.; DeKock, R.L. *J. Am. Chem. Soc.* **1999**, *121*, 3666.

89. Torkelson, J. R.; McDonald, R.; Cowie, M. *J. Am. Chem. Soc.* **1998**, *120*, 4047.

90. Kiplinger, J. L.; Richmond, T. G.; Osterberg, C. E. *Chem. Rev.* **1994**, *94*, 373.

91. Richmond, T. G. in "Topics in Organometallic Chemistry: Activation of Unreactive Bonds and Organic Synthesis" Springer-Verlag, New York, 1999. Vol. 3, pp. 243-269.

92. Richmond, T. G. *Angew. Chem. Int. Ed.* **2000**, *39*, 3241.

93. Schlosser, M. *Angew. Chem. Int. Ed. Engl.* **1998**, *110*, 1496.

94. *Biochemistry Involving the Carbon-fluorine Bond*, Filler, R. (Ed); American Chemical Society, Washington, DC 1976.

95. Selective Fluorination in Organic and Bioorganic Chemistry, Welch, J.T. (Ed) American Chemical Society, Washington, DC 1991.

96. Welch, J. T.; Lin, J. *Tetrahedron*, **1996**, *52*, 291.

97. Hughes, R. P. *Adv. Organometal. Chem.*, **1990**, *31*, 183

98. Kobayashi, Y.; Kumadaki, I. *Acc. Chem. Res.* **1981**, *14*, 76.

99. Dewar, M. J. S. *Bull. Chem. Soc. Fr.* **1951**, *18*, C71.

100. Chatt, J.; Duncanson, L. A. *J. Chem. Soc.* **1953**, 2939.

101. Albright, T. A.; Hoffmann, R.; Thibeault, J. C.; Thorn, D. L. *J. Am. Chem. Soc.* **1979**, *101*, 3801.

102. Curnow, O.; Hughes, R. P.; Rheingold, A. L. *J. Am. Chem. Soc.* 1992, 114, 3153.

103. Curnow, O.; Hughes, R. P.; Mairs, E. N.; Rheingold, A. L. *Organometallics* 1993, 12, 3102.

104. Hughes, R. P. *Organometallics* **1993**, *12*, 4736.

105. Akermark, B.; Blomberg, M. R. A.; Glaser, J.; Ohrstrom, L.; Wahlberg, S.; Warnmark, K.; Zetterberg, K. *J. Am. Chem. Soc.* **1994**, *116*, 3405.

106. Green, M.; Osborn, R. B. L.; Rest, A. J.; Stone, F. G. A. *J. Chem. Soc. A* **1968**, 2525.

107. Fornies, J.; Green, M.; Laguna, A.; Murray, M.; Spencer, J. L.; Stone, F. G. A. *J. Chem. Soc., Dalton Trans.* **1977**, 1515.

108. Green, M.; Howard, J. A. K.; Spencer, J. L.; Stone, F. G. A. *J. Chem. Soc., Chem. Commun.* **1975**, 449.

109. Empsall, H. D.; Green, M.; Shakshooki, S. K.; Stone, F. G. A. *J. Chem. Soc. A* **1971**, 3472.

110. Cooke, M.; Green, M.; Kuc, T. A.; *J. Chem. Soc.* A **1971**, 1200.

111. Burt, R.; Cooke, M.; Green, M. *J. Chem. Soc. A* **1970**, 2975.

112. Cooke, M.; Green, M. *J. Chem. Soc. A* **1969**, 651.

113. Parshall, G. W.; Jones, F. W. *J. Am. Chem. Soc.* **1965**, *87*, 5356.

114. Green, M.; Taylor, S. H. *J. Chem. Soc., Dalton Trans.* **1975**, 1128.

115. Oliver, A. J.; Graham, W. A. G. *Inorg. Chem.* **1971**, *10*, 1165.

116. Tolman, C. A. *J. Am. Chem. Soc.* **1974**, *96*, 2780.

117. Browning, J.; Cook, D. J.; Cundy, C. S.; Green, M.; Stone, F. G. A. *Chem. Commun.* **1968**, 929.

118. Cundy, C. S.; Green, M.; Stone, F. G. A., *J. Chem. Soc. A* **1970**, 1647.

119. Green, M.; Shakshooki, S. K.; Stone, F. G. A. *J. Chem. Soc. A* **1971**, 2828.

120. Maples, P. K.; Green, M.; Stone, F. G. A. *J. Chem. Soc., Dalton Trans.* **1973**, 388.

121. Browning, J.; Penfold, B. R. *J. Chem. Soc., Chem. Commun.* **1973**, 198.

122. Maples, P. K.; Green, M.; Stone, F. G. A.; Spencer, J. L. *J. Chem. Soc., Dalton Trans.* **1974**, 1194.

123. Clark, H. C.; Manzer, L. E. *J. Chem. Soc., Chem. Commun.* **1973**, 870.

124. Clark, H. C.; Manzer, L. E. *Inorg. Chem.* **1974**, 13, 1996.

125. Cramer, R.; Parshall, G. W. *J. Am. Chem. Soc.* **1965**, 87, 1392.

126. Burch, R. B.; Harlow, R. L.; Ittel, S. D. *Organometallics* **1987**, *6*, 982.

127. Booth, B. L.; Casey, S.; Haszeldine, R. N. *J. Organomet. Chem.* **1982**, *226*, 289.

128. Mukhedkar, V. A.; Mukhedkar, A. J. *J. Inorg. Nucl. Chem.* **1981**, *43*, 2801.

129. Howard, J. A. K.; Mitrprachachon, P.; Roy, A. *J. Organomet. Chem.* **1982**, *235*, 375.

130. Guggenberger, L. J.; Cramer, R. *J. Am. Chem. Soc.* **1972**, *94*, 3779.

131. Burch, R. R.; Harlow, R. L.; Ittel, S. D. *Organometallics* **1987**, 6,982.

132. Baraban, J. M. J.; McGinnety, A. *J. Am. Chem. Soc.* **1975**, *97*, 4232.

133. Burrel, A. K.; Clark, G. R.; Rickard, C. E. F.; Roper, W. R.; Wright, A. H. *J. Chem. Soc., Dalton Trans.* **1991**, 609.

134. Burrel, A. K.; Clark, G. R.; Rickard, C. E. F.; Roper, W. R.; Ware, D. C. *J. Organomet. Chem.* **1990**, 398.

135. Curnow, O. J.; Hughes, R. P.; Rheingold, A. L. *J Am. Chem. Soc.* **1992**, *114*, 3153.

136. Brothers, P. J.; Burrell, A. K.; Clark, G. R.; Rickard, C. E. F.; Roper, W. R. *J. Organomet. Chem.* **1990**, *394*, 615.

137. Kaschube, W.; Schroder, W.; Porschke, K. R.; Angermund, K.; Kruger, C. *J. Organomet. Chem.* **1990**, *389*, 399.

138. Russel, D. R.; Tucker, P. A. *J. Chem. Soc., Dalton Trans.* **1975**, 1752.

139. Curnow, O. J.; Hughes, R. P.; Mairs, E. N.; Rheingold, A. L. *Organometallics* **1993**, *12*, 3102.

140. Francis, J. N.; McAdam, A.; Ibers, J. A. J. *Organomet. Chem.* **1971**, *29*, 131.

141. Howard, J. A. K.; Knox, S. A. R.; Terrill, N. J.; Yates, M. T. *J. Chem. Soc., Chem. Commun.* **1989**, 640.

142. Arthurs, M. A.; Bickerton, J.; Stobart, S. R.; J. Wang *Organometallics* **1998**, *17*, 2743.

143. Hughes, R.P; Smith, J. M.; Incarvito, C. D.; Lam, K.; Rhatigan, B.; Rheingold, A. L. *Organometallics* **2002**, *21*, 2136.

144. Koola, J. D.; Roddick, D. M. *Organometallics* **1991**, 10, 591.

145. Brothers, P. J.; Roper, W. R. *Chem. Rev.* **1988**, *88*, 1293.

146. Gallop, M. A.; Roper, W. R. *Adv. Organometal. Chem.* **1986**, *25*, 121.

147. Roper, W.R.. *J. Organomet. Chem.* **1986**, *300*, 167.

148. Crespi, A. M.; Shriver, D. F. *Organometallics* **1985**, *4*, 1830.

149. Richmond, T. G.; Crespi, A. M.; Shriver, D. F. *Organometallics* **1984**, *3*, 314.

150. Richmond, T. G.; Shriver, D. F. *Organometallics* **1984**, *3*, 305.

151. Richmond, T. G.; Shriver, D. F. *Organometallics* **1983**, *2*, 1061.

152. Reger, D. L.; Dukes, M. D. *J. Organomet. Chem.* **1978**, *153*, 67.

153. Maples, P. K.; Green, M.; Stone, F. G. A. *J. Chem. Soc. Dalton Trans.* **1973**, 2069.

154. Maples, P. K.; Green, M.; Stone, F. G. A.; Spencer, J. L. *J. Chem. Soc., Dalton Trans.* **1974**, 1194.

155. Appleton, T. G.; Berry, R. D.; Hall, J. R.; Neale, D. W. *J. Organomet. Chem.* **1989**, *364*, 249.

156. Clark, G. R.; Hoskins, S. V.; Roper, W. R. *J. Organomet. Chem.* **1982**, *234*, C9.

157. Ferraris, D; Cox, C; Anand, R.; Lectka, T. *J. Am. Chem. Soc.* **1997**, *119*, 4319.

158. Burrell, A. K.; Clark, G. R.; Rickard, C. E. F.; Roper, W. R. *J. Organomet. Chem.* **1994**, 482, 261.

159. Michelin, R. A.; Ros, R.; Guadalupi, G.; Bombieri, G.; Benetollo, F.; Chapuis, G. *Inorg. Chem.* **1989**, *28*, 840.

160. Treichel, P.M., *Comprehensive Organometallic Chemistry* Vol. 4; Chpt. 29; Pergamon: Oxford, 1982, pp 98-99.

161. Tolman, C. A. *J. Am. Chem. Soc.* **1974**, *96*, 2780.

162. Cedeno, D. L.; Weitz, E. *J. Am. Chem. Soc.* **2001**, *123*, 12857.

163. Torkelson, J. R. Ph. D. Thesis, University of Alberta, 1998.

164. Antwi-Nsiah, F. H.; Cowie, M. *Organometallics* **1992**, *11*, 3157.

Chapter 2

Olefin coordination to $[Ir_2(CH_3)(CO)_2(dppm)_2][CF_3SO_3]$ [1]

Introduction

The compound $[Ir_2(CH_3)(CO)_2(dppm)_2][CF_3SO_3]$ (**1**) has demonstrated a rich chemistry with a range of substrate molecules.[1 - 4] With carbon monoxide, phosphines and isocyanide molecules, **1** underwent C-H activation of the methyl ligand upon coordination of these substrates to give methylene hydride products (see Scheme 2.1).[2 - 4] This reactivity was subsequently exploited in reactions of **1** with allenes ultimately giving vinyl carbene products which were presumed to form via methylene hydride intermediates, although species in which the allene ligand acts as a four electron donor wherein one metal is bonded to the central allene carbon, while the other is bonded to the allene ligand in an η^3 fashion, were isolated after shorter reaction times (compounds **3E** and **4E** in Scheme 2.2).[4] Surprisingly, the reaction of **1** with ethene or 1,1-dimethylallene gave simple adducts that could be formulated as $[Ir_2(CH_3)(L)(CO)_2(dppm)_2][CF_3SO_3]$ (L = C_2H_4, 1,1-dimethylallene).[2, 4, 5] The absence of methylene hydrides, which would have been analogous to the products from the reaction of **1** with carbon monoxide, phosphines and isocyanides, upon initial coordination of the olefins was puzzling. We therefore have investigated these reactions to determine whether the reaction with ethene or 1,1-dimethylallene was fundamentally different than with CO, PR_3 or RNC, and to further elucidate the C-H activation in **1** promoted by ligand coordination.

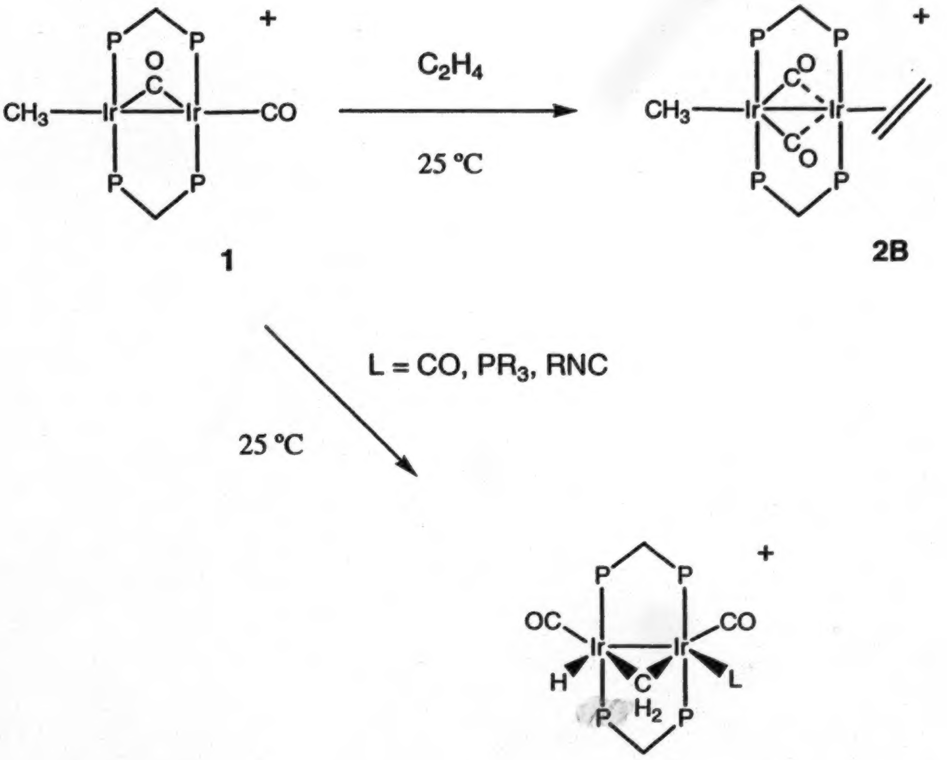

Scheme 2.1. Products obtained at ambient temperature from the reaction of ethene, carbon monoxide and phosphines with **1** in CH_2Cl_2[2-5].

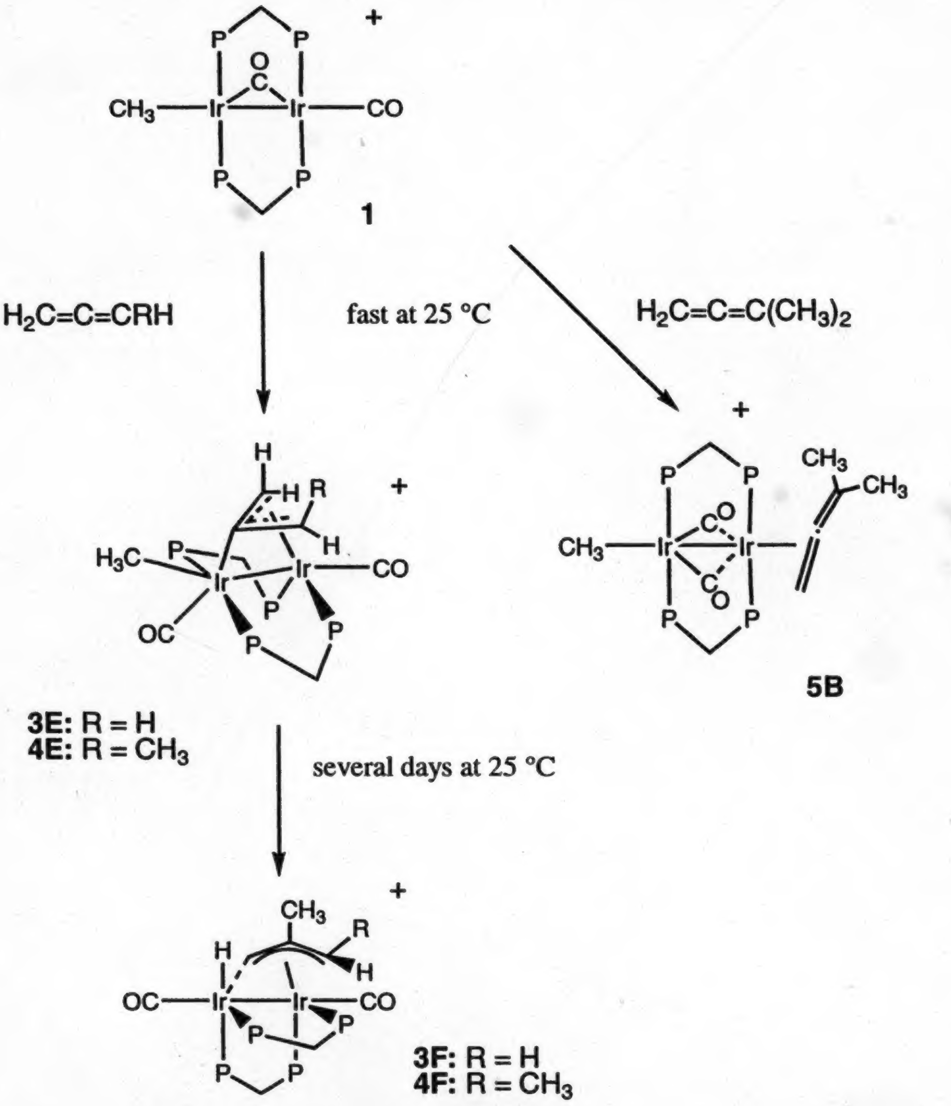
+
P
P
O
C
CH$_3$
Ir
Ir
CO
P
P
1
H$_2$C=C=CRH
fast at 25 °C
H$_2$C=C=C(CH$_3$)$_2$
H
H
R
+
H$_3$C
P
Ir
Ir
H
CO
OC
P
P
P
3E: R = H
4E: R = CH$_3$
several days at 25 °C
+
P
P
CH$_3$
CH$_3$
O
C
CH$_3$
Ir
Ir
C
O
P
P
5B
+
CH$_3$
R
H
H
OC
Ir
Ir
CO
P
P
P
P
3F: R = H
4F: R = CH$_3$

Scheme 2.2. Reaction of allene, methylallene and 1,1-dimethylallene with **1** in CH_2Cl_2 solution.

In addition, 1,3-butadiene also reacted differently with compound **1** yielding the unusual vinylvinylidene-bridged product $[Ir_2(CH_3)(H)(CO)_2(\mu\text{-}H)(\mu\text{-}CC(H)C(H)CH_2)(dppm)_2][CF_3SO_3]$ (**6B**)[1, 2] by double activation of two geminal C-H bonds in the substrate (see Scheme 2.3). The absence of information on the nature of any intermediates in this reaction involving the butadiene molecule, or information that could help explain why this diolefin molecule gave rise to C-H activation of the substrate rather than C-H activation of the methyl ligand in **1** suggested that a reinvestigation of this reaction was needed. To address these questions, a series of variable temperature NMR studies was undertaken using the above-mentioned olefins and cumulenes as well as several other diolefins.

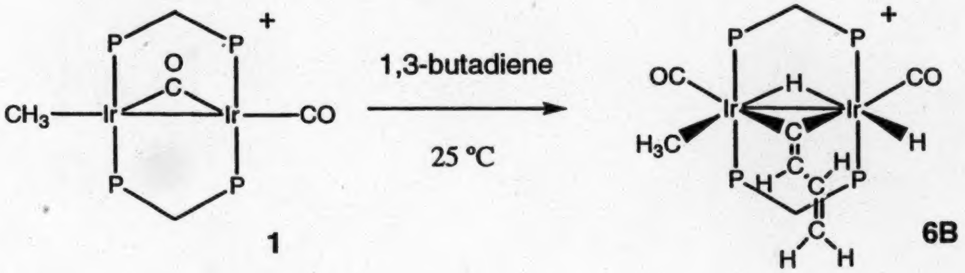

Scheme 2.3. Reaction of butadiene with **1** in CH_2Cl_2 forming $[Ir_2(CH_3)(H)(CO)(\mu\text{-}H)(\mu\text{-}CC(H)C(H)CH_2)(dppm)_2][CF_3SO_3]$ (**6B**).[1,2]

Experimental

General Comments. All solvents were dried (using appropriate drying agents), distilled before use and stored under dinitrogen. Deuterated solvents used for NMR experiments were freeze-pump-thaw degassed (three cycles) and stored under nitrogen or argon over molecular sieves. Reactions were carried out under argon using standard Schlenk techniques, and compounds that were used as solids were purified by recrystallization. Prepurified argon and nitrogen were purchased from Linde, carbon-13 enriched CO (99%) was supplied by Isotec Inc., ethene was supplied by Praxair and methylallene by Fluka. All gases were used as received and all other reagents were purchased from Aldrich and were used as received, except as noted. The compound $[Ir_2(CH_3)(CO)(\mu\text{-}CO)(dppm)_2][CF_3SO_3]$ (**1**) was prepared as previously reported.[3] The perdeuteromethyl analog, **1-*d*₃** was prepared by the literature method, except that methyl-d_3 trifluoromethanesulfonate was reacted with $[Ir_2(CO)_3(dppm)_2]$, and the trimethylamine N-oxide used to remove one of the carbonyls was purified to avoid incorporation of protium into the methyl group of the product, by first recrystallizing commercial anhydrous timethylamine N-oxide from D_2O and then subliming it *in vacuo.*

Proton NMR spectra were recorded on Varian Unity 400, 500 or 600 spectrometers, or on a Bruker AM400 spectrometer. Carbon-13 NMR spectra were recorded on Varian Unity 400 or Bruker AM300 spectrometers. Phosphorus and fluorine NMR spectra were recorded on Varian Unity 400 or Bruker AM400 spectrometers. Two-dimensional NMR experiments (COSY, ROESY, TOCSY and ^{13}C-^{1}H HMQC) were obtained on Varian Unity 400 or 500 spectrometers.

Preparation of Compounds

Low temperature reaction of 1 with allene, methylallene, 1,1-dimethylallene, ethene, butadiene, 2-methyl-1,3-butadiene, *cis*- and *trans*-1,3-pentadiene. In a typical experiment 1-3 equiv. of the gaseous olefin was added slowly by means of a gas-tight syringe to a solution of 30 mg (0.02 mmol) of **1** in 0.7 mL of CD_2Cl_2 in an NMR tube cooled to -78 °C in a solid CO_2/acetone bath. One-dimensional NMR spectra (^{1}H, ^{31}P) were recorded from -80 °C to ambient temperature at 10 °C intervals. As discussed in the Results section, two-dimensional NMR studies (^{1}H - COSY, TOCSY, ROESY, and ^{13}C-^{1}H HMQC) were carried out for certain compounds at particular temperatures. The results of these studies are summarized in Table 2.1.

Table 2.1. NMR Data for the Compounds[a, b]

compounds[c]	temperature, °C	$\delta(^{31}P\{^1H\})^d$	$\delta(^1H)^{,fe}$	$\delta(^{13}C\{^1H\})^{e,f}$
$[Ir_2(H)(CO)_2(\eta^2\text{-}C_2H_4)(\mu\text{-}CH_2)(dppm)_2]^+$ **(2A)**	-80	-2.0 (m, 2P), -3.7 (m, 2P)	5.02 (b, 2H), 4.91 (b, 2H), 3.16 (b, 2H), 1.16 (b, 4H), -12.3 (b, 1H)	189.1 (b), 178.4 (t, $^2J_{PC}$ = 10 Hz)
$[Ir_2(H)(CO)_2($*anti*$\text{-}\eta^2\text{-}H_2C{=}C{=}CH_2)(\mu\text{-}CH_2)(dppm)_2]^+$ **(3A)** and $[Ir_2(H)(CO)_2($*syn*$\text{-}\eta^2\text{-}H_2C{=}C{=}CH_2)(\mu\text{-}CH_2)(dppm)_2]^+$ **(3B)**	-80	-1.6 (m, 4P), -6.7 (m, 2P), -9.0 (m, 2P)	4.99 (b, 4H), -12.3 (b, 2H)	190.3 (b), 189.3 (b), 176.1 (b), 174.8 (b)
$[Ir_2(CH_3)(\eta^2\text{-}H_2C{=}C{=}CH_2)(CO)_2(dppm)_2]^+$ **(3C)**	-30	19.5 (m, 2P), -4.8 (m, 2P)	3.71 (m, 2H), 3.53 (m, 2H), 2.54 – 2.30 (b, 4H), 0.18 (t, 3H, $^3J_{PH}$ = 6.4 Hz)	195.1 (b)
$[Ir_2(CH_3)(\mu\text{-}H_2C{=}C{=}CH_2)(CO)_2(dppm)_2]^+$ **(3D)**	10	19.5 (m, 2P), 2.5 (m, 2P)	5.61 (b, 1H), 4.81 (b, 1H), 4.24 (b, 2H), 3.34 (m, 4H), 1.23 (t, 3H, $^3J_{PH}$ = 8.6 Hz)	208.3 (b), 172.9 (b)
$[Ir_2(H)(CO)_2($*anti*$\text{-}\eta^2\text{-}H_2C{=}C{=}CH(CH_3))(\mu\text{-}CH_2)(dppm)_2]^+$ **(4A)** and $[Ir_2(H)(CO)_2($*syn*$\text{-}\eta^2\text{-}H_2C{=}C{=}CH(CH_3))(\mu\text{-}CH_2)(dppm)_2]^+$ **(4B)**	-80	-0.4 (m, 2P), -6.9 (m, 2P) -2.6 (m, 2P), -8.0 (m, 2P)	-12.0 (b, 1H), -12.6 (b, 1H)	189.9 (b), 189.5 (b), 176.5 (b), 175.9 (b)
$[Ir_2(CH_3)(\mu\text{-}H_2C{=}C{=}CH(CH_3))(CO)_2(dppm)_2]^+$ **(4C)**	-40	27.6 (m, 2P), -5.9 (m, 2P)	3.80 (s, 1H), 3.45 (m, 4H), 2.07 (t, 2H, $^3J_{PH}$ = 11.4 Hz), 1.76 (d, 3H, $^3J_{HH}$ = 3.0 Hz), 0.23 (t, 3H, $^3J_{PH}$ = 6.6 Hz)	191.7 (t, $^2J_{PC}$ = 8.0 Hz), 186.4 (b)
$[Ir_2(CH_3)(\mu\text{-}H_2C{=}C{=}CH(CH_3))(CO)_2(dppm)_2]^+$ **(4D)**	-10	19.9 (m, 2P), 2.9 (m, 2P)	1.25 (t, 3H, $^3J_{PH}$ = 8.5 Hz), 0.95 (d, $^3J_{HH}$ = 3.4 Hz)	

Table 2.1. NMR Data for the Compounds, continued

$[Ir_2(H)(\mu\text{-}CH_2)(CO)_2(\eta^2\text{-}H_2C{=}C{=}CH(CH_3))(dppm)_2]^+$ **(5A)**	-80	1.3 (m, 2P), -13.7 (m, 2P)	5.96 (b, 2H), 5.16 (b, 2H), 4.50 (b, 2H), 3.48 (b, 2H), 1.90 (b, 2H), 1,13 (b, 3H), 0.19 (b, 3H), -12.1 (b, 1H)	191.1 (b), 178.2 (b)
$[Ir_2(CH_3)(CO)_2(\mu\text{-}\eta^2{:}\eta^2\text{-}H_2C{=}CH\text{-}CH{=}CH_2)(dppm)_2]^+$ **(6A)**	-55	-3.22 (m, 1P),-9.42 (m, 1P), -22.66 (m, 1P), -25.64 (m, 1P)	4.89 (m, 1H), 4.51 (m, 1H), 3.59 (m, 1H), 3.27 (m, 1H), 2.67 (d, 1H, $^3J_{HH}$ = 6 Hz), 2.54 (ddd, 1H, $^3J_{HH}$ = 9, 8, 6 Hz), 2.40 (dm, 1H, $^3J_{HH}$ = 9 Hz), 1.62 (dm, 1H, $^3J_{HH}$ = 9 Hz), 1.28 (m, 1H), 1.24 (m, 1H), 0.38 (t, 3H, $^3J_{PH}$ = 6.5 Hz)	186.9 (t, $^2J_{PC}$ = 14 Hz), 184.7 (b), 72.1 ($^1J_{HC}$ = 160 Hz), 64.5 ($^1J_{HC}$ = 147 Hz), 47.9 ($^1J_{HC}$ = 161 Hz), 35.9, 34.4, -3.5 ($^1J_{HC}$ = 139 Hz), -20.2 ($^1J_{HC}$ = 132 Hz)

---

[a] NMR abbreviations: s = singlet, d = doublet, t = triplet, m = multiplet, b = broad. [b] NMR data CD_2Cl_2 unless otherwise stated. [c] In all cases trifluoromethanesulfonate is the accompanying anion. [d] $^{31}P\{^1H\}$ chemical shifts are referenced vs. external 85% H_3PO_4 [e] ^1H and ^{13}C chemical shifts are referenced vs. external TMS. [f] Chemical shifts for the phenyl hydrogens are not given in the ^1H data. [g] C-H coupling constants are from a separate ^1H - coupled experiment

Results

2.1. Reaction of ethene with $[Ir_2(CH_3)(CO)_2(dppm)_2][CF_3SO_3]$ (1).

As previously reported, the reaction of $[Ir_2(CH_3)(CO)_2(dppm)_2][CF_3SO_3]$ with ethene at room temperature forms a π-olefin complex as shown in Scheme 2.4.[4] This product, $[Ir_2(CH_3)(CO)_2(\eta^2\text{-}C_2H_4)(dppm)_2][CF_3SO_3]$ (**2B**), has two semi-bridging carbonyl groups symmetrically disposed about the plane formed by the two pairs of trans-phosphines and two metal atoms; hence the $^{13}C\{^1H\}$ NMR spectrum shows a single NMR resonance in the carbonyl region at 204.0 ppm.[2,4] The ^{31}P spectrum shows a pair of multiplets due to an AA'BB' spin system at 19.9 and 7.2 ppm.[2,4]

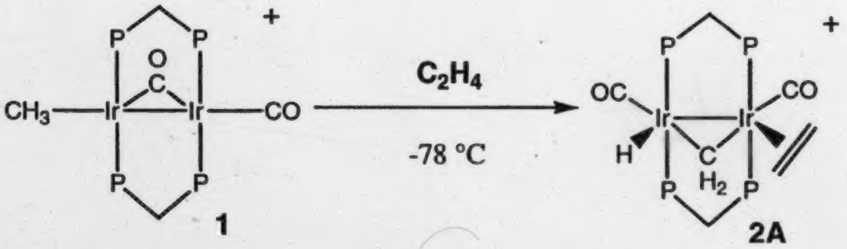

Scheme 2.4. Reaction of **1** with ethene to form **2A**.

When ethene is added slowly via syringe to a -78 °C solution of **1** in CD_2Cl_2 another product, in addition to **2B**, is observed. This product, $[Ir_2(H)(CO)_2(\eta^2\text{-}C_2H_4)(\mu\text{-}CH_2)(dppm)_2][CF_3SO_3]$ (**2A**) may be immediately distinguished by its $^{31}P\{^1H\}$ NMR spectrum, which shows two multiplets at -2.0 and -3.7 ppm, respectively. The very slow addition of ethene using a cold syringe is essential to observing **2A** since any local warming above approximately -60 °C results in its irreversible conversion to **2B,** as verified by warming a sample above this temperature followed by re-cooling to below -60 °C, which resulted in only **2B** being apparent in the ^{31}P NMR spectrum. The $^{31}P\{^1H\}$ NMR spectrum of a typical mixture of compounds **2A** and **2B** is shown in Figure 2.1.

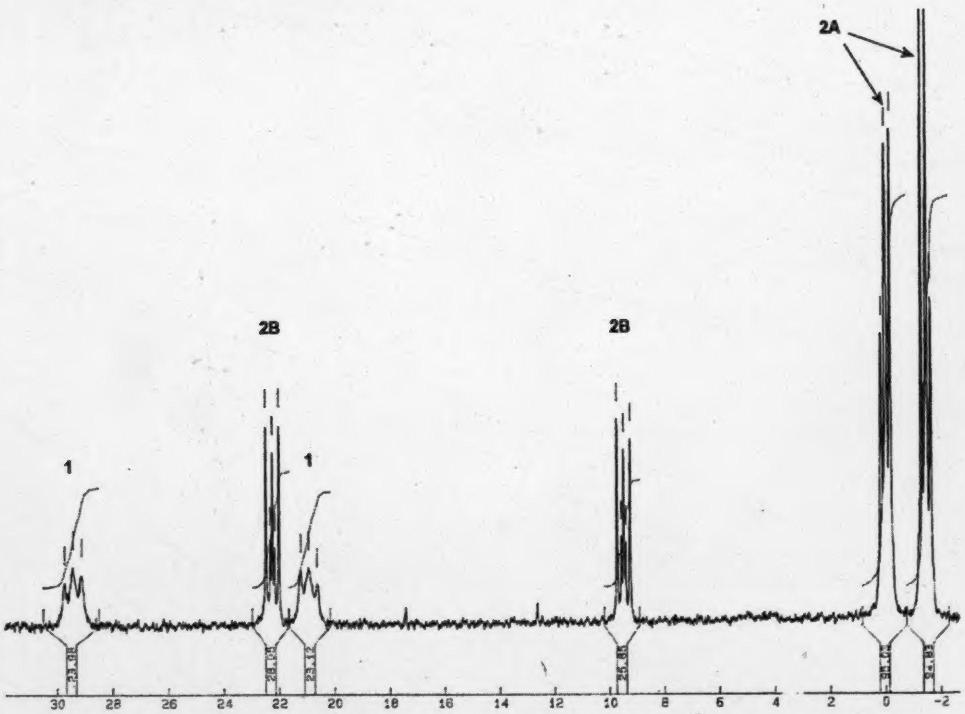

Figure 2.1. $^{31}P\{^1H\}$ spectrum of the reaction mixture of ethene and **1** at -80 °C in CD_2Cl_2.

The $^{13}C\{^1H\}$ NMR spectrum at -80 °C of **2A** shows two distinct signals, a broad singlet at 189.1 ppm and a triplet at 178.4 ppm ($J_{P\text{-}C}$ = 10 Hz). At this temperature the lone signal due to **2B** has shifted slightly from the value observed at ambient temperature (204.0 ppm) to 207.5 ppm. The proton NMR spectrum has, as its most distinctive feature, a broad hydride resonance at -12.3 ppm. The compound appears fluxional on the ^{1}N-NMR time scale at this temperature, so that all the ^{1}H NMR signals are broad. A bridging methylene, showing some partially resolved coupling approximating a quintet, is visible at 5.02 ppm, comparable to that reported for the bridging methylene group of $[Ir_2(H)(CO)_3(\mu\text{-}CH_2)(dppm)_2][CF_3SO_3]$ which appears at 5.19 ppm.[11] A very broad peak at 1.16 ppm integrating for four protons is attributed to the coordinated ethene molecule, and does not differ greatly from the chemical shift of the coordinated ethene in **2B** (1.05 ppm). The fluxional nature of **2A** is confirmed by the observation of decoalescence of the low field multiplet in the ^{31}P spectrum when the sample is cooled to -90 °C. Since the other multiplet remains sharp, it is likely that the low field multiplet is due to the two phosphorus nuclei attached to the iridium to which the ethene ligand is bound, since as the sample is cooled, ethene rotation slows causing the two phosphorus environments to differ slightly, and the signals to broaden. This implies up-down asymmetry in **2A** (with respect to the $Ir_2(\mu\text{-}CH_2)$ plane), presumably because the ethene ligand is twisted with respect to the Ir-Ir axis so that in a static structure the two phosphorus nuclei attached to the iridium to which the olefin is bound are in different environments. The average structure in the fast-exchange limit of rapid ethene rotation gives rise to the observed pair of multiplets in the $^{31}P\{^1H\}$ NMR spectrum. Conversely, the ^{31}P signals due to **2B** remain sharp at all of the temperatures studied. Here the ethene ligand is coordinated in the equatorial plane of the complex and there is no up-down asymmetry.

To investigate the possibility of reversible C-H activation of the ethene ligand accompanied by scrambling of the resulting hydride with a hydride resulting from intramolecular activation of the iridium bound methyl group (i.e. to form a methylene hydride such as **2A**), the perdeuteromethyl analog of **1**, i.e. **1-*d*$_3$**, was prepared and combined with ethene in CH_2Cl_2 solvent at -78 °C. The sample was warmed to 27 °C forming **2B-*d*$_3$** and unreacted **1-*d*$_3$**. No ^2D signals other than the deuterated methyl groups of these compounds were observed. After the solvent was removed *in vacuo* and replaced with CD_2Cl_2 the ^1H spectrum did not show incorporation of protons into the deuterated methyl groups. Hence, no evidence of exchange between the protons of the coordinated ethene and the iridium-bound methyl group could be found. This does not, however, rule out the possibility of reversible C-H activation of the ethene ligand, but *without* scrambling with deuterons from the iridium-bound methyl group.

2.2. Reactions of 1,2-dienes with $[Ir_2(CH_3)(CO)_2(dppm)_2][CF_3SO_3]$ (1).

2.2.1. Reaction of allene with $[Ir_2(CH_3)(CO)_2(dppm)_2][CF_3SO_3]$ (1).

Figures 2.2.1 - 2.2.4 show the $^{31}P\{^1H\}$ NMR spectra of **1** + allene at different temperatures between -90 °C and 5 °C. When allene is added to **1** in an NMR tube at -78 °C a pair of major products, **3A** and **3B**, are seen in the ^{31}P NMR spectra, as shown in Figure 2.2.1. At this temperature, the ^{31}P NMR spectrum consists of three resonances: overlapping multiplets at -1.6 ppm and partially resolved multiplets -6.7 ppm and -9.0 ppm, having the integral ratios 2:1:1, respectively. Upon warming to about -60 °C the resonances sharpen, whereas upon cooling to -90 °C they broaden further, suggestive of a fluxional process involving the phosphorus nuclei. The lowest field resonance at -1.6 ppm is due to two overlapping pairs of phosphorus nuclei and the two higher field resonances are due to the other two nuclei of the $Ir_2(dppm)_2$ framework of **3A** and **3B**. The ^1H NMR spectrum is complicated with overlapping broad resonances; however, a hydride signal appears as a broad resonance at -12.3 ppm. Also there is a broad signal at 4.99 ppm corresponding to a bridging methylene group, indicating that the iridium-bound methyl of **1** has undergone an intramolecular C-H activation upon η^2 coordination of the allene ligand, as noted earlier for $[Ir_2(H)(\mu\text{-}CH_2)(CO)_2(\eta^2\text{-}C_2H_4)(dppm)_2]^+$, **2A**. The ^{13}C NMR spectrum of a ^{13}CO-enriched sample, recorded at -80 °C shows four broad

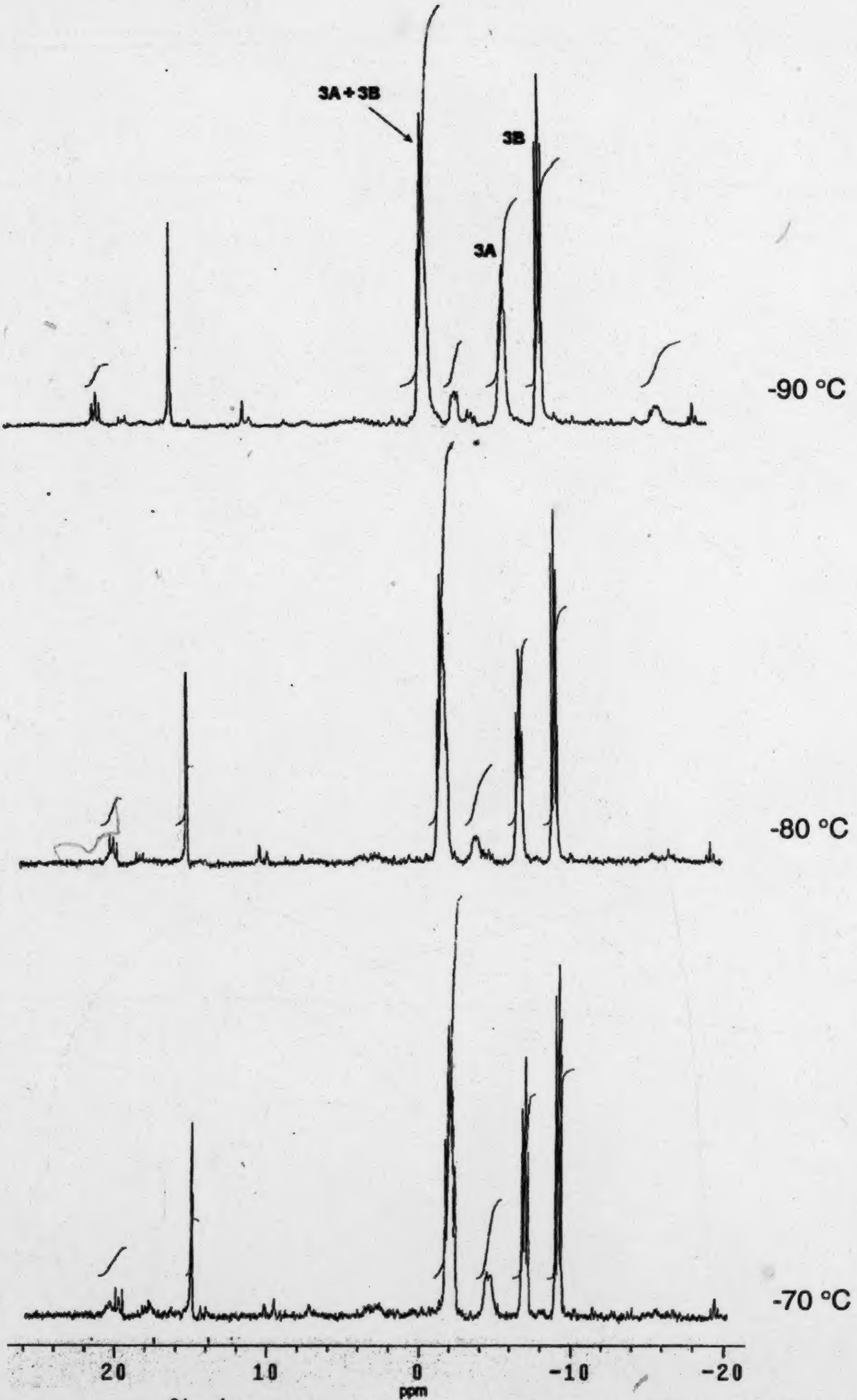

Figure 2.2.1. $^{31}P\{^1H\}$ NMR of the reaction of allene with **1** in CD_2Cl_2, -90 to -70 °C.

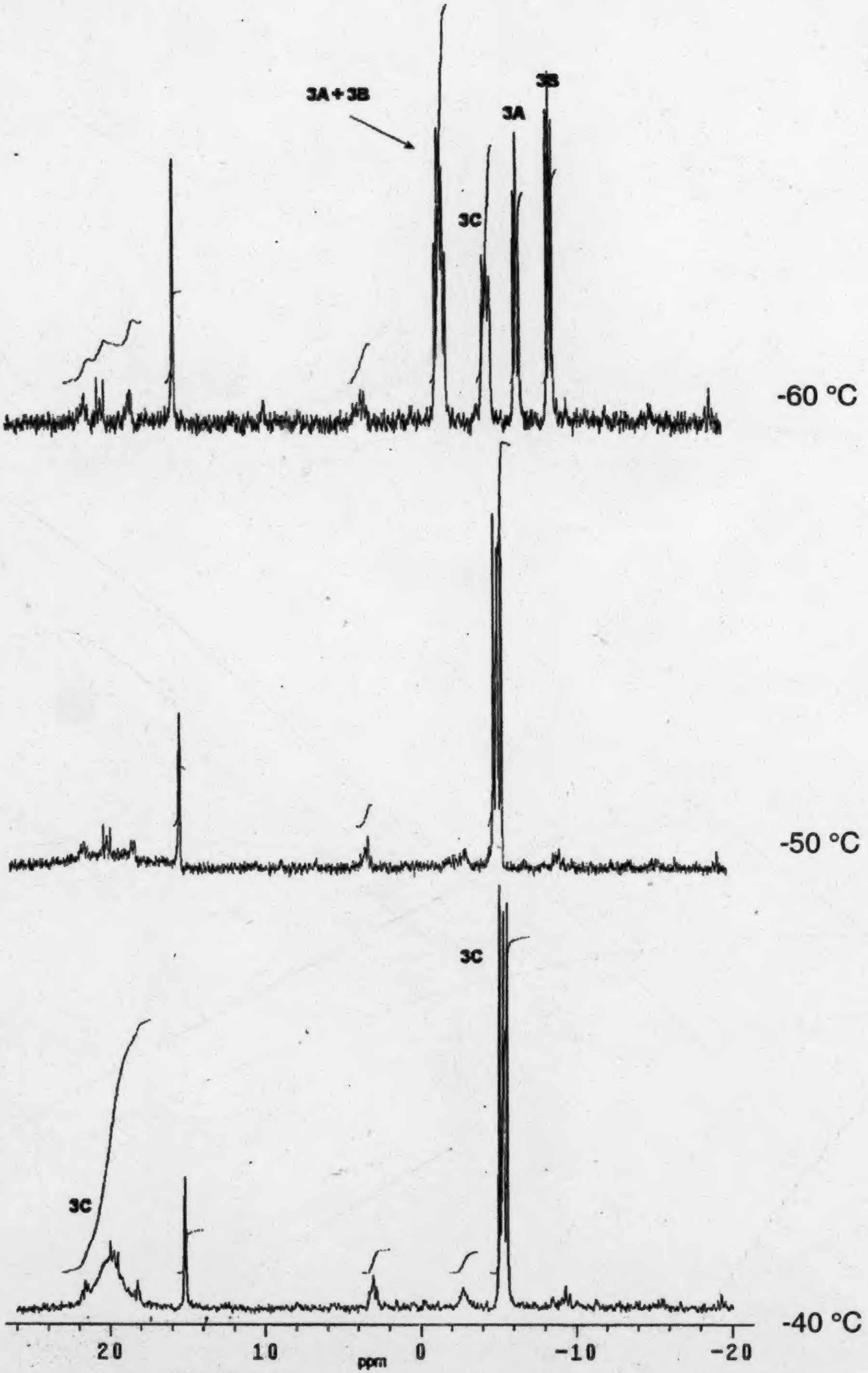

Figure 2.2.2. $^{31}P\{^1H\}$ NMR of the reaction of allene with **1** in CD_2Cl_2, -60 to -40 °C.

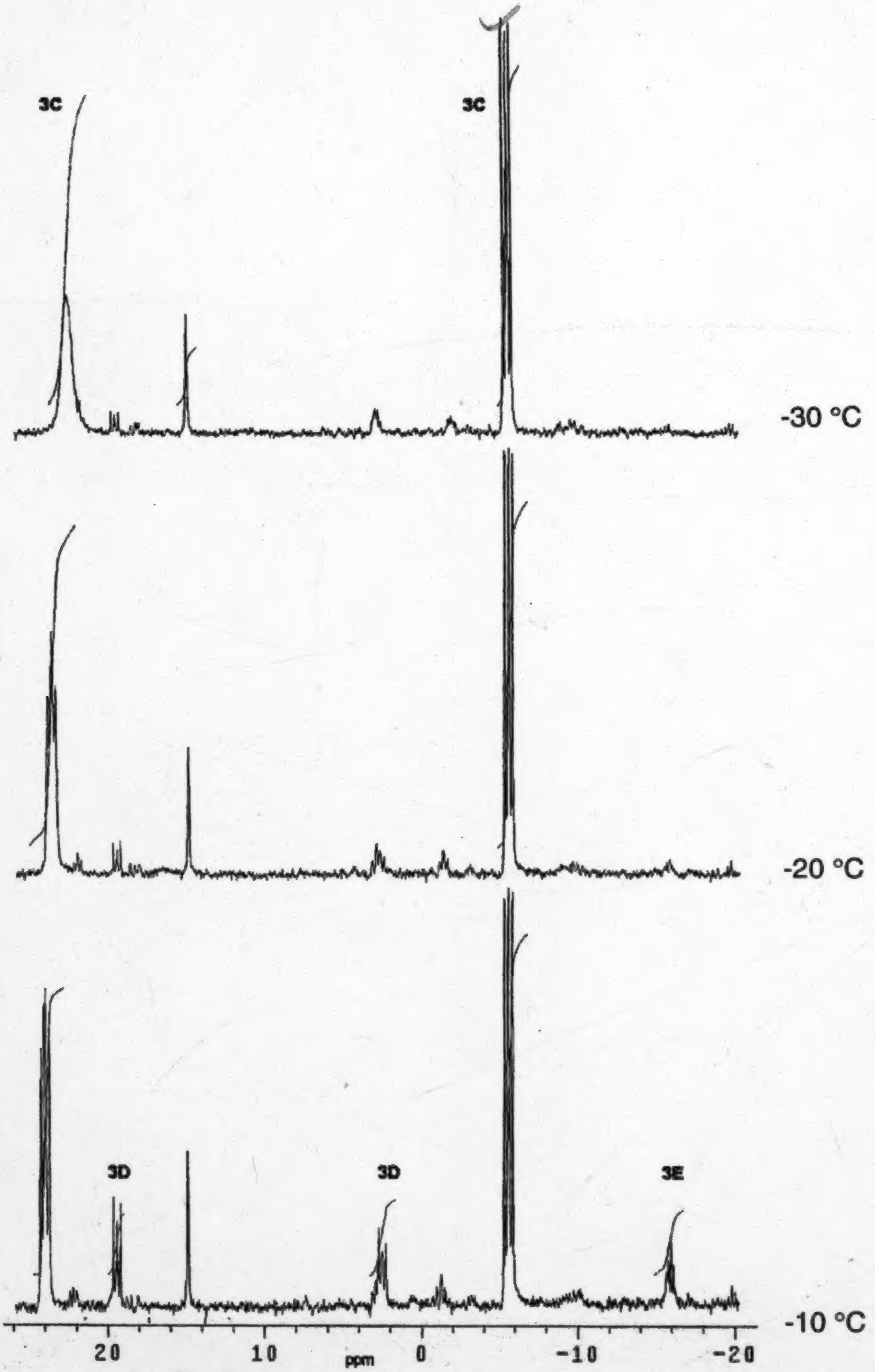

Figure 2.2.3. $^{31}P\{^{1}H\}$ NMR of the reaction of allene with **1** in CD_2Cl_2, -40 to -10 °C.

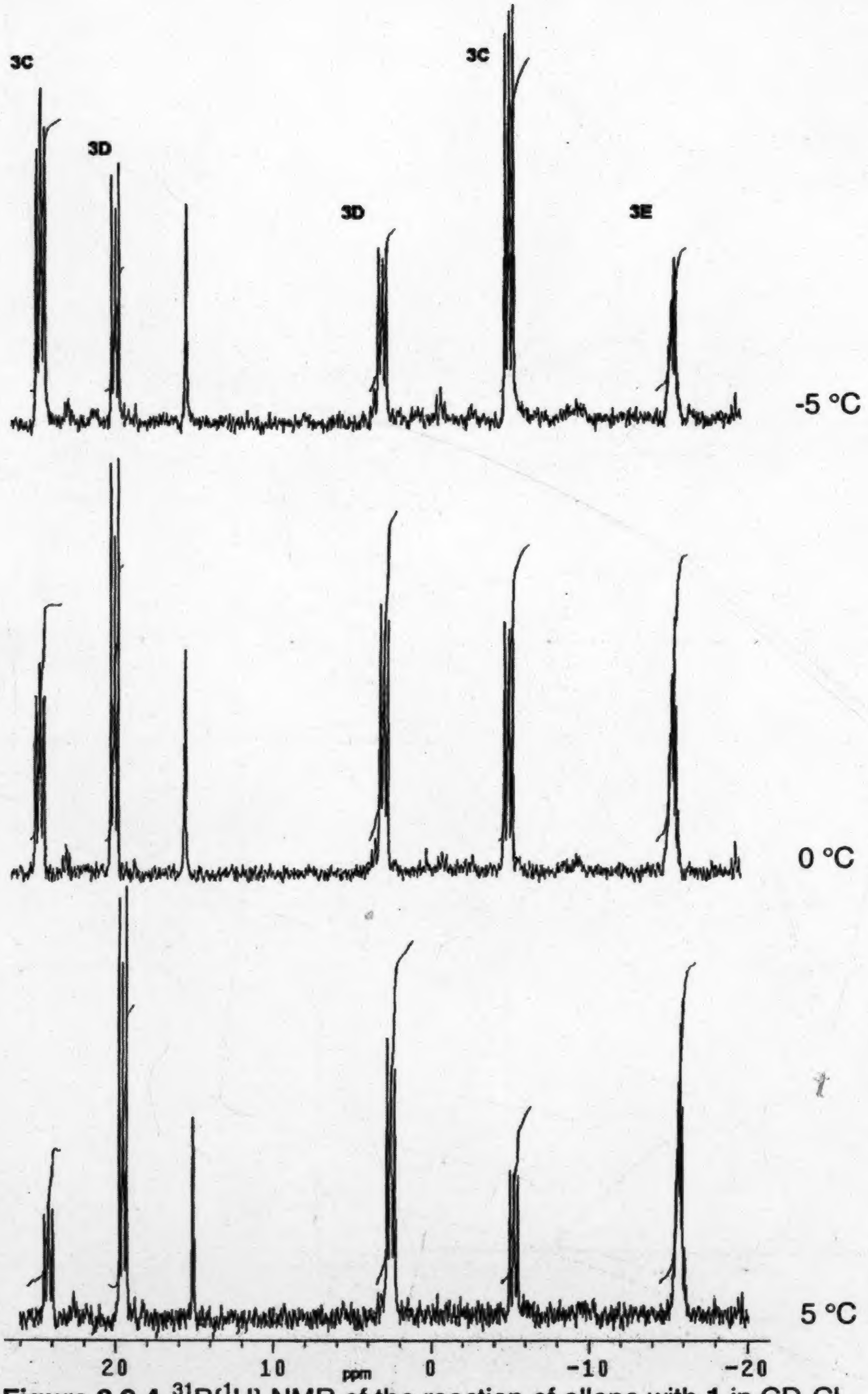

Figure 2.2.4. $^{31}P\{^1H\}$ NMR of the reaction of allene with **1** in CD_2Cl_2, -5 to 5 °C.

carbonyl signals of comparable intensity at 190.3, 189.3, 176.1 and 174.8 ppm, suggesting the presence of two rather similar dicarbonyl complexes at this temperature.

In order to obtain additional information about the presumed isomers **3A** and **3B** a series of ^{31}P decoupling experiments were carried out. The effect of this decoupling on the hydride resonance at -12.3 ppm in the ^{1}H NMR is shown in Figure 2.3. While at higher temperatures the signal appears as a broad singlet, at -90 °C some structure is visible in the ^{31}P-coupled spectrum (spectrum *(a)* in Figure 2.3). Broadband ^{31}P decoupling causes the signal to appear as a broad singlet and a doublet (spectrum *(b)*), clearly showing the two different ^{1}H resonances. Selective decoupling of the -9.0 ppm or -6.7 ppm ^{31}P resonance gives two broad peaks in the ^{1}H spectra (spectra *(d)* and *(e)*), whereas decoupling the ^{31}P resonance at -1.6 ppm (spectrum *(c)*) gives a spectrum similar to that involving broadband decoupling (spectrum *(b)*) . The overall geometry of the two complexes must be quite similar since there are two pairs of very similar carbonyls in the ^{13}C NMR spectrum, making a large change in the environment of the carbonyl carbons between the two isomers unlikely. These observations are consistent with **3A** and **3B** differing in the orientation of the allene ligand with respect to the face of the complex, as shown in Scheme 2.5. Compound **3A** is arbitrarily assigned as being

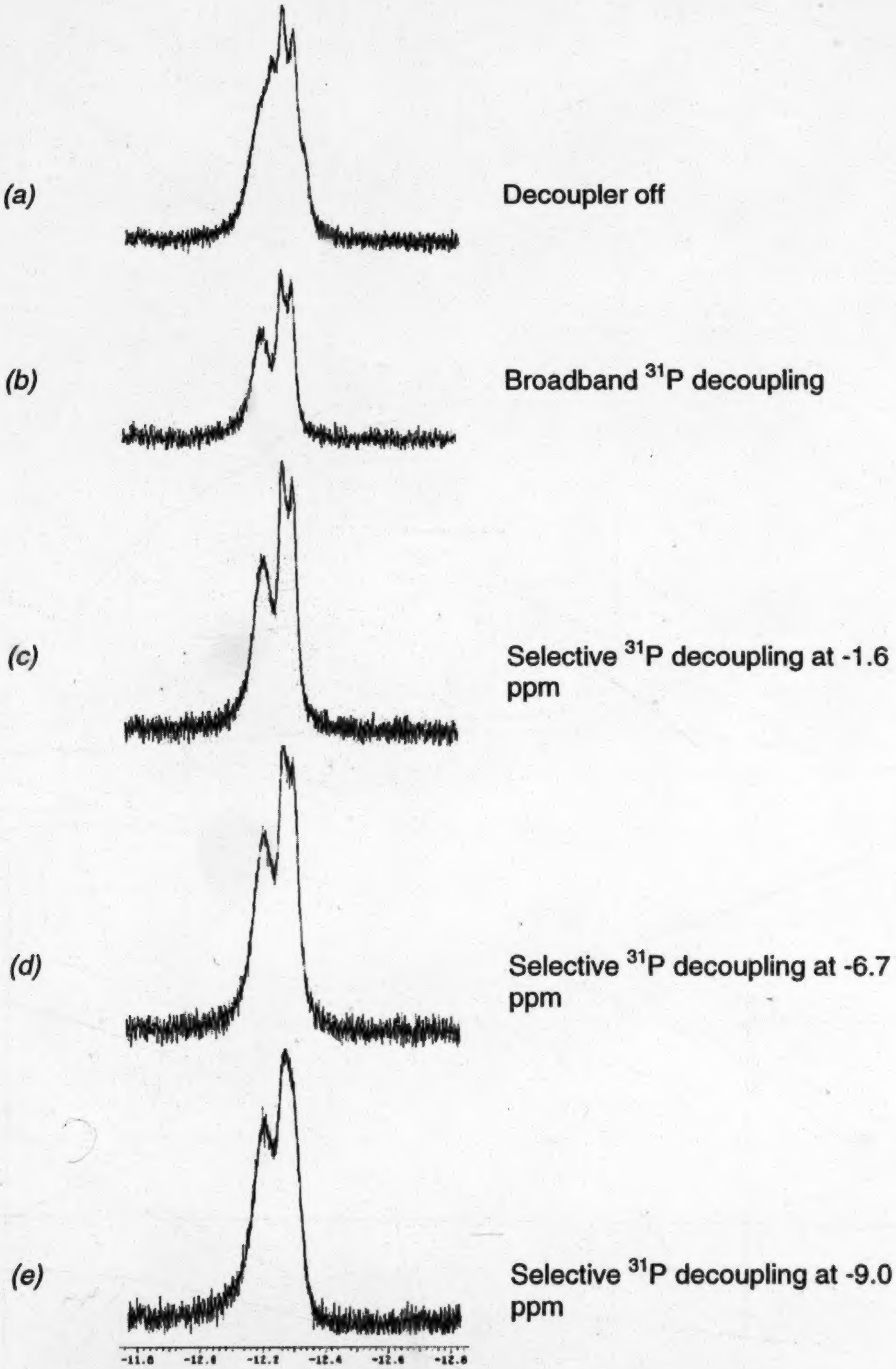

(a) Decoupler off

(b) Broadband ^{31}P decoupling

(c) Selective ^{31}P decoupling at -1.6 ppm

(d) Selective ^{31}P decoupling at -6.7 ppm

(e) Selective ^{31}P decoupling at -9.0 ppm

Figure 2.3. Hydride region of the ^{1}H spectrum of **3A** and **3B** at -90 °C.

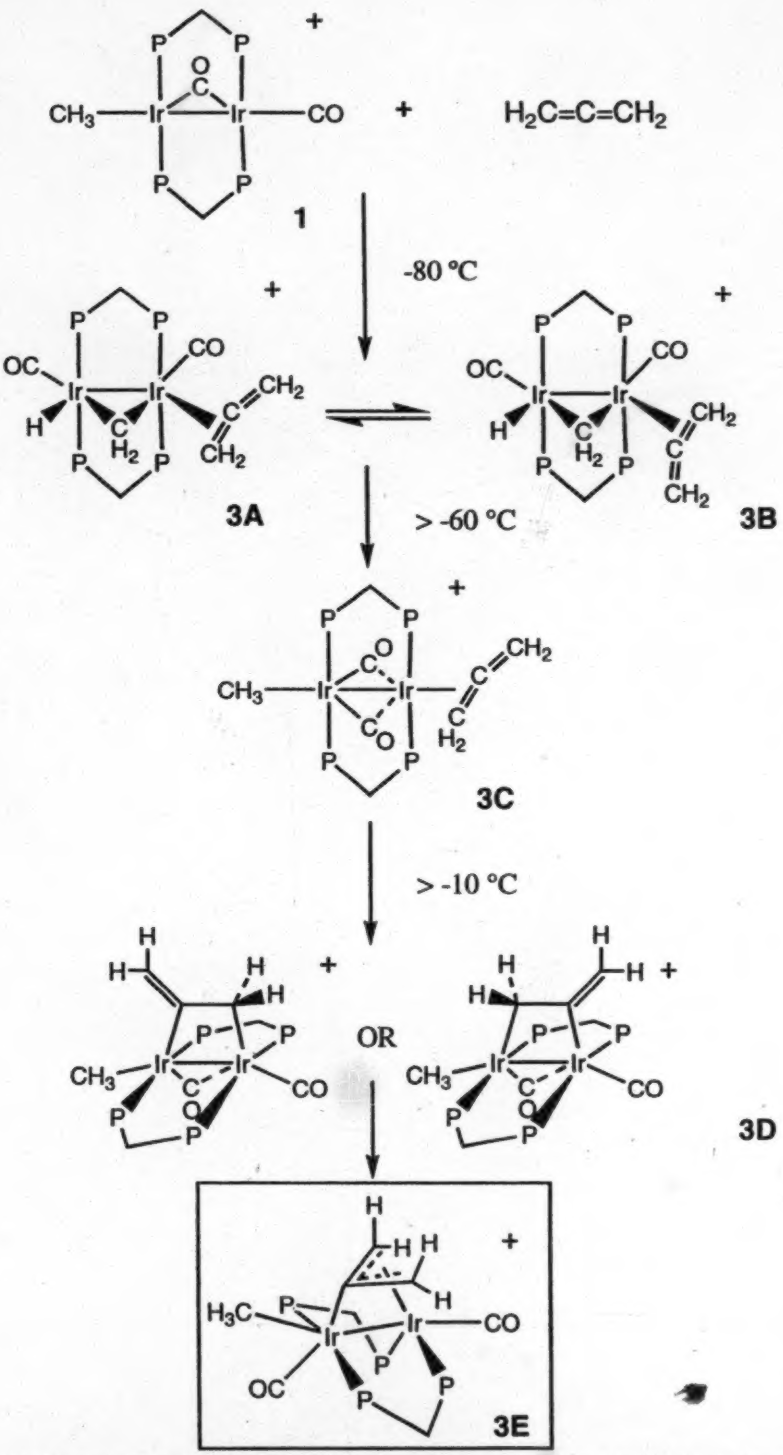
1
-80 °C
3A
3B
> -60 °C
3C
> -10 °C
OR
3D
3E

Scheme 2.5. Products of the reaction of allene with **1**. The species in the box has been previously characterized.[4]

the *anti* isomer with respect to the bridging methylene group and compound **3B** as the *syn* isomer.

At approximately -60 °C a new species, **3C**, begins to appear in the ^{31}P NMR spectrum as a multiplet at -4.8 ppm and a very broad and barely discernable signal at 19.5 ppm (Figure 2.2.2). At -50 °C **3A** and **3B** have disappeared leaving **3C** as the major species. The low-field multiplet of **3C** is exceedingly broad at this temperature and begins to coalesce at -40 °C. At -20 °C a multiplet structure is visible in the low field resonance (Figure 2.2.3). From -50 °C to -20 °C, **3C** is the only species present in appreciable quantity in the ^{31}P NMR spectrum. The ^{1}H NMR spectrum at -30 °C shows no hydride signal, instead a triplet appears at 0.18 ppm (J_{P-C} = 6.4 Hz) due to an iridium-bound methyl group, indicating that the methylene hydrides **3A** and **3B** have been replaced by the more stable methyl complex **3C**. The allene protons in **3C** appear as broad unresolved multiplets from 2.54 to 2.30 ppm, integrating for a total of four protons. The dppm methylene proton resonances appear as complex, overlapped multiplets at 3.71 (2H) and 3.53 ppm (2H). The ^{13}C NMR spectrum shows a single broad peak at 195.1 ppm, due to two equivalent carbonyls. The spectroscopic data are consistent with a terminal η^2 adduct of the type that has been previously isolated from the reaction of ethene with **1** at room temperature[5].

At approximately -10 °C a fourth product, **3D**, starts to appear as a pair of multiplets at 19.5 and 2.5 ppm in the ^{31}P NMR spectrum, and by 5 °C this is the predominant species in solution (Figure 2.2.4). Notably, the formation of **3D** is accompanied by the formation of **3E** (complex multiplet at -15.7 ppm), which is the previously reported $[Ir_2(CH_3)(CO)_2(\mu\text{-}\eta^1\text{-}\eta^3\text{-}H_2C{=}C{=}CH_2)(dppm)_2][CF_3SO_3]$ (**3E**).[4] When the solution is warmed to 10 °C, **3C** disappears, and on maintaining the reaction mixture at this temperature results in the disappearance of **3D** over 1-2 hours, at which time only **3E** is visible in the ^{31}P NMR spectrum. In the ^{1}H NMR spectrum at 10 °C, compound **3D** displays a typical iridium-bound methyl group as a triplet at 1.23 ppm, and broad signals at 5.61 (1H), 4.81 (1H), and 4.24 (2H) ppm for the coordinated allene. Given that the $^{31}P\{^1H\}$ NMR spectrum shows two resonances for the two chemically distinct phosphorus environments (by virtue of the chemically inequivalent metal centres), the signals due to the allene ligand are consistent with it being coordinated so that one CH_2 group is bisected by the symmetry plane of the complex ion. The dppm methylene protons appear as a complex multiplet at 3.34 ppm (4H) in the ^{1}H NMR spectrum. The ^{13}C NMR spectrum indicates that there are two distinct carbonyls, resonating at 208.3 and 172.9 ppm, both of which appear broad. Therefore, the allene is coordinated with one double bond parallel to the iridium-iridium axis. Unfortunately, because of the exchange broadening of the allene proton resonances, neither metrical information in the form of through-space NOE's nor the orientation of the ligand from ^{31}P decoupling experiments could be obtained. The available data are consistent with the allene ligand occupying a bridging position as shown in Scheme 2.5, although the preferred orientation of the uncoordinated methylene cannot be determined. The proposed dimetallacyclobutane arrangement is repeated in the methylallene product **4C**, where NOE information is available with which to establish the structure (see below). A known homobimetallic example of this bonding mode for allene is $C_3H_4Os_2(CO)_8$ which is thermally unstable and was characterized in solution.[7]

2.2.2. Reaction of methylallene with $[Ir_2(CH_3)(CO)_2(dppm)_2][CF_3SO_3]$ (1)

Figures 2.4.1 - 2.4.3 show the $^{31}P\{^1H\}$ NMR spectra of a mixture of **1** with methylallene at various temperatures over the range from -80 °C to 27 °C. The $^{31}P\{^1H\}$ NMR spectrum of this mixture at -80 °C, shown in Figure 2.4.1, is complex. As well as a small amount of unreacted **1** (small multiplets at 27.0 and 18.8 ppm), three major products of reaction with methylallene, **4A**, **4B** and **4C**, may be identified. Species **4C** appears as a pair of multiplets at 27.6 and -5.9 ppm. Species **4A** appears as broad resonances at -0.4 and -6.9 ppm, whereas species **4B** displays a pair of multiplets at -2.6 ppm and -8.0 ppm.

At the lowest temperatures studied all three of **4A**, **4B** and **4C** are present in similar amounts. The ^{1}H NMR spectrum is complicated with broad and

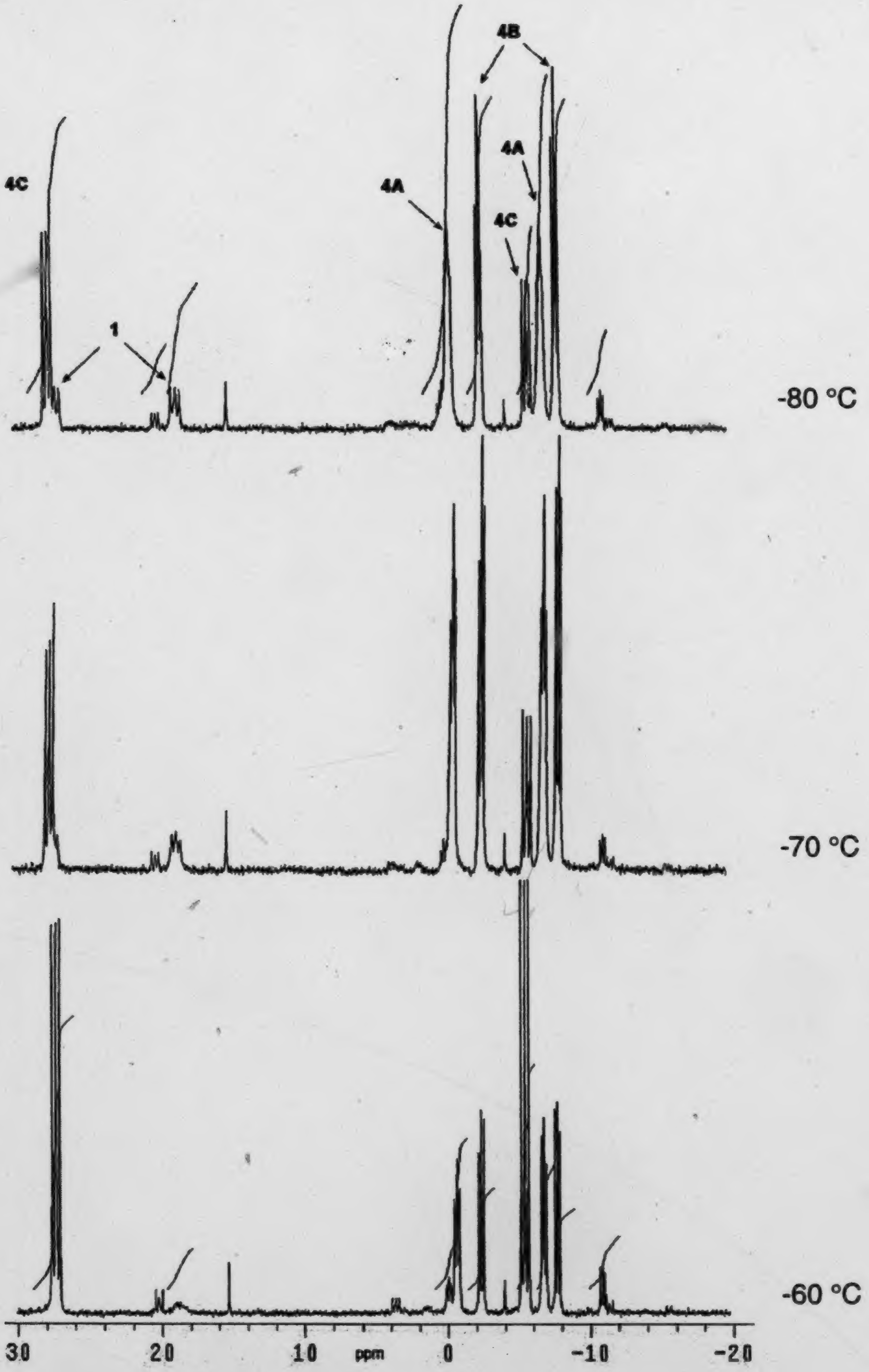

Figure 2.4.1. ^{31}P NMR spectra of the mixture of **1** and methylallene in CD_2Cl_2 from -80 °C to -60 °C.

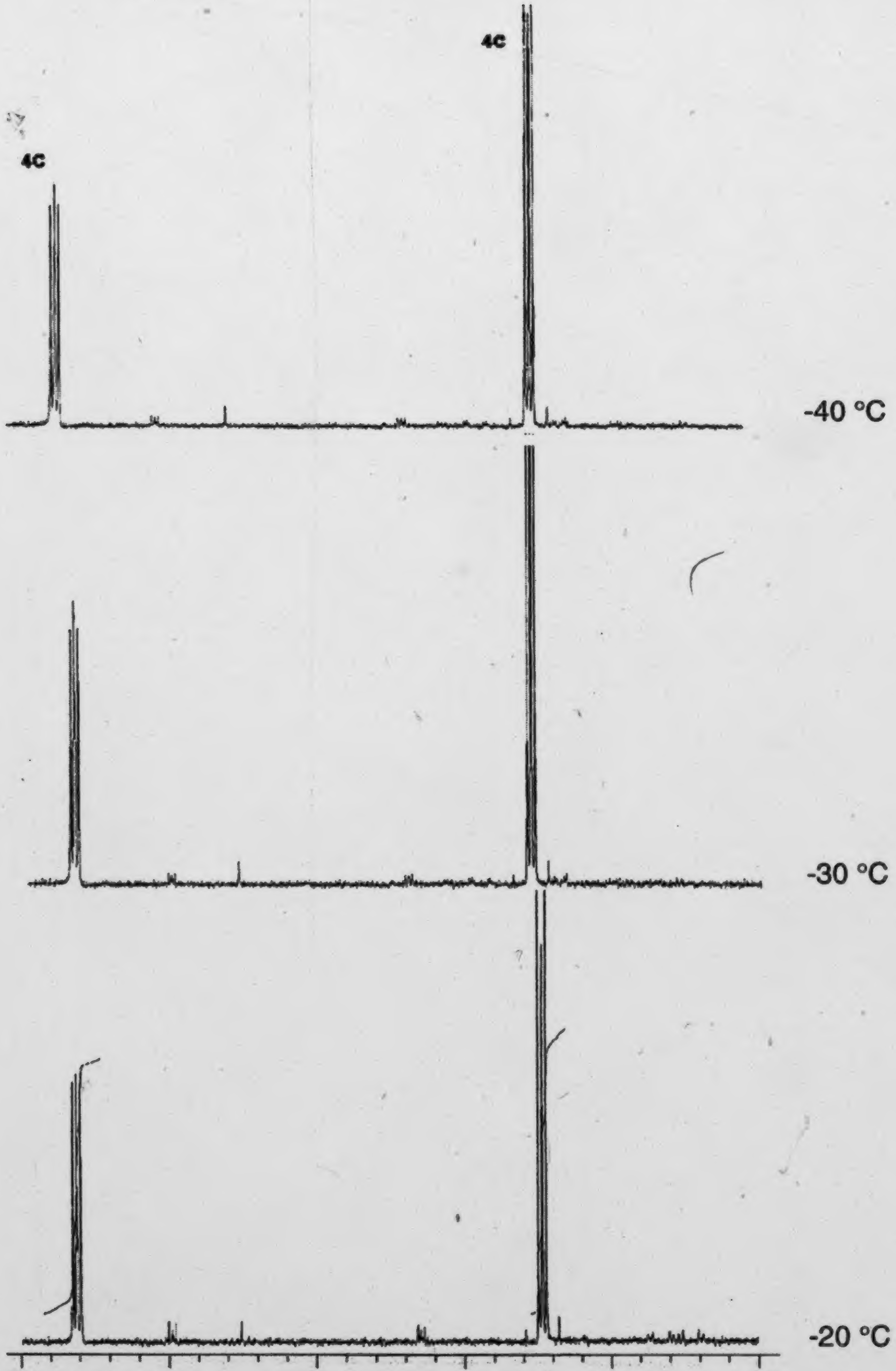

Figure 2.4.2. ^{31}P NMR spectra of the mixture of **1** and methylallene in CD_2Cl_2 from -40 °C to -20 °C.

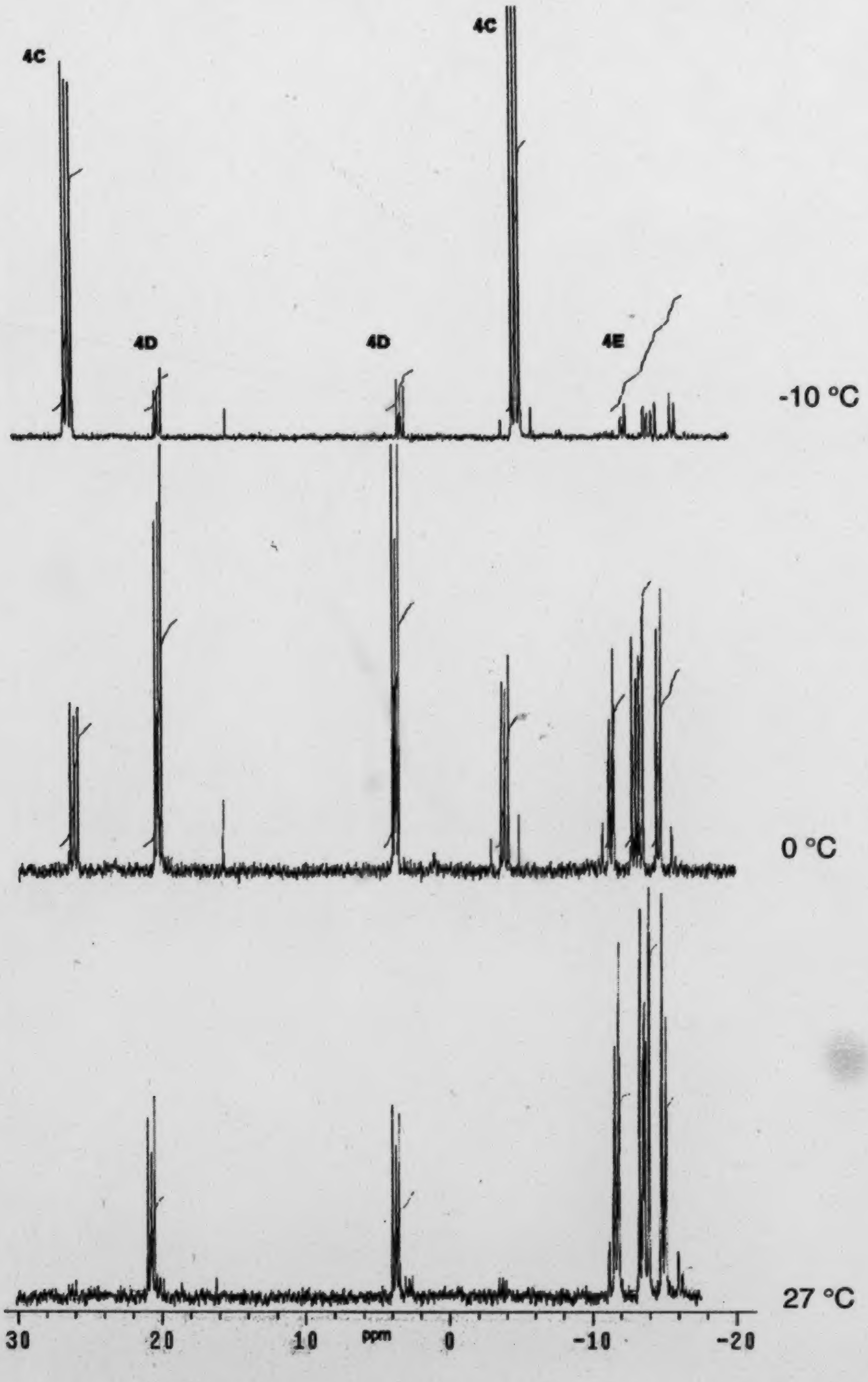

Figure 2.4.3. ^{31}P NMR spectra of the mixture of **1** and methylallene in CD_2Cl_2 from -10 °C to 27 °C.

overlapping resonances; however, the hydride region shows two hydrides as broad signals at -12.0 and -12.6 ppm, due to **4A** and **4B**. Also, the ^{13}C NMR spectrum shows two pairs of broad carbonyl resonances corresponding to **4A** and **4B**: the first pair at 189.9 and 176.5 ppm and the second at 189.5 and 175.9 ppm. It would appear that **4A** and **4B** are a pair of isomeric hydrides in which the iridium-methyl group has been intramolecularly activated upon methylallene coordination, as was observed with **3A** and **3B**.

As the sample is warmed to -60 °C the proportions of species changes, leaving **4C** is the major species in solution at this temperature. Compound **4A** has decreased in intensity relative to **4C** and has resolved into a pair of multiplets at this temperature. Peaks due to **4B** have also decreased in intensity at this temperature. Between -40 °C and -20 °C compound **4C** is the predominant species in solution, with only traces of other species being visible.

At -10 °C a new species, **4D**, appearing as an AA'BB' multiplet at 19.9 and 2.9 ppm is seen, as well as a complicated pattern centred at -14.4 ppm due to **4E**, $[Ir_2(CH_3)(CO)_2(\mu\text{-}\eta^1\text{-}\eta^3\text{-}H_2C{=}C{=}C(H)CH_3)(dppm)_2][CF_3SO_3]$.[4] Upon standing at 0 °C in the NMR tube, the proportion of **4E** increases and **4C** disappears. When a sample is warmed from -10°C to room temperature, **4D** disappears within 0.5 h, leaving only the final product **4E**.

The subsequent rearrangement to $[Ir_2(H)(CO)_2(\mu\text{-}\eta^1\text{-}\eta^3\text{-}HCC(Me)=CH_2)(dppm)_2][CF_3SO_3]$ (**4F**) occurs over a period of about a day in solution (see Scheme 2.2).[2,4]

Since the species **4C** is the dominant one in solution from -50 °C to -20 °C, a series of two-dimensional NMR studies was undertaken in this temperature range to shed light on its structure. In the one-dimensional ^1H NMR spectrum at -40 °C, **4C** displays a triplet corresponding to an iridium-bound methyl group at 0.23 ppm ($^3J_{P\text{-}H}$ = 6.6 Hz), a doublet at 1.76 ppm ($^3J_{H\text{-}H}$ = 3 Hz) due to the methyl group of the coordinated methylallene, a multiplet at 3.45 ppm due to the isochronous dppm methylenes, a singlet at 3.80 ppm due to the unique C-H proton of the methylallene ligand and a triplet at 2.07 ppm ($^3J_{P\text{-}H}$ = 11.4 Hz) due to the ligand $=CH_2$ group. Selective ^{31}P decoupling with observation of the ^1H NMR spectrum indicates that the $=CH_2$ group of the ligand is coupled to the phosphorus ligands at 27.6 ppm whereas the iridium-bound methyl group is coupled to the phosphorus ligands at -5.9 ppm. Also, the methylallene methyl group resonance at 1.76 ppm and the signal at 3.80 ppm become sharper and better resolved when the phosphorus resonating at -5.9 ppm is selectively irradiated, indicating that there is a small coupling from the methyl end of the methylallene ligand to these phosphorus nuclei. This suggests a structure in which methylallene is bridging the two iridium centres, with the methyl-substituted end oriented towards the iridium that bears a methyl group, as shown in Scheme 2.6. This formulation was confirmed by a ROESY experiment, in which NOE was observed between the hydrogen of the C-H at the methyl end and the iridium-bound methyl group, but *not* between the methylallene methyl and the iridium methyl group (the expected strong intra-ligand NOE between the C-H and methyl *was* observed). NOE was also seen between the $=CH_2$ group of methylallene and the dppm methylene resonance. The structure is proposed to be one in which the 1- and 2- carbons of the methylallene group bridge the two metal atoms forming a dimetallacyclobutane-like arrangement. Since the double bonds are cumulated, their filled π orbitals are mutually orthogonal and so both pairs cannot be simultaneously involved in bonding to the metals, if the major axis of the ligand is parallel to the iridium-iridium vector. In the bonding mode shown for **4C**, there are two possible orientations of the methyl group: one away from the iridium methyl (up) and the other towards the iridium methyl (down). On steric grounds the former arrangement should be favoured, and it is the structure we propose for **4C** based upon the NOE information.

This type of dimetallacyclobutane structure has previously been reported in the reaction of tetrafluoroethene with **1** to form $[Ir_2(CH_3)(CO)_2(\mu\text{-}C_2F_4)(dppm)_2][CF_3SO_3]$, the analogous tricarbonyl complex having been structurally characterized using X-ray

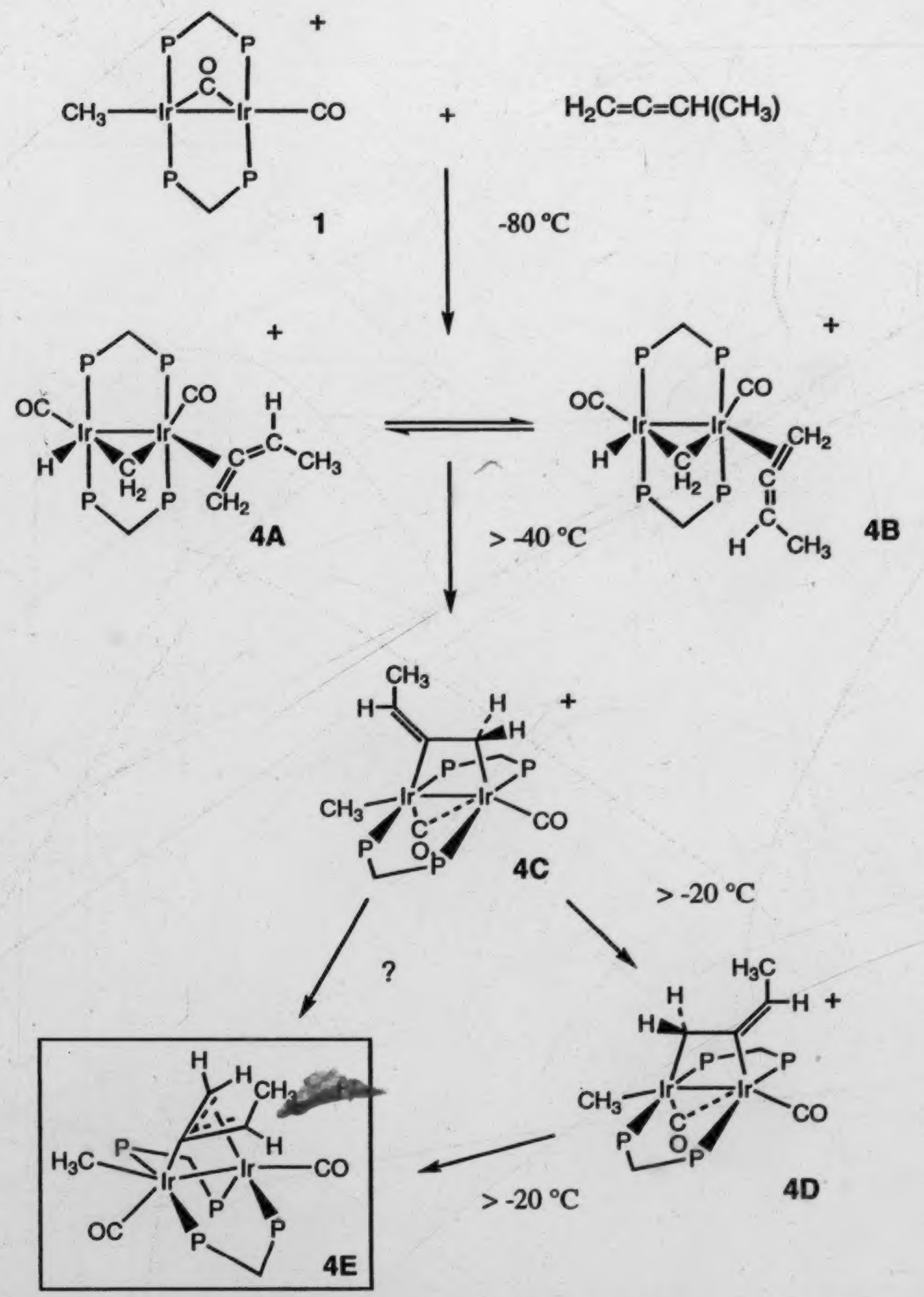
1
H₂C=C=CH(CH₃)
-80 °C
4A
4B
> -40 °C
4C
> -20 °C
?
4D
> -20 °C
4E

Scheme 2.6. Products of the reaction of methylallene with **1**. The species in the box has been previously characterized.[4]

crystallography.[2] Also, a weakly bound complex in which the tetrafluoroethene ligand is readily lost in the absence of excess olefin, $[Ir_2(H)_2(\mu\text{-}H)(\mu\text{-}C_2F_4)(dppm)_2][BF_4]$, has been reported.[6] As discussed in Chapter 3, dimetallacyclobutane products also form in solution from di- and trifluoroethenes at low temperature, but dissociate below room temperature.

The identity of **4D** is less easily ascertained, since at no temperature could it be obtained as the sole or even major species in solution. However, there is no hydride resonance apparent in the ^1H NMR spectrum, but there is an iridium-bound methyl group appearing as a triplet at 1.25 ppm in the ^1H NMR spectrum. Also, the methylallene ligand methyl group is a doublet at 0.95 ppm. Based upon the range of structural types we have seen for these complexes, it could be either a terminal-olefin complex like **3C** or **2B**, or a bridged species, isomeric with **4C**. Unfortunately, attempts at obtaining useful NOE information at temperatures at which **4D** was detected were frustrated by the presence of overlapping peaks in the NMR spectra and by the transformation of **4D** to **4E**, which also takes place in this temperature regime. The second conceivable isomer of a dimetallacyclobutane **(4C)** type has the methyl-end of the methylallene ligand oriented towards the iridium atom *not* bearing a methyl group. When the reaction mixture is maintained at 0 °C **4C** gradually disappears over 1-2 hours and the only species visible in the ^{31}P NMR spectrum at that point are **4D** and **4E**, with the ratio of **4E**:**4D** being approximately 2:1. At this temperature, **4D** also disappears slowly and is replaced, irreversibly, by **4E**. Warming a solution containing **4D** and **4E** to 27 °C results in the more rapid disappearance of **4D**, leaving only **4E** after *ca.* 30 min. This is similar to the situation for the allene reaction, in which the bridged complex **3D** converts to **3E**.

2.2.3. Reaction of 1,1-dimethylallene with $[Ir_2(CH_3)(CO)_2(dppm)_2][CF_3SO_3]$ (1).

At room temperature 1,1-dimethylallene forms a simple π adduct similar to that of ethene[2], and at low temperature it forms a C-H activated methylene hydride, $[Ir_2(H)(\mu\text{-}CH_2)(CO)_2(\eta^2\text{-}H_2C{=}C{=}CH(CH_3))(dppm)_2][CF_3SO_3]$ (**5A**), again paralleling the ethene adduct. Scheme 2.7 shows the products obtained from the reaction of 1,1-dimethylallene with **1**.

At -80 °C, only the methylene/hydride product **5A** is apparent in the ^{31}P NMR spectrum, as a pair of multiplets at 1.3 and -13.7 ppm, consistent with an AA'BB' spin system resulting from a trans arrangement of phosphines. The ^{13}C NMR spectrum of a ^{13}CO-enriched sample displays broad carbonyl resonances at 191.1 and 178.2 ppm. The proton NMR spectrum of **5A** shows broad signals at -12.1 ppm and 5.96 ppm, due to a hydride ligand and a bridging methylene group, respectively. The signals at 3.48 and 5.16 ppm are due to the dppm methylene protons, while the $=CH_2$ protons of the cumulene ligand resonate at 1.90 ppm.

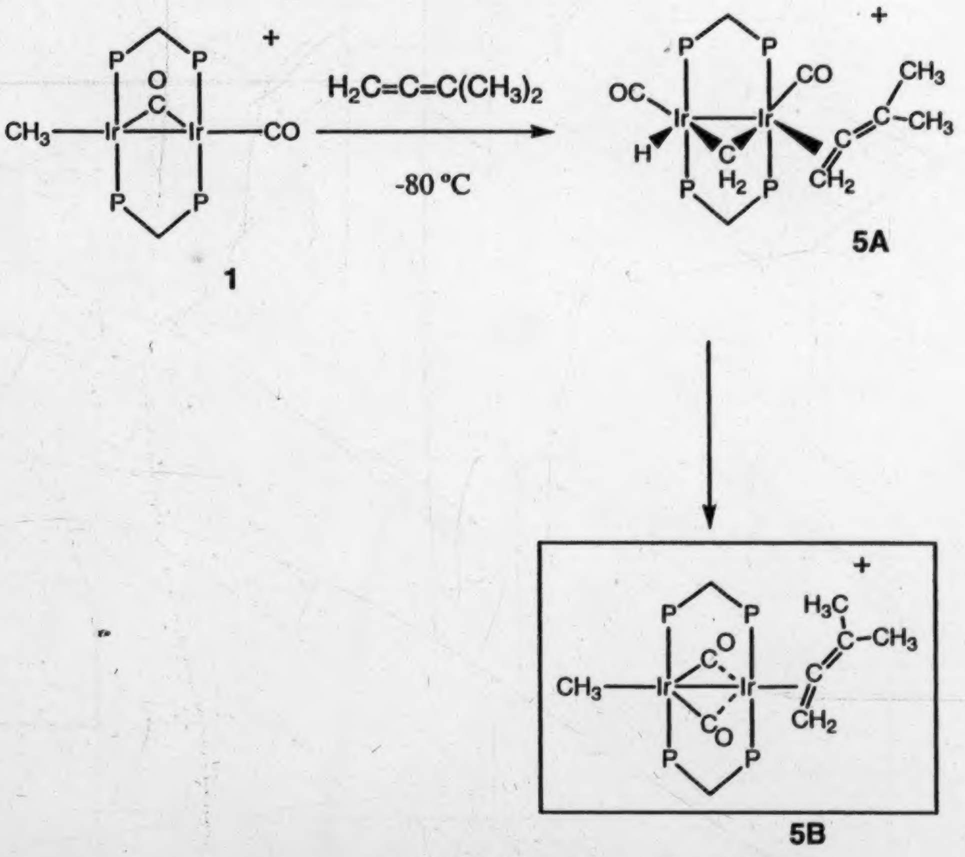

Scheme 2.7. Products obtained from the reaction of 1,1-dimethylallene with **1**. The species in the box has been previously characterized.[2]

Two distinct ligand methyl signals due to the cumulene ligand are seen at 1.13 and 0.19 ppm. This assignment was confirmed from the ROESY spectrum, wherein a strong NOE between the two methyls was observed. The large chemical shift difference between the two methyl signals points to markedly different chemical environments for each, suggesting that the methyl groups are at the end of the ligand *not* coordinated to the metal centre. Since the other double bond is orthogonal to the coordinated one, one of the methyl groups is *endo* with respect to the metal and the other is *exo*. This orientation is in accord with the steric requirements of the ligand, which would be expected to disfavour coordination at the dimethyl end.

No subsequent transformations of the 1,1-dimethylallene adduct **5B** is observed, setting it apart from the previous allene adducts.

2.3. Reactions of 1,3-dienes with $[Ir_2(CH_3)(CO)_2(dppm)_2][CF_3SO_3]$ (1)

We have attempted to observe intermediates in the unusual double oxidative addition of 1,3-butadiene to form $[Ir_2(CH_3)(H)(CO)(\mu\text{-}H)(\mu\text{-}CC(H)C(H)CH_2)(dppm)_2][CF_3SO_3]$ (**6B**) by carrying out the reaction at low temperature in an NMR tube. Between -95 °C and -50 °C in CD_2Cl_2 solution, the diolefin adduct $[Ir_2(CH_3)(CO)_2(\mu\text{-}\eta^2\text{:}\eta^2\text{-}H_2C{=}CH\text{-}CH{=}CH_2)(dppm)_2][CF_3SO_3]$ (**6A**) is observed in equilibrium with free 1,3-butadiene and **1**. The $^{31}P\{^1H\}$ spectrum, shown in Figure 2.5, indicates that all four phosphorus atoms of **6A** are chemically inequivalent, displaying a pattern characteristic of an ABCD spin system.

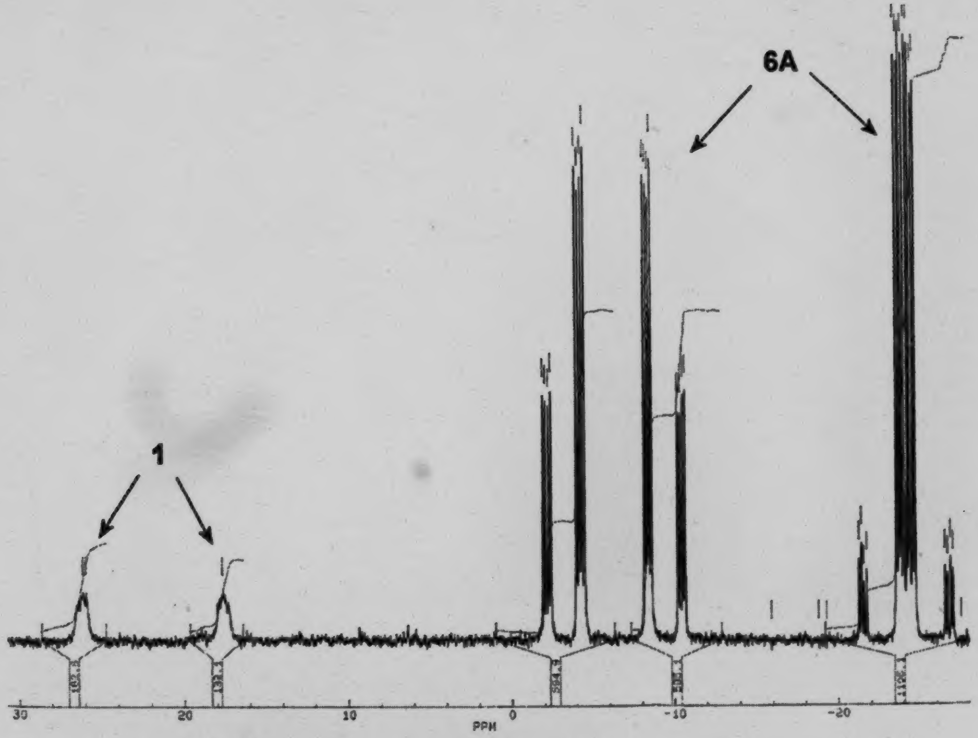

Figure 2.5. $^{31}P\{^1H\}$ spectrum of a mixture of $[Ir_2(CH_3)(CO)_2(\mu\text{-}\eta^2\text{:}\eta^2\text{-}H_2C\text{=}CH\text{-}CH\text{=}CH_2)(dppm)_2][CF_3SO_3]$ (**6A**) and **1** in CD_2Cl_2 at -55 °C.

Although the appropriate number of resonances for the coordinated 1,3-butadiene moiety is seen in the ^1H NMR spectrum, their unambiguous identification required a series of 2D NMR experiments (COSY, ROESY, and TOCSY), and selective ^{31}P decoupling of ^1H spectra. The ROESY spectrum established the placement of the butadiene moiety in an s-trans bridging fashion, since NOE's, as shown in Figure 2.6, could be seen as well as the intraligand NOE's expected for the s-trans arrangement. A portion of the ROESY spectrum is shown in Figure 2.7.

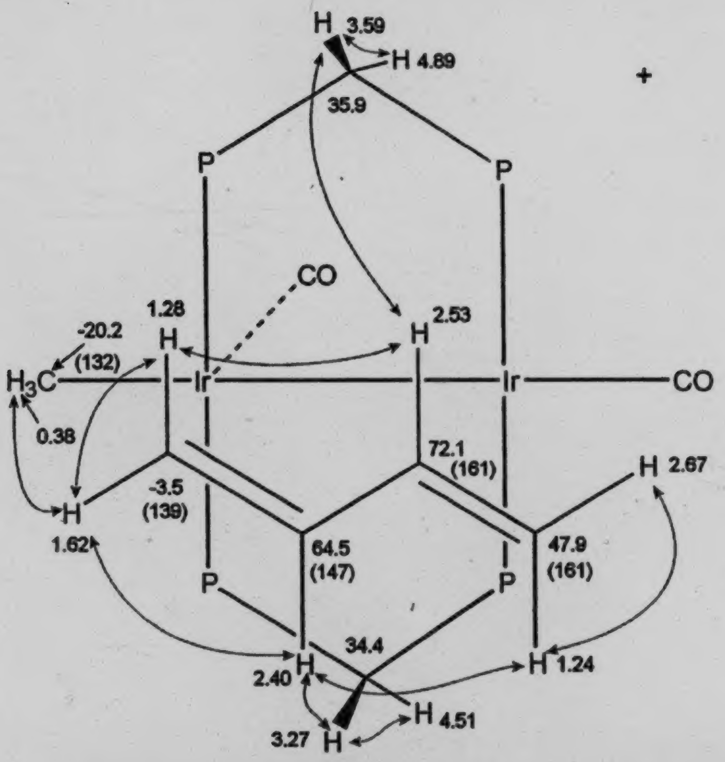
H 3.59
H 4.89
35.9
+
P
P
CO
1.28
H
2.53
H
-20.2
(132)
H3C
Ir
Ir
CO
0.38
72.1
(161)
H 2.67
-3.5
(139)
H
1.62
64.5
(147)
47.9
(161)
P
P
34.4
2.40 H
H 1.24
H 4.51
3.27 H

Figure 2.6. Schematic drawing of the complex cation of **6A** showing ^{1}H and ^{13}C chemical shifts in ppm. One-bond C-H coupling constants in Hz are shown in parentheses. NOE's are shown as double-headed arrows.

The orientation of the butadiene ligand was determined from the NOE between the proton at 1.62 ppm and the protons of the iridium-bound methyl group at 0.38 ppm. NOE was also observed between each of the 2- and 3- hydrogens and one hydrogen of each of the dppm methylene groups, consistent with the structure shown. The ^{13}C chemical shifts for three of the carbons of the ligand (between 47.9 and 72.1 ppm) and the C-H coupling constants involving the attached hydrogens (between 147 and 161 Hz) appear typical for a coordinated olefin;[11] however, the ^{13}C chemical shift for the carbon at the iridium-methyl end is at unusually high field (-3.50 ppm) and together with the associated C-H coupling constants ($^1J_{CH}$ = 139 Hz) suggests a substantial rehybridization of this carbon toward sp^3. This is consistent with this metal being more electron rich due to the electron donating properties of the methyl ligand.

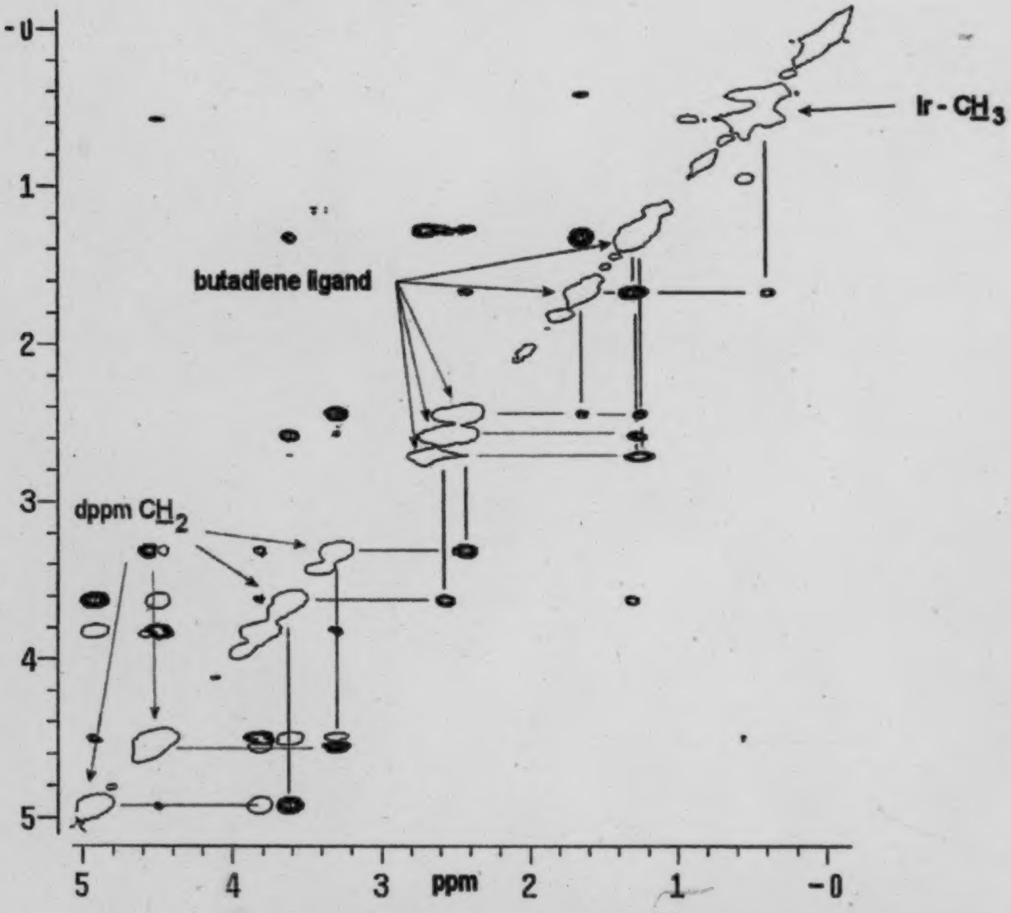

Figure 2.7. Portion of the ROESY spectrum of **6A** in CD_2Cl_2 at -55 °C. Positive peaks are shown as a single contour, negative peaks (due to NOE) are shown as multiple contours.

Exchange between 1,3-butadiene in solution and the complex (**6A**) was confirmed by the observation of an unsymmetrical off diagonal "stripe" in the TOCSY spectrum due to chemical exchange of the protons in coordinated 1,3-butadiene with those of the free 1,3-butadiene molecule.[8]

Several butadiene-bridged complexes have been reported[9, 10] including examples of s-trans-butadiene coordination[10] similar to that proposed for **6A**.

Discussion

Ethene, allene, methylallene and 1,1-dimethylallene form olefin adducts at low temperature in which a C-H bond of the iridium-bound methyl group has been cleaved to form a methylene hydride complex. This demonstrates an interesting example involving the transmission of electronic effects from one metal to the other, by which coordination of the substrate at one metal results in C-H bond activation of the methyl group at the *adjacent* metal. The geometry of these olefin adducts suggests that olefin attack occurs at the site between the methyl group and the bridging carbonyl of **1**, as shown in equation (2.1).

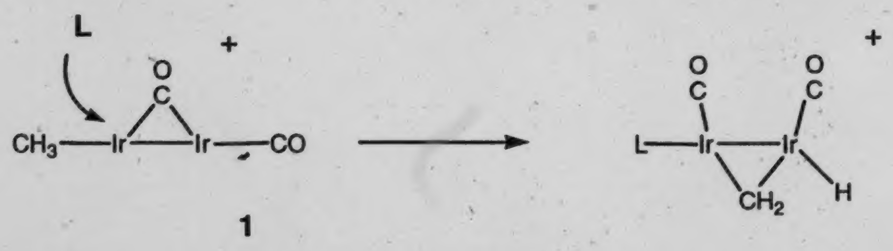

(2.1)

These methylene-hydride species undergo what can be viewed as an internal reductive elimination and subsequent rearrangement as the temperature is raised reforming the iridium-methyl group, a process which apparently is not reversible. The fact that cooling a sample does not reform the kinetic product shows that the stability of the iridium methyl complex is greater than that of the methylene hydride form.

Thus, the reaction of **1** with ethene forms the kinetic product **2A**, which can only be observed at temperatures below -60 °C. Above this temperature it is irreversibly replaced by **2B**, which is isolable at room temperature. Allene and methylallene also form C-H activated products at -80 °C, but in these cases there is a pair of products (**3A** + **3B**, and **4A** + **4B**, respectively) for each. Since either member of the pair is present in equal abundance, the energy difference between them is quite small, and their structures quite similar, as suggested by the spectroscopic parameters.

The pair of isomers observed for the allene adduct (**3A** and **3B**) can have only one origin, since all substituents (hydrogens) are the same. Thus the isomers differ based on whether the uncoordinated π bond is *syn* or *anti* to the bridging methylene group, as shown in Scheme 2.5. For methylallene, however, the isomers can have several origins. First, coordination to the metal could occur at the substituted or the unsubstituted π bond. We rule out this possibility since coordination by the more substituted olefinic linkage should be significantly less favoured and should give rise to substantially different populations of the isomers, in contrast to the equal populations observed. Otherwise, coordination *via* the unsubstituted π bond could give rise to isomers having an *exo* or *endo* orientation of the methyl substituent and the methylene group, as shown in Figure 2.8. Again *exo*-**4B** should be favoured and have a higher population. The equal populations of **4A** and **4B** suggest that the isomerism observed is a result of the rotation of the *exo* isomer about the Ir-olefin bond such that the uncoordinated π bond is on the same face of the Ir_2P_4 plane as the bridging methylene group or on the opposite face adjacent to the carbonyl, as shown in Scheme 2.6. On the basis of steric repulsions involving the methyl substituents and the methylene or carbonyl groups, there seems to be no obvious reason why only one isomer is observed for 1,1-dimethylallene. In this case, the lower stability of the second (unobserved) isomer may result from unfavourable interactions with the dppm phenyl groups.

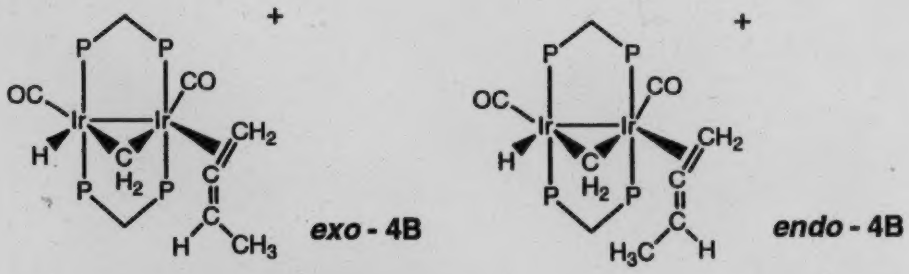

exo **- 4B**

endo **- 4B**

Figure 2.8. *Endo* and *exo* isomers of $[Ir_2(H)(CO)_2(syn\text{-}\eta^2\text{-}H_2C{=}C{=}CH(CH_3))(\mu\text{-}CH_2)(dppm)_2]$ $[CF_3SO_3]$ (**4B**)

Methylallene forms a bridged species, **4C**, but no isomer in which the methyl group is intact and the methylallene ligand is η^2-bound, corresponding to the allene adduct **3C**, could be detected. In contrast, ethene does not form a bridged species up to room temperature. 1,1-dimethylallene also does not form a bridged species like **4C** up to room temperature, presumably because of the extra steric crowding associated with the second methyl substituent. Placement of a ligand in the bridging position requires some degree of reorganization of the dppm ligands of the complex. In the equilibrium solution structure of **1**, phenyl groups surround an area of coordinative unsaturation (see Appendix). The phenyl groups must move out of the way for an incoming ligand to occupy this position. The barrier to the formation of the bridged complexes is due in part to this reorganization. In contrast, coordination of an olefin in the terminal position has a lower activation barrier, since this site is less crowded by the phenyls, and so these are the kinetic products. Since the steric crowding at the terminal position is less than that in the bridging position, the thermodynamic preference for the bridging position must be due to electronic factors. Useful here is a comparison of the preferred bonding modes of ethene with those of tetrafluoroethene. Tetrafluoroethene forms a stable diiridacyclobutane (bridging) structure whereas ethene prefers an η^2 structure at room temperature.[2,3] As will be seen in the Chapter 3 of this thesis, partially fluorinated ethenes form either bridged or terminal species in accordance with the metal-carbon bond strength predicted on the basis of the acceptor ability of the fluoroolefin. Hence, one might expect fluorinated cumulenes to lead to bridged species of greater stability than those of the parent allenes. However, 1,1-difluoroallene differs from allene in that the HOMO is localized at the $=CF_2$ end, whereas the LUMO is localized at the other end.[12] The regiochemistry of the product of the reaction of **1** with 1,1-difluoroallene would offer insight into the nature of the bonding interaction in these bridged complexes, however, this reaction has not yet been attempted.

The room-temperature products **3E** and **4E**, obtained from allene and methylallene, respectively, represent a small rearrangement from the complexes seen in solution just below room temperature. For this reason, and because the transformation of **3D** or **4D** into **3E** or **4E** is irreversible and occurs at the expense of the former, it would appear that the former compounds are intermediates in the formation of **3E** and **4E**. However, as shown in Scheme 2.6, the formation of **4E** from the bridged compound **4C** in which the methyl group of the methylallene ligand is in the up position on the same side as the iridium-methyl, would entail smaller nuclear motion than its formation from **4D**. From the ^{31}P NMR spectra in Figure 2.4.3 it can be seen that the formation of **4E** is coincident with that of **4D** and that at 27 °C only **4D** and **4E** are visible; moreover, as mentioned, **4E** is formed as **4D** disappears. Compounds **4C** and **4D** are kinetic products,

4D being more stable than **4C**. Compound **4E** is more stable than either **4C** or **4D**. A proposal to rationalize these observations and the apparent formation of **4E** from **4D** is shown in Scheme 2.8.

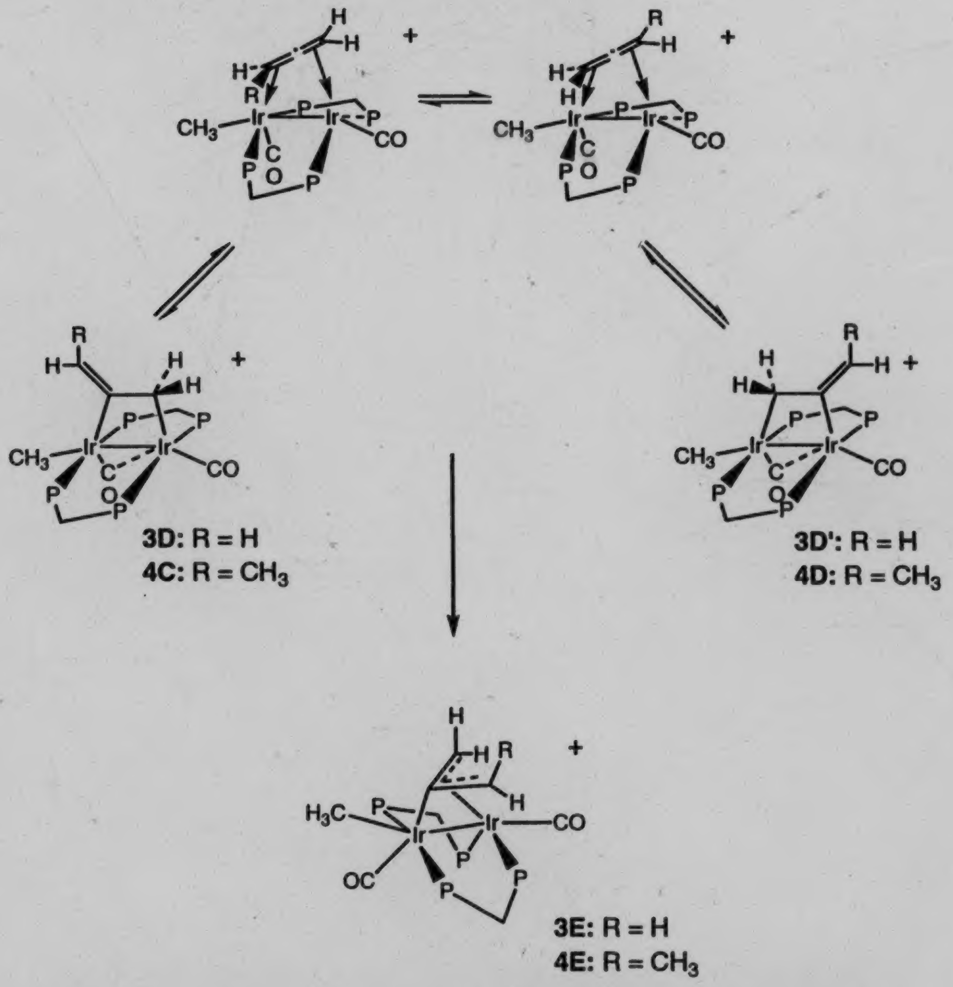

3D: R = H
4C: R = CH_3

3D': R = H
4D: R = CH_3

3E: R = H
4E: R = CH_3

Scheme 2.8. Isomerization of μ-η^2-bridging allenyl complexes and conversion to η^1-η^3 allenyl bridged complexes. The two possible isomers of $[Ir_2(CH_3)(\mu\text{-}H_2C{=}C{=}CH_2)(CO)_2(dppm)_2]^+$ are shown as **3D** and **3D'**.

In the proposed mechanism the first bridged form, **3D** or **4C**, is in equilibrium with a bridged η^2:η^2 allenyl complex which is also in equilibrium with the second kinetic bridged form, **3D'** or **4D**, respectively. For methylallene, the isomer **4C** predominates at lower temperature, but as the mixture is warmed the activation barrier to the formation of **4D** is overcome. The isomer **4D** predominates at higher temperature since it is slightly more stable, possibly because of less steric interference with the iridium-bound methyl group. At temperatures sufficiently high for this equilibrium to be established, the allenyl bridged complexes **3E** or **4E** also form, directly from the $\eta^2:\eta^2$ intermediate. The equilibrium concentration of the $\eta^2:\eta^2$ complex is small (in fact, it is not observed in the ^{31}P NMR spectra) because it is less stable than the other species due to the cis/cis arrangement of the dppm ligands, which is necessary to allow both of the cumulated double bonds to be coordinated to the metals simultaneously.

The conversion to the ultimate vinyl carbene products **3F** and **4F** may occur via a direct coupling of the iridium-bound methyl group and the central carbon of the bridging allenyl ligand, as shown in Scheme 2.9 for the reaction involving allene. Earlier results in our group showed that when compound **1** with a ^{13}C labeled methyl group was employed in the reaction with allene, the label was incorporated into three positions as shown in Scheme 2.9.[2] In our proposal, one of the C-H bonds of the iridium-bound methyl group is cleaved either concurrently with or after migration to the central allyl carbon. This forms an η^4 trimethylenemethane intermediate which can then undergo a 1,3-

sigmatropic shift, as shown by the curved arrows in Scheme 2.9, to form the vinyl carbene product **3F**. Rotation of the trimethylenemethane moiety[13] allows the label to be incorporated in all three positions as previously observed.

In contrast to the other olefins studied, for 1,3-butadiene, an η^2 complex was not observed, nor was a methylene hydride species detected. The only π adduct observed had each π bond coordinated to a different metal, in an s-trans geometry as shown in Scheme 2.6. The related substrate, 2-methyl-1,3-butadiene did not form any complex with **1** under the conditions studied (down to -95 °C). Cis- and trans-1,3-pentadiene, where the methyl is at one end of the ligand, formed much weaker complexes than the parent 1,3-butadiene, presumably due to the increased steric repulsions involving the bridging site. Thus, adding even a single methyl substituent had a substantial effect on olefin binding.

Although the direct transformation of the 1,3-butadiene adduct **6A** to the vinylvinylidene product **6B** could not be observed, since **6A** is only detectable at low temperatures, at which C-H activation of the butadiene ligand does not occur, we propose that **6A** is an intermediate in the formation of **6B**. We suggest that C-H activation occurs stepwise, with the first activation occurring at the iridium having the methyl group attached.

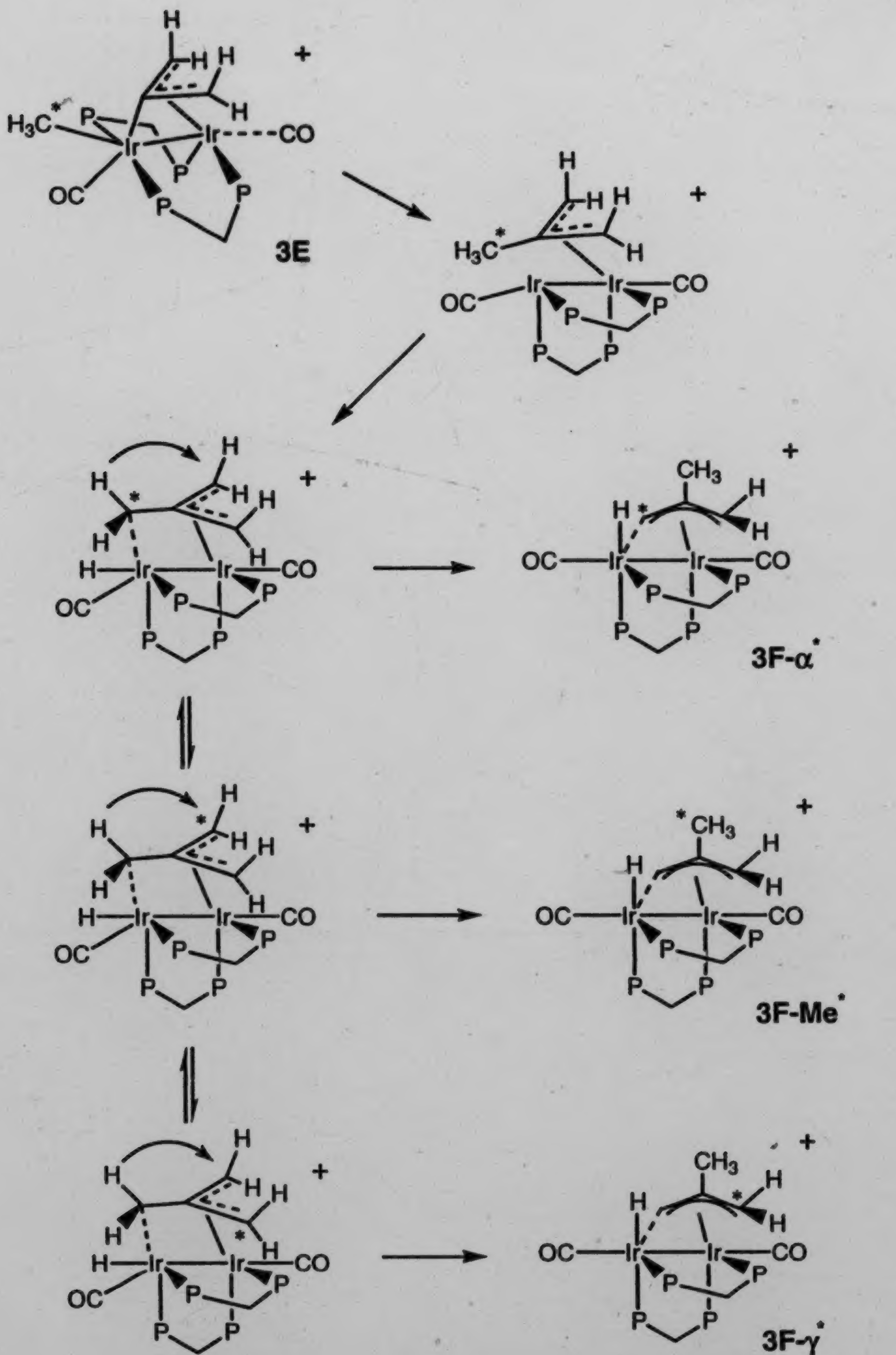
3E
3F-α*
3F-Me*
3F-γ*
H₃C*
Ir
P
OC
CO
CH₃
*CH₃
H
+

Scheme 2.9. Formation of the vinyl carbene **3F** product from the allenyl bridged complex **3E** via a trimethylenemethane intermediate. Curved arrows indicate 1,3-sigmatropic shifts.

This metal should be more electron-rich and more susceptible to oxidative addition owing to the donor properties of the methyl ligand; moreover, the adjacent metal should be less prone to oxidative addition because of its positive charge. These suggestions are consistent with the proposed rehybridization noted earlier for the carbon at the iridium-methyl end (as evidenced by the upfield chemical shift of 3.5 ppm), indicating greater back-donation to this end of the diolefin. Although structure **6A** has a carbonyl on each metal, carbonyl transfer might accompany C-H activation from one metal to the other, generating the requisite unsaturation. Oxidative addition of the first C-H bond would yield a vinyl hydride as shown in structure *(a)* of Scheme 2.11 (dppm ligands, perpendicular to the plane of the drawing, are not shown). Activation of a single terminal vinylic C-H bond of 1,3-butadiene by a binuclear species to give a bridging butadienyl moiety has been observed previously.[14] Inversion of the "$Ir_2(\mu\text{-}H)$" core, as diagrammed, is common[15] and would yield a species such as *(b)* in which the hydride ligand is now on the opposite face of the Ir_2P_4 plane from the resulting hydrocarbyl fragment, as observed in the structure of the final product **6B**. This "hydride inversion" brings the vinyl group into proximity with the adjacent metal, leading to activation of the second C-H bond to give **6B**.

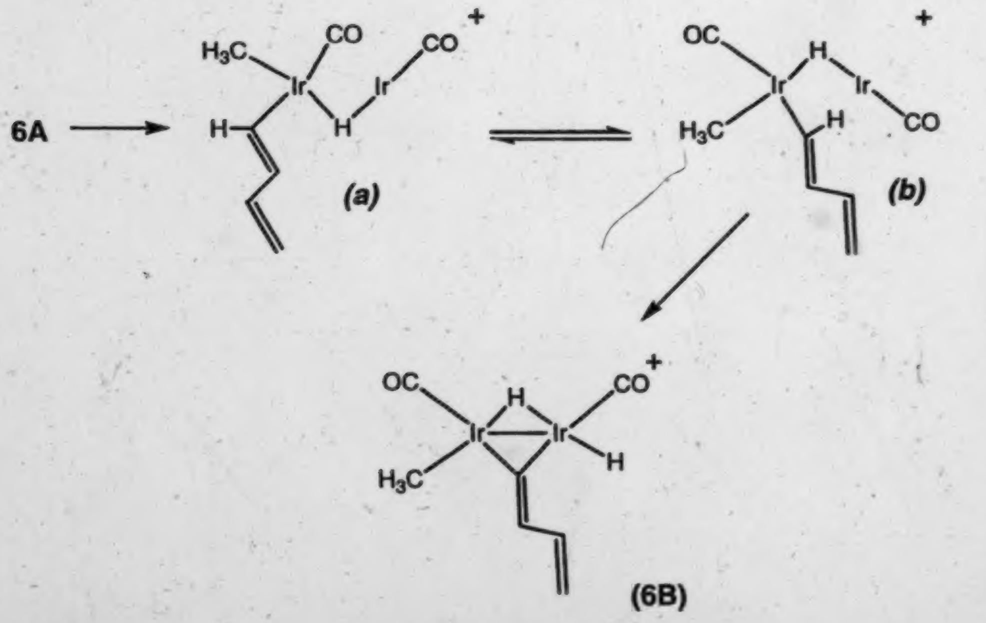

Scheme 2.10. Proposed route for the double olefinic C-H activation of **6A** to form **6B**.

Support for our proposal that precoordination of butadiene at both metals precedes the double C-H activation comes from attempted reactions of **1** with other 1,3-dienes. Therefore, compound **1** in the presence of 2-methyl-1,3-butadiene or either cis- or trans- 1,3-pentadiene results in no reaction after several days at ambient temperature or after 24 h in refluxing CH_2Cl_2 or THF. The failure of the pentadiene compounds to give a C-H activation product strongly suggests that coordination of both olefin functionalities is required; otherwise substitution at one end of the butadiene unit would not be expected to inhibit C-H activation at the other end. Additional support that prior coordination of both π bonds of butadiene facilitates the C-H activation observed comes from the reaction with ethene, which does not give olefin C-H activation products, yielding only the π complex, **2B**.[5]

Conclusions

In these systems the simple π-complex, without activation of the iridium-bound methyl group, is more stable than the methylene hydride species that results from methyl C-H activation. This suggests the possibility that other bimetallic methylene hydride complexes of this type might undergo a corresponding internal C-H reductive elimination if the temperature were raised. Also, taking into account the reactions of fluoroolefins discussed in Chapter 3, it would appear that more electron withdrawing ligands prefer the bridging site, if the steric demands are not too great.

Finally, we have shown that the same steric effects that preclude bridged complex formation also block the formation of olefinic C-H activation products, and we have argued that prior coordination of both olefin double bonds is required for this reaction to proceed.

References and Footnotes

1. A portion of the work reported in this Chapter has been previously published: Ristic-Petrovic, D.; Torkelson, J. R.; Hilts, R. W.; McDonald, R.; Cowie, M. *Organometallics* **2000**, *19*, 4432.
2. Torkelson, J. R. Ph. D. Thesis, University of Alberta, 1998.
3. Torkelson, J.R.; Antwi-Nsiah, F.H.; McDonald, R.; Cowie, M.; J.G. Prius, J.G.; Jalkanen, K.J.; DeKock, R.L. *J. Am. Chem. Soc.* **1999**, *121*, 3666.
4. Torkelson, J. R.; McDonald, R.; Cowie, M. *J. Am. Chem. Soc.* **1998**, *120*, 4047.
5. Antwi-Nsiah, F. H.; Cowie, M. *Organometallics* **1992**, *11*, 3157.
6. Antwi-Nsiah, F.; Torkelson, J. R.; Cowie, M. *Inorg. Chim. Acta.* **1997**, *259*, 213.
7. Spetseris, N.; Norton, J. R.; Hunter, D. R. *Organometallics* **1995**, *14*, 603.
8. Nakashima, T. T.; McClung, R. E. D.; Kotovych, G. *J. Magn. Reson.* **1998**, *133*, 222.
9. (a) King, J. A.; Vollhardt, K. P. C. *Organometallics* **1983**, *2*, 684.
   (b) Fryzuk, M. D.; Piers, W. E.; Rettig, S. J. *J. Am. Chem. Soc.* **1985**, *107*, 8259.
   (c) Kaneko, Y.; Suzuki, T.; Isobe, K. *Organometallics* **1995**, *17*, 996.

10. (a) Adam, V. C.; Jarvis, J. A. J.; Kilboum, B. T.; Owston, P. G. *Chem. Commun.* **1971**, 467.

    (b) Sasse, Von H. E.; Ziegler, M. L. Z. *Anorg. Allg. Chem.* **1972**, *392*, 167.

    (c) Tachikawa, M.; Shapley, J. R.; Haltimanger, R. C.; Pierpont, C. G. *J. Am. Chem. Soc.* **1976**, *98*, 4651.

    (d) Pierpont, C. G. *Inorg. Chem.* **1975**, *17*, 1976.

    (e) Franzreb, K.-H.; Kreiter, C. G. *Z. Naturforsch.* **1952**, *37B*, 1058.

11. Mann, B. E. *Adv. Organometal. Chem.* **1974**, *12*, 135.

12. a) Lentz, D.; Willemsen, S. *Organometallics* **1999**, *18*, 3962.

    b) Dixon, D. A.; Mart, B. E. *J. Phys. Chem.* **1989**, *93*, 7772.

13.. Russell P. Hughes, David S. Tucker, Arnold L. Rheingold; *Organometallics;* **1993**; *12*, 3069-3074.

14. Fryzuk, M. D.; Jones, T.; Einstein, F. W. B. *Chem. Commun.* **1984**, 1556.

15. Antonelli, D. M.; Cowie, M. *Inorg. Chem.* **1990**, *17*, 2553, and references therein.

Chapter 3

Reactions of $[Ir_2(CH_3)(CO)_2(dppm)_2][CF_3SO_3]$ with fluoroethenes

Introduction

In the previous chapter of this thesis, the reactions of $[Ir_2(CH_3)(CO)(\mu\text{-}CO)(dppm)_2][CF_3SO_3]$ (**1**) with a variety of olefins were explored. A central conclusion of that study was that olefins may form complexes with **1** in which they are coordinated in a terminal, η^2 position or in a bridging fashion, depending on the nature of the olefin and the temperature. We have proposed that the subsequent C-H activation reaction of 1,3-butadiene proceeds via such a bridged species as an intermediate.[1]

A recent study in this group found that tetrafluoroethene forms a stable bridged complex[2] as shown in Scheme 3.1. This is in contrast to ethene which forms an η^2 complex.[3] This difference in reactivity between ethene and tetrafluoroethene led us to wonder how the electronic nature of the olefin, i.e. the presence of electron-withdrawing fluorines, influenced the coordination mode of the olefin in binuclear dppm-bridged complexes such as **1**. We have therefore investigated the low temperature reactions of a series of partially fluorinated ethenes with **1**, to determine the olefin coordination modes and how they are related to those of ethene or tetrafluoroethene.

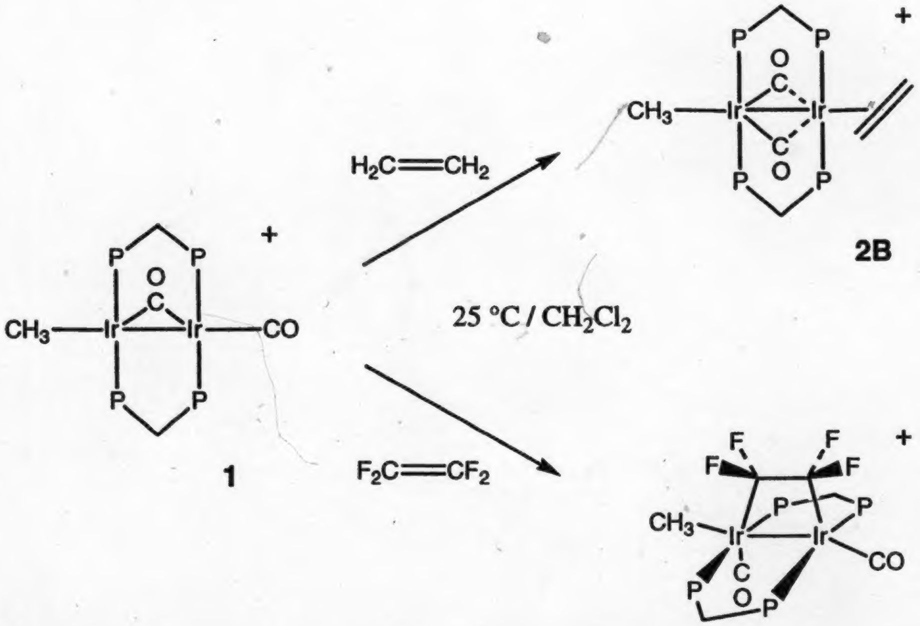

Scheme 3.1. Comparison of bonding modes of tetrafluoroethene[2] and ethene.[3]

Experimental

General Comments. All solvents were dried (using appropriate drying agents), distilled before use and stored under dinitrogen. Deuterated solvents used for NMR experiments were freeze-pump-thaw degassed (three cycles) and stored under nitrogen or argon over molecular sieves. Reactions were carried out under argon using standard Schlenk techniques, and compounds that were used as solids were purified by recrystallization. Prepurified argon and nitrogen were purchased from Linde, carbon-13 enriched CO (99%) was supplied by Isotec Inc, certain fluoroolefins (fluoroethene, Z-1,2-difluoroethene, and 1,1-difluoroethene) were supplied by Lancaster; trifluoroethene was supplied by PCR or prepared by a literature method[4]. All purchased gases were used as received. All other reagents were obtained from Aldrich and were used as received (unless otherwise stated). The compound $[Ir_2(CH_3)(CO)(\mu\text{-}CO)(dppm)_2][CF_3SO_3]$ (**1**) was prepared as previously reported.[5]

Proton NMR spectra were recorded on Varian Unity 400, 500 or 600 spectrometers, or on a Bruker AM400 spectrometer. Carbon-13 NMR spectra were recorded on Varian Unity 400 or Bruker AM300 spectrometers. Phosphorus and fluorine spectra were recorded on Varian Unity 400 or Bruker AM400 spectrometers. Two-dimensional NMR experiments (COSY, ROESY and TOCSY) were obtained on Varian Unity 400 or 500 spectrometers.

Preparation of Compounds

Low temperature reaction of 1 with fluoroethene, Z-1,2-difluoroethene, and 1,1-difluoroethene. In a typical experiment, between 1 and 5 equiv. of the gaseous fluoroolefin was added slowly by means of a gas-tight syringe to a solution of 30 mg (0.022 mmol) of **1** in 0.7 mL of CD_2Cl_2 or acetone-d^6 in an NMR tube at -78 °C in a solid CO_2/acetone bath. NMR spectra (^1H, ^{31}P and ^{19}F) were recorded from -80 °C to ambient temperature at 10 °C intervals. The results of these studies are summarized in Table 3.1. In the reaction of **1** with fluoroethene

Table 3.1. NMR data[a, b] for reactions of **1** with fluoroolefins

fluoroolefin	Product[c]	$\delta(^{31}P\{^1H\})$[d]	$\delta(^1H)$[e, f]	$\delta(^{13}C)$[e]	$\delta(^{19}F)$[g]	free olefin $\delta(^{19}F)$[g]
fluoroethene	$[Ir_2(CH_3)(CO)_2(\eta^2\text{-}CHF{=}CH_2)(dppm)_2]^+$ (**7**)	18.8 (m), 6.1 (m)	3.50 (b, 2H), 3.10 (b, 1H), 3.00 (b, 1H), 2.2 (b, 1H), 1.13 (t, 3H, $^3J_{P\text{-}C}$ = 8.5 Hz), 0.96 (b, 2H)	208.3 (b), 209.8 (b)	-79.1 (s), -172.1 (b)	-116.7 (m)
Z-1,2-difluoroethene	$[Ir_2(CH_3)(CO)_2(\eta^2\text{-}CHF{=}CHF)(dppm)_2]^+$ (**8**)	17.2 (m), 2.6 (m)	1.18 (t, $^3J_{PH}$ = 9.0 Hz)	207.4 (b)	-79.1 (s), -211.6 (b)	-164.4 (m)
1,1-difluoroethene	$[Ir_2(H)(\mu\text{-}CH_2)(CO)_2(\eta^2\text{-}CF_2{=}CH_2)(dppm)_2]^+$ (**9A**)	-2.8 (m), -4.3 (m)	5.37 (b, 2H), 5.11 (b, 2H), 3.28 (b, 2H), 0.08 (b, 2H), -12.4 (b, 1H)	191.3 (b)	-79.4 (s), -80.4 (b)	-82.2 (m)
	$[Ir_2(CH_3)(CO)_2(\eta^2\text{-}CH_2{=}CF_2)(dppm)_2]^+$ (**9B**)	16.1 (m), 6.4 (m)	3.80 (m, 2H), 3.02 (m, 2H), 1.15 (t, 3H, $^3J_{PH}$ = 8.8 Hz), 0.37 (m, 2H)	210.7 (b), 202.3 (b)	-79.4 (s), -83.7 (b)	
	$[Ir_2(CH_3)(CO)_2(\mu\text{-}CH_2{=}CF_2)(dppm)_2]^+$ (**9C**)	16.1 (m), 5.9 (m)	4.44 (m, 2H), 3.60 (m, 2H), 2.47 (m, 2H), 0.18 t, $^3J_{PH}$ = 4.8 Hz)	196.6 (b), 185.6 (b)[h]	-79.4 (s), -45.8 (m)	
trifluoroethene	$[Ir_2(CH_3)(CO)_2(\mu\text{-}CHF{=}CF_2)(dppm)_2]^+$ (**10**)	14.9 (m), 5.1 (m)	3.97 (m, 1H), 3.92 (m, 2H), 3.56(m, 1H), 0.36 (t, 3H, $^3J_{PH}$ = 6.0 Hz)	196.9 (t, J = 8.6 Hz), 184.5 (b)[h]	-79.4 (s), -52.6 (d, $^2J_{FF}$ = 253 Hz), -81.6 (d, $^2J_{FF}$ = 253 Hz), -193.8 (b)	-100.0 (m), -125.9 (m), -205.0 (m)

Notes: [a] NMR abbreviations: s = singlet, d = doublet, t = triplet, q = quintet, m = multiplet, b = broad. [b] NMR data in CD_2Cl_2 unless otherwise stated. [c] The anion in all cases is trifluoromethanesulfonate. [d] $^{31}P\{^1H\}$ chemical shifts are referenced vs. external 85% H_3PO_4

Table 3.1 NMR data[a, b] for reactions of **1** with fluoroolefins, continued.

Notes: (continued) [e] ^1H and ^{13}C chemical shifts are referenced vs. external TMS. [f] Chemical shifts for the phenyl hydrogens are not given in the ^1H data. [g] ^{19}F chemical shifts are referenced vs. external $CFCl_3$. [h] Recorded in acetone-d^6.

only a single product, $[Ir_2(CH_3)(CO)_2(\eta^2\text{-}CHF{=}CH_2)(dppm)_2][CF_3SO_3]$ (**7**), was observed by NMR from -80 °C to -50 °C, whereupon it decomposed to **1** and free fluoroethene. Similarly, Z-1,2-difluoroethene gave a single, thermally unstable product in solution, $[Ir_2(CH_3)(CO)_2(\eta^2\text{-}CHF{=}CHF)(dppm)_2][CF_3SO_3]$ (**8**), which decomposed in a similar manner as **7** above -40 °C. The compound 1,1-difluoroethene formed three different thermally unstable products, starting with $[Ir_2(H)(\mu\text{-}CH_2)(CO)_2(\eta^2\text{-}CF_2{=}CH_2)(dppm)_2][CF_3SO_3]$ (**9A**) observed from -80 °C to -40 °C. From -80 °C to 0 °C $[Ir_2(CH_3)(CO)_2(\eta^2\text{-}CH_2{=}CF_2)(dppm)_2][CF_3SO_3]$ (**9B**) is present in solution. Above -20 °C there is slow conversion (*ca.* 50% in 18 h at -20 °C) to a third species $[Ir_2(CH_3)(CO)_2(\mu\text{-}CH_2{=}CF_2)(dppm)_2][CF_3SO_3]$ (**9C**) which decomposes above 0 °C.

Reaction of trifluoroethene with 1. In a typical experiment 2 equiv. of trifluoroethene was added slowly by means of a gas-tight syringe to a solution of 30 mg (0.022 mmol) of **1** in 0.7 mL of CD_2Cl_2 or acetone-d^6 in an NMR tube at -78 °C, causing a gradual colour change from red to orange. NMR spectra (^1H, ^{31}P and ^{19}F) were recorded from -80 °C to ambient temperature at 10 °C intervals, showing the presence of $[Ir_2(CH_3)(CO)_2(\mu\text{-}CHF{=}CF_2)(dppm)_2][CF_3SO_3]$ (**10**), which persisted in solution up to room temperature, but decomposed to unidentified products over a period of several hours. In one instance, the compound $[Ir_2CH_3(H)(CO)_2(\mu\text{-}X)(\mu\text{-}C{=}CF_2)(dppm)_2][CF_3SO_3]$ (**11**), X = F or OH (see Discussion section) was obtained as orange crystals when an acetone-d^6 solution was layered with diethyl ether. Experimental details of the X-ray structural determination carried out on **11** are contained in Table 3.2. Numerous attempts to duplicate the reaction leading to **11** all met with failure; only unidentified mixtures of decomposition products were obtained. Compound **11** was prepared using our last commercial sample of trifluoroethene. Our inability to obtain further samples of trifluoroethene commercially necessitated that the gas be prepared by us using a literature preparation.[4] All subsequent reactions involving this reagent relied on samples being prepared in-house. Owing to our inability to duplicate our original observations, we considered the possibility that the presence of limonene as an inhibitor in the original commercial sample may have affected the outcome of the reaction with **1**, but found that limonene added to our prepared trifluoroethene had no salutary effect on the outcome. We also attempted the reaction in other solvents (toluene, acetonitrile, methanol and benzene) to no avail.

Results

3.1. Reaction of fluoroethene with $[Ir_2(CH_3)(CO)_2(dppm)_2][CF_3SO_3]$ (1).

Addition of a threefold excess of fluoroethene to a CD_2Cl_2 solution of $[Ir_2(CH_3)(CO)_2(dppm)_2][CF_3SO_3]$ (**1**) in an NMR tube at -80 °C gives *ca.* 90% conversion to $[Ir_2(CH_3)(CO)_2(\eta^2\text{-}CH_2{=}CHF)(dppm)_2][CF_3SO_3]$ (**7**). As the sample is warmed from -80 °C the amount of adduct decreases until above -50 °C none

Table 3.2. Crystallographic Experimental Details.

A. Crystal Data	
compound	$[Ir_2(H)(CO)_2(Me)(\mu\text{–}F)(\mu\text{–}C{=}CF_2)\text{-}(dppm)_2][CF_3SO_3]\bullet 0.4CH_2Cl_2$
formula	$C_{56.4}H_{48.8}Cl_{0.8}F_6Ir_2O_5P_4S$
formula weight	1489.25
crystal dimensions (mm)	0.22 × 0.19 × 0.13
crystal system	triclinic
space group	$P\bar{1}$ (No. 2)
unit cell parameters[a]	
a (Å)	12.3421 (7)
b (Å)	21.7915 (12)
c (Å)	23.1391 (12)
α (deg)	73.5466 (15)
β (deg)	79.5885 (11)
γ (deg)	89.4378 (12)
V (Å^3)	5864.6 (6)
Z	4
ρ_{calcd} (g cm^{-3})	1.687
μ (mm^{-1})	4.779
B. Data Collection and Refinement Conditions	
diffractometer	Bruker P4/RA/SMART 1000 CCD[b]
radiation (λ [Å])	graphite-monochromated Mo Kα (0.71073)
temperature (°C)	–80
scan type	ϕ rotations (0.3°) / ω scans (0.3°) (30 s exposures)
data collection 2θ limit (deg)	52.88
total data collected	30565 ($-14 \le h \le 15$, $-16 \le k \le 27$, $-28 \le l \le 28$)
independent reflections	23781 ($R_{int} = 0.0321$)
number of observed reflections (*NO*)	13089 [$F_o^2 \ge 2\sigma(F_o^2)$]
structure solution method	Patterson search/structure expansion (*DIRDIF–96*[c])
refinement method	full-matrix least-squares on F^2 (*SHELXL–93*[d])
absorption correction method	Gaussian integration (face-indexed)
range of transmission factors	0.5755–0.4195
data/restraints/parameters	23781 [$F_o^2 \ge -3\sigma(F_o^2)$] / 21[e] / 1317
goodness-of-fit (S)[f]	0.996 [$F_o^2 \ge -3\sigma(F_o^2)$]

Table 3.2. continued

final R indices[g]	
R_1 [$F_o^2 \ge 2\sigma(F_o^2)$]	0.0751
wR_2 [$F_o^2 \ge -3\sigma(F_o^2)$]	0.2357
largest difference peak and hole	3.320 and –2.491 e Å^{-3}

[a] Obtained from least-squares refinement of 8192 centered reflections.

[b] Programs for diffractometer operation, data collection, data reduction and absorption correction were those supplied by Bruker.

[c] Beurskens, P. T.; Beurskens, G.; Bosman, W. P.; de Gelder, R.; Garcia Granda, S.; Gould, R. O.; Israel, R.; Smits, J. M. M. (1996). The *DIRDIF-96* program system. Crystallography Laboratory, University of Nijmegen, The Netherlands.

[d] Sheldrick, G. M. *SHELXL-93*. Program for crystal structure determination. University of Göttingen, Germany, 1993. Refinement on F_o^2 for all reflections (all of these having $F_o^2 \ge -3\sigma(F_o^2)$). Weighted R-factors wR_2 and all goodnesses of fit S are based on F_o^2; conventional R-factors R_1 are based on F_o, with F_o set to zero for negative F_o^2. The observed criterion of $F_o^2 > 2\sigma(F_o^2)$ is used only for calculating R_1, and is not relevant to the choice of reflections for refinement. R-factors based on F_o^2 are statistically about twice as large as those based on F_o, and R-factors based on ALL data will be even larger.

[e] The Ir(1)–H(1) distances in both independent [$Ir_2(H)(CO)_2(Me)(\mu\text{–}F)(\mu\text{–}C{=}CF_2)(dppm)_2]^+$ units were fixed at 1.75 Å. Furthermore, to enforce an idealized geometry upon one of the triflate ions, the following distance restraints were employed: d(S(2)–C(92)) = 1.80 Å; d(S(2)–O(94)) = d(S(2)–O(95)) = d(S(2)–O(96)) = 1.45 Å; d(F(94)–C(92)) = d(F(95)–C(92)) = d(F(96)–C(92)) = 1.45 Å; d(F(94)···F(95)) = d(F(94)···F(96)) = d(F(95)···F(96)) = 2.20 Å; d(O(94)···O(95)) = d(O(94)···O(96)) = d(O(95)···O(96)) = 2.37 Å; d(F(94)···O(95)) = d(F(94)···O(96)) = d(F(95)···O(94)) = d(F(95)···O(96)) = d(F(96)···O(94)) = d(F(96)···O(95)) = 3.04 Å.

[f] $S = [\Sigma w(F_o^2 - F_c^2)^2/(n - p)]^{1/2}$ (n = number of data; p = number of parameters varied; $w = [\sigma^2(F_o^2) + (0.1309P)^2]^{-1}$ where $P = [\mathrm{Max}(F_o^2, 0) + 2F_c^2]/3$).

[g] $R_1 = \Sigma||F_o| - |F_c||/\Sigma|F_o|$; $wR_2 = [\Sigma w(F_o^2 - F_c^2)^2/\Sigma w(F_o^4)]^{1/2}$.

is observed. The complex **7** appears in the $^{31}P\{^{1}H\}$ NMR spectrum as two equal intensity multiplets at 18.8 and 6.1 ppm, with the higher field multiplet having a more complex appearance, suggesting that it is due to two inequivalent phosphorus nuclei, while the lower field multiplet is due to two almost equivalent phosphorus nuclei. Overall, the pattern is characteristic of an ABCD spin system, where the nuclei A and B are in similar environments, so that the AB part appears at 18.8 ppm, whereas the C and D nuclei are in slightly different environments and the CD part is a complex multiplet centred at 6.1 ppm.

Exchange between free and coordinated fluoroethene was demonstrated by a 500 MHz ^{1}H-TOCSY experiment at -60 °C which showed exchange of the methylene end of free fluoroethene (4.78 and 4.52 ppm) and the broad peak at 0.96 ppm due to the coordinated ligand. In comparison, the protons of the ethylene ligand in $[Ir_2(CH_3)(CO)_2(\eta^2\text{-}C_2H_4)(dppm)_2][CF_3SO_3]$ appear as a triplet at 1.16 ppm at room temperature.[3] A very broad resonance at *ca.* 2.2 ppm is assigned to the vinylic proton, geminal to fluorine, in the complex **7**. The dppm methylene protons are also broad and appear at 3.50 (2H), 3.10 (1H) and 3.00 (1H) ppm. The iridium-bound methyl appears as a triplet at 1.13 ppm ($^{3}J_{PH}$ = 8.5 Hz), with equal coupling to two adjacent phosphorus nuclei and is shifted downfield from the 0.58 ppm seen for unreacted **1**. Coordination of fluoroethene, shown in Scheme 3.2, does not induce activation of the iridium-bound methyl group at the temperatures studied since it apparently remains intact. The exchange of the fluoroethene ligand is consistent with it remaining intact upon

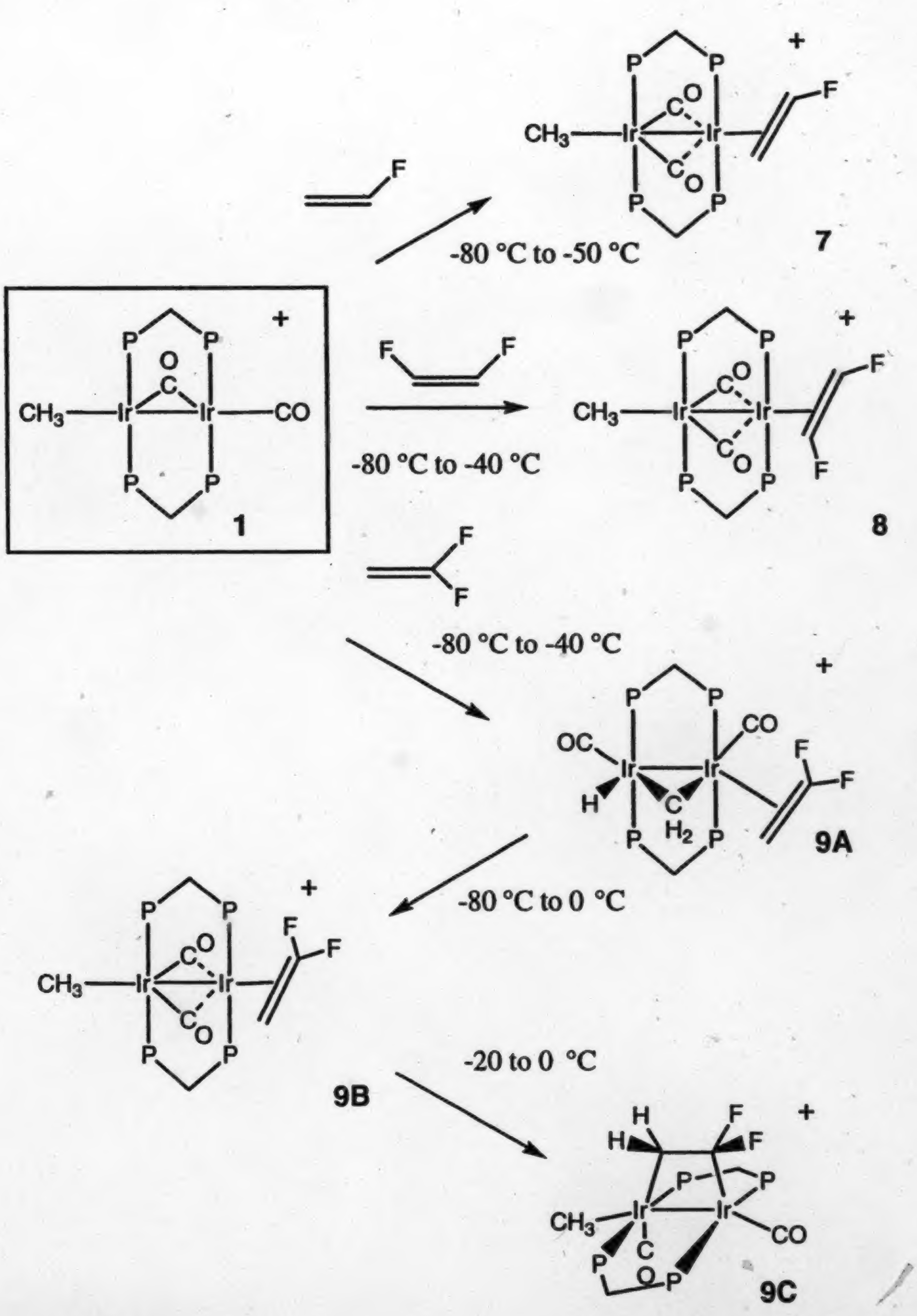

-80 °C to -50 °C
7
1
-80 °C to -40 °C
8
-80 °C to -40 °C
9A
-80 °C to 0 °C
9B
-20 to 0 °C
9C

Scheme 3.2. Reactions of mono- and di- fluoroolefins with $[Ir_2(CH_3)(CO)_2(dppm)_2][CF_3SO_3]$ (**1**), in CD_2Cl_2. Temperatures quoted indicate the range over which the compound was observed by ^{31}P NMR spectroscopy. For the compounds **9A** and **9C** only one of the two possible orientations of the fluoroolefin ligand is shown. Phenyl groups of the dppm ligands have been omitted for clarity.

coordination, but the possibility of reversible C-H or C-F activation cannot be ruled out on this basis. However, the absence of a metal hydride signal does militate against appreciable amounts of C-H activated products. The $^{13}C\{^{1}H\}$ spectrum of a ^{13}CO-enriched sample of **7** shows two broad carbonyl resonances at 209.8 and 208.3 ppm, comparable to the chemical shift of the carbonyls in $[Ir_2(CH_3)(CO)_2(\eta^2\text{-}C_2H_4)(dppm)_2][CF_3SO_3]$ (**2B**), which appears at 204.0 ppm.[3] These resonances are at somewhat lower field than is normally observed for terminally bound carbonyls in late transition metal dppm-bridged bimetallic complexes, and at higher field than is usual for bridged carbonyls, suggesting a possible semi-bridging interaction.[3, 5] The ^{19}F NMR spectrum shows an upfield shift for the coordinated ligand, from -116.4 ppm to -172.1 ppm (broad) in the complex **7**.

3.2. Reaction of Z-1,2-difluoroethene with $[Ir_2(CH_3)(CO)_2(dppm)_2][CF_3SO_3]$ (1).

The compound Z-1,2-difluoroethene binds reversibly to **1** forming the adduct $[Ir_2(CH_3)(CO)_2(\eta^2\text{-}Z\text{-}CHF{=}CHF)(dppm)_2][CF_3SO_3]$ (**8**), visible in the ^{31}P NMR spectrum between -80 °C and -40 °C. At the lower temperature there is only about 60 % conversion when five equivalents of olefin are employed. By -40 °C conversion to the adduct is reduced to about 20%, and above this temperature it is not seen.

The $^{31}P\{^1H\}$ NMR spectrum of **8** shows a pair of complex multiplets at 17.2 and 2.6 ppm, consistent with an ABCD spin system due to four chemically inequivalent phosphorus nuclei. The ^1H NMR spectrum shows the methyl resonance as a triplet at 1.18 ppm ($^3J_{PH}$ = 9.0 Hz), indicating that it is terminally bound to one metal. Unfortunately, it is not possible to assign the remaining resonances in this spectrum because of the poor quality of the spectra resulting from the presence of a large excess of the free olefin, impurities in the olefin and exchange broadening. The ^{13}C NMR spectrum shows a single broad peak at 207.4 ppm, consistent with the proposed structure shown in Scheme 3.2. The ^{19}F NMR spectrum shows a single broad peak at -211.6 ppm due to the two equivalent fluorine nuclei in the η^2 complex. In a bridged complex, two inequivalent fluorines would have been expected owing to the inequivalence of the metals (one has a methyl ligand); furthermore, a single ^{13}CO resonance, again corresponding to a pair of chemically equivalent semi-bridging carbonyls would not have been observed. The NMR spectral parameters of the η^2 adducts **7** and **8** resemble those of the ethene adduct $[Ir_2(CH_3)(CO)_2(\eta^2\text{-}C_2H_4)(dppm)_2][CF_3SO_3]$ (**2B**).

3.3. Reaction of 1,1-difluoroethene with $[Ir_2(CH_3)(CO)_2(dppm)_2][CF_3SO_3]$ (1)

When a large (> 5 eq.) excess of 1,1-difluoroethene is passed through a solution of **1** at -78 °C, the ^{31}P NMR spectrum typically shows approximately 44 % of unreacted **1**, 15 % of **9A**, 30 % of **9B** and 13 % of several uncharacterized species.

The adduct $[Ir_2(H)(\mu\text{-}CH_2)(CO)_2(\eta^2\text{-}CF_2{=}CH_2)(dppm)_2][CF_3SO_3]$ (**9A**), in which the iridium-bound methyl of the starting complex **1** has undergone intramolecular C-H activation to form a hydride and a methylene ligand bridging the two metals, is characterized in the $^{31}P\{^1H\}$ NMR spectrum by equal intensity resonances at -2.8 and -4.3 ppm which are broad with some multiplet structure visible. The proton NMR spectrum displays a broad hydride signal at -12.4 ppm, and a broad resonance at 5.37 ppm, integrating for 2H (relative to the hydride) due to the bridging methylene group. Warming the solution from -80 °C to -40 °C causes both resonances to disappear, being replaced by the methyl signal of **9B** (*vide infra*) as **9A** transforms into **9B**. The dppm methylene protons of **9A** appear as broad peaks at 5.11 and 3.28 ppm with some partially resolved coupling to the ^{31}P nuclei, while the methylene group of the coordinated 1,1-difluoroethene appears as a broad resonance at 0.08 ppm, displaying the upfield shift expected of the protons of a coordinated olefin.[7] Only a tentative assignment of the ^{13}C NMR spectrum could be made because of the difficulty encountered in producing sufficient quantities of **9A** in solution, and the presence of other products. Only a single very broad carbonyl resonance at 191.3 ppm could be attributed to **9A**, whereas a pair of resonances would normally be expected, unless the carbonyl carbons were accidentally isochronous. In the ^{19}F NMR spectrum a single broad peak is observed at -80.4 ppm, shifted only slightly downfield form the free olefin at -82.2 ppm.

The observed NMR spectral features are consistent with either rapid exchange of the *syn* and *anti* isomers of the 1,1-difluoroethene ligand (shown in Figure 3.1), or with only one isomer being present. Presumably, the *anti* isomer would be favoured on steric grounds; moreover, the repulsive effect of the fluorine lone pairs on the bridging methylene moiety may enhance this effect, decreasing the population of the *syn* isomer.

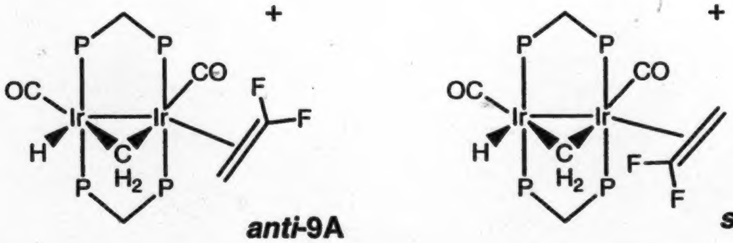

***anti*-9A** ***syn*-9A**

Figure 3.1. Orientations of the 1,1-difluoroethene ligand in **9A**.

The complex $[Ir_2(CH_3)(CO)_2(\eta^2\text{-}CF_2{=}CH_2)(dppm)_2]^+$ (**9B**) is characterized by equal intensity multiplets at 16.1 and 6.4 ppm in the $^{31}P\{^1H\}$ NMR spectrum, consistent with an AA'BB' spin system. Because **9B** predominates in solution at -30 °C, detailed NMR studies of this species were carried out at this temperature. Compared to $[Ir_2(CH_3)(CO)_2(\eta^2\text{-}CH_2{=}CHF)(dppm)_2][CF_3SO_3]$ (**7**), the dppm methylene resonances at 3.80 and 3.28 ppm in the ^1H NMR spectrum of $[Ir_2(CH_3)(CO)_2(\eta^2\text{-}CF_2{=}CH_2)(dppm)_2][CF_3SO_3]$ (**9B**) are sharper, and the difluoroethene methylene signal in the complex shows resolved coupling (this signal is a broad envelope for the fluoroethene complex, **7**). The methylene signal of the difluoroethene ligand is a virtual quintet at 0.37 ppm in the ^{1}H NMR spectrum, and collapses to a triplet ($^3J_{HF}$ = 9.2 Hz) upon broadband ^{31}P decoupling, indicating that this group is coupled approximately equally to two phosphorus nuclei, and also to two equivalent fluorines of the difluoromethylene group. The iridium-bound methyl group appears as a triplet at 0.37 ppm, with a coupling of 8.8 Hz to two equivalent phosphorus nuclei. In the ^{19}F NMR spectrum, the difluoromethylene resonance appears as a broad peak at -83.7 ppm. Decoupling experiments (^{31}P or ^{1}H decoupling) did not succeed in resolving this resonance into a multiplet. The ^{13}C NMR spectrum of a ^{13}CO-enriched ample reveals two inequivalent, semi-bridging carbonyls at 210.7 and 202.3 ppm.

Warming the sample to -40 °C results in a decrease in the amount of **9A** present, such that **9B** is the predominant species in solution, and at -30 °C the conversion to **9B** is essentially complete. Warming above this temperature results in its diminution until by 10 °C only starting material is observed. When a solution containing **9B** is maintained at *ca.* -20 °C overnight there is approximately 50 % conversion to a third species, $[Ir_2(CH_3)(CO)_2(\mu\text{-}CF_2{=}CH_2)(dppm)_2][CF_3SO_3]$ (**9C**).

The final species in the transformation, **9C**, appears in the ^{31}P NMR spectrum as multiplets at 16.1 ppm and 5.9 ppm; the lower field multiplet is coincident with the lower field multiplet of compound **9B**. As **9C** forms, the integral ratio of the 16.1 ppm multiplet to the sum of the 5.9 ppm and 6.4 ppm resonances remains constant, indicating that this low field resonance is due to both compounds. The ^{1}H NMR spectrum shows dppm methylenes for **9C** at 4.44 and 3.60 ppm, the difluoroethene methylene resonance as a multiplet at 2.47 ppm and the intact iridium-bound methyl group as a triplet at 0.18 ppm, with a 4.8 Hz coupling to two equivalent phosphorus nuclei. The olefinic methylene resonance at 2.47 ppm simplifies to a triplet (J = 20 Hz) upon broadband ^{31}P irradiation, and this coupling is also found in the resonance for the difluoromethylene group in the ^{19}F{^{31}P} spectrum which appears as a triplet at -45.8 ppm with 20 Hz coupling. The olefinic methylene resonance appears at somewhat lower field than that in the η^2-coordinated complexes **9A** and **9B** where it appears at 0.08 ppm and 0.37 ppm, respectively, and is consistent with the proposed dimetallacyclobutane formulation. The ^{13}C NMR spectrum of a ^{13}CO-enriched sample shows two inequivalent terminal carbonyls at 196.6 ppm and 185.6 ppm.

The olefinic fluorine signals are shifted downfield in the ^{19}F NMR spectrum by 36.4 ppm from the free olefin, comparable to the coordination shift displayed in the formation of the tetrafluoroethene-bridged complex $[Ir_2(CH_3)(CO)_2(\mu\text{-}C_2F_4)(dppm)_2]^+$ where the reported shift averages 52.5 ppm downfield.[2]

3.4. Reaction of trifluoroethene with $[Ir_2(CH_3)(CO)_2(dppm)_2][CF_3SO_3]$ (1).

Trifluoroethene reacts with **1** at -80 °C forming $[Ir_2(CH_3)(CO)_2(\mu\text{-}CHF{=}CF_2)(dppm)_2][CF_3SO_3]$ (**10**), as shown in Scheme 3.3. The ^{19}F NMR spectrum shows three broad signals, at -52.6, -81.6 and -193.8 ppm, all of which are shifted to low field from the free ligand, the corresponding resonances of which appear at -100.0, -125.9 and -205.0 ppm, respectively. The two lower field resonances show mutual coupling of 253 Hz, which is consistent with an sp^3 hybridized $-CF_2$ group.[8] Coupling to the high-field fluorine at -193.8 ppm is not discernible. The broadness of the peaks in the ^{19}F NMR spectrum is not due to unresolved coupling to phosphorus, as revealed by the failure of the resonances to sharpen upon broadband ^{31}P decoupling.

All three fluorine nuclei of trifluoroethene have moved to lower field upon complexation, the geminal fluorines having moved the furthest. The average coordination shift is 45.9 ppm for these nuclei and is consistent with rehybridization towards sp^3 for the carbon bearing two fluorines, due to substantial back donation from the metals. This shift is similar to that observed for the analogous tetrafluoroethene complex.[2] As noted, the coordination shift of the remaining fluorine, while not as pronounced, is also downfield.

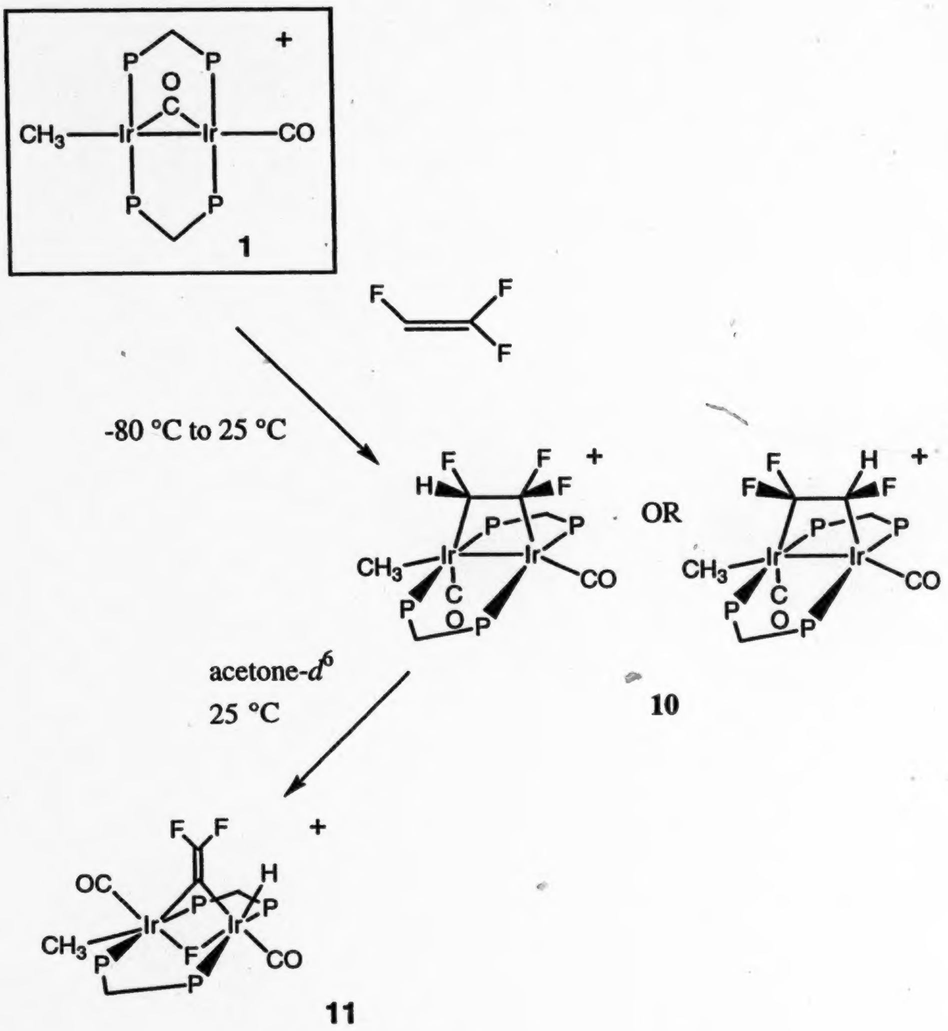

Scheme 3.3. Reactions of trifluoroethene with $[Ir_2(CH_3)(CO)_2(dppm)_2][CF_3SO_3]$ (**1**), in CD_2Cl_2. Phenyl groups of the dppm ligands have been omitted for clarity.

The $^{31}P\{^1H\}$ NMR spectrum reveals the presence of a pair of complex multiplets at 14.9 ppm and 5.1 ppm, consistent with four inequivalent phosphorus nuclei. The ^1H NMR spectrum shows the dppm protons as multiplets at 3.97 (1H), 3.92 (2H) and 3.56 (1H) ppm, while the iridium-bound methyl appears as a triplet at

0.36 ppm ($^3J_{PH}$ = 6.0 Hz), indicating that there is a single terminally-bound methyl, the protons of which couple approximately equally to a pair of phosphorus nuclei. We were unable to locate the single vinylic proton of the coordinated trifluoroethene moiety, perhaps because of exchange broadening. The ^{13}C NMR spectrum of a ^{13}CO-enriched sample of **10** shows two inequivalent terminal carbonyl resonances at 196.9 and 184.5 ppm, which are very similar to the terminal carbonyls of the 1,1-difluoroethene bridged compound **9C** (196.6 and 185.6 ppm).

The product **10** persists in CD_2Cl_2 solution upon warming to room temperature, but decomposes after several hours to a mixture of unidentified products. In one trial that we were subsequently unable to reproduce, we obtained a limited quantity of orange crystals by slow diffusion of Et_2O into the acetone-d^6 reaction mixture, and these have been identified as $[Ir_2CH_3(H)(CO)_2(\mu\text{-}X)(\mu\text{-}C{=}CF_2)(dppm)_2][CF_3SO_3]$ (**11**) , X = F or OH, based on an X-ray structural determination. While the crystals were not of ideal quality the structure refined reasonably well (although the hydrogen atoms could not be located). A representation of **11** is shown in Figure 3.2 and important bond lengths and angles are found in Table 3.3. The structure is best described as a difluorovinylidene-bridged A-frame, with an additional bridging ligand on the other face of the complex. In Figure 3.2 this second bridge is represented as a fluoride, but because of the poor quality of the data set cannot be unequivocally identified as such, and could also be a bridging hydroxide formed by hydrolysis by adventitious moisture. Facile ionization of iridium-fluoride bonds has been reported[9] and may account for such hydrolysis. The hydride ligand was not located and is shown in an idealized position. Unfortunately, the limited amount of sample did not allow the necessary spectroscopy to be carried out and an inability to reproduce the reaction did not allow follow-up investigations.

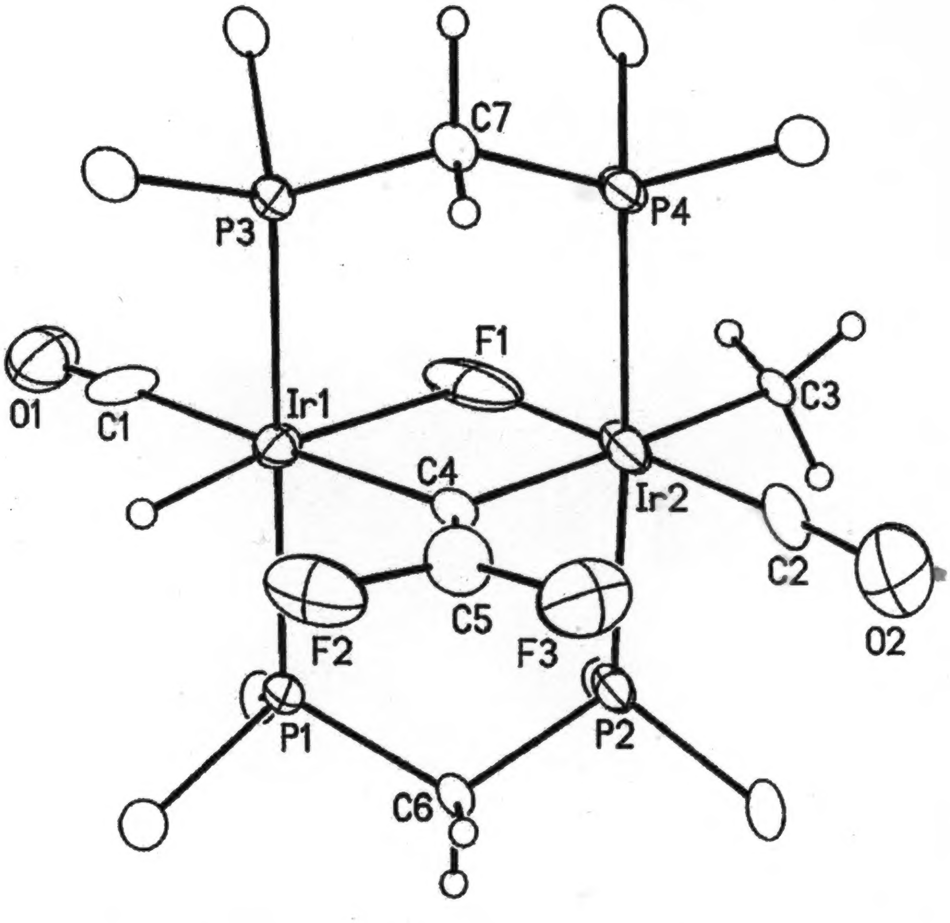

Figure 3.2. Representation of the X-ray structure of the cation of **11**. The bridging group has been tentatively labeled as F1. Only the ipso carbons of the phenyl groups of dppm are shown.

Table 3.3. Selected Interatomic Distances (Å) and Angles (deg).

(a) Distances (Å)

(i) Molecule A			*(ii) Molecule B*		
Atom1	**Atom2**	**Distance**	**Atom1**	**Atom2**	**Distance**
Ir(1)	P(1)	2.344(3)	Ir(1)	P(1)	2.350(3)
Ir(1)	P(3)	2.341(3)	Ir(1)	P(3)	2.343(3)
Ir(1)	F(1)	2.280(11)	Ir(1)	F(1)	2.285(10)
Ir(1)	C(1)	1.881(19)	Ir(1)	C(1)	1.908(14)
Ir(1)	C(4)	2.048(14)	Ir(1)	C(4)	2.084(12)
Ir(1)	H(1)	1.75†	Ir(1)	H(1)	1.75†
Ir(2)	P(2)	2.358(3)	Ir(2)	P(2)	2.356(3)
Ir(2)	P(4)	2.366(3)	Ir(2)	P(4)	2.371(3)
Ir(2)	F(1)	1.86(2)	Ir(2)	F(1)	1.902(15)
Ir(2)	C(2)	1.94(2)	Ir(2)	C(2)	1.848(15)
Ir(2)	C(3)	2.020(10)	Ir(2)	C(3)	2.049(9)
Ir(2)	C(4)	2.050(12)	Ir(2)	C(4)	2.069(12)
P(1)	C(6)	1.834(13)	P(1)	C(6)	1.801(14)
P(2)	C(6)	1.824(11)	P(2)	C(6)	1.832(13)
P(3)	C(7)	1.833(12)	P(3)	C(7)	1.840(13)
P(4)	C(7)	1.827(13)	P(4)	C(7)	1.829(14)
F(2)	C(5)	1.422(19)	F(2)	C(5)	1.376(16)
F(3)	C(5)	1.320(19)	F(3)	C(5)	1.334(15)
O(1)	C(1)	1.031(19)	O(1)	C(1)	1.109(16)
O(2)	C(2)	1.19(2)	O(2)	C(2)	1.149(17)
C(4)	C(5)	1.243(19)	C(4)	C(5)	1.239(17)

†Distance fixed during refinement.

Table 3.3 (continued)

(b) Angles (deg)

(i) Molecule A				*(ii) Molecule B*			
Atom1	**Atom2**	**Atom3**	**Angle**	**Atom1**	**Atom2**	**Atom3**	**Angle**
P(1)	Ir(1)	P(3)	173.07(13)	P(1)	Ir(1)	P(3)	173.00(11)
P(1)	Ir(1)	F(1)	91.8(2)	P(1)	Ir(1)	F(1)	91.7(2)
P(1)	Ir(1)	C(1)	94.1(4)	P(1)	Ir(1)	C(1)	92.1(4)
P(1)	Ir(1)	C(4)	88.0(3)	P(1)	Ir(1)	C(4)	87.2(3)
P(1)	Ir(1)	H(1)	85(3)	P(1)	Ir(1)	H(1)	90(3)
P(3)	Ir(1)	F(1)	91.5(2)	P(3)	Ir(1)	F(1)	90.5(2)
P(3)	Ir(1)	C(1)	90.8(4)	P(3)	Ir(1)	C(1)	93.6(4)
P(3)	Ir(1)	C(4)	87.1(3)	P(3)	Ir(1)	C(4)	86.9(3)
P(3)	Ir(1)	H(1)	90(3)	P(3)	Ir(1)	H(1)	85(3)
F(1)	Ir(1)	C(1)	105.8(9)	F(1)	Ir(1)	C(1)	106.0(7)
F(1)	Ir(1)	C(4)	74.8(6)	F(1)	Ir(1)	C(4)	75.8(5)
F(1)	Ir(1)	H(1)	166(4)	F(1)	Ir(1)	H(1)	159(3)
C(1)	Ir(1)	C(4)	177.8(6)	C(1)	Ir(1)	C(4)	178.1(6)
C(1)	Ir(1)	H(1)	88(4)	C(1)	Ir(1)	H(1)	95(3)
C(4)	Ir(1)	H(1)	91(4)	C(4)	Ir(1)	H(1)	83(3)
P(2)	Ir(2)	P(4)	176.70(13)	P(2)	Ir(2)	P(4)	175.67(13)
P(2)	Ir(2)	F(1)	89.4(3)	P(2)	Ir(2)	F(1)	87.8(3)
P(2)	Ir(2)	C(2)	91.8(5)	P(2)	Ir(2)	C(2)	92.3(5)
P(2)	Ir(2)	C(3)	90.6(3)	P(2)	Ir(2)	C(3)	89.5(3)
P(2)	Ir(2)	C(4)	89.8(3)	P(2)	Ir(2)	C(4)	90.3(3)
P(4)	Ir(2)	F(1)	87.8(3)	P(4)	Ir(2)	F(1)	87.9(3)
P(4)	Ir(2)	C(2)	90.9(5)	P(4)	Ir(2)	C(2)	92.0(5)
P(4)	Ir(2)	C(3)	91.3(3)	P(4)	Ir(2)	C(3)	90.4(3)
P(4)	Ir(2)	C(4)	88.2(3)	P(4)	Ir(2)	C(4)	89.4(3)
F(1)	Ir(2)	C(2)	176.2(7)	F(1)	Ir(2)	C(2)	178.4(6)
F(1)	Ir(2)	C(3)	93.0(5)	F(1)	Ir(2)	C(3)	91.4(4)
F(1)	Ir(2)	C(4)	84.6(5)	F(1)	Ir(2)	C(4)	85.1(4)
C(2)	Ir(2)	C(3)	90.5(7)	C(2)	Ir(2)	C(3)	90.2(6)
C(2)	Ir(2)	C(4)	91.8(7)	C(2)	Ir(2)	C(4)	93.3(6)
C(3)	Ir(2)	C(4)	177.6(6)	C(3)	Ir(2)	C(4)	176.5(4)
Ir(1)	P(1)	C(6)	112.8(4)	Ir(1)	P(1)	C(6)	112.9(4)
Ir(2)	P(2)	C(6)	111.5(4)	Ir(2)	P(2)	C(6)	110.6(5)
Ir(1)	P(3)	C(7)	112.9(4)	Ir(1)	P(3)	C(7)	114.2(5)

Table 3.3 (continued)

(b) Angles (deg)

(i) Molecule A				*(ii) Molecule B*			
Atom1	**Atom2**	**Atom3**	**Angle**	**Atom1**	**Atom2**	**Atom3**	**Angle**
Ir(2)	P(4)	C(7)	112.1(4)	Ir(2)	P(4)	C(7)	111.7(4)
Ir(1)	F(1)	Ir(2)	99.3(6)	Ir(1)	F(1)	Ir(2)	98.8(4)
Ir(1)	C(1)	O(1)	176.6(17)	Ir(1)	C(1)	O(1)	176.5(18)
Ir(2)	C(2)	O(2)	177(2)	Ir(2)	C(2)	O(2)	179.7(16)
Ir(1)	C(4)	Ir(2)	101.2(6)	Ir(1)	C(4)	Ir(2)	100.3(5)
Ir(1)	C(4)	C(5)	129.6(11)	Ir(1)	C(4)	C(5)	128.5(10)

Discussion

As anticipated, the coordination mode of the fluoroethenes varies depending on the number of fluorine substituents on the ethene ligand. If the fluoroethene ligand contains only a single fluorine it binds terminally in an η^2 fashion to a single iridium centre, as observed for the ethene adduct $[Ir_2(CH_3)(CO)_2(\eta^2\text{-}C_2H_4)(dppm)_2][CF_3SO_3]$ (**2B**).[3] If three or more fluorine substituents are present, the fluoroolefin bridges the metals, as observed with the complexes $[Ir_2(CH_3)(CO)_2(\mu\text{-olefin})(dppm)_2][CF_3SO_3]$ (olefin = C_2F_3H, C_2F_4). This bridging coordination mode was previously confirmed by the X-ray structure determination of $[Ir_2(CH_3)(CO)_3(\mu\text{-}C_2F_4)(dppm)_2][CF_3SO_3]$, which was formed from the above tetrafluoroethene adduct by addition of CO.[2] With two fluorine substituents both coordination modes can be observed, depending on the olefin isomer.

The π complex $[Ir_2(CH_3)(CO)_2(\eta^2\text{-}CF_2{=}CH_2)(dppm)_2][CF_3SO_3]$ (**9B**) appears to have similar stability to the bridged form **9C**, since both coexist at the same temperature and the conversion of **9B** to **9C** is incomplete. With the fluorine atoms on different carbon atoms, as in Z-1,2-difluoroethene, the bridged form is not observed at all, and the π complex $[Ir_2(CH_3)(CO)_2(\eta^2\text{-}Z\text{-}CHF{=}CHF)(dppm)_2][CF_3SO_3]$ (**8**) is only stable below -40 °C. With only a single fluorine substituent, fluoroethene also forms a labile π complex, $[Ir_2(CH_3)(CO)_2(\eta^2\text{-}CH_2{=}CHF)(dppm)_2][CF_3SO_3]$ (**7**). There appear to be two distinct trends at work here: the effect of the degree of fluorine substitution on the stability of the π complex and the effect of fluorine substitution on the stability of the bridged form. Complexes of partially fluorinated ethenes are thought to be less stable than ethene complexes or tetrafluoroethene π complexes.[10] The present results tend to support that proposition, especially in light of the observation that the non-fluorinated ethene complex $[Ir_2(CH_3)(CO)_2(\eta^2\text{-}C_2H_4)(dppm)_2][CF_3SO_3]$ (**2B**) may be isolated as a stable solid at room temperature.[3] There is, however, a remarkable dearth of fluoroethene or difluoroethene complexes in the literature, so that generalizations regarding their stability must be regarded with caution.

It is notable that bridging adducts are observed in all cases in which the olefin has two fluorines on the same carbon, whereas olefins without such a substitution pattern (fluoroethene, Z-1,2-difluoroethene) form only a π complex (e.g. **7** and **8**). As discussed in the Appendix, the steric requirements in the bridging position in complexes of olefins derived from **1** are rather severe because of the bulky phenyl groups of the dppm ligands. Moreover, movement of a ligand from the terminal π-bound position to the bridging position presumably requires a rearrangement of the phenyl groups to accommodate the bridging ligand. For a bridged complex to form the reorganization energy associated with these changes must be compensated for by the greater bonding interaction when the olefin ligand is bonded to two metal atoms simultaneously. Accordingly, the increase in the metal-olefin bonding interactions in the 1,1-difluoroethene complex upon moving from the π-complex **9B** where the bonding is with one metal only to the bridged complex **9C** must be at least as large as the reorganization energy. Hence, the sum of one M-CF_2 and one M-CH_2 bonding interaction must exceed that of two M-CHF bonding interactions since Z-1,2-difluoroethene does not form a bridged complex whereas 1,1-difluoroethene does. Therefore, we assume that the formation of a hypothetical bridging complex from Z-1,2-difluoroethene would not release sufficient energy necessary to reorganize the dppm framework to form the bridged complex. The entropic contribution to the overall free energy change is assumed to be small, since there is no change in the number of particles in these transformations. Figure 3.3 schematically depicts the relative energies of the bridged and terminal adducts for olefin complexes of **1**.

In all the cases we have studied the kinetic product is a *terminal* adduct, presumably because this involves attack at the least crowded site in the equilibrium solution

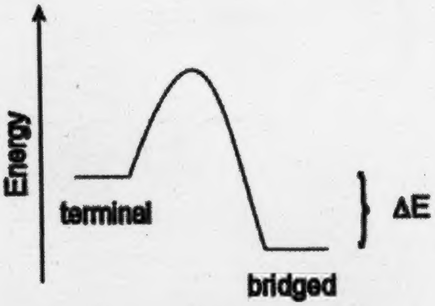

Figure 3.3. Potential energy diagram showing the proposed relationship of the bridged and terminal olefin adducts of **1**.

geometry of **1** (see Appendix). It is constructive at this point to consider the olefins that do not form any bridged products and the possible reasons for this. We have seen that ethene, fluoroethene, Z-1,2-difluoroethene, 2-methyl-1,3-butadiene and 1,1-dimethylallene (Chapter 2) do not form bridged species. For 1,1-dimethylallene and 2-methyl-1,3-butadiene this is probably due to the steric crowding that would be imparted by their methyl substituents. The other olefins (i.e. fluoroethene and Z-1,2-difluoroethene) would result in less crowding in the bridging position but the additional bonding interaction in the bridged position must be insufficiently strong to overcome the reorganization energy.

With ligands that are less sterically demanding than dppm, such as dmpm (dmpm = bis(dimethylphosphino)methane, see Chapter 5) bridged complexes would be expected to form at lower temperatures, and to form with olefins that do not bridge when bonded to the dppm complex, **1**. Based on the observed increase in propensity towards bridging as the degree of fluorination increases, we would expect ethene to form the least stable bridged complex.

We have found that the ^{19}F chemical shifts in the fluoroolefin complexes where the iridium-bound methyl group is not activated can be diagnostic for the olefin coordination mode. Thus, in the η^2 complexes (**7**, **8**, and **9B**) the coordination shift of the fluorine nuclei in the ^{19}F NMR spectrum of the ligand is towards higher field, whereas in the bridged complexes (**9C** and **10**) the coordination shift is to lower field. The changes in the chemical shift ($\Delta\delta$) upon complex formation are summarized in Table 3.4.

The magnitude and the sign of the change in chemical shift upon complexation ($\Delta\delta$) for the two geminal fluorine nuclei of compound **10** is similar to that observed for the complex $[Ir_2(CH_3)(CO)_2(\eta^2\text{-}CF_2{=}CF_2)(dppm)_2][CF_3SO_3]$. Although the ^{19}F chemical shift for the olefinic fluorine nuclei in **8** are similar to that of the lone vinylic fluorine in **10** (i.e. -211.6 *vs.* -193.8 ppm), it is the *change* in chemical shift from that of the free olefin that is important. Here a comparison of the π-bound and bridged isomers of the 1,1-difluoroethene complex (**9B** and **9C**, respectively) is helpful. In the bridged form **9C** there is a large downfield shift upon complexation of 37 ppm, whereas the terminal olefin ligand in **9B** experiences an upfield shift of -2 ppm.

Table 3.4. Chemical shift change upon coordination for partially fluorinated ethenes

Compound[a]	**Change in chemical shift upon complex formation in ppm, $\Delta\delta = \delta(\text{complex}) - \delta(\text{ligand})$**
$[Ir_2(CH_3)(CO)_2(\eta^2\text{-}CHF{=}CH_2)(dppm)_2]^+$ **(7)**	-56
$[Ir_2(CH_3)(CO)_2(\eta^2\text{-}CHF{=}CHF)(dppm)_2]^+$ **(8)**	-47
$[Ir_2(H)(\mu\text{-}CH_2)(CO)_2(\eta^2\text{-}CF_2{=}CH_2)(dppm)_2]^+$ **(9A)**	2
$[Ir_2(CH_3)(CO)_2(\eta^2\text{-}CH_2{=}CF_2)(dppm)_2]^+$ **(9B)**	-2
$[Ir_2(CH_3)(CO)_2(\mu\text{-}CH_2{=}CF_2)(dppm)_2]^+$ **(9C)**	37
$[Ir_2(CH_3)(CO)_2(\mu\text{-}CHF{=}CF_2)(dppm)_2]^+$ **(10)**	47, 44, 11
$[Ir_2(CH_3)(CO)_2(\eta^2\text{-}CF_2{=}CF_2)(dppm)_2]^{+\,b}$	56, 49

Notes: [a] In all cases the anion is $CF_3SO_3^-$ [b] Calculated from data in reference 3. δ (C_2F_4) = -135 ppm

A large downfield coordination shift upon bridge formation is seen for the three cases where there are two fluorine atoms on the same carbon in the ligand (i.e. for 1,1-difluoroethene, trifluoroethene and tetrafluoroethene), whereas the downfield coordination shift is much smaller (11 ppm) when there is only a single fluorine on a bridging carbon. This suggests that the downfield coordination shift is related to the ability of the ligated carbon to form a strong bond with a metal atom which is not involved in back donation to another olefin ligand carbon. In all cases when there are two fluorine substituents on the same ethene carbon the bridged adduct forms as the thermodynamic product.

Without doubt, the most interesting and perplexing result to come out of this study is the apparent C-H and C-F activation of trifluoroethene to give the difluorovinylidene-bridged product $[Ir_2CH_3(H)(CO)_2(\mu\text{-}X)(\mu\text{-}CHF{=}CF_2)(dppm)_2]$-$[CF_3SO_3]$ (**11**). Clearly, the difficulty in activating the strong C-F bond makes this an unusual transformation. In addition, a number of obvious questions arise concerning the mechanism, such as which bond (C-H or C-F) is activated first and what the roles of the adjacent metals are. Unfortunately, we have not yet succeeded in repeating this fascinating transformation, so mechanistic information is lacking. Nevertheless, the X-ray structure offers some clues in the form of the relative positions of the ligands in the equatorial plane.

The initial attack of the fluoroolefin to form a bridged complex (compound **10** in the case of trifluoroethene) could occur at two different sites, as shown in Scheme 3.4. Attack at site (a), between the methyl group and the bridging carbonyl, would lead to an olefin-bridged product where the bridge is *cis* with respect to the methyl group, and *trans* with respect to a carbonyl ligand (which has migrated from the other metal, where it was the terminal carbonyl of **1**). This is indeed the geometry determined crystallographically for the tetrafluoroethene adduct $[Ir_2(CH_3)(CO)_3(\mu\text{-}C_2F_4)(dppm)_2][CF_3SO_3]$, where the third carbonyl occupies a position along the iridium-iridium axis on the metal not bearing the methyl group.[2] However, the observed geometry of the difluorovinylidene **11** shows the difluorovinylidene situated *trans* to the methyl group, suggesting that either an initial *cis* bridge isomerizes to *trans* or that the site of attack that leads to **11** is (b) in Scheme 3.4. Support for the formulation of the fluoroolefin complexes in this study (**9C** and **10**) as having the *cis*-bridged geometry is found in the ^{13}C chemical shifts of the carbonyls. The lower field carbonyl resonances (196.6 and 196.9 ppm, respectively) suggest some semi-bridging interaction with a second metal, which is only feasible in the *cis* geometry.[10]

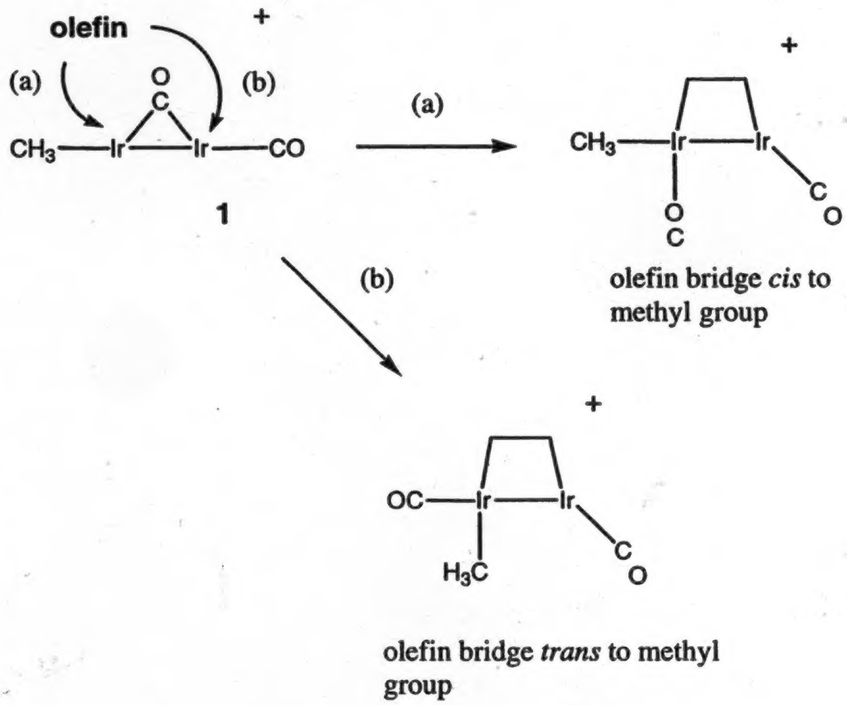
olefin
(a)
(b)
+
O
C
CH3—Ir—Ir—CO
1
(a)
CH3—Ir—Ir
O C
C O
+
olefin bridge cis to methyl group
(b)
+
OC—Ir—Ir
H3C
C O
olefin bridge trans to methyl group

Scheme 3.4. Possible sites of attack of olefin ligands on **1** to form a dimetallacyclobutane complex. Dppm ligands and substituents on the olefin have been omitted for clarity.

We suggest a possible mechanism, starting with **10** in the *cis* geometry described above, for the transformation of **10** to **11**, as shown in Scheme 3.5. In this proposal, HF is eliminated from the coordinated trifluoroethene molecule in

11 leading to the coordinatively unsaturated species **(a)**, which rapidly rearranges to the difluorovinylidene **(b)**, which then recombines with HF to form the product **11**. The initial loss of HF could lead, in a concerted fashion, directly to the difluorovinylidene **(b)**, without the intermediacy of **(a)**. Intramolecular HF elimination in a complex containing a coordinated fluorocarbon ligand has been previously reported.[12] The loss of HF and its subsequent recoordination helps rationalize the location of the μ-F group on the face of the complex opposite the μ-C=CF_2 group. Since the trifluoroethene ligand is unsymmetrical, and since we have argued that the bonding interaction of the -CF_2- end with the metal is stronger than that of the -CHF- end with the other metal centre, it is likely that the coordination geometry of the bridged form has the -CHF- end closer to the midpoint of the iridium-iridium bond than expected for a symmetrical arrangement as shown in Scheme 3.5. Hence, upon elimination of HF a smaller movement of the carbenoid carbon is required to form the difluorovinylidene **(b)**. Accompanying these transformations, the carbonyl ligand on the iridium bearing a methyl group moves to a position *cis* to the μ-C=CF_2 group, leaving the methyl group *trans*. After HF re-coordination the final step required is the migration of a hydride ligand to the opposite face of the Ir_2P_4 plane.[13] Support for this scheme comes from the observation that C-F bonds α to a metal centre are susceptible to abstraction by Lewis acids.[14] Also, intramolecular Lewis acid abstraction occurs in the thermal decomposition of lithiofluoroolefins via the elimination of lithium fluoride and the transient formation of difluoroethyne or difluorovinylidene.[15]

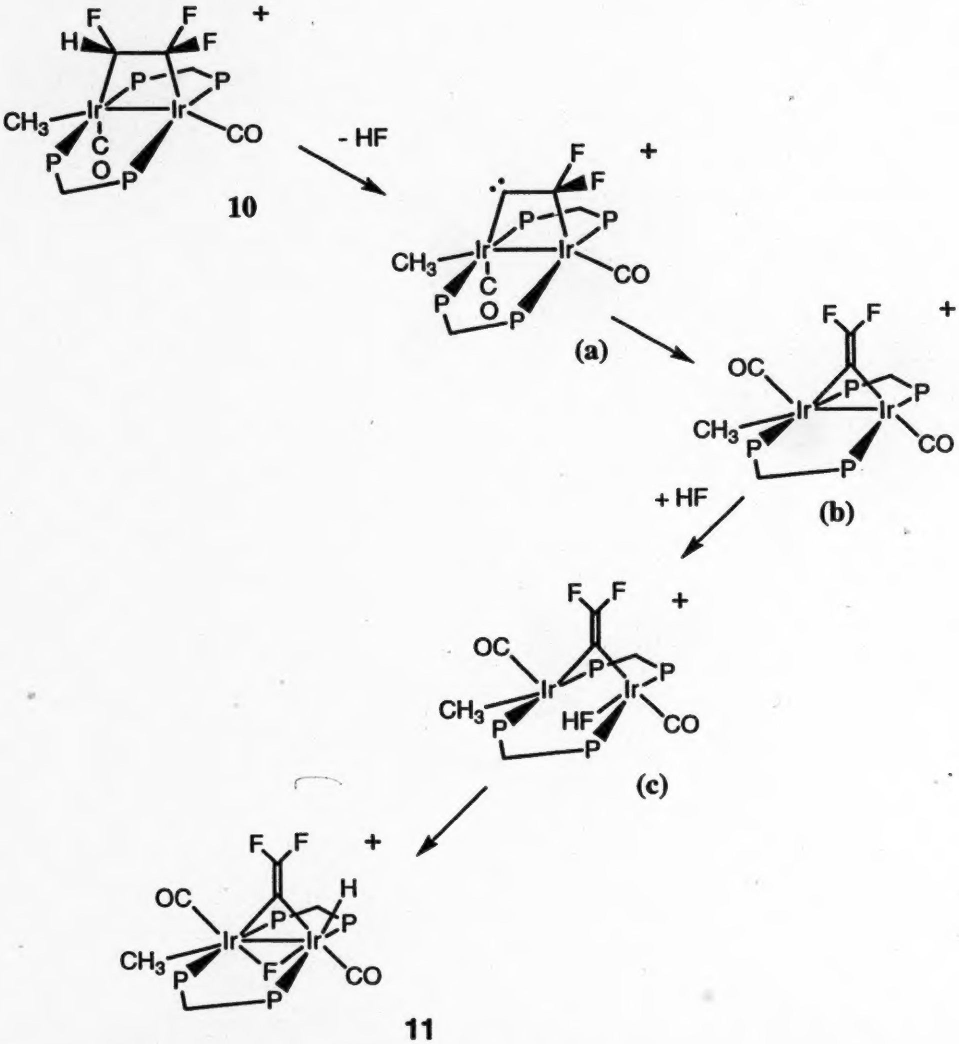

Scheme 3.5. Proposed route for the transformation of $[Ir_2(CH_3)(CO)_2(\mu\text{-}CHF{=}CF_2)(dppm)_2][CF_3SO_3]$ (**10**) to $[Ir_2CH_3(H)(CO)_2(\mu\text{-}X)(\mu\text{-}CHF{=}CF_2)(dppm)_2][CF_3SO_3]$ (**11**) , X = F or H. Structures **(a)**, **(b)**, and **(c)** are proposed intermediates. Dppm phenyl groups have been omitted for clarity.

Alternatively, while the observed species in solution is **10**, reversible loss of trifluoroethene and its subsequent recoordination at an alternate site to give the isomer where the olefin bridge is *trans* to the methyl group (Scheme 3.4) could lead to products. Also, recoordination of HF could be concerted, as implied in Scheme 3.5, or could occur *via* protonation followed by fluoride attack.

Conclusions

We have found that, within the series of fluoroolefins studied, the propensity towards bridged complex formation is related to the degree of fluorine substitution of the olefin. Bridging complexes form where the additional bonding interaction in a bridged complex is sufficient to overcome the energy penalty incurred in moving the dppm ligands out of the way of the bridging site. The stability order of the complexes parallels that seen in Chapter 2 for the allene complexes of **1**, that is, for a given olefin, the least stable is the terminal π-complex in which a C-H bond of the methyl group has been activated (for example, $[Ir_2(H)(\mu\text{-}CH_2)(CO)_2(\eta^2\text{-}CF_2{=}CH_2)(dppm)_2][CF_3SO_3]$ **9A**), followed by the more stable π complex with an intact iridium-methyl (e.g. $[Ir_2(CH_3)(CO)_2(\eta^2\text{-}CH_2{=}CF_2)(dppm)_2][CF_3SO_3]$, **9B**), and finally the most stable is the bridged complex (e.g. $[Ir_2(CH_3)(CO)_2(\mu\text{-}CH_2{=}CF_2)(dppm)_2][CF_3SO_3]$, **9C**). This leads to the prediction that with a less sterically demanding biphosphine ligand than dppm, bridged complexes might also form in the reaction of **1** with Z-1,2-difluoroethene or fluoroethene.

Finally, the transformation of the bridged trifluoroethene complex **10** to the difluorovinylidene **11** represents a facile formal C-H and C-F activation, which, unfortunately has not been repeated. To better understand this process we have undertaken the study of some halogen-substituted fluoroolefins, which are described in Chapter 4 of this thesis.

References

1. Ristic-Petrovic, D.; Torkelson, J. R.; Hilts, R. W.; McDonald, R.; Cowie, M. *Organometallics* **2000**, *19*, 4432.
2. Torkelson, J. R., Ph. D. Thesis, University of Alberta, Edmonton, Alberta, 1998.
3. (a) Antwi-Nsiah, F. H., Ph. D. Thesis, University of Alberta, Edmonton, Alberta, 1994.
   (b) Antwi-Nsiah, F. H.; Cowie, M. *Organometallics* **1992**, *11*, 3157.
4. Kotora, M.; Hajek, M. *J. Fluorine Chem.* **1991**, *55*, 57.
5. (a) Xiao, J.; Cowie, M. *Organometallics* **1993**, *12*, 463.
   (b) Antonelli, D. M.; Cowie, M. *Organometallics* **1991**, *10*, 2550.
   (c)Hilts, R. W.; Franchuk, R. A.; Cowie, M. *Organometallics* **1991**, *10*, 1297.
6. Torkelson, J. R.; Antwi-Nsiah, F. H.; McDonald, R.; Cowie, M.; Prius, J. G.; Jalkanen, K. J.; DeKock, R. L. *J. Am. Chem. Soc.* **1999**, *121*, 3666.

7. Elsenbroich, C.; Salzer, A. *Organometallics: A Concise Introduction*, VCH, Weinheim, Germany, 1989. p. 298.

8. Dungan, C. H.; Van Wazer, J. R. *Compilation of Reported F^{19} NMR Chemical Shifts*, Wiley-Interscience, New York, 1970.

9. Veltheer, J. E.; Burger, P.; Bergman, R. G. *J. Am. Chem. Soc.* **1995**, *117*, 12478.

10. George, D. S. A.; McDonald, R.; Cowie, M. *Organometallics* **1998**, *17*, 2553.

11. a) Cramer, R. *J. Am. Chem. Soc.* **1967**, *89*, 4621,

    b) Tolman, C. A. *J. Am. Chem. Soc.* **1974**, *96*, 2780,

    c) Cedeno, D. L.; Weitz, E. *J. Am. Chem. Soc* **2001**, *123*, 12857.

12. Howard, J. A. K.; Knox, S. A. R.; Terrill, N. J.; Yates, M. I. *Chem. Commun.* **1989**, 640.

13. Antonelli, D. M.; Cowie, M. *Inorg. Chem.* **1990**, *17*, 2553, and references therein.

14. Richmond, T. G. *Angew. Chem. Int. Ed.* **2000**, *39*, 3241.

15. Brisdon, A. K., Banger, K. K. *J. Fluorine Chem.* **1999**, *100*, 35.

Chapter 4

Fluoroethenyl complexes from the reaction of $[Ir_2(CH_3)(CO)_2(dppm)_2][CF_3SO_3]$ with halofluoroolefins[1]

Introduction

The activation of carbon-fluorine bonds is of importance from a number of perspectives. Fluorocarbons are global-warming gases,[2] having long atmospheric lifetimes,[3] so methods for transforming them into more innocuous substances are being sought. In addition, fluorocarbons are finding applications as agrochemicals and pharmaceuticals,[4] necessitating new methods for selectively transforming or creating C-F bonds in relevant synthons. The challenges in achieving the goals of C-F activation are due, in a large measure, to the strength of the C-F bond, which is the strongest single bond involving carbon.[5] The paucity of nucleophilic substitutions of alkyl fluorides highlights the diminished reactivity of the C-F bond relative to other C-X bonds; this reaction is more than two orders of magnitude slower for alkyl fluorides than for alkyl chlorides.[6]

In Chapter 3 we described the apparent C-H and C-F activation of trifluoroethene by the diiridium complex, $[Ir_2(CH_3)(CO)_2(dppm)_2][CF_3SO_3]$ (**1**) to yield a difluorovinylidene-bridged product (**10**).[7] However, a number of factors, including the capricious nature of the reaction (which took place over a period of days at ambient temperature and was only observed on one occasion) and the increasing difficulty of obtaining trifluoroethene or its synthons, have to date prevented us from studying this transformation further. Two questions that we had hoped to address in this apparent double-activation process was whether C-H or C-F activation occurred first, and what the functions of the adjacent metals might be in such a transformation. Compound **1** had previously been demonstrated to undergo double C-H activation of 1,3-butadiene,[8] suggesting a role for adjacent metals in olefin activation (Chapter 2). Our inability to obtain the desired information directly from the reaction of **1** with trifluoroethene encouraged us to seek this information indirectly. If C-H activation was the first activation step the first species produced would be a trifluoroethenyl complex, whereas, initial C-F activation would yield a 2,2-difluoroethenyl group. We therefore sought routes to complexes containing these fluoroethenyl ligands. Several fluorovinyl complexes of transition metals are known, including a few of iridium.[9] However, we are unaware of any binuclear complexes of iridium containing fluorovinyl groups. Our interest in binuclear complexes of fluorovinyl ligands relates to the functions of the adjacent metals in the activation of fluorocarbon ligands - a topic that seems to have been only briefly addressed in the past.[10] Vinyl fluorides are normally quite inert, however, examples of C-F bond cleavage reactions in the presence of nucleophiles have been reported.[1-13] In this chapter preliminary results on the preparation of fluorovinyl complexes of diiridium and on some subsequent transformations are described.

Experimental

General Comments. All solvents were dried (using appropriate drying agents), distilled before use and stored under dinitrogen. Deuterated solvents used for NMR experiments were freeze-pump-thaw degassed (three cycles) and stored under nitrogen or argon over molecular sieves. Reactions were carried out at ambient temperature under argon using standard Schlenk techniques, and compounds that were used as solids were purified by recrystallization. Prepurified argon and nitrogen were purchased from Linde, carbon-13 enriched CO (99%) was supplied by Isotec Inc., fluoroolefins (chlorotrifluoroethene, iodotrifluoroethene and 1-bromo-2,2-difluoroethene) were supplied by Lancaster. All gases were used as received and all other reagents were purchased from Aldrich and were used as received. The compound $[Ir_2(CH_3)(CO)(\mu\text{-}CO)(dppm)_2][CF_3SO_3]$ (**1**) was prepared as previously reported.[14]

Proton NMR spectra were recorded on Varian Unity 400, 500 or 600 spectrometers, or on a Bruker AM400 spectrometer. Carbon-13 NMR spectra were recorded on Varian Unity 400 or Bruker AM300 spectrometers. Phosphorus and fluorine spectra were recorded on Varian Unity 400 or Bruker AM400 spectrometers. Two-dimensional NMR experiments (GCOSY, TROESY, GTOCSY and ^{13}C-^{1}H HMQC) were obtained on Varian Unity 400 or 500 spectrometers. Infrared spectra were obtained on a Bio-Rad RTS-60 Fourier transform infrared spectrometer as solutions in KCl cells with 0.5-mm-window path lengths, or as solids using a Nicolet Magna 750 with a Nic-Plan infrared microscope. Carbonyl stretches reported are for non-isotopically enriched samples. Mass spectrometric analyses were performed by positive ion electrospray ionization on a Micromass ZabSpec Hybrid Sector-TOF. Elemental analyses were performed by the microanalytical service within the department. Spectroscopic data for all compounds are given in Table 4.1.

Preparation of Compounds.

(a) $[Ir_2(C_2F_3)(CH_3)(CO)_2(\mu\text{-}Cl)(dppm)_2][CF_3SO_3]$. (11). A brick-red solution of $[Ir_2(CH_3)(CO)(\mu\text{-}CO)(dppm)_2][CF_3SO_3]$ (**1**) (93 mg, 0.066 mmol) dissolved in 15 mL of dichloromethane was cooled to -78°C using a solid CO_2/acetone bath. Excess chlorotrifluoroethene gas was condensed onto the stirred solution, which was stirred at this temperature for 1/2 h at which time the cooling bath was removed and the vessel allowed to warm to room temperature (*ca.* 4 h). After stirring at room temperature overnight, the yellow solution was reduced *in vacuo* to *ca.* 3 mL. Slow addition of 10 mL of Et_2O afforded a bright yellow powder. The product was triturated twice with 10 mL of Et_2O, the supernatant decanted, and then the solid was dried briefly under a stream of argon and then *in vacuo* (89% yield). Anal. Calcd. for $Ir_2SClP_4F_6O_5C_{56}H_{14}$: C, 44.74; H, 3.18; Cl, 2.38. Found: C, 45.15; H, 3.15; Cl, 2.69%. MS (ESI) $P^+ = 1341.1$.

Table 4.1. Spectroscopic Data for the Compounds

compound	NMR[a,b]				IR, cm^{-1} [g,h]
	$\delta(^{31}P\{^1H\})$ [c]	$\delta(^1H)$ [d,e]	$\delta(^{19}F)$ [f]	$\delta(^{13}C\{^1H\})$ [d]	
$[Ir_2(C_2F_3)(CH_3)(CO)_2(\mu\text{-}Cl)(dppm)_2][CF_3SO_3]$ (**11**)[i]	-6.9 (m), -11.3(m)	5.80 (m, 2H), 4.35 (m, 2H), 1.17 (t, 3H, $^3J_{P\text{-}H}$ = 5.4 Hz))	-78.8 (s, 3F), -92.8 (ddt, 1F, $^4J_{P\text{-}F}$ = 5 Hz, $^2J_{F\text{-}F}$ = 89 Hz, $^3J_{F\text{-}F}$ = 37 Hz), -126.9 (dd, 1F, $^2J_{F\text{-}F}$ = 89 Hz, $^3J_{F\text{-}F}$ = 110 Hz), -139.1 (dd, 1F, $^3J_{F\text{-}F}$ = 110, 37 Hz)	172.5 (t, $^2J_{C\text{-}P}$ = 9 Hz), 170.8 (t, $^2J_{C\text{-}P}$ = 11 Hz), -24.0 (m)	2024(s), 1709 (w)
$[Ir_2(C_2F_2H)(CH_3)(CO)_2(\mu\text{-}Br)(dppm)_2][CF_3SO_3]$ (**12**)	-6.8 (m), -10.3 (m)	4.93 (m, 2H), 3.76 (m, 2H), 4.62 (ddt, $^3J_{H\text{-}F}$ = 42 Hz, $^3J_{H\text{-}F}$ = 12 Hz, $^3J_{P\text{-}H}$ = 5 Hz), 0.88 (t, 3H, $^3J_{P\text{-}H}$ = 5 Hz)	-79.1 (s, 3F), -65.9 (ddt, 1F, $^2J_{F\text{-}F}$ = 59 Hz, $^3J_{H\text{-}F}$ = 12 Hz, $^4J_{P\text{-}F}$ = 5 Hz), -84.9 (ddt, 1F, $^3J_{H\text{-}F}$ = 42 Hz, $^2J_{F\text{-}F}$ = 59 Hz, $^4J_{P\text{-}F}$ = 5 Hz)	174.4 (t, $^2J_{C\text{-}P}$ = 9 Hz), 169.5 (t, $^2J_{C\text{-}P}$ = 11 Hz), -24.4 (m)	2021 (s), 1672 (w)
$[Ir_2(C_2F_3)(CH_3)(CO)_2(\mu\text{-}H)(dppm)_2][CF_3SO_3]_2$ (**13**)	-12.9 (m), -20.8 (m)	5.26 (m, 2H), 5.13 (m, 2H), 1.40 (t, 3H, $^3J_{P\text{-}H}$ = 6 Hz) -13.00 (b, 1H)	-78.8 (s, 3F), -92.5 (dd, 1F, $^3J_{F\text{-}F}$ = 110 Hz, $^2J_{F\text{-}F}$ = 86 Hz), -122.1 (pt, 1F, J = 100 Hz), -133.6 (dd, $^3J_{F\text{-}F}$ = 110 Hz, $^3J_{F\text{-}F}$ = 43 Hz)		2021 (s), 1706 (w)

(continued)

Table 4.1. continued

compound	NMR[a,b]				IR, cm^{-1} [g,h]
	δ(^{31}P{^{1}H})[c]	δ(^{1}H)[d,e]	δ(^{19}F)[f]	δ(^{13}C{^{1}H})[d]	
[$Ir_2(C_2F_2CH_3)(CH_3)(CO)_2(\mu\text{-}Cl)(dppm)_2$] [$CF_3SO_3$] (**14**)	1.2 (m), -15.7 (m)	4.08 (m, 2H), 3.44 (m, 2H), 1.22 (t, 3H, $J_{F\text{-}F}$ = 12 Hz), 1.07 (t, 3H, $^3J_{P\text{-}H}$ = 7 Hz)	-78.8 (s, 3F), -126 (b, 2F)	196.8 (b), 174.0 (b), 20.2 (m) -24.8 (m)	2019 (s), 1676 (w, ν(C=C))

[a]NMR abbreviations: s = singlet, d = doublet, t = triplet, pt = psueudotriplet, m = multiplet, b = broad. [b]NMR data at 398K in CD_2Cl_2 unless otherwise stated. [c] ^{31}P{^{1}H} chemical shifts are referenced *vs.* external 85% H_3PO_4. [d] ^{1}H and ^{13}C chemical shifts are referenced *vs.* external TMS. [e]Chemical shifts for the phenyl hydrogens are not given in the ^{1}H data. [f] ^{19}F chemical shifts are referenced *vs.* external $CFCl_3$. [g]IR abbreviations (n(CO) unless otherwise stated): vs = very strong, s = strong, m = medium, w = weak, sh = shoulder, b = broad. [h]CH_2Cl_2 solution unless otherwise stated. [i]NMR data in acetone-d^6 solution.

(b) $[Ir_2(C_2F_2H)(CH_3)(CO)_2(\mu\text{-}Br)(dppm)_2][CF_3SO_3]$ (12). The procedure was the same as that described for **11** except that 1-bromo-2,2-difluoroethene was used instead of chlorotrifluoroethene. The yield of the orange powder was 78%. Anal. Calcd for $Ir_2BrSP_4F_5O_5C_{56}H_{48}$: C, 44.36, H, 3.19. Found: C, 44.15; H, 3.06%. MS(ESI)P+ = 1367.

(c) Reaction of 1 with iodotrifluoroethene. In and NMR tube, 25 mg (0.018 mmol) of **1** was dissolved in 0.7 mL of CD_2Cl_2 and cooled to -78°C giving a brick-red solution. Iodotrifluoroethene (18 μL, 0.018 mmol) was added by syringe. The NMR spectra were recorded at -78°C and at 20° intervals until approximately ambient temperature was reached by which time the solution had become the bright red colour of $[Ir_2(CO)_2(\mu\text{-}CH_2)(\mu\text{-}I)(dppm)_2][CF_3SO_3]$[15] Throughout the NMR monitoring of this reaction the NMR spectra (^1H, ^{19}F, ^{31}P) showed only this compound, unreacted **1** and iodotrifluoroethene. The labeled product $[Ir_2(^*CO)_2(\mu\text{-}^*CH_2)(\mu\text{-}I)(dppm)_2][CF_3SO_3]$ was prepared using the same procedure except that $[Ir_2(^{13}CH_3)(^{13}CO)(\mu\text{-}^{13}CO)(dppm)_2][CF_3SO_3]$ (**1***) was used as the precursor.

(d) $[Ir_2(C_2F_3)(CH_3)(CO)_2(\mu\text{-}H)(\mu\text{-}Cl)(dppm)_2][CF_3SO_3]_2$ (13). Compound **11** (48 mg, 0.032 mmol) was dissolved in 10 mL of dichloromethane forming a yellow solution. To this was added trifluoromethanesulfonic acid (3 mL 0.034 mmol) causing the solution to lighten in colour and become slightly cloudy. The mixture was stirred for 15 min and then reduced *in vacuo* to 5 mL. The supernatant liquid was decanted and the remaining powder triturated twice with 10 mL volumes of Et_2O, leaving 37 mg (70%) of a pale yellow powder. Anal. Calcd for $Ir_2ClS_2P_4F_9O_8C_{57}H_{49}$: C, 41.75; H, 3.01. Found: C, 41.92; H, 2.82%.

(e) $[Ir_2(C_2F_2CH_3)(CH_3)(CO)_2(\mu\text{-}Cl)(dppm)_2][CF_3SO_3]$ (14). Compound **11** (29 mg, 0.020 mmol) was dissolved in 20 mL of THF and the yellow solution was cooled in a dry ice/acetone bath to -78°C, at which time 0.1 mL of a 1.4 M solution of methyl lithium in Et_2O (Aldrich) was added. The solution was stirred at this temperature for 10 min and then allowed to warm to room temperature. Stirring was continued at room temperature for a further hour, at which time the solution was transferred into another vessel that had been charged with approximately 5 g of dry Florisil. The solution was stirred over Florisil for 5 min, during which time the yellow colour of the solution was discharged and the Florisil became bright yellow. The colourless supernatant was decanted, and the Florisil with adsorbed compound **14** was extracted with 10 mL of acetonitrile. The yellow extract was filtered through Celite and then reduced *in vacuo* to a pale yellow powder, which was found by ^{31}P NMR spectroscopy to consist of approximately 60% of **14**, with the remainder being unreacted **11**. The labeled product, $[Ir_2(C_2F_2CH_3)(^{13}CH_3)(^{13}CO)_2(\mu\text{-}Cl)(dppm)_2][CF_3SO_3]$ (**14**), was obtained by the same procedure except that $[Ir_2(^{13}CH_3)(^{13}CO)(\mu\text{-}^{13}CO)(dppm)_2][CF_3SO_3]$ (**1***) was used as the precursor. All attempts to separate **14** from unreacted **11** failed, as did attempts to effect complete transformation of **11** to **14**, so elemental analyses were not obtained.

(f) Reaction of 11 with hydride sources. In a typical experiment, 40 mg of **11** was dissolved in 20 mL of THF. To this was added a solution of the test reagent (10 eq. $NaBH_4$ (10 mg) in 35 mL THF, or 4 eq. of 1.0 M $KHB(sec\text{-}bu)_3$ in THF (100 μL)). In the case of the reaction with KH, a solution of **11** was added to a suspension of 20 eq. (2 mg) KH in 15 mL THF. In all cases, progress of the reaction was assessed by pumping the mixture to dryness after 1 h and observing the ^{31}P, ^{1}H and ^{19}F NMR in CD_2Cl_2 solution, and, in a replicate experiment, pumping the mixture to dryness after 24 h and again running the NMR. From the hydride-source reactions, unreacted **11** was recovered after 24 h, accompanied by variable amounts of unidentified decomposition products.

(g) Reaction of 11 with Lewis acids. In a typical experiment, 40 mg of **11** was dissolved in 20 mL of benzene (trimethylaluminum, methyl trifluoromethanesulfonate, trimethylsilyl trifluoromethanesulfonate) or acetonitrile (silver trifluoromethanesulfonate). To this was added *ca.* 1 eq. the test reagent as a solution (15 μL 2.0M trimethylaluminum in toluene, 3.5 μL of methyl trifluoromethanesulfonate in 20 mL benzene, 5 μL of trimethylsilyl trifluoromethanesulfonate in 20 mL benzene, or 10 mg silver trifluoromethanesulfonate in 20 mL acetonitrile). In all cases, progress of the reaction was assessed by pumping the mixture to dryness after 1 h and observing the ^{31}P, ^{1}H and ^{19}F NMR in CD_2Cl_2 solution, and, in a replicate experiment, pumping the mixture to dryness after 24 h and again running the

NMR. Partial conversion to the dication **13** was observed after 1 h in the reactions with Lewis acids, except the reaction with silver trifluoromethanesulfonate which led to decomposition to unidentified products.

X-Ray Data Collection. Data collection and structure solution (*vide infra*) were carried out by R. McDonald and M. Wang. Yellow crystals of $[Ir_2(CF{=}CF_2)(Me)(CO)_2(\mu\text{-}Cl)(dppm)_2][CF_3SO_3]\cdot 1.5Me_2CO$ (**11**) were obtained *via* slow diffusion of *n*-pentane into an acetone solution of the complex. Data were collected on a Bruker PLATFORM/SMART 1000 CCD diffractometer[16] using Mo K_α radiation at -80°C. Unit cell parameters were obtained from a least-squares refinement of the setting angles of 5737 reflections from the data collection. The space group was determined to be $P2_1/n$ (an alternate setting of $P2_1/c$ [No. 14]). The data were corrected for absorption through use of the SADABS procedure. See Table 4.2 for a summary of crystal data and X-ray data collection information.

Colourless crystals of $[Ir_2(CF{=}CF_2)(Me)(CO)_2(\mu\text{-}Cl)(\mu\text{-}H)(dppm)_2][CF_3SO_3]_2$ (**13**) were obtained *via* slow diffusion of diethyl ether into a dichloromethane solution of the compound. Data were collected and corrected for absorption as for **11** above. Unit cell parameters were obtained from a least-squares refinement of the setting angles of 5118 reflections from the data collection, and the space group was determined to be $P2_1/c$ (No. 14).

Table 4.2. Crystallographic Experimental Details for Compounds **11, 13** and **14.**

A. Crystal Data			
formula	$C_{60.5}H_{56}ClF_6Ir_2O_{6.5}P_4S$	$C_{57}H_{48}ClF_9Ir_2O_8P_4S_2$	$C_{60.5}H_{58}ClF_5Ir_2O_6P_4S$
formula weight	1576.84	1639.80	1551.86
crystal dimensions (mm)	0.30 X 0.10 X 0.09	0.24 X 0.15 X 0.12	0.36 X 0.19 X 0.09
crystal system	monoclinic	monoclinic	monoclinic
space group	*P*2₁/*n* (an alternate setting of *P*2₁/*c* [No. 14])	*P*2₁/*c* (No. 14)	*C*2/*c* (No. 15)
unit cell parameters[a]			
a (Å)	12.2660 (8)	11.3860 (7)	29.974 (2)
b (Å)	32.721 (2)	11.8677 (8)	15.2663 (10)
c (Å)	15.4317 (10)	21.8526 (14)	27.8913 (19)
β (deg)	106.1367 (12)	97.5621 (12)	95.9674 (14)
V (Å^3)	5949.6 (7)	2927.2 (3)	12693.6 (15)
Z	4	2	8
ρ_{calcd} (g cm^{-3})	1.760	1.860	1.624
μ (mm^{-1})	4.726	4.850	4.426
B. Data Collection and Refinement Conditions			
diffractometer	Bruker PLATFORM/ SMART 1000 CCD	Bruker PLATFORM/ SMART 1000 CCD	Bruker PLATFORM/ SMART 1000 CCD
radiation (λ [Å])	graphite-monochromated Mo Kα (0.71073)	graphite-monochromated Mo Kα (0.71073)	graphite-monochromated Mo Kα (0.71073)

(continued)

Table 4.2. (continued)

temperature (°C)	-80	-80	-80
scan type	ω scans (0.2°) (30 s exposures)	ω scans (0.2°) (25 s exposures)	ω scans (0.2°) (30 s exposures)
data collection 2θ limit (deg)	52.80	52.78	52.78
total data collected	28714 ($-15 \leq h \leq 14$, $-33 \leq k \leq 40$, $-19 \leq l \leq 16$)	15804 ($-14 \leq h \leq 14$, $-14 \leq k \leq 14$, $-24 \leq l \leq 27$)	30695 ($-37 \leq h \leq 27$, $-19 \leq k \leq 18$, $-34 \leq l \leq 34$)
independent reflections	12165	5980 ($R_{\mathrm{int}} = 0.0313$)	12952 ($R_{\mathrm{int}} = 0.0424$)
number of observed reflections (*NO*)	9911 [$F_o^2 \geq 2\sigma(F_o^2)$]	5217 [$F_o^2 \geq 2\sigma(F_o^2)$]	9444 [$F_o^2 \geq 2\sigma(F_o^2)$]
structure solution method	direct methods/fragment search (*DIRDIF-96*)	direct methods (*SHELXS-86*)	Patterson search/structure expansion (*DIRDIF-96*)
refinement method[b]	full-matrix least-squares on F^2 (*SHELXL-93*)	full-matrix least-squares on F^2 (*SHELXL-93*)	full-matrix least-squares on F^2 (*SHELXL-93*)
absorption correction method	*SADABS*	empirical (*SADABS*)	empirical (*SADABS*)
range of transmission factors	0.6757-0.3313	0.5937-0.3890	0.6914-0.2987
data/restraints/ parameters	12165 [$F_o^2 \geq -3\sigma(F_o^2)$] / 6[c] / 710	5980 [$F_o^2 \geq -3\sigma(F_o^2)$] / 3[d] / 384	12952 [$F_o^2 \geq -3\sigma(F_o^2)$] / 32[e] / 695
goodness-of-fit (*S*)[f]	1.044 [$F_o^2 \geq -3\sigma(F_o^2)$]	1.108 [$F_o^2 \geq -3\sigma(F_o^2)$]	1.051 [$F_o^2 \geq -3\sigma(F_o^2)$]
final *R* indices[g]			
R_1 [$F_o^2 \geq 2\sigma(F_o^2)$]	0.0386	0.0387	0.0479

(continued)

Table 4.2. (continued)

wR_2 $[F_o^2 \geq -3\sigma(F_o^2)]$	0.0860	0.0935	0.1398
largest difference peak and hole	2.115 and -1.114 e Å^{-3}	1.721 and -1.411 e Å^{-3}	3.319 and -1.071 e Å^{-3}

[a] Obtained from least-squares refinement of 5737 centered reflections for compound **2**, 5118 reflections for **4** and 5438 reflections for **5**.

[b] Refinement on F_o^2 for all reflections (all of these having $F_o^2 \geq -3\sigma(F_o^2)$). Weighted *R*-factors wR_2 and all goodnesses of fit *S* are based on F_o^2; conventional *R*-factors R_1 are based on F_o, with F_o set to zero for negative F_o^2. The observed criterion of $F_o^2 > 2\sigma(F_o^2)$ is used only for calculating R_1, and is not relevant to the choice of reflections for refinement. *R*-factors based on F_o^2 are statistically about twice as large as those based on F_o, and *R*-factors based on ALL data will be even larger.

[c] An idealized geometry was imposed upon the inversion-disordered half-occupancy solvent acetone molecule using the following restraints: d(C(4S)-C(5S)) = d(C(5S)-C(6S)) = 1.47 Å; d(O(2S)-C(5S)) = 1.23 Å; d(C(4S)···C(6S)) = 2.55 Å; d(O(2S)···C(4S)) = d(O(2S)···C(6S)) = 2.34 Å.

[d] An idealized geometry was imposed upon the hydrido ligand by fixing the Ir-H(1) and Ir'-H(1) distances to equal 1.85 Å, and by constraining the P(1)···H(1) and P(2')···H(1) distances to be equal (to within 0.002 Å).

[e] One of the half-occupancy trifluoromethanesulfonate ion positions was found to be disordered about a crystallographic twofold axis, leading to employment of the following restraints: d(S(2)-C(92)) = 1.80 Å; d(S(2)-O(94)) = d(S(2)-O(95)) = d(S(2)-O(96)) = 1.45 Å; d(F(94)-C(92)) = d(F(95)-C(92)) = d(F(96)-C(92)) = 1.35 Å; d(F(94)···F(95)) = d(F(94)···F(96)) = d(F(95)···F(96)) = 2.20 Å; d(O(94)···O(95)) = d(O(94)···O(96)) = d(O(95)···O(96)) = 2.37 Å; d(F(94)···O(95)) = d(F(94)···O(96)) = d(F(95)···O(94)) = d(F(95)···O(96)) = d(F(96)···O(94)) = d(F(96)···O(95)) = 3.04 Å. Distances were also assigned idealized values for the half-occupancy solvent diethyl ether (d(O(1S)-C(1S)) = d(O(1S)-C(3S)) = 1.43 Å; d(C(1S)-C(2S)) = d(C(3S)-C(4S)) = 1.54 Å; d(O(1S)···C(2S)) = d(O(1S)···C(4S)) = 2.43 Å; d(C(1S)···C(3S)) = 2.34 Å) and acetone (d(O(2S)-C(6S)) = 1.20 Å; d(C(5S)-C(6S)) = d(C(6S)-C(7S)) = 1.54 Å; d(O(2S)···C(5S)) = d(O(2S)···C(7S)) = 2.38 Å; d(C(5S)···C(7S)) = 2.67 Å) molecules.

[f] $S = [\Sigma w(F_o^2 - F_c^2)^2/(n - p)]^{1/2}$ (n = number of data; p = number of parameters varied; $w = [\sigma^2(F_o^2) + (AP)^2 + BP]^{-1}$ where $P = [\mathrm{Max}(F_o^2, 0) + 2F_c^2]/3$). For compound **2**, A = 0.0381, B = 6.2180; for **4**, A = 0.0378, B = 13.5695; for **5**, A = 0.0670, B = 151.3170.

[g] $R_1 = \Sigma||F_o| - |F_c||/\Sigma|F_o|$; $wR_2 = [\Sigma w(F_o^2 - F_c^2)^2/\Sigma w(F_o^4)]^{1/2}$.

Yellow crystals of $[Ir_2(CF{=}CFMe)Me(CO)(\mu\text{-}Cl)(\mu\text{-}CO)(dppm)_2][CF_3SO_3]\bullet 0.5\text{-}Et_2O\bullet 0.5Me_2CO$ (**14**) were obtained *via* slow diffusion of diethyl ether into an acetone solution of a mixture of compounds **11** and **14**. A crystal of **14** was hand picked from a mixture of crystals of the two compounds. Redissolving the crystals afterward gave compounds **11** and **14** in the same ratio as before crystallization. Data were collected and corrected for absorption as for **11** above. Unit cell parameters were obtained from a least-squares refinement of the setting angles of 5438 reflections from the data collection, and the space group was determined to be *C*2/*c* (No. 15).

Structure Solution and Refinement. The structure of **11** was solved using automated Patterson location of the heavy metal atoms and structure expansion *via* the *DIRDIF-96* program system.[17] Refinement was completed using the program *SHELXL-93*.[18] Hydrogen atoms were assigned positions based on the geometries of their attached carbon atoms, and were given thermal parameters 20% greater than those of the attached carbons. An idealized geometry was imposed upon the inversion-disordered half-occupancy solvent acetone molecule using the following restraints: d(C(4S)-C(5S) = d(C(5S)-C(6S)) = 1.47 Å; d(O(2S)-C(5S)) = 1.23 Å; d(C(4S)•••C(6S)) = 2.55Å; d(O(2S)•••C(4S)) = d(O(2S)•••C(6S)) = 2.34 Å. The final model for **2** refined to values of $R_1(F)$ = 0.0386 (for 9911 data with $F_o^2 \geq 2\sigma(F_o^2)$) and $wR_2(F^2)$ = 0.0860 (for all 12165 independent data).

The structure of **13** was solved using direct methods (*SHELXS-86*[19]), and refinement was completed using the program *SHELXL-93*. Hydrogen atoms were treated as for **2** except for the hydrido ligand, which was assigned a fixed isotropic displacement parameter and idealized interatomic distances (Ir-H(1) = Ir'-H(1) = 1.85 Å; P(1)···H(1) = P(2')···H(1) to within 0.002 Å). The final model for **4** refined to values of $R_1(F) = 0.0387$ (for 5217 data with $F_o^2 \geq 2\sigma(F_o^2)$) and $wR_2(F^2) = 0.0935$ (for all 5980 independent data).

The structure of **14** was solved using the *DIRDIF-96* program system in the same manner as for **11** above. Refinement was completed using the program *SHELXL-93*, during which the hydrogen atoms were treated as for **11**. Idealized geometries were imposed upon one of the half-occupancy trifluoromethanesulfonate ion positions and upon the half-occupancy solvent diethyl ether and acetone molecules through use of intramolecular distance restraints (fully detailed in the support information). The final model for **14** refined to values of $R_1(F) = 0.0479$ (for 9444 data with $F_o^2 \geq 2\sigma(F_o^2)$) and $wR_2(F^2) = 0.1398$ (for all 12952 independent data).

Results and Compound Characterization

The trifluoroethenyl compound, $[Ir_2(CF{=}CF_2)(CH_3)(CO)_2(\mu\text{-}Cl)(dppm)_2][CF_3SO_3]$ (**11**), is readily obtained by the oxidative addition of the C-Cl bond of chlorotrifluoroethene to $[Ir_2(CH_3)(CO)(\mu\text{-}CO)(dppm)_2][CF_3SO_3]$ (**1**), as shown in

Scheme 4.1. Attempts to detect intermediates in this transformation, such as a chlorotrifluoroethene adduct, were not successful. At -80°C no reaction between **1** and $ClFC=CF_2$ was observed over a 2 h period by NMR, whereas warming to room temperature resulted in the slow but complete conversion to **11** overnight (*ca.* 18 h). At intermediate temperatures the only species observed were the reactants and product in varying amounts.

The $^{31}P\{^1H\}$ NMR spectrum of **11** shows the characteristic, second-order multiplets at -6.9 and -11.3 ppm, belonging to an AA'BB' spin system. In the ^1H NMR spectrum the methylene protons of the dppm ligands appear normal and the methyl group appears as a triplet at 1.17 ppm, with coupling of 5 Hz to the two adjacent ^{31}P nuclei on one iridium. The $^{13}C\{^1H\}$ NMR spectrum of the ^{13}C-enriched, $[Ir_2(C_2F_3)(^{13}CH_3)(^{13}CO)_2(\mu\text{-}Cl)(dppm)_2][CF_3SO_3]$ (**11***), displays resonances typical of terminally bound Ir-carbonyls (172.5, 170.8 ppm) and a high-field resonance at -24.0 ppm corresponding to the methyl group. In the ^{19}F NMR spectrum the three trifluoroethenyl fluorines appear at -97.8, -126.9 and -139.1 ppm, in the normal range for fluorines attached to sp^2-hybridized carbon atoms.[20]

The assignment of the ^{19}F spectrum is aided by comparisons to other trifluorovinyl groups in which the coupling between geminal fluorines ($^2J_{FF}$) is found in the range 75-107 Hz. For example, in trifluoroethene and chlorotrifluoroethene $^2J_{FF}$ = 87 and 76 Hz, respectively, while in a series of

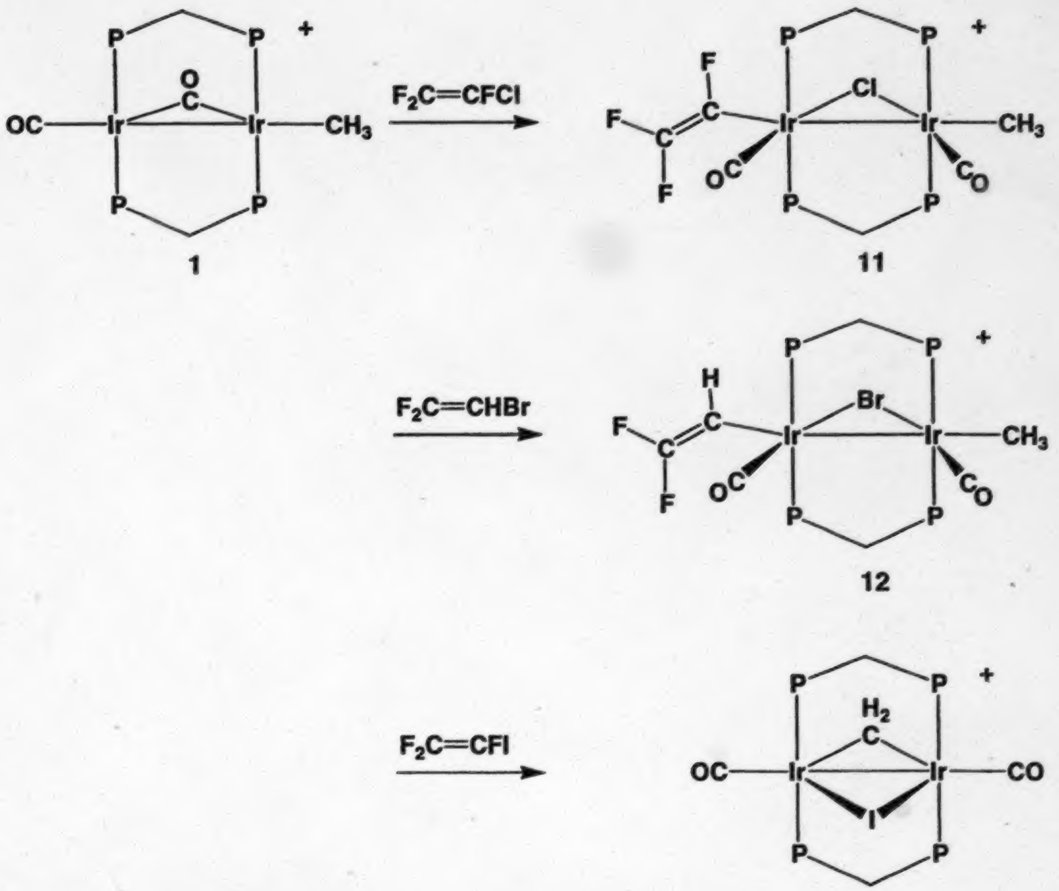

Scheme 4.1. Reaction of **1** with chlorotrifluoroethene, 1-bromo-2,2-difluoroethene and iodotrifluoroethene.

trifluorovinyl complexes, $[M(X)(Y)(PEt_3)_2]$ (M = Ni, Pd, Pt; X = C_2F_3; Y = C_2F_3, Br),[21] *cis*-$[Pt(CF{=}CF_2)_2(PPh_3)_2]$ and *cis*-$[PtCl(CF{=}CF_2)(PBu_3)_2]$[22] values near 100 Hz have been reported. For the aforementioned compounds cis coupling $(^3J_{FF})_{cis}$ is in the range 32-40 Hz, whereas trans coupling $(^3J_{FF})_{trans}$ between 101 and 120 Hz is observed. On the basis of the coupling constants, the two ^{19}F resonances of **11** at -92.8 and -126.9 ppm are assigned to the geminal fluorines on the β carbon, having a mutual coupling of 89 Hz. The former signal appears as a doublet of doublets of triplets and is assigned as cis to the lone fluorine on the α carbon (at -139.1 ppm) on the basis of the 37 Hz coupling between the two. The triplet coupling (5 Hz) of this β-fluorine (-126.9 ppm) results from 4-bond coupling with the ^{31}P nuclei that are bound to the same metal as the C_2F_3 ligand. Neither of the other two fluorines shows coupling to the ^{31}P nuclei. The two mutually trans fluorines show mutual coupling of 110 Hz.

The structure proposed for **11** has been confirmed by an X-ray structure determination, as shown for the complex cation in Figure 4.1. Selected bond lengths and angles are given in Table 4.3. Compound **11** has an unsymmetrical A-frame structure in which the chloro ligand bridges the metals in an essentially symmetrical manner. One carbonyl on each metal lies approximately opposite the Ir-Cl bonds while the methyl and trifluorovinyl groups occupy positions on each metal opposite the metal-metal bond, but bent slightly towards the bridging chloride ligand (Ir(1)-Ir(2)-C(3) = 156.8(2)°, Ir(2)-Ir(1)-C(4) = 165.7(2)°). The Ir-Ir separation (2.8116(3)Å) is consistent with a single bond and is noticeably shorter than the intraligand P-P separations (P(1)-P(2) = 3.026(3)Å, P(3)-P(4) = 3.033(2)Å), consistent with a bonding interaction between the two metals. Both C-F distances on the β-carbon (C(5)-F(2) = 1.351(8)Å, C(5)-F(3) = 1.337(8)Å) are somewhat shorter than C(4)-F(1) of 1.376(7)Å; the shortening of C-F bonds as the number of fluorines on a carbon is increased has previously been noted.[23] Metal-fluorocarbon bonds are also generally observed to be shorter and stronger than those involving non-fluorinated hydrocarbon-metal bonds,[24] and the same is

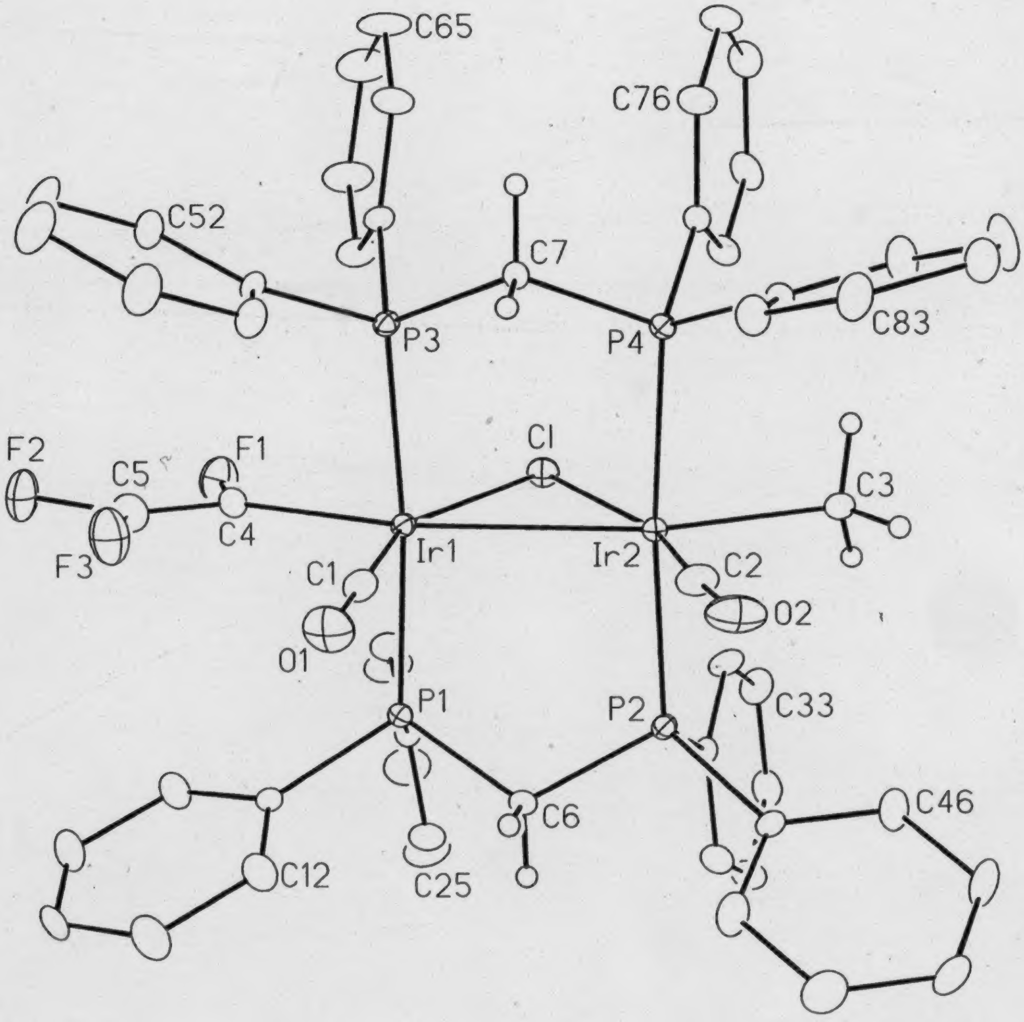
C65
C76
C52
C7
C83
P3
P4
Cl
F2
F1
C5
C3
C4
Ir1
Ir2
F3
C1
C2
O2
O1
P1
C33
P2
C46
C6
C12
C25

Figure 4.1. Perspective view of the $[Ir_2(CF{=}CF_2)(CH_3)(CO)_2(\mu\text{-}Cl)(dppm)_2]^+$ cation of complex **11** showing the atom-labeling scheme. Non-hydrogen atoms are represented by Gaussian ellipsoids at the 20% probability level. The methylene and methyl hydrogens are shown with arbitrarily small thermal parameters, while the phenyl hydrogens are not shown.

Table 4.3. Selected Interatomic Distances and Angles for Compound **11**.

(a) Distances (Å)

Atom1	*Atom2*	*Distance*
Ir(1)	Ir(2)	2.8116(3)
Ir(1)	Cl	2.416(1)
Ir(1)	P(1)	2.350(1)
Ir(1)	P(3)	2.353(1)
Ir(1)	C(1)	1.863(7)
Ir(1)	C(4)	2.090(6)
Ir(2)	Cl	2.449(1)
Ir(2)	P(2)	2.353(1)
Ir(2)	P(4)	2.346(1)
Ir(2)	C(2)	1.809(6)
Ir(2)	C(3)	2.182(6)
P(1)	P(2)	3.026(2)[a]
P(1)	C(6)	1.822(5)
P(2)	C(6)	1.821(5)
P(3)	C(7)	1.817(5)
P(3)	P(4)	3.033(2)[a]
P(4)	C(7)	1.823(5)
F(1)	C(4)	1.376(7)
F(2)	C(5)	1.351(8)
F(3)	C(5)	1.337(8)
O(1)	C(1)	1.143(7)
O(2)	C(2)	1.142(7)
C(4)	C(5)	1.298(9)

(b) Angles (deg)

Atom1	*Atom2*	*Atom3*	*Angle*
Ir(2)	Ir(1)	Cl	55.24(3)
Ir(2)	Ir(1)	P(1)	92.95(3)
Ir(2)	Ir(1)	P(3)	92.60(3)
Ir(2)	Ir(1)	C(1)	96.7(2)
Ir(2)	Ir(1)	C(4)	165.7(2)
Cl	Ir(1)	P(1)	90.69(5)
Cl	Ir(1)	P(3)	91.23(5)
Cl	Ir(1)	C(1)	151.9(2)
Cl	Ir(1)	C(4)	110.6(2)
P(1)	Ir(1)	P(3)	174.25(5)
P(1)	Ir(1)	C(1)	88.9(2)
P(1)	Ir(1)	C(4)	88.6(2)
P(3)	Ir(1)	C(1)	92.0(2)
P(3)	Ir(1)	C(4)	85.7(2)
C(1)	Ir(1)	C(4)	97.5(3)
Ir(1)	Ir(2)	Cl	54.14(3)
Ir(1)	Ir(2)	P(2)	92.19(3)
Ir(1)	Ir(2)	P(4)	92.80(3)
Ir(1)	Ir(2)	C(2)	108.2(2)
Ir(1)	Ir(2)	C(3)	156.8(2)
Cl	Ir(2)	P(2)	93.42(5)
Cl	Ir(2)	P(4)	91.06(5)
Cl	Ir(2)	C(2)	162.3(2)
Cl	Ir(2)	C(3)	102.7(2)
P(2)	Ir(2)	P(4)	174.66(5)
P(2)	Ir(2)	C(2)	87.6(2)

Table 4.3.

(b) Angles, continued

Atom1	*Atom2*	*Atom3*	*Angle*
P(2)	Ir(2)	C(3)	89.6(2)
P(4)	Ir(2)	C(2)	89.1(2)
P(4)	Ir(2)	C(3)	86.6(2)
C(2)	Ir(2)	C(3)	94.9(3)
Ir(1)	Cl	Ir(2)	70.62(4)
Ir(1)	P(1)	C(6)	110.0(2)
Ir(2)	P(2)	C(6)	112.1(2)
Ir(1)	P(3)	C(7)	111.8(17)
Ir(2)	P(4)	C(7)	111.6(2)
Ir(1)	C(1)	O(1)	177.0(6)
Ir(2)	C(2)	O(2)	174.9(7)
Ir(1)	C(4)	F(1)	121.4(4)
Ir(1)	C(4)	C(5)	127.7(5)
F(1)	C(4)	C(5)	110.7(5)
F(2)	C(5)	F(3)	106.8(6)
F(2)	C(5)	C(4)	127.5(7)
F(3)	C(5)	C(4)	125.5(6)
P(1)	C(6)	P(2)	112.4(3)
P(3)	C(7)	P(4)	112.8(3)

[a]Nonbonded distance.

observed in **11**, in which the Ir(1)-C(4) bond (2.090(6)Å) is significantly shorter than Ir(2)-C(3) (2.182(6)Å). Although some of this difference results from the different hybridizations of the trifluorovinyl and methyl carbons (r(sp^2) = 0.74Å. r(sp^3) = 0.77Å), some shortening certainly must be due to fluorine substituents on the former. However, the Ir(1)-C_2F_3 bond is not substantially different than related Rh-vinyl distances in the isopropenyl and trimethylvinyl compounds, [RhOs(C(CH$_3$)=CH$_2$)(CO)$_3$(dppm)$_2$] and [RhOs(C(CH$_3$)=C(CH$_3$)$_2$)(CH$_3$)-(CO)$_3$(dppm)$_2$][CF$_3$SO$_3$] (2.04(2) and 1.955(5)Å, respectively)[25] and is also comparable to the Ir-vinyl distances (2.0(2)-2.13(1)Å) in [Ir$_2$Cl$_2$(CR=CHR)$_2$(CO)$_2$(dppm)$_2$][26] and [Ir$_2$ClH(CR=CHR)(CO)$_2$(μ-H)(dppm)$_2$]-[BF$_4$][27] (R = CO$_2$Me). The olefinic C(4)-C(5) separation(1.298(9)Å) is consistent with a C=C double bond, although is somewhat shorter than for non-fluorinated olefins.[28]

An analogous 2,2-difluorovinyl complex, $[Ir_2(CH=CF_2)(CH_3)(CO)_2(\mu\text{-}Br)(dppm)_2][CF_3SO_3]$ (**12**), is prepared, much as is **11**, by the oxidative addition of 1-bromo-2,2-difluoroethene to **1** (see Scheme 4.1). This reaction occurs more readily than that involving **11** and chlorotrifluoroethene, with small amounts of **12** being detected by NMR even at -80°C, and the reaction proceeding to completion within 1 h at ambient temperature. This is in accord with the expectation of more facile C-Br oxidative addition to an electron-rich transition metal compared to addition of a C-Cl bond.[29] Spectroscopically, compound **12** is quite comparable to **11**; in particular, their $^{31}P\{^1H\}$ NMR spectra are very similar (see Table 4.1). The methyl protons of **12** again appear as a triplet ($^3J_{PH}$ = 5 Hz) at typically high field (0.88 ppm), and the hydrogen of the difluorovinyl ligand, at 4.62 ppm, shows 42 Hz coupling to the trans fluorine (at -84.9 ppm) and 12 Hz to the cis fluorine (at -65.9 ppm). This vinyl hydrogen also displays coupling (5 Hz) to the adjacent pair of ^{31}P nuclei. In the ^{19}F NMR spectrum, both fluorines display coupling of 59 Hz, significantly less than the geminal coupling observed in **11**. Smaller geminal coupling has previously been observed when a fluorine on the adjacent α-carbon has been replaced by a less electronegative group.[30]

Attempts to prepare the fluoro-bridged analogue of **12**, which would be related to a presumed C-F bond-activation product of trifluoroethene, by bromide replacement in **12** using KF/18-crown-6 in THF gave no reaction overnight. Similarly, the reaction of **12** with AgF in THF gave only decomposition products.

In an attempt to generate the iodo-bridged, trifluorovinyl analogue of **11**, the reaction between **1** and iodotrifluoroethene was attempted. However, instead of a simple oxidative-addition reaction paralleling the formation of **11** and **12**, the only product obtained is the iodo- and methylene-bridged product, $[Ir_2(CO)_2(\mu\text{-}I)(\mu\text{-}CH_2)(dppm)_2][CF_3SO_3]$, shown in Scheme 4.1. This product, previously prepared by a different route and characterized in this group,[15] displays the protons of the bridging methylene group at 10.0 ppm in the ^1H NMR spectrum. The other presumed product in the reaction, trifluoroethene, was not detected by ^{19}F NMR spectroscopy. Although this methylene-bridged species could result from oxidative addition of the iodo-olefin followed by reductive elimination of trifluoroethene, the reaction more likely is a free-radical process, as previously observed in the reactions of ICH_2CN and I_2CH_2 with analogous diiridium complexes.[15] Confirmation that the bridging methylene group comes form the methyl of **1** (and not from the solvent) was obtained by using the methyl and carbonyl ^{13}C-labeled analogue $\mathbf{1}^*$ which gave the product with the label in the bridging methylene, and no trace of unlabelled product (by ^1H NMR).

Attempts to replace the bridging chloro ligand in **11** with either hydride or alkyl groups have met with failure. Compound **11** was unreactive to $NaBH_4$, KH or $KHB(\textit{sec}\text{-bu})_3$ in THF at ambient temperature, and was also unreactive to the

Lewis acids, trimethylaluminum, methyl trifluoromethanesulfonate and trimethylsilyl trifluoromethanesulfonate. In all cases **11** was recovered, as the sole or major product, although in the attempted reactions of the Lewis acids, varying amounts of a hydride species was recovered. This hydride product, the complex cation of which was identified as $[Ir_2(CF=CF_2)(CH_3)(CO)_2(\mu\text{-}H)(\mu\text{-}Cl)(dppm)_2]^+$, presumably results from hydrolysis of the Lewis acid by adventitious water and subsequent protonation of **11**; this species was subsequently generated quantitatively by reaction of **11** with triflic acid to give $[Ir_2(CF=CF_2)(CH_3)(CO)_2(\mu\text{-}H)(\mu\text{-}Cl)(dppm)_2][CF_3SO_3]$ (**13**) (see Scheme 4.2).

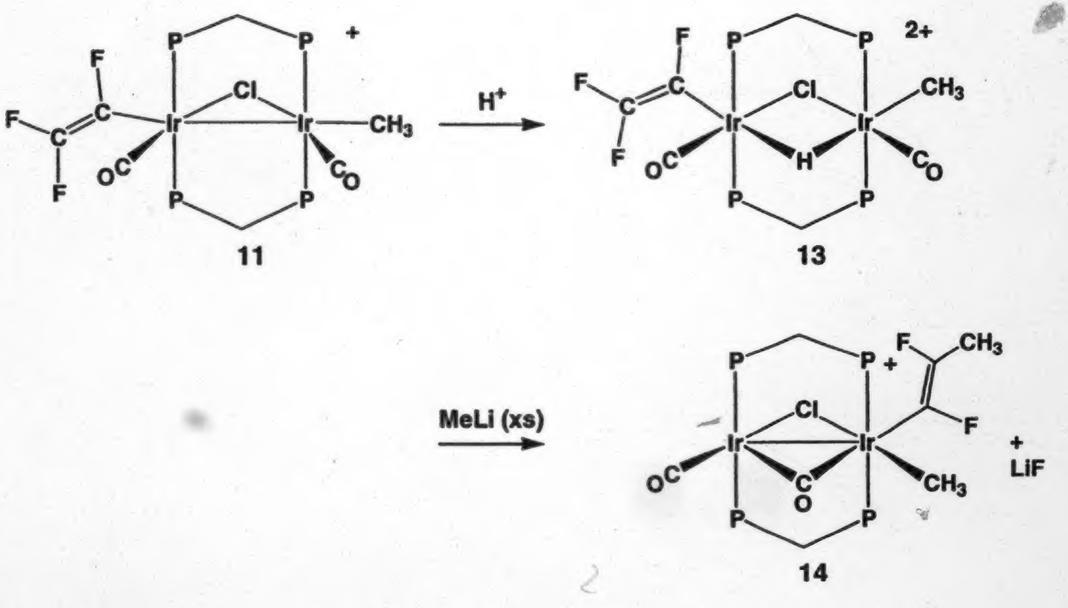

Scheme 4.2. Reaction of **11** with H⁺ or methyl lithium.

Spectroscopically, compound **13** bears a strong resemblance to **11**, and in particular the ^{19}F NMR spectrum displays similar chemical shifts and coupling constants for the trifluorovinyl group in both compounds (see Table 4.1). The ^{1}H NMR spectrum shows the methyl group as a triplet at 1.40 ppm ($^{3}J_{PH}$ = 6 Hz), and the hydride ligand appears as a broad unresolved resonance at -13.00 ppm; the breadth of the hydride resonance presumably results from coupling to all four phosphorus nuclei, suggesting a bridging arrangement, which has been confirmed by ^{31}P-decoupling experiments. This structural assignment has been confirmed by an X-ray determination, and the final structure of the cation is shown in Figure 4.2, with selected bond lengths and angles given in Table 4.4.

The molecule was found to be disordered about an inversion center, meaning that the trifluoroethenyl group and C(2)O(2) are superimposed at 50% occupancy, as are the methyl group and C(1)O(1) as well as Cl and H(1); nevertheless, the non-hydrogen atoms are readily resolved and least-squares refinement proceeded without incident. Although, the disorder precludes unambiguous location of the hydride ligand, its position bridging the metals, is supported by the substantial lengthening of the Ir-Ir bond from 2.8116(3)Å in **11** to 3.0315(5)Å in **13**. Also consistent with the bridging location of the hydride ligand, is the opening up of the pocket between the carbonyls on protonation. As a consequence, the Ir-Ir-CO angles in **11** (96.7(2)°, 108.2(2)°) have increased substantially to 124.7(5)° and 128.7(5)° in **13**. Both effects are well documented in hydride-bridged metal-carbonyl clusters.[31]

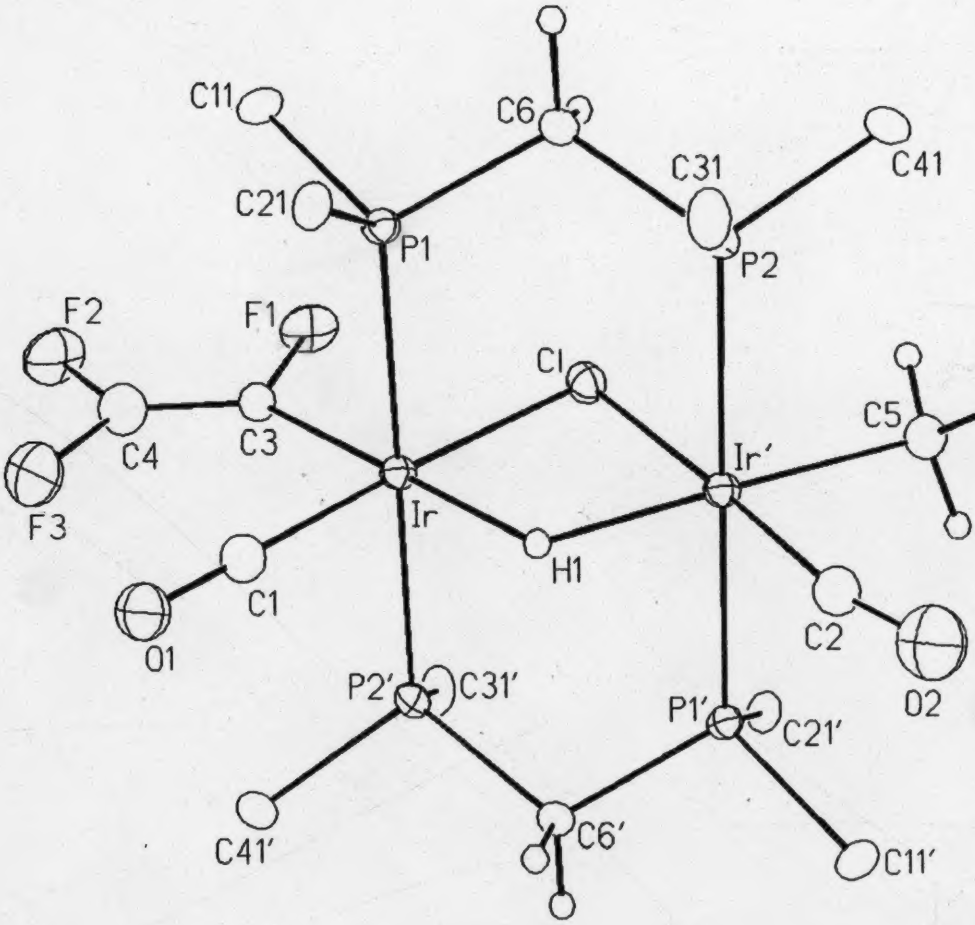
C11
C6
C31
C41
C21
P1
P2
F2
F1
Cl
C5
C4
C3
Ir
Ir'
F3
H1
C1
C2
O1
O2
P2'
C31'
P1'
C21'
C41'
C6'
C11'

Figure 4.2. Perspective view of the $[Ir_2(CF{=}CF_2)(CH_3)(CO)_2(\mu\text{-}H)(\mu\text{-}Cl)(dppm)_2]^{2+}$ cation of complex **13** showing the atom-labeling scheme. The bridging hydride ligand was not located in the X-ray study. Thermal parameters are as described for Figure 4.1. Only one of the disordered molecules is shown. For an explanation of the disorder see the Experimental Section.

Table 4.4. Selected Interatomic Distances and Angles for Compound **13**.

(a) Distances (Å)

Atom1	*Atom2*	*Distance*
Ir	Ir'	3.0315(5)^a
Ir	Cl	2.318(3)
Ir	P(1)	2.372(1)
Ir	P(2')	2.381(1)
Ir	C(1)	1.90(1)
Ir	C(3)	2.02(1)
Ir	H(1)	1.85b
Ir'	Cl	2.369(3)
Ir'	C(2)	1.89(2)
Ir'	C(5)	2.15(1)
Ir'	H(1)	1.85b
P(1)	P(2)	3.051(2)^c
P(1)	C(6)	1.818(6)
P(2)	C(6)	1.834(6)
F(1)	C(3)	1.39(2)
F(2)	C(4)	1.29(2)
F(3)	C(4)	1.34(2)
O(1)	C(1)	1.11(2)
O(2)	C(2)	1.09(2)
C(3)	C(4)	1.33(2)

(b) Angles (deg)

Atom1	*Atom2*	*Atom3*	*Angle*	*Atom1*	*Atom2*	*Atom3*	*Angle*
Ir'	Ir	Cl	50.45(8)	Cl	Ir	C(1)	175.1(5)
Ir'	Ir	P(1)	89.48(4)	Cl	Ir	C(3)	95.4(4)
Ir'	Ir	P(2')	90.98(4)	Cl	Ir	H(1)	85.4^d
Ir'	Ir	C(1)	124.7(5)	P(1)	Ir	P(2')	179.25(5)
Ir'	Ir	C(3)	145.9(4)	P(1)	Ir	C(1)	91.7(4)
Ir'	Ir	H(1)	35.0^d	P(1)	Ir	C(3)	89.5(4)
Cl	Ir	P(1)	88.20(8)	P(1)	Ir	H(1)	90.5^d
Cl	Ir	P(2')	91.64(8)	P(2')	Ir	C(1)	88.6(4)

(continued)

Table 4.4. (continued)

(b) Angles (deg)

Atom1	**Atom2**	**Atom3**	**Angle**
P(2')	Ir	C(3)	89.8(4)
P(2')	Ir	H(1)	90.2[d]
C(1)	Ir	C(3)	89.5(6)
C(1)	Ir	H(1)	89.7[d]
C(3)	Ir	H(1)	179.2[d]
Ir	Ir'	Cl	48.97(7)
Ir	Ir'	C(2)	128.7(5)
Ir	Ir'	C(5)	143.7(4)
Ir	Ir'	H(1)	35.0[d]
Cl	Ir'	P(1')	91.10(8)
Cl	Ir'	P(2)	89.65(8)
Cl	Ir'	C(2)	177.6(5)
Cl	Ir'	C(5)	94.8(4)
Cl	Ir'	H(1)	84.0[d]
P(1')	Ir'	C(2)	88.1(4)
P(1')	Ir'	C(5)	88.9(4)
P(1')	Ir'	H(1)	88.6[d]
P(2)	Ir'	C(2)	91.1(4)
P(2)	Ir'	C(5)	91.1(4)
P(2)	Ir'	H(1)	91.4[d]
C(2)	Ir'	C(5)	87.5(6)
C(2)	Ir'	H(1)	93.7[d]
C(5)	Ir'	H(1)	110.0[d]
Ir	Cl	Ir'	80.58(9)
Ir	P(1)	C(6)	111.5(2)
Ir'	P(2)	C(6)	109.4(2)
Ir	C(1)	O(1)	177(1)
Ir'	C(2)	O(2)	166(2)
Ir	C(3)	F(1)	116(1)
Ir	C(3)	C(4)	137(1)
F(1)	C(3)	C(4)	106(1)
F(2)	C(4)	F(3)	110(1)
F(2)	C(4)	C(3)	130(2)
F(3)	C(4)	C(3)	120(1)
P(1)	C(6)	P(2)	113.3(3)
Ir	H(1)	Ir'	110.0[d]

Primed atoms are related to unprimed ones via the crystallographic inversion center (0, 0, 0).

[b] Distance fixed during refinement.

[c] Nonbonded distance.

[d] Angle includes Ir-H distances fixed during refinement.

Although the observed disorder would normally preclude a discussion of bond lengths, the parameters involving the trifluorovinyl group give us confidence that our disordered model accounts accurately for the atom positions. The C-F bond lengths in compound **13** agree well with those of **11** and show the same trend

(C_β-F > C_α-F). In the geometry shown, both the trifluoroethenyl and methyl groups are opposite the bridging hydride ligand and might be expected to show somewhat elongated metal-carbon bonds owing to the high trans influence of the hydride ligand.[32] However, both of these bonds in **13** (Ir-C(3) = 2.02(1)Å, Ir'-C(5) = 2.15(1)Å) are actually somewhat *shorter* than the corresponding distances in **11** (2.090(6), 2.182(6)Å). It should be recalled however that metal-metal bonds can also display a significant trans influence,[33] which in these compounds appears to exceed that of the bridging hydride ligand. It may also be that the methyl and trifluorovinyl ligands in **11** are exerting a trans influence on each other *via* the metal-metal bond. The transmission of electronic effects from one metal to another in binuclear complexes has been observed.[34] All other parameters within the complex are as expected.

Attempts to replace the chloro ligand in **11** by a methyl group by reaction with methyl lithium also did not succeed, although in this case a reaction did occur. In the presence of a seven-fold excess of methyl lithium, 65% conversion to a new product **14** occurred (Scheme 4.2). However, NMR studies demonstrated that chloride replacement did not occur; instead, replacement of one fluorine on the trifluoroethenyl group by a methyl group occurred yielding $[Ir_2(CF{=}CFMe)(CH_3)(CO)(\mu\text{-}Cl)(\mu\text{-}CO)(dppm)_2][CF_3SO_3]$ (**14**). The ^1H NMR spectrum of **14** shows two methyl resonances. The signal at 1.22 ppm appears as a pseudo triplet and is assigned to the methyl group on the vinyl ligand, in which the coupling to both fluorine nuclei is essentially the same ($J_{FH} \simeq$ 12 Hz), whereas the higher-field resonance at 1.07 ppm is due to the methyl that is bound to one metal, showing coupling to two adjacent ^{31}P nuclei. Surprisingly, the two chemically inequivalent fluorine atoms of the methyl difluorovinyl group resonate at approximately the same chemical shift as a broad unresolved signal at -126 ppm, and this signal integrates well compared to that of the trifluoromethanesulfonate anion. The $^{13}C\{^1H\}$ NMR and the IR spectra are consistent with one terminal and one bridging carbonyl ligand. In order to establish which methyl group in **14** results from the Ir-bound methyl group in the precursor and which is obtained from methyl lithium, the ^{13}C-enriched precursor $[Ir_2(CF=CF_2)(^{13}CH_3)(^{13}CO)_2(\mu\text{-}Cl)(dppm)_2][CF_3SO_3]$ was reacted with unenriched MeLi. The product had the $^{13}CH_3$ group exclusively on iridium, with no significant $^{13}CH_3$ enrichment of the methyldifluoroethenyl group. Clearly, the iridium-bound methyl group remains on the metals, while replacement of a fluoride is effected by MeLi. In the $^{13}C\{^1H\}$ NMR spectrum of this $^{13}CH_3$-enriched sample the iridium-bound methyl signal appears at -24.8 ppm while that for the vinylic methyl group is at lower field (20.2 ppm) and is very weak since no enrichment occurred at this site (observation of the ^{13}C signal for the vinyl-substituted methyl group required overnight data acquisition). Both signals are broad and unresolved so coupling to ^{31}P or ^{19}F nuclei can not be determined.

Although spectroscopy clearly establishes the formation of a methyldifluoroethenyl group in **14**, it did not enable us to establish the geometry of this group or the relative positions of the methyl and vinyl ligands. However, these details were established by an X-ray structural determination of **14**, which is shown for the cation in Figure 4.3.

Relevant bond lengths and angles are given in Table 4.5. Two details immediately stand out in the structure of **14**; first, the methyl and methyldifluoroethenyl groups are mutually cis *on the same metal*, and second, fluoride substitution has occurred trans to the Ir-vinyl bond to give the trans isomer of the methyldifluoroethenyl group. The Ir-Ir distance (2.9603(4)Å) is substantially longer than a normal single bond (*cf.* 2.8116(3)Å in **11**), but is compressed compared to non-bonded distances in comparable compounds, for which separations are usually substantially greater than 3Å. This Ir(1)-Ir(2) separation is also less than the non-bonded intraligand P(1)-P(2) and P(3)-P(4) separations of 3.057(3) and 3.113(3)Å, respectively, indicating some compression along the metal-metal axis. The bonding can therefore be considered in terms of two extremes. In the first scenario the metals are non-bonded and the bridging carbonyl is semibridging, in which it is primarily bound to Ir(2) while simultaneously functioning as a π acceptor from Ir(1). This view is consistent with the long Ir(1)-Ir(2) separation noted and with the unsymmetrical geometry of the bridging carbonyl (Ir(2)-C(2) = 2.083(8)Å, Ir(1)-C(2) = 2.116(8)Å; Ir(2)-C(2)-O(2) = 141.5(7)°, Ir(1)-C(2)-O(2) = 128.5(6)°), which is more linear with respect to the metal to which it is more strongly bound. In the second extreme a symmetrically bridging carbonyl would be accompanied by an Ir-Ir bond.

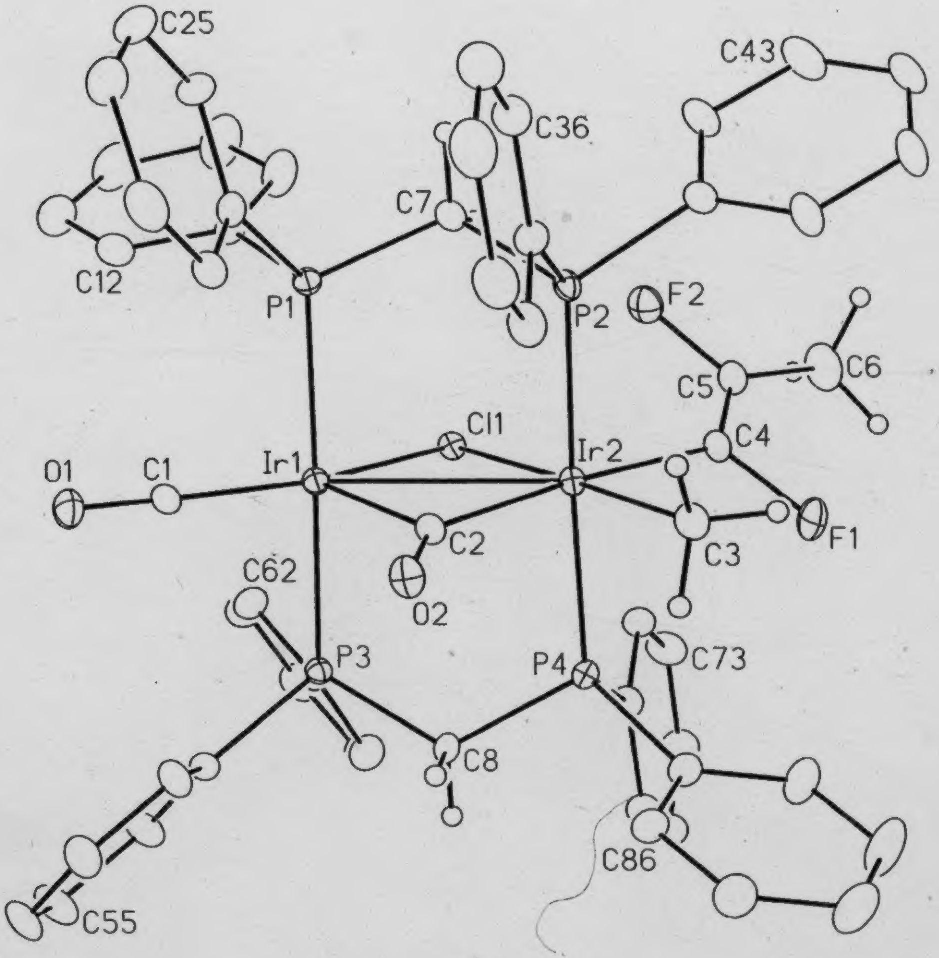
C25
C43
C36
C7
C12
P1
P2
F2
C6
C5
Cl1
C4
O1
C1
Ir1
Ir2
F1
C2
C3
C62
O2
P3
P4
C73
C8
C86
C55

Figure 4.3. Perspective view of the $[Ir_2(CF{=}C(F)CH_3)(CH_3)(CO)_2(\mu\text{-}Cl)(dppm)_2]^+$ cation of complex **14** showing the atom-labeling scheme. Thermal parameters are as described for Figure 4.1.

Table 4.5. Selected Interatomic Distances and Angles for Compound **14**.

(a) Distances (Å)

Atom1	*Atom2*	*Distance*	*Atom1*	*Atom2*	*Distance*
Ir(1)	Ir(2)	2.9603(4)	P(1)	P(2)	3.057(3)a
Ir(1)	Cl(1)	2.401(2)	P(1)	C(7)	1.828(8)
Ir(1)	P(1)	2.358(2)	P(2)	C(7)	1.840(9)
Ir(1)	P(3)	2.349(2)	P(3)	P(4)	3.133(3)[a]
Ir(1)	C(1)	1.834(8)	P(3)	C(8)	1.818(8)
Ir(1)	C(2)	2.116(8)	P(4)	C(8)	1.829(8)
Ir(2)	Cl(1)	2.552(2)	F(1)	C(4)	1.40(1)
Ir(2)	P(2)	2.358(2)	F(2)	C(5)	1.39(1)
Ir(2)	P(4)	2.361(2)	O(1)	C(1)	1.14(1)
Ir(2)	C(2)	2.083(8)	O(2)	C(2)	1.158(9)
Ir(2)	C(3)	2.099(8)	C(4)	C(5)	1.30(1)
Ir(2)	C(4)	2.066(8)	C(5)	C(6)	1.48(1)

(b) Angles (deg)

Atom1	*Atom2*	*Atom3*	*Angle*	*Atom1*	*Atom2*	*Atom3*	*Angle*
Ir(2)	Ir(1)	Cl(1)	55.68(5)	Ir(1)	Ir(2)	Cl(1)	50.99(4)
Ir(2)	Ir(1)	P(1)	91.05(5)	Ir(1)	Ir(2)	P(2)	90.36(5)
Ir(2)	Ir(1)	P(3)	92.19(5)	Ir(1)	Ir(2)	P(4)	92.02(5)
Ir(2)	Ir(1)	C(1)	147.8(2)	Ir(1)	Ir(2)	C(2)	45.6(2)
Ir(2)	Ir(1)	C(2)	44.7(2)	Ir(1)	Ir(2)	C(3)	132.4(2)
Cl(1)	Ir(1)	P(1)	84.70(7)	Ir(1)	Ir(2)	C(4)	140.0(2)
Cl(1)	Ir(1)	P(3)	87.25(7)	Cl(1)	Ir(2)	P(2)	93.87(7)
Cl(1)	Ir(1)	C(1)	156.5(3)	Cl(1)	Ir(2)	P(4)	88.17(6)
Cl(1)	Ir(1)	C(2)	100.0(2)	Cl(1)	Ir(2)	C(2)	96.3(2)
P(1)	Ir(1)	P(3)	167.60(7)	Cl(1)	Ir(2)	C(3)	175.5(2)
P(1)	Ir(1)	C(1)	92.6(3)	Cl(1)	Ir(2)	C(4)	89.2(2)
P(1)	Ir(1)	C(2)	101.6(2)	P(2)	Ir(2)	P(4)	177.52(7)
P(3)	Ir(1)	C(1)	91.0(3)	P(2)	Ir(2)	C(2)	92.8(2)
P(3)	Ir(1)	C(2)	89.1(2)	P(2)	Ir(2)	C(3)	89.2(2)
C(1)	Ir(1)	C(2)	103.4(3)	P(2)	Ir(2)	C(4)	89.0(2)

(continued)

Table 4.5. (continued)

(b) Angles (deg)

Atom1	*Atom2*	*Atom3*	*Angle*	*Atom1*	*Atom2*	*Atom3*	*Angle*
P(4)	Ir(2)	C(2)	88.3(2)	Ir(2)	P(4)	C(8)	111.1(3)
P(4)	Ir(2)	C(3)	88.7(2)	Ir(1)	C(1)	O(1)	177.6(7)
P(4)	Ir(2)	C(4)	89.6(2)	Ir(1)	C(2)	Ir(2)	89.7(3)
C(2)	Ir(2)	C(3)	86.8(3)	Ir(1)	C(2)	O(2)	128.5(6)
C(2)	Ir(2)	C(4)	174.1(3)	Ir(2)	C(2)	O(2)	141.5(7)
C(3)	Ir(2)	C(4)	87.6(3)	Ir(2)	C(4)	F(1)	115.7(6)
Ir(1)	Cl(1)	Ir(2)	73.33(5)	Ir(2)	C(4)	C(5)	132.3(7)
Ir(1)	P(1)	C(7)	112.9(3)	F(1)	C(4)	C(5)	111.6(7)
Ir(2)	P(2)	C(7)	108.4(3)	F(2)	C(5)	C(4)	117.1(7)
Ir(1)	P(3)	C(8)	111.2(3)	F(2)	C(5)	C(6)	111.4(8)
				C(4)	C(5)	C(6)	131.4(9)
				P(1)	C(7)	P(2)	113.0(4)
				P(3)	C(8)	P(4)	118.4(4)

[a] Nonbonded distance

The observed structure is probably best described as lying somewhere between the two extremes. In the former description the geometry about Ir(2) is octahedral while that about Ir(1) is tetragonal pyramidal having the weaker π interaction to the semibridging carbonyl in the apical site.

Both the Ir-vinyl and Ir-methyl bonds in **14** (2.066(8), 2.099(8)Å, respectively) are shorter than the analogous distances in **11** (2.090(6), 2.182(6)Å) probably reflecting the movement of these groups away from their locations in **11** opposite the Ir-Ir bond (recall our argument earlier about the high trans influence of this bond). In **14** the trans influence of the methyl group appears responsible for the significantly longer Ir(2)-Cl(1) bond compared to Ir(1)-Cl(1) (2.552(2) *vs.* 2.401(2)Å). Within the methyldifluoroethenyl group, both C-F bonds are essentially identical, and consistent with earlier arguments, removal of a fluorine substituent from **11** has resulted in a lengthening of the remaining C-F bond on the β-carbon.

Discussion

As noted earlier, our one-time observation that geminal C-H and C-F activation of trifluoroethene by the diiridium complex **1** yielded a difluorovinylidene group[7] prompted us to investigate related trifluoroethenyl and 2,2-difluoroethenyl complexes in order to gain information on the order of C-H *vs.* C-F activation in partially fluorinated olefins. If C-H activation of trifluoroethene occurred first, we were interested in determining how the adjacent metals effected subsequent C-F activation of the resulting trifluoroethenyl group. Similarly, if C-F activation was first, the resulting 2,2-difluoroethenyl group would yield a difluorovinylidene group by subsequent C-H activation.

The targeted trifluorovinyl and 2,2-difluorovinyl complexes, $[Ir_2(R)(CH_3)(CO)_2(\mu\text{-}X)(dppm)_2][CF_3SO_3]$ (R = $FC{=}CF_2$, X = Cl (**11**); R = $HC{=}CF_2$, X = Br (**12**)) were readily prepared by the oxidative addition of $ClFC{=}CF_2$ and $BrHC{=}CF_2$, respectively, to $[Ir_2(CH_3)(CO)(\mu\text{-}CO)$-

(dppm)$_2$][CF$_3$SO$_3$] (**1**). The structure of both species has the fluoroethenyl and the methyl groups on the outside of the complex, essentially opposite the metal-metal bond. Unfortunately, this is not a suitable position for activation of the fluoroethenyl substrates by the adjacent metal, and attempts to induce such activation in these halide-bridged species, under refluxing conditions (CH_2Cl_2 or THF solvent) failed. Attempts to substitute the bridging chloride ligand in **11** by hydride, in order to give species analogous to that proposed in an initial C-H activation of trifluoroethene failed with a number of hydride sources. Furthermore, attempts to remove the chloride ligand using Lewis acids such as $(CH_3)_3SiOSO_2CF_3$ also failed. The only reaction observed in these cases was protonation of **11**, by the acids derived from hydrolysis of the Lewis acid by adventitious water. It is noteworthy that protonation of **11** did not result in subsequent reductive elimination of either methane or trifluoroethene. However, protonation at the metal-metal bond, as observed, leaves the hydride trans to both organic ligands and unable to readily eliminate. Given the facile protonation of **11**, it is perhaps surprising that analogous methylation by methyl trifluoromethanesulfonate did not occur, although we have previously observed that similar cationic species can be basic enough to be protonated, yet remain unreactive to the weaker electrophile, methyl trifluoromethanesulfonate.

In an attempt to replace the bridging chloride ligand in **11** by a methyl group using methyl lithium, one of the fluorines on the trifluoroethenyl group was instead replaced. We were initially surprised that replacement of an olefin-bound fluorine was preferred to replacement of the metal-bound chloride, and were also subsequently surprised by the stereoselective replacement of the fluorine trans to iridium, and by the final geometry of the complex in which both the methyldifluoroethenyl group and the methyl ligand are mutually cis on the same metal. Clearly transfer of either the methyl or the vinyl group from one metal to the other has occurred.

Substitution on vinyl fluorides by strong nucleophiles has been reported to proceed by an addition-elimination sequence to give the substituted vinyl derivative.[35] It is reasonable to expect nucleophilic attack to occur at the β-carbon which should be more electrophilic as a consequence of the two fluorine substituents. The transfer of the vinyl group in **11** to the metal bearing the methyl group in **14** suggests a bridging arrangement for this vinylic group at some stage. We therefore suggest that nucleophilic attack is accompanied by movement of the resulting fragment to the bridging site yielding a fluorocarbene-bridged (**B**) as shown in Scheme 4.3 (dppm ligands are omitted for clarity). Analogous fluorocarbene-bridged species have been reported.[10] Subsequent loss of fluoride ion (as LiF), with movement of the new methyl-substituted vinyl group to the second metal, would yield the observed product (**14**) as shown. Alternately, nucleophilic attack on a putative trifluorovinyl-bridged intermediate would yield the same fluorocarbene-bridged species (**B**). Although bridging vinyl groups have not been observed in the chemistry reported herein, binuclear complexes containing such groups are well

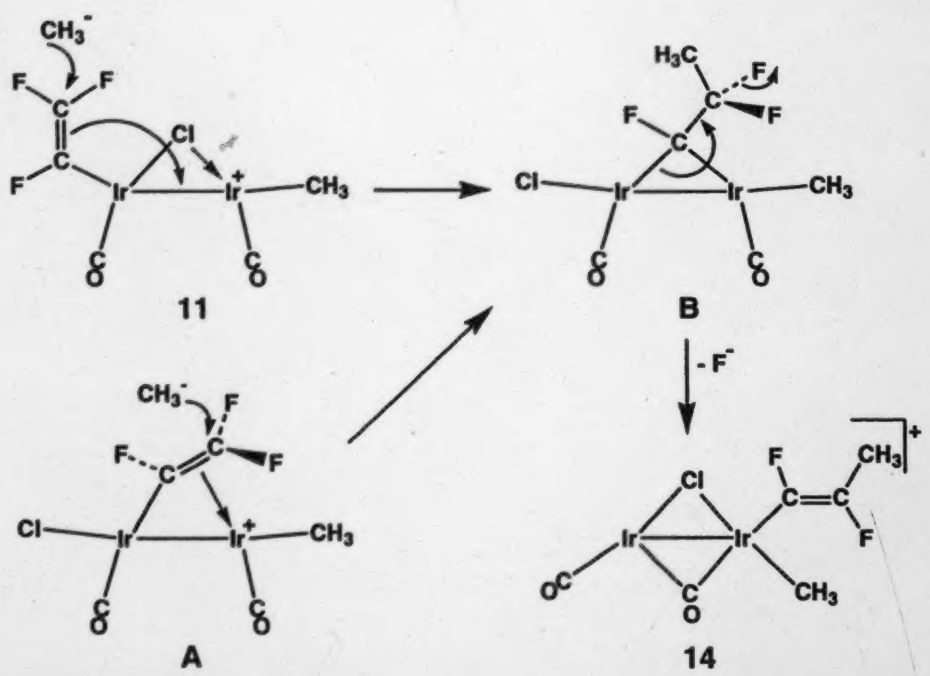

Scheme 4.3. Reaction of $[Ir_2(CF{=}CF_2)(CH_3)(CO)_2(\mu\text{-}Cl)(dppm)_2][CF_3SO_3]$ with methyl lithium forming $[Ir_2(CF{=}CFMe)(CH_3)(CO)(\mu\text{-}Cl)(\mu\text{-}CO)(dppm)_2][CF_3SO_3]$ (**14**).

documented.[36] Consequently, an intermediate such as **A** cannot be ruled out in the transformation of **11** to **14**. This scheme does not explain the trans arrangement of substituents on the vinyl group, however, we note that other related substitutions on fluorovinyl groups also gave trans products.[11,12,13b] This may result from steric factors favoring a trans arrangement of the bulkier methyl and metal substituents.

The mutually cis arrangement of methyl and vinyl ligands on the same metal suggests the possibility of reductive elimination of *trans*-2,3-difluoro-2-butene generating the known[37] A-frame complex cation $[Ir_2(CO)_2(\mu\text{-}Cl)(dppm)_2]^+$.

Certainly, the reductive elimination involving unsaturated substrates is known to be more facile than that involving saturated substrates.[38] This has not been achieved under relatively mild conditions (refluxing CH_2Cl_2), presumably reflecting the strong Ir-fluorovinyl bond,[24] but attempts will be made to promote reductive elimination through the use of oxidizing agents.[39]

Conclusions

Although binuclear complexes containing the trifluoroethenyl and 2,2-difluoroethenyl ligands have been synthesized, attempts to activate the C-F and C-H bonds on the α-carbons of these ligands by the adjacent metal have failed. Certainly one factor inhibiting the targeted activation steps is the location of the fluoroethenyl groups on the outside of the respective complexes, in a position remote from the adjacent metal. Attempts to replace or remove the bridging chloride ligand in **11** in attempts to bring the trifluorovinyl group towards the bridging site have failed. Subsequent studies will be aimed at related complexes in which halide removal or replacement can be achieved in order to probe the functions of adjacent metals in the activation of fluorocarbyl groups.

We have discovered that the fluorine atom trans to Ir in the trifluorovinyl complex **11** can be selectively replaced by a methyl group and we propose that this occurs via a fluorocarbene-bridged intermediate.

References and Footnotes

1. A version of this chapter has been accepted for publication: Ristic-Petrovic, D.; Wang, M.; McDonald, R.; Cowie, M. *Organometallics*, **2002**, *21*.
2. (a) Intergovernmental Panel on Climate Change, *Climate Change - The IPCC Scientific Assessment*, Cambridge U. Press, Cambridge **1990**.
   (b) Zurer, P. *Chem. Eng. News* **1993**, *71*, 16.
3. Ravishankara, A.R.; Soloman, S.; Turnipseed, A.A.; Warren, R.F. *Science* **1993**, *259*, 194.
4. (a) *Biochemistry Involving the Carbon-fluorine Bond*, Filler, R. (Ed); American Chemical Society, Washington, DC 1976.
   (b) *Selective Fluorination in Organic and Bioorganic Chemistry*, Welch, J.T. (Ed) American Chemical Society, Washington, DC 1991.
5. (a) Smart, B.E. *Mol. Struct. Energ.* **1986**, *3*, 141.
   (b) McMillen, D.F.; Golden, D.M. *Annu. Rev. Phys. Chem.* **1982**, *33*, 493.
6. Satai, P. (ed.) *The Chemistry of the Carbon-Halogen Bond, Part 1*, J. Wiley and Sons, New York, 1973, p. 416.
7. (a) Ristic-Petrovic, D.; Cowie, M. unpublished results.
   (b) Although an X-ray structure determination of the product from our initial attempt clearly indicated a bridging difluorovinylidene group, we have been unable to duplicate this result subsequently.
8. Ristic-Petrovic, D.; Torkelson, J.R.; Hilts, R.W.; McDonald, R.; Cowie, M. *Organometallics* **2000**, *19*, 1432.

9. (a) Hughes, R.P.; Kovacik, I.; Lindner, D.C.; Smith, J.M.; Willemsen, S.; Zhang, D.; Guzei, I.A.; Rheingold, A.L. *Organometallics* **2001**, *20*, 3190.
   (b) Siedle, A.R.; Newmark, R.A. *Organometallics* **1989**, *8*, 1442.
10. (a) Booth, R.L.; Haszeldine, R.N.; Mitchell, R.R.; Cox, J.J. *J. Chem. Soc. Chem. Commun.* **1967**, 529.
    (b) Bonnet, J.J.; Mathieu, R.; Poilblanc, R.; Ibers, J.A. *J. Am. Chem. Soc.* **1979**, *101*, 7487.
11. Tamborski, C.; Soloski, E.J.; de Pasquale, R.J. *J. Organomet. Chem.* **1968**, *15*, 494.
12. (a) Seyferth, D.; Wada, T. *Inorg. Chem.* **1962**, *1*, 78.
    (b) Martin, S.; Sauvetre, R.; Normant, J.-F. *Tet. Lett.* **1983**, *24*, 5615.
13. (a) de Cadenet, K.G.; Rumin, R.; Pétillon, F.Y.; Yufit, D.S.; Muir, K.W. *Eur. J. Inorg. Chem.* **2002**, 639. (b) Peterson, T.H.; Golden, J.T.; Bergman, R.G. *Organometallics* **1999**, *18*, 2005. (c) Fujiwara, M.; Ichikawa, J.; Okauchi, T.; Minami, T. *Tet. Lett.* **1999**, *40*, 7261. (d) de Cadenet, K.G.; Rumin, R.; Pétillon, F.Y. *Organometallics* **2000**, *19*, 1912.
14. Torkelson, J.R.; Antwi-Nsiah, F.H.; McDonald, R.; Cowie, M.; Pruis, J.G.; Jalkanen, K.J.; DeKock, R.L. *J. Am. Chem. Soc.* **1999**, *121*, 3666.
15. (a) Torkelson, J.R., Ph.D. Thesis, University of Alberta **1998**, Chapter 5.
    (b) Torkelson, J.R.; Oke, O.; Muritu, J.; McDonald, R.; Cowie, M. *Organometallics* **2000**, *19*, 854.
16. Programs for diffractometer operation, data collection, data reduction and absorption correction were those supplied by Bruker.

17. Beurskens, P.T.; Beurskens, G.; Bosman, W.P.; deGelder, R.; Garcia Granda, S.; Gould, R.O.; Israel, R.; Smits, J.M.M. (1996). The *DIRDIF-96* program system. Crystallography Laboratory, University of Nijmegen, The Netherlands.

18. Sheldrick, G.M. *SHELXL-93.* Program for crystal structure determination. University of Göttingen, Germany, 1993.

19. Sheldrick, G.M. *Acta Crystallogr.* **1990**, *A46*, 467-473.

20. Dungan, C.H.; van Wazer, J.R. "Compilation of Reported F19 NMR Chemical Shifts", Wiley-Interscience, New York, 1970.

21. Rest, A.J.; Rosevear, D.T.; Stone, F.G.A. *J. Chem. Soc. (A)* **1967**, 66.

22. Banger, K.K.; Brisdon, A.K.; Gupta, A. *Chem. Commun.* **1997**, 139.

23. Peters, D. *Chem. Phys.* **1963** *38*, 561.

24. (a) Kiplinger, J.L.; Richmond, T.G.; Osterberg, C.E. *Chem. Rev.* **1994**, *94*, 373. (b) Brothers, P.J.; Roper, W.R. *Chem. Rev.* **1988**, *88*, 1293.

25. Sterenberg, B.T.; McDonald, R.; Cowie, M. *Organometallics* **1997**, *16*, 2297.

26. Sutherland, B.R.; Cowie, M. *Organometallics* **1985**, *4*, 1801.

27. Vaartstra, B.A.; Cowie, M. *Organometallics* **1990**, *9*, 1594.

28. Allen, F.H.; Kennard, O.; Watson, D.G.; Brammer, L.; Orpen, A.G.; Taylor, R. *J. Chem. Soc. Perkin Trans.* **1987**, 51.

29. Collman, J.P.; Hegedus, L.S.; Norton, J.R.; Finke, R.G. In *Principles and Applications of Organotransition Metal Chemistry*, University Science Books: Mill Valley CA, 1987; Section 5.5.

30. Manatt, S.L.; Bowers, M.T. *J. Am. Chem. Soc. 1969*, 91, *4381.*

31. (a) Churchill, M.R.; deBoer, B.G.; Rotella, F.J. *Inorg. Chem.* **1976**, *15*, 1843. (b) Teller, R.G.; Bau, R. *Structure and Bonding* **1981**, *44*, 1.

32. Huheey, J.E.; Keiter, E.A.; Keiter, R.L. *Inorganic Chemistry, Principles of Structure and Reactivity*, 4th ed.; Harper Collins, New York, NY 1993, Chapter 13.

33. (a) Sutherland, B.R.; Cowie, M. *Organometallics* **1984**, *3*, 1869. (b) Cowie, M.; Dwight, S.K. *Inorg. Chem.* **1980**, *19*, 209. (c) Cowie, M.; Gibson, J.A.E. *Organometallics* **1984**, *3*, 984. (d) Farr, J.P.; Olmstead, M.M.; Balch, A.L. *Inorg. Chem.* **1983**, *22*, 1229.

34. (a) Cowie, M.; Vasapollo, G.; Sutherland, B.R.; Ennett, J.P. Ennett, J.P. *Inorg. Chem.* **1986**, *25*, 2648. (b) Sola, E.; Torres, F.; Jimenez, M.V.; López, J.A.; Ruiz, S.E.; Lahoz, F.J.; Elduque, A.; Oro, L.A. *J. Am. Chem. Soc.* **2001**, *123*, 11925. (c) Rowsell, B.D.; Tepanier, S.J.; Lam, R.; McDonald, R.; Cowie, M. *Organometallics* **2002**, *21*, 3228.

35. March, J. In *Advanced Organic Chemistry*; John Wiley & Sons: New York, 1985; p671.

36. See for example: (a) Knox, S.A.R.; *J. Organomet. Chem.* **1990**, *400*, 255, and references therein. (b) Akita, M.; Hua, R.; Knox, S.A.R.; Moro-oka, Y.; Nakanishi, S.; Yates, M.I., *Chem. Commun.* **1997**, 51. (c) Nubel, P.O.; Brown, T.L. *J. Am. Chem. Soc.* **1984**, *106*, 3474. (d) Casey, C.P.; Meszaros, M.W.; Fagan, P.J.; Bly, R.K.; Colborn, R.E. *J. Am. Chem. Soc.* **1986**, *108*, 4053. (e) Casey, C.P.; Austin, E.A.; Rheingold, A.L. *Organometallics* **1987**, *6*, 2157. (f) Casey, C.P.; Austin, E.A. *J. Am. Chem.*

Soc. **1988**, *110*, 7106. (g) Cao, D.H.; Stang, P.J.; Arif, A.M. *Organometallics* **1995**, *14*, 2733. (h) Ting, C.; Messerle, L. *J. Am. Chem. Soc.* **1987**, *109*, 6506. (i) Suzuki, H.; Omori, H.; Lee, D.H.; Yoshida, Y.; Fukushima, M.; Tanaka, M.; Moro-oka, Y. *Organometallics* **1984**, *13*, 1129.

37. Sutherland, B.R.; Cowie, M. *Inorg. Chem.* **1984**, *23*, 2324.
38. Calhorda, M.J.; Brown, J.M.; Cooley, N.A. *Organometallics* **1991**, *10*, 1431.
39. Collman, J.P.; Hegedus, L.S.; Norton, J.R.; Finke, R.G. In *Principles and Applications of Organotransition Metal Chemistry*, University Science Books: Mill Valley CA, 1987; p324.

Chapter 5

Complexes containing the dmpm ligand

Introduction

In an earlier study it was reported that 1,3-butadiene reacted with the diiridium complex, $[Ir_2(CH_3)(CO)(\mu\text{-}CO)(dppm)_2][CF_3SO_3]$ (**1**) to yield the vinylvinylidene-bridged product $[Ir_2(CH_3)(H)(CO)_2(\mu\text{-}H)(\mu\text{-}CC(H)C(H)CH_2)(dppm)_2][CF_3SO_3]$ (**6B**) by the double activation of a pair of geminal C-H bonds at one end of the butadiene molecule.[1, 2] In attempts to discover how the two metal centres were involved in the double activation process we probed the reaction at low temperatures and observed the butadiene adduct $[Ir_2(CH_3)(CO)_2(\mu\text{-}\eta^2\text{:}\eta^2\text{-}H_2C{=}CH\text{-}CH{=}CH_2)(dppm)_2][CF_3SO_3]$ (**6A**) (see Chapter 2).[1] However, we were unable to determine the relationship of this adduct to the final product since the π adduct is labile, binding butadiene reversibly even at -50 °C, while the C-H activation process is slow, requiring days at room temperature. We therefore sought ways to both stabilize the π adduct and to facilitate the C-H activation steps, hopefully bringing both processes onto comparable time scales. One strategy for achieving both of these goals was to replace the bridging dppm ligands of **1** by dmpm. The smaller methyl substituents in dmpm should facilitate access of 1,3-butadiene to the metals and the reduced steric repulsions should stabilize the 1,3-butadiene adduct. Moreover, the complex containing the more basic dmpm ligands should favour oxidative addition over the complex containing dppm.

The targeted dmpm analogue of **1**, namely $[Ir_2(CH_3)(CO)_2(dmpm)_2][CF_3SO_3]$ (**1-dmpm**) has been reported,[3, 4] however, in our hands all attempts to duplicate its synthesis met with failure. In addition, monitoring the reaction by ^{31}P NMR spectroscopy indicated that complex mixtures of species were present at most stages of the reaction, from which the successful isolation of **1-dmpm** in a repeatable manner seemed unlikely. It also became clear that subtle changes in reaction conditions give rise to substantially different results. We therefore set out to characterize some of the species obtained in this reaction in order to gain a better understanding of the differences between dmpm and dppm in these binuclear complexes and to achieve a rational synthesis of **1-dmpm**.

Experimental

General Comments. All solvents were dried (using appropriate drying agents), distilled before use and stored under dinitrogen. Deuterated solvents used for NMR experiments were freeze-pump-thaw degassed (three cycles) and stored under nitrogen or argon over molecular sieves. Reactions were carried out under argon using standard Schlenk techniques, and compounds that were used as solids were purified by recrystallization. Prepurified argon, nitrogen and carbon monoxide were purchased from Linde. All purchased gases were used as received. The compound bis(dimethylphosphino)methane was purchased from

Strem. All other reagents were obtained from Aldrich and were used as received. The compounds $[IrCl(COD)]_2$ and $[IrCl(CO)(PPh_3)_2]$ were prepared using standard procedures.[7, 8]

Proton NMR spectra were recorded on Varian Unity 400, 500 or 600 spectrometers, or on a Bruker AM400 spectrometer. Phosphorus and fluorine spectra were recorded on Varian Unity 400 or Bruker AM400 spectrometers. Two-dimensional NMR experiments (COSY and TOCSY) were obtained on Varian Unity 400 or 500 spectrometers. Infrared spectra were obtained on a Bio-Rad RTS-60 Fourier transform infrared spectrometer as solutions in KCl cells with 0.5-mm-window path lengths, or as solids using a Nicolet Magna 750 with a Nic-Plan infrared microscope. Carbonyl stretches reported are for non-isotopically enriched samples. Mass spectrometric analyses were performed by positive ion electrospray ionization on a Micromass ZabSpec Hybrid Sector-TOF. Elemental analyses were performed by the microanalytical service within the department. Spectroscopic data for all compounds are given in Table 5.1. Except as noted, satisfactory elemental analyses were not obtained on the majority of the compounds because of their extreme air sensitivity and because their insolubility in solvents with which they do not react precluded preparative scale recrystallization.

Preparation of Compounds. (a) $[Ir_2(CO)_4(dmpm)_2]$ (15). A solution containing 408.5 mg of $[IrCl(COD)]_2$ (0.608 mmol) in 40 mL of THF was cooled in solid CO_2/acetone to -78 °C. To this stirred solution was added 200 µL of dmpm, (1.26 mmol) causing a yellow precipitate to form. Carbon monoxide was passed over the solution and the cooling bath was removed. As the mixture warmed to room temperature the solids dissolved yielding a burgundy solution. At this time, 0.5 mL of liquid Na/K alloy (1:1 mole ratio of Na to K) was added and stirring was continued under CO for 18 h, after which a yellow solution and gray precipitate remained. The IR spectrum of the supernatant showed quantitative conversion to $[Ir_2(CO)_4(dmpm)_2]$.[9] The supernatant was decanted and filtered through a pad of Celite on a glass fritte, and the contents of the reaction vessel extracted with a further 3 X 20 mL of THF. The combined filtrates were reduced *in vacuo* to an 88% yield of an orange glass, which was shown to be the only observed ^{31}P-containing product by ^{31}P NMR spectroscopy, and was identified as **15** based on a comparison of its spectral parameters with those reported [9]

Table 5.1. Spectroscopic data for the compounds

compound	$\delta(^{31}P\{^1H\})$[c]	$\delta(^1H)$[d]	IR, cm^{-1} [g,l]	MS: *m/z*
$[Ir_2(CO)_4(dmpm)_2]$ **(15)**	-65.4 (s) [m]	3.46 (q, 4H), 1.80 (s, 24H) [m]	1954 (m), 1927 (s), 1891 (s), 1863 (w)[n]	
$[Ir_2(CH_3)_2(CO)_4(dmpm)_2][CF_3SO_3]_2$ **(16)**	-42.2 ppm (s)[f]	3.43 (m, 4H), 2.06 (m, 24H), 1.12 (t, $^3J_{PH}$ = 7.0 Hz)[f]	2009 (s)[h]	399.0 (M^{2+})
$[Ir_2Cl(CO)(\mu\text{-}CO)(dmpm)_3][Cl]$ **(17)**	δ = -28.4 (m, 2P); -32.3 (dt, 1P, $^2J_{PP}$ = 185 Hz, $^2J_{PP}$ = 28 Hz); -36.7 (m, 2P); -52.0 (dt, $^2J_{PP}$ = 185 Hz, $^2J_{PP}$ = 16 Hz).	3.42 (m, 2H); 3.25 (m,2H); 2.83 (m, 2H); 1.68 - 1.98 (24 H)	1956 (s), 1722 (m)[i]	909 (M^+ + Na)
$[Ir(COD)(dmpm)_2]Cl$ **(18)**	-7.20 (d, 1P, $^2J_{PP}$ = 30 Hz); -50.8 (dt, 1P, $^2J_{PP}$ = 30 Hz, $^2J_{PP}$ = 14 Hz), -86.4 (d, 2P, $^2J_{PP}$ = 14 Hz)	3.80 (b, 2H),m 3.17 (b, 4H), 3.02 (m, 2H), 2.45 (b, 8H), 2.21 (d, 6H, $^2J_{PH}$ = 6.0 Hz), 1.91 (m, 6H), 1.69 (m, 6H), 1.62 (d, $^2J_{PH}$ = 5.5 Hz)		437 (M^+ - dmpm)
$[Ir_2(CH_3)Cl_2(CO)_2(dmpm)_2][CF_3SO_3]$ **(19)**	-12.2 (m), -29.2 (m)	3.24 (m, 2H), 3.08 (m, 2H), 1.72-2.00 (m, 24 H), 1.04 (t, 3H, $^3J_{PH}$ = 8 Hz)	1967 (s)[i]	799 (M^+)
$[Ir_2Cl_4(CO)_2(dmpm)_2]$ **(20)**.	-27.4 (m), -31.6 (m)	3.42 (m, 2H), 3.25 (m, 2H), 1.70-2.16 (m, 24H)		

Notes: [a] NMR abbreviations: s = singlet, d = doublet, t = triplet, q = quintet, m = multiplet, b = broad. [b] NMR data in CD_2Cl_2 unless otherwise stated. [c] $^{31}P\{^1H\}$ chemical shifts are referenced vs. external 85% H_3PO_4 [d] ^1H chemical shifts are referenced vs. external TMS. [f]. CD_3NO_2 [g] ν(CO) [h] Nujol [i] CH_2Cl_2 [j] C_6H_6 [k] C_6D_6 [l] IR abbreviations: s = strong, m = medium, w = weak [m] Data from ref. 9 [n] THF

(b) $[Ir_2(CH_3)_2(CO)_4(dmpm)_2][CF_3SO_3]_2$ (16). To a solution of 81 mg (0.11 mmol) of $[Ir_2(CO)_4(dmpm)_2]$ in 10 mL of nitromethane was added 28 μL (0.22 mmol) methyl trifluoromethanesulfonate in 5 mL of nitromethane causing the solution to change rapidly from orange to yellow. The solution was stirred overnight whereupon it was reduced *in vacuo* to *ca.* 5 mL. Et_2O (20 mL) was added to precipitate a brown oil, which was dried *in vacuo* to yield 75 mg of a brown glass.

(c) $[Ir_2Cl(CO)(\mu\text{-}CO)(dmpm)_3][Cl]$ (17). 0.475 mL (3.0 mmol) of dmpm was added dropwise to a stirred suspension of $[Ir(Cl)(CO)(PPh_3)_2]$ (1.18 g, 1.5 mmol) in 60 mL of benzene resulting in a lemon-yellow powder and nearly colourless supernatant. The supernatant was decanted and the solid was washed with 20 mL of benzene followed by 20 mL of Et_2O. After drying overnight *in vacuo*, a 91% yield of lemon-yellow microcrystalline powder was obtained. Analysis calculated for $Ir_2Cl_2O_2P_6C_{17}H_{42}$: C, 22.20, H 4.60, Cl 7.71; Found: C, 21.78, H 4.73, Cl, 7.87.

(d) $[Ir(COD)(dmpm)_2]Cl$ (18). To a stirred solution of $[IrCl(COD)]_2$ (143 mg; 0.21 mmol) in 35 mL of CH_2Cl_2, a solution of dmpm (40 μL; 0.25 mmol) in 35 mL of CH_2Cl_2 was added dropwise, over 15 min. The resulting yellow solution was reduced *in vacuo* to 5 mL. 20 mL of Et_2O was added to precipitate a yellow powder, which was further washed with 20 mL of pentane and then dried in vacuo to afford 98 mg (76 %) of lemon-yellow **18**.

(e) $[Ir_2(CH_3)Cl_2(CO)_2(dmpm)_2][CF_3SO_3]$ (19). To a solution of 55 mg of $[IrCl(COD)]_2$ (0.082 mmol), dissolved in 30 mL of CH_2Cl_2 was added dmpm (25 µL, 0.016 mmol) yielding a yellow solution. CO was passed over the solution for 1 min. The excess CO was removed by three cycles of pumping under vacuum followed by admitting Ar to the reaction mixture. To the resulting red solution was added 10 µL methyl trifluoromethanesulfonate (0.078 mmol), causing an immediate colour change to yellow. The solution was reduced *in vacuo* to *ca.* 5 mL and Et_2O was added to precipitate 58 mg (75 %) of yellow microcrystalline compound **19**.

(f) $[Ir_2Cl_4(CO)_2(dmpm)_2]$ (20). A solution consisting of *ca.* 30 mg of $[Ir_2(CH_3)(Cl_2)(CO)_2(dmpm)_2][CF_3SO_3]$ (**19**) in 0.7 mL of CD_2Cl_2 was allowed to stand in an NMR tube overnight, yielding complete conversion to compound **20** (by ^1H and ^{31}P NMR).

Table 5.2. Crystallographic Experimental Details for compounds **16**, **17** and **20**.

A. Crystal Data			
formula	$C_{24}H_{46}F_6Ir_2O_{12}P_4S_2$	$C_{19}H_{46}Cl_6Ir_2O_2P_6$	$C_{12.5}H_{29}Cl_5Ir_2O_2P_4$
formula weight	1213.01	1089.48	896.89
crystal dimensions (mm)	0.41 × 0.36 × 0.15	0.49 × 0.33 × 0.32	0.57 × 0.12 × 0.10
crystal system	triclinic	monoclinic	orthorhombic
space group	$P\bar{1}$ (No. 2)	$P2_1/n$ (an alternate setting of $P2_1/c$ [No. 14])	*Pbcn* (No. 60)
unit cell parameters[a]			
a (Å)	8.9815 (5)	8.9735 (7)	30.2861 (19)
b (Å)	11.4386 (7)	19.6999 (14)	13.4542 (8)
c (Å)	11.8183 (7)	20.9679 (14)	12.6612 (8)
β (deg)	64.1746 (9)	91.2714 (13)	
V (Å^3)	79.6330 (11)	3705.7 (5)	5159.1 (6)
Z	67.8402 (9)	4	8
ρ_{calcd} (g cm^{-3})	1011.99 (10)	1.953	2.309
μ (mm^{-1})	1	7.884	11.08
	1.990		
	6.908		
B. Data Collection and Refinement Conditions			
diffractometer	Bruker P4/RA/SMART 1000 CCD[b]	Bruker P4/RA/SMART 1000 CCD[b]	Bruker PLATFORM/SMART 1000 CCD[b]

(continued)

Table 5.2. (continued)

radiation (λ [Å])	graphite-monochromated Mo Kα (0.71073)	graphite-monochromated Mo Kα (0.71073)	graphite-monochromated Mo Kα (0.71073)
temperature (°C)	–80	–80	–80
scan type	ϕ rotations (0.3°) / ω scans (0.3°) (30 s exposures)	ϕ rotations (0.3°) / ω scans (0.3°) (30 s exposures)	ω scans (0.2°) (25 s exposures)
data collection 2θ limit (deg)	52.74	52.76	52.84
total data collected	5003 ($-4 \leq h \leq 11$, $-13 \leq k \leq 14$, $-14 \leq l \leq 14$)	18941 ($-11 \leq h \leq 11$, $-24 \leq k \leq 21$, $-26 \leq l \leq 25$)	27173 ($-37 \leq h \leq 36$, $-16 \leq k \leq 13$, $-15 \leq l \leq 15$)
independent reflections	4099 ($R_{\mathrm{int}} = 0.0256$)	7565 ($R_{\mathrm{int}} = 0.0241$)	5284 ($R_{\mathrm{int}} = 0.0317$)
number of observed reflections (*NO*)	3692 [$F_o^2 \geq 2\sigma(F_o^2)$]	6750 [$F_o^2 \geq 2\sigma(F_o^2)$]	4640 [$F_o^2 \geq 2\sigma(F_o^2)$]
structure solution method	Patterson search/structure expansion (*DIRDIF–96*[c])	Patterson search/structure expansion (*DIRDIF–96*[c])	direct methods (*SHELXS–86*[h])
refinement method	full-matrix least-squares on F^2 (*SHELXL–93*[d])	full-matrix least-squares on F^2 (*SHELXL–93*[d])	full-matrix least-squares on F^2 (*SHELXL–93*[d])
absorption correction method	Gaussian integration (face-indexed)	empirical (*SADABS*)	empirical (*SADABS*)
range of transmission factors	0.3930–0.0688	0.1870–0.1131	0.4037–0.0614
data/restraints/parameters	4099 [$F_o^2 \geq -3\sigma(F_o^2)$] / 0 / 229	7565 [$F_o^2 \geq -3\sigma(F_o^2)$] / 3[g] / 342	5284 [$F_o^2 \geq -3\sigma(F_o^2)$] / 3[i] / 227
goodness-of-fit (S)[f]	1.085 [$F_o^2 \geq -3\sigma(F_o^2)$]	1.250 [$F_o^2 \geq -3\sigma(F_o^2)$]	1.081 [$F_o^2 \geq -3\sigma(F_o^2)$]
final R indices[g]			

(continued)

Table 5.2. (continued)

R_1 [$F_o^2 \geq 2\sigma(F_o^2)$]	0.0232	0.0332	0.0288
wR_2 [$F_o^2 \geq -3\sigma(F_o^2)$]	0.0589	0.0712	0.0722
largest difference peak and hole	1.307 and –1.172 e Å^{-3}	1.166 and –0.991 e Å^{-3}	2.806 and –2.169 e Å^{-3}

[a] Obtained from least-squares refinement of 5798 centered reflections for compound **16**, 7016 centered reflections for **17**, and 8164 centered reflections for **20**.

[b] Programs for diffractometer operation, data collection, data reduction and absorption correction were those supplied by Bruker.

[c] Beurskens, P. T.; Beurskens, G.; Bosman, W. P.; de Gelder, R.; Garcia Granda, S.; Gould, R. O.; Israel, R.; Smits, J. M. M. (1996). The *DIRDIF-96* program system. Crystallography Laboratory, University of Nijmegen, The Netherlands.

[d] Sheldrick, G. M. *SHELXL-93*. Program for crystal structure determination. University of Göttingen, Germany, 1993. Refinement on F_o^2 for all reflections (all of these having $F_o^2 \geq -3\sigma(F_o^2)$). Weighted *R*-factors wR_2 and all goodnesses of fit S are based on F_o^2; conventional *R*-factors R_1 are based on F_o, with F_o set to zero for negative F_o^2. The observed criterion of $F_o^2 > 2\sigma(F_o^2)$ is used only for calculating R_1, and is not relevant to the choice of reflections for refinement. *R*-factors based on F_o^2 are statistically about twice as large as those based on F_o, and *R*-factors based on ALL data will be even larger.

[e] $S = [\Sigma w(F_o^2 - F_c^2)^2/(n - p)]^{1/2}$ (n = number of data; p = number of parameters varied; $w = [\sigma^2(F_o^2) + (0.0354P)^2]^{-1}$ where $P = [\mathrm{Max}(F_o^2, 0) + 2F_c^2]/3$).

[f] $R_1 = \Sigma||F_o| - |F_c||/\Sigma|F_o|$; $wR_2 = [\Sigma w(F_o^2 - F_c^2)^2/\Sigma w(F_o^4)]^{1/2}$.

[g] Distance restraints were applied to attain an idealized geometry for the minority-occupancy terminal carbonyl group: d(O(2B)–C(2B)) = 1.10 Å; d(Ir(1)–C(2B)) = 1.90 Å; d(Ir(1)···O(2B)) = 3.00 Å (these restraints were based upon the distances observed for the Ir(2)–C(2A)–O(2A) carbonyl group).

Table 5.2. (continued)

[h] Sheldrick, G. M. *Acta Crystallogr.* **1990**, *A46*, 467–473.

[i] Due to the disorder of the solvent dichloromethane molecule about the crystallographic twofold axis (0, *y*, $-1/4$), the Cl–C (1.80 Å) and Cl···Cl (2.95 Å) distances were given fixed idealized values.

Results and Discussion

As noted in the Introduction, we set out to duplicate the synthesis of $[Ir_2(CH_3)(CO)(\mu\text{-}CO)(dmpm)_2][CF_3SO_3]$ (**1-dmpm**) by the reported procedure.[3] The first step in the original procedure involved the synthesis of $[Ir_2(CO)_4(dmpm)_2]$ (**15**) by the reduction of an ill-characterized reaction mixture presumed to contain $[Ir_2Cl(\mu\text{-}CO)(CO)_3(dmpm_2)][Cl]$, with Na/Hg under CO (Scheme 5.1).[3, 10] However, we have been unable to obtain synthetically useful amounts of $[Ir_2(CO)_4(dmpm)_2]$ by this route. A better route to **15** was developed in which Na/K in THF was used as the reductant (eqn. 5.1). In spite of our success at achieving the synthesis of **15**, we were unable to satisfactorily reproduce the remainder of the reported synthesis of **1-dmpm**.

$$[Ir(COD)Cl]_2 \xrightarrow[\text{2. CO, Na/K, THF, 25 °C}]{\text{1. dmpm, THF, -78 °C}} [Ir_2(CO)_4(dmpm)_2] \qquad (5.1)$$

Our procedure gives a clean conversion to **15**, and may conveniently be monitored by infrared spectroscopy of the solution. Compound **15** reacts instantly with air in solution giving unknown decomposition products, and decomposes as a solid in air in a few seconds.

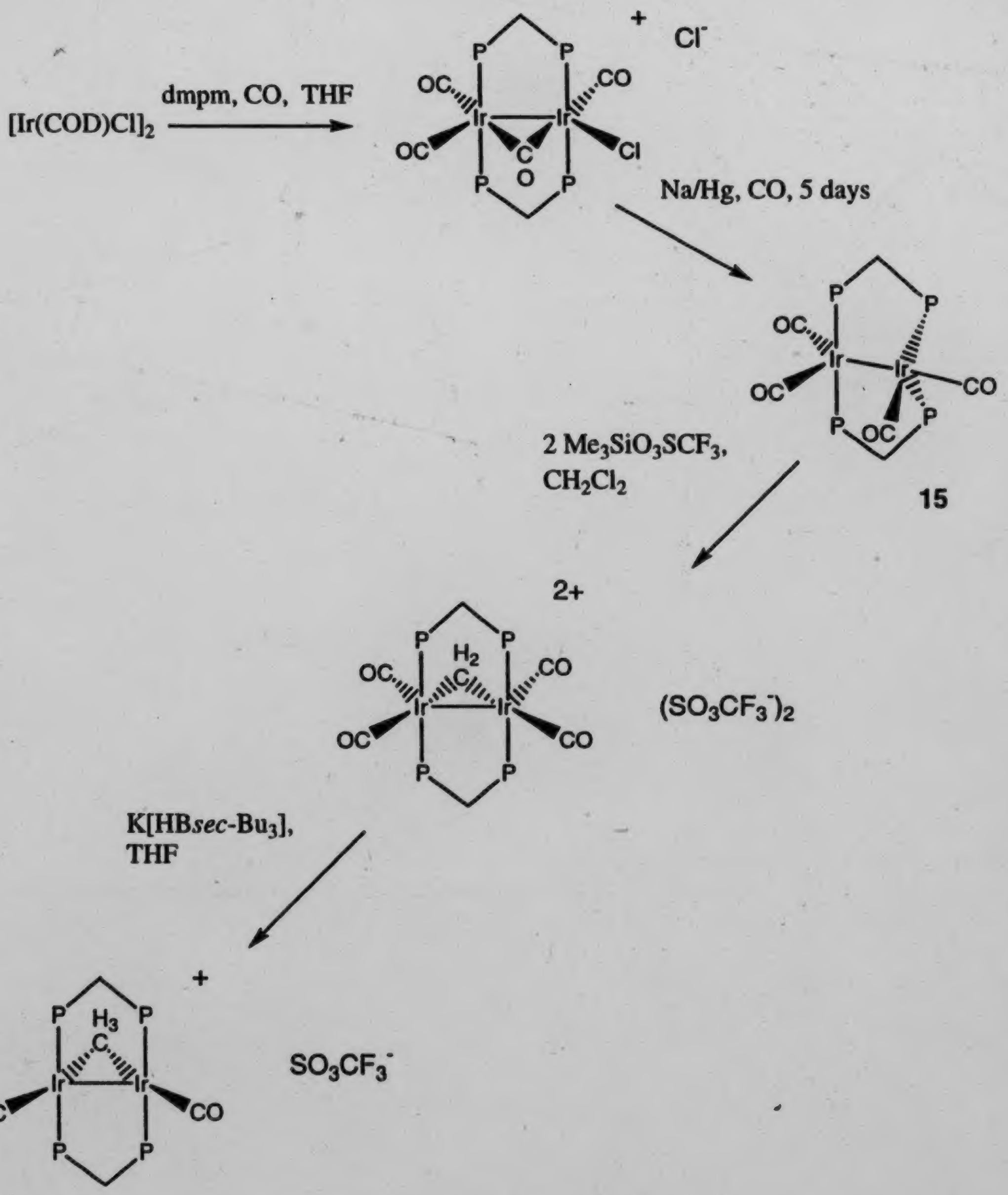
[Ir(COD)Cl]$_2$
dmpm, CO, THF
Cl$^-$
Na/Hg, CO, 5 days
15
2 Me$_3$SiO$_3$SCF$_3$,
CH$_2$Cl$_2$
2+
(SO$_3$CF$_3^-$)$_2$
K[HB*sec*-Bu$_3$],
THF
+
SO$_3$CF$_3^-$

Scheme 5.1. Preparation of **1-dmpm** according to Reinking *et al.*[3, 9] Methyl groups of the dmpm ligand are not shown.

We therefore turned our attention to the introduction of an iridium-bound methyl group by the reaction of methyl trifluoromethanesulfonate with $[Ir_2(CO)_4(dmpm)_2]$, which had been reported to give $[Ir_2(CH_3)(CO)_4(dmpm)_2][CF_3SO_3]$ when toluene was the solvent.[3b] In our hands, this reaction gave complex mixtures containing $[Ir_2(CH_3)_2(CO)_4(dmpm)_2][CF_3SO_3]_2$ (**16**) as the major product, which has resulted from the addition of two equivalents of methyl trifluoromethanesulfonate. In addition to the dicationic species (**16**), mass spectra of the evaporated reaction mixture showed the presence of higher nuclearity clusters of the general formula $[Ir_3(CH_3)(CO)_x(dmpm)_3]^+$. These trinuclear species were not pursued further. By changing the reaction solvent to nitromethane we were able to obtain nearly quantitative conversion to $[Ir_2(CH_3)_2(CO)_4(dmpm)_2][CF_3SO_3]_2$ (**16**). The $^{31}P\{^1H\}$ NMR spectrum of **16** shows a singlet at -42.2 ppm, as expected for a symmetrical species. The mass spectrum shows a parent molecular ion at m/z = 399.0 dalton, which is due to a dication. The IR spectrum shows a peak at 2009 cm^{-1}, which is at somewhat higher frequency than that previously reported for the monocationic $[Ir_2(CH_3)(CO)_4(dmpm)_2][CF_3SO_3]$ (1942 (s), 1910 (sh)), as is consistent with decreased back donation to the carbonyl in the dication.

A related dppm complex, $[Ir_2(CO)_3(dppm)_3]$, reacts with only one equivalent of methyl trifluoromethanesulfonate.[11] To form a dication in the dppm compound, the stronger electrophile trifluoromethanesulfonic acid is required, suggesting that the metals in $[Ir_2(CO)_4(dmpm)_2]$ are more nucleophilic than in $[Ir_2(CO)_3(dppm)_2]$.[12] In addition, and in contrast to $[Ir_2(CO)_4(dppm)_2]$ which is only stable under an atmosphere of CO the dmpm analogue, $[Ir_2(CO)_4(dmpm)_2]$, is stable to CO loss *in vacuo*,[12] again indicative of the greater electron-richness of the dmpm system, consistent with the greater basicity of the dmpm ligand vs. dppm.[5] Surprisingly, this compound is very air sensitive even as a solid. Also, its solubility is very low, in keeping with the general trend we observed of dmpm complexes being less soluble than related dppm derivatives.

Crystals of **16** suitable for X-ray structure determination were obtained by the slow diffusion of Et_2O into a saturated acetone solution of **16**. The structure of the complex dication is shown in Figure 5.1, with relevant bond lengths and angles in Table 5.3. The structure consists of two octahedral iridium centres bridged by two dmpm ligands in a trans orientation (P(1)-Ir-P(2') = 176.32(3)°). The octahedral coordination geometry of each metal is comprised of the mutually trans dmpm groups, two mutually trans carbonyls (C(1)-Ir-C(2) = 179.2(2)°), the metal-metal bond and a methyl ligand that lies along the metal-metal bond axis. The Ir-C(3) bond distance of 2.178(3) is slightly longer than that of the monocationic dppm-bridged complex $[Ir_2(CH_3)(CO)(\mu\text{-}CO)(dppm)_2][CF_3SO_3]$ (**1**) (2.15(2) Å).[13] This may be an effect of the trans influence of the Ir-Ir bond[14] or a transmission of the trans influence of the methyl ligand on the adjacent metal. The transmission of electronic effects *via* the metal-metal bond has been described.[15]

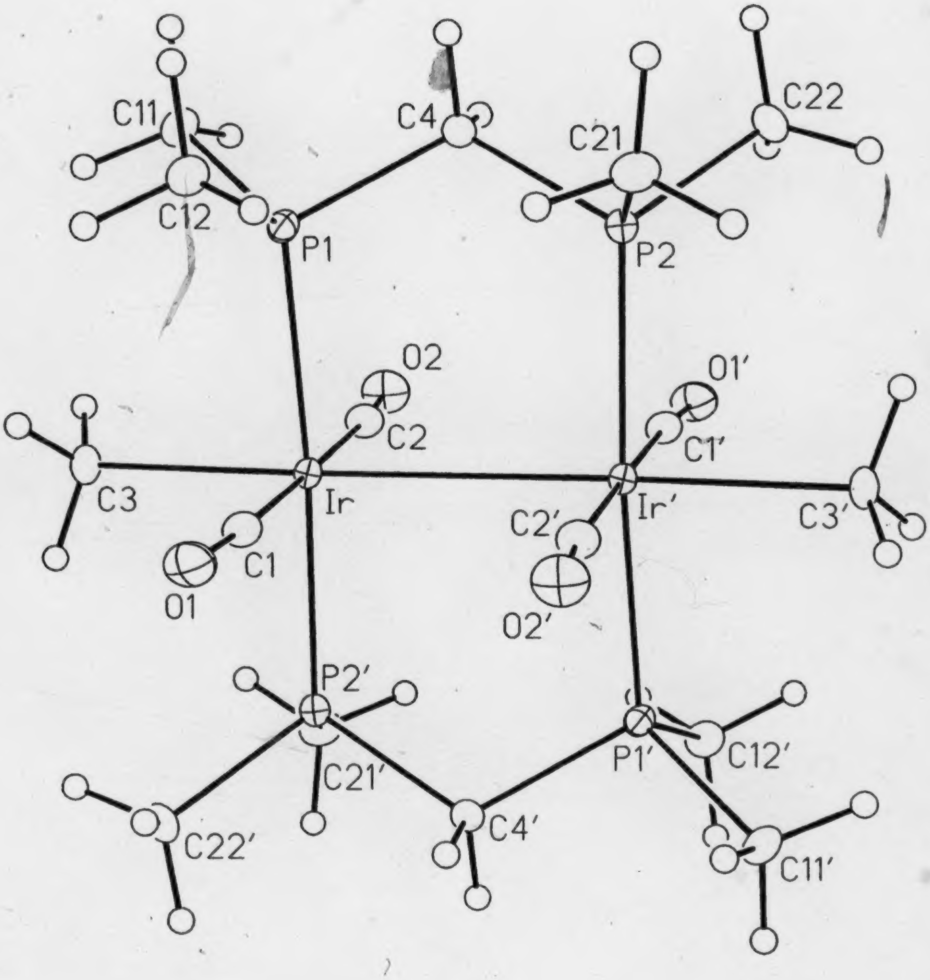
C11
C4
C21
C22
C12
P1
P2
O2
O1'
C2
C1'
C3
Ir
Ir'
C3'
C2'
C1
O1
O2'
P2'
P1'
C12'
C21'
C4'
C22'
C11'

Figure 5.1. Perspective view of the $[Ir_2(CO)_4(Me)_2(dmpm)_2]^{2+}$ ion of **16** showing the atom-labeling scheme. Non-hydrogen atoms are represented by Gaussian ellipsoids at the 20% probability level. Hydrogen atoms are shown with arbitrarily small thermal parameters. Primed atoms are related to unprimed ones via the crystallographic inversion center (0, 0, 0) at the midpoint of the Ir-Ir' bond.

Table 5.3. Selected interatomic distances (Å) and angles (deg) within the complex cation of **16**.

(a) Distances (Å)

Atom1	*Atom2*	*Distance*	*Atom1*	*Atom2*	*Distance*
Ir	Ir'	2.9286(2)	P(1)	C(11)	1.815(4)
Ir	P(1)	2.3500(10)	P(1)	C(12)	1.813(4)
Ir	P(2')	2.3496(10)	P(2)	C(4)	1.818(4)
Ir	C(1)	1.915(4)	P(2)	C(21)	1.811(4)
Ir	C(2)	1.912(4)	P(2)	C(22)	1.813(3)
Ir	C(3)	2.178(3)	O(1)	C(1)	1.134(5)
P(1)	C(4)	1.815(3)	O(2)	C(2)	1.135(5)

(a) Angles (deg)

Atom1	*Atom2*	*Atom3*	*Angle*	*Atom1*	*Atom2*	*Atom3*	*Angle*
Ir'	Ir	P(1)	92.05(2)	Ir	P(1)	C(4)	113.27(13)
Ir'	Ir	P(2')	91.54(2)	Ir	P(1)	C(11)	115.37(17)
Ir'	Ir	C(1)	92.87(11)	Ir	P(1)	C(12)	115.10(15)
Ir'	Ir	C(2)	87.53(12)	C(4)	P(1)	C(11)	101.65(18)
Ir'	Ir	C(3)	176.37(12)	C(4)	P(1)	C(12)	106.56(19)
P(1)	Ir	P(2')	176.32(3)	C(11)	P(1)	C(12)	103.5(2)
P(1)	Ir	C(1)	89.66(13)	Ir'	P(2)	C(4)	113.96(13)
P(1)	Ir	C(2)	89.58(13)	Ir'	P(2)	C(21)	114.88(15)
P(1)	Ir	C(3)	87.90(12)	Ir'	P(2)	C(22)	115.65(15)
P(2')	Ir	C(1)	89.36(13)	C(4)	P(2)	C(21)	105.87(19)
P(2')	Ir	C(2)	91.37(13)	C(4)	P(2)	C(22)	100.97(18)
P(2')	Ir	C(3)	88.57(13)	C(21)	P(2)	C(22)	104.0(2)
C(1)	Ir	C(2)	179.15(17)	Ir	C(1)	O(1)	175.9(4)
C(1)	Ir	C(3)	90.76(17)	Ir	C(2)	O(2)	175.2(4)
C(2)	Ir	C(3)	88.84(17)	P(1)	C(4)	P(2)	115.7(2)

[a] Primed atoms are related to unprimed ones via the crystallographic inversion center (0, 0, 0).

The Ir-Ir' bond length of 2.9286(2) Å is substantially longer than a normal Ir-Ir single bond, which is generally found to be *ca.* 2.8 Å in similar complexes. This lengthening has previously been observed when there are eclipsing interactions at adjacent octahedral metal centres.[5] However, a metal-metal bond is formulated to complete the valence shell of the metals. It may also be that the metal-ligand bond is lengthened due to the high trans influence of the methyl groups.

Since the initial reaction mixture resulting from the combination of $[IrCl(COD)]_2$, dmpm and CO was not well characterized we investigated the effects of changing conditions (solvent, concentration and temperature) on the reaction, in the hope of selectively forming one or more of the products to aid in their characterization. While we were unable to definitively characterize all of the species present in these reaction mixtures, we were able to obtain some interesting new products. At an early stage we found that a yellow species would often form, rather than the red to violet colour that is typical of binuclear species such as $[Ir_2Cl(\mu\text{-}CO)(CO)_3(dmpm)]_2[Cl]$, particularly when the reagents were combined in a small solvent volume. This yellow compound could be prepared as a pure compound using a different route, given below, and was found to be the triply dmpm-bridged compound, $[Ir_2Cl(CO)(\mu\text{-}CO)(dmpm)_3][Cl]$, **17**.

This triply dmpm-bridged compound (**17**) could be obtained nearly quantitatively by the reaction of Vaska's compound with excess dmpm. The ^{31}P NMR spectrum of **17** indicates a formulation in which there are two equivalent bridging biphosphines, and one that is distinct. Two sets of multiplets appear at -28.4 and -36.7 ppm each integrating as two phosphorus nuclei; these correspond to two trans-bridged dmpm ligands. The simpler patterns at -32.3 ppm and -52.0 ppm, integrate as one phosphorus nuclei each. The signal at -32.3 ppm is a doublet of triplets, with a coupling of 185 Hz to the phosphorus resonating at -52.0 ppm and a 28 Hz coupling to two equivalent phosphorus nuclei giving rise to the triplet. The signal at -52.0 ppm is also a doublet of triplets, with the same 185 Hz coupling observed above and a 16 Hz, two-bond coupling to two equivalent phosphorus nuclei. Taken together, the ^{31}P data show a pair of trans bridging phosphines, with the pair at either metal being equivalent, and a third bridging the metals at approximate right angles to the other two, as indicated by the small coupling constants (16 Hz and 28 Hz). The infrared spectrum shows that there is one terminal (1956 cm^{-1}) and one bridging (1722 cm^{-1}) carbonyl, and the mass spectrum shows a parent ion at 909 dalton with the correct isotope pattern for two iridium atoms and one chlorine atom, the other having been lost as a chloride ion.

In order to confirm the formulation predicted on the basis of the NMR study, an X-ray structure determination was carried out. The results, represented in Figure 5.2, with the relevant bond lengths and angles in Tables 5.4, confirm the predicted geometry of the complex cation of **17**, in that the structure may be described as an "A-frame" complex having two biphosphines in a trans arrangement and a third (also bridging) in the plane essentially perpendicular to the first two. A carbonyl also bridges the metals on the face of the complex opposite the unique dmpm ligand, while the coordination sphere of one metal is completed by a terminally bound carbonyl. Both terminal ligands are almost opposite the Ir-Ir bond (Ir(2)-Ir(1)-Cl = 162.55(8)°; Ir(1)-Ir(2)-C(2A) = 158.2(3)°). Presumably, both groups are bent away from the unique biphosphine ligand to avoid repulsions with the methyl substituents. The mutually trans dmpm groups are also bent away from the third dmpm group resulting in P-Ir-P angles of 162.46(6)° and 163.42(6)°. These distortions are shown in Figure 5.3, which clearly indicates the bending back of these groups.

In this compound the Ir(1)-Ir(2) bond length (2.7448(3) Å) is typical of an Ir-Ir single bond. The chloride ligand and the terminal carbonyl were found to be disordered, precluding detailed discussion of the structural parameters. Nevertheless, refinement proceeded well and the general arrangement, with the dmpm ligands being significantly bent away from the facially bridging dmpm ligand is clear. The structure of compound **3** bears some similarity to that proposed for the butadiene-bridged complex $[Ir_2(CH_3)(CO)_2(\mu\text{-}\eta^2:\eta^2\text{-}H_2C{=}CH\text{-}CH{=}CH_2)(dppm)_2][CF_3SO_3]$ (**6A**) in which the smaller diolefin is able to bridge the two metals across one face of the complex (Chapter 2).

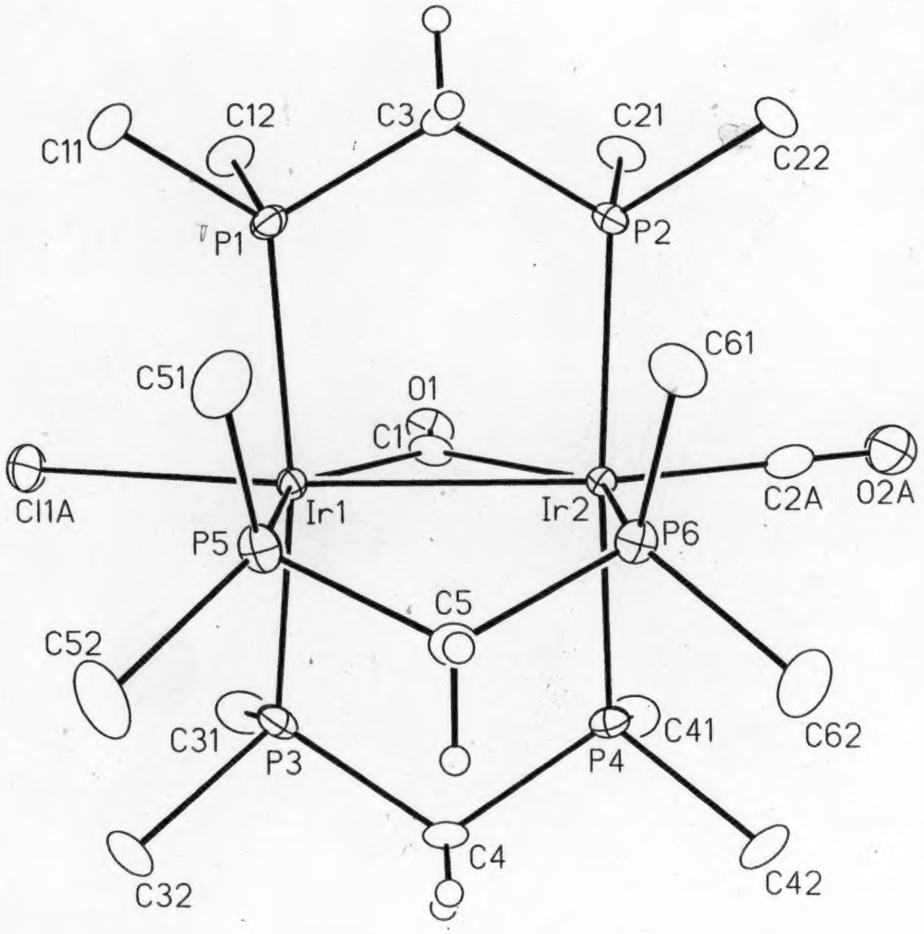
C11
C12
C3
C21
C22
P1
P2
C51
O1
C1
C61
Cl1A
Ir1
Ir2
C2A
O2A
P5
P6
C5
C52
C31
P3
P4
C41
C62
C4
C32
C42

Figure 5.2. Perspective view of the $[Ir_2Cl(CO)(\mu\text{-}CO)(dmpm)_3]^+$ ion of **17** showing the atom labeling scheme. Non-hydrogen atoms are represented by Gaussian ellipsoids at the 20% probability level. Hydrogen atoms are shown with arbitrarily small thermal parameters for the dmpm methylene groups, and are not shown for the dmpm methyl groups.

Table 5.4. Selected interatomic distances (Å) and angles (deg) within the complex cation of **17**.

(a) Distances (Å)

Atom1	*Atom2*	*Distance*	*Atom1*	*Atom2*	*Distance*
Ir(1)	Ir(2)	2.7448(3)	P(2)	C(21)	1.823(6)
Ir(1)	Cl(1A)	2.486(2)	P(2)	C(22)	1.816(6)
Ir(1)	P(1)	2.3219(15)	P(3)	C(4)	1.828(7)
Ir(1)	P(3)	2.3302(16)	P(3)	C(31)	1.821(7)
Ir(1)	P(5)	2.3717(16)	P(3)	C(32)	1.823(7)
Ir(1)	C(1)	2.025(6)	P(4)	C(4)	1.812(6)
Ir(1)	C(2B)	1.90†	P(4)	C(41)	1.832(7)
Ir(2)	Cl(1B)	2.464(18)	P(4)	C(42)	1.821(7)
Ir(2)	P(2)	2.3422(14)	P(5)	C(5)	1.834(7)
Ir(2)	P(4)	2.3394(15)	P(5)	C(51)	1.835(8)
Ir(2)	P(6)	2.3947(15)	P(5)	C(52)	1.840(7)
Ir(2)	C(1)	2.111(6)	P(6)	C(5)	1.832(6)
Ir(2)	C(2A)	1.902(12)	P(6)	C(61)	1.828(7)
P(1)	C(3)	1.822(6)	P(6)	C(62)	1.835(7)
P(1)	C(11)	1.825(7)	O(1)	C(1)	1.191(7)
P(1)	C(12)	1.819(7)	O(2A)	C(2A)	1.088(14)
P(2)	C(3)	1.833(6)	O(2B)	C(2B)	1.10†

†Distance fixed during refinement.

(b) Angles (deg)

Atom1	*Atom2*	*Atom3*	*Angle*	*Atom1*	*Atom2*	*Atom3*	*Angle*
Ir(2)	Ir(1)	Cl(1A)	162.55(8)	Cl(1A)	Ir(1)	P(3)	84.08(8)
Ir(2)	Ir(1)	P(1)	94.13(4)	Cl(1A)	Ir(1)	P(5)	100.72(9)
Ir(2)	Ir(1)	P(3)	93.71(4)	Cl(1A)	Ir(1)	C(1)	112.8(2)
Ir(2)	Ir(1)	P(5)	96.72(4)	P(1)	Ir(1)	P(3)	162.16(6)
Ir(2)	Ir(1)	C(1)	49.77(18)	P(1)	Ir(1)	P(5)	98.71(6)
Ir(2)	Ir(1)	C(2B)	159.0(10)	P(1)	Ir(1)	C(1)	86.88(17)
Cl(1A)	Ir(1)	P(1)	83.64(8)	P(1)	Ir(1)	C(2B)	85.1(11)

(continued)

Table 5.4. (continued)

(a) Angles (deg)

Atom1	*Atom2*	*Atom3*	*Angle*	*Atom1*	*Atom2*	*Atom3*	*Angle*
P(3)	Ir(1)	P(5)	96.25(6)	C(11)	P(1)	C(12)	100.4(4)
P(3)	Ir(1)	C(1)	86.00(17)	Ir(2)	P(2)	C(3)	115.6(2)
P(3)	Ir(1)	C(2B)	81.9(12)	Ir(2)	P(2)	C(21)	111.7(2)
P(5)	Ir(1)	C(1)	146.46(19)	Ir(2)	P(2)	C(22)	119.9(2)
P(5)	Ir(1)	C(2B)	104.2(10)	C(3)	P(2)	C(21)	104.3(3)
C(1)	Ir(1)	C(2B)	109.3(10)	C(3)	P(2)	C(22)	103.5(3)
Ir(1)	Ir(2)	Cl(1B)	166.1(3)	C(21)	P(2)	C(22)	99.7(3)
Ir(1)	Ir(2)	P(2)	92.50(4)	Ir(1)	P(3)	C(4)	115.1(2)
Ir(1)	Ir(2)	P(4)	92.90(4)	Ir(1)	P(3)	C(31)	111.3(3)
Ir(1)	Ir(2)	P(6)	91.11(4)	Ir(1)	P(3)	C(32)	119.9(3)
Ir(1)	Ir(2)	C(1)	47.10(17)	C(4)	P(3)	C(31)	105.1(4)
Ir(1)	Ir(2)	C(2A)	158.2(3)	C(4)	P(3)	C(32)	102.3(3)
Cl(1B)	Ir(2)	P(2)	86.7(3)	C(31)	P(3)	C(32)	101.2(4)
Cl(1B)	Ir(2)	P(4)	84.3(4)	Ir(2)	P(4)	C(4)	116.2(2)
Cl(1B)	Ir(2)	P(6)	102.8(3)	Ir(2)	P(4)	C(41)	111.0(2)
Cl(1B)	Ir(2)	C(1)	119.0(4)	Ir(2)	P(4)	C(42)	117.7(3)
P(2)	Ir(2)	P(4)	163.42(6)	C(4)	P(4)	C(41)	104.8(3)
P(2)	Ir(2)	P(6)	99.40(5)	C(4)	P(4)	C(42)	103.4(3)
P(2)	Ir(2)	C(1)	85.29(16)	C(41)	P(4)	C(42)	102.1(4)
P(2)	Ir(2)	C(2A)	83.5(3)	Ir(1)	P(5)	C(5)	109.4(2)
P(4)	Ir(2)	P(6)	96.14(6)	Ir(1)	P(5)	C(51)	120.5(3)
P(4)	Ir(2)	C(1)	86.95(16)	Ir(1)	P(5)	C(52)	122.8(3)
P(4)	Ir(2)	C(2A)	85.7(3)	C(5)	P(5)	C(51)	101.6(3)
P(6)	Ir(2)	C(1)	138.20(18)	C(5)	P(5)	C(52)	100.7(4)
P(6)	Ir(2)	C(2A)	110.7(3)	C(51)	P(5)	C(52)	98.4(4)
C(1)	Ir(2)	C(2A)	111.1(4)	Ir(2)	P(6)	C(5)	112.9(2)
Ir(1)	P(1)	C(3)	115.46(19)	Ir(2)	P(6)	C(61)	118.4(2)
Ir(1)	P(1)	C(11)	119.9(2)	Ir(2)	P(6)	C(62)	121.3(3)
Ir(1)	P(1)	C(12)	111.3(2)	C(5)	P(6)	C(61)	103.0(3)
C(3)	P(1)	C(11)	103.6(3)	C(5)	P(6)	C(62)	99.8(3)
C(3)	P(1)	C(12)	104.1(3)	C(61)	P(6)	C(62)	98.2(4)

(continued)

Table 5.4. (continued)

(b) Angles (deg)

Atom1	*Atom2*	*Atom3*	*Angle*	*Atom1*	*Atom2*	*Atom3*	*Angle*
Ir(1)	C(1)	Ir(2)	83.1(2)	Ir(1)	C(2B)	O(2B)	180†
Ir(1)	C(1)	O(1)	142.0(5)	P(1)	C(3)	P(2)	111.1(3)
Ir(2)	C(1)	O(1)	134.9(5)	P(3)	C(4)	P(4)	111.9(3)
Ir(2)	C(2A)	O(2A)	179.1(13)	P(5)	C(5)	P(6)	113.7(3)

†Angle fixed during refinement.

When an excess of dmpm is added at room temperature to a solution of $[IrCl(COD)]_2$ in dry THF or benzene, a yellow solution containing the air-sensitive mononuclear complex having the formulation $[IrCl(dmpm)_2(COD)]$ (**4**) is obtained, as shown in eqn. (5.2), and this compound can be isolated as a yellow microcrystalline powder. The compound slowly decomposes in dichloromethane solution.

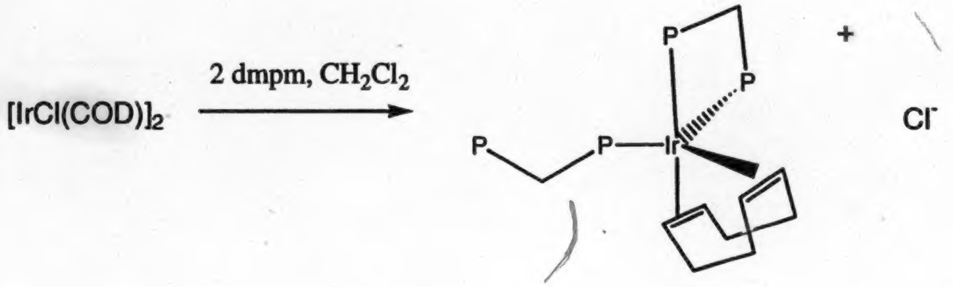

(5.2)

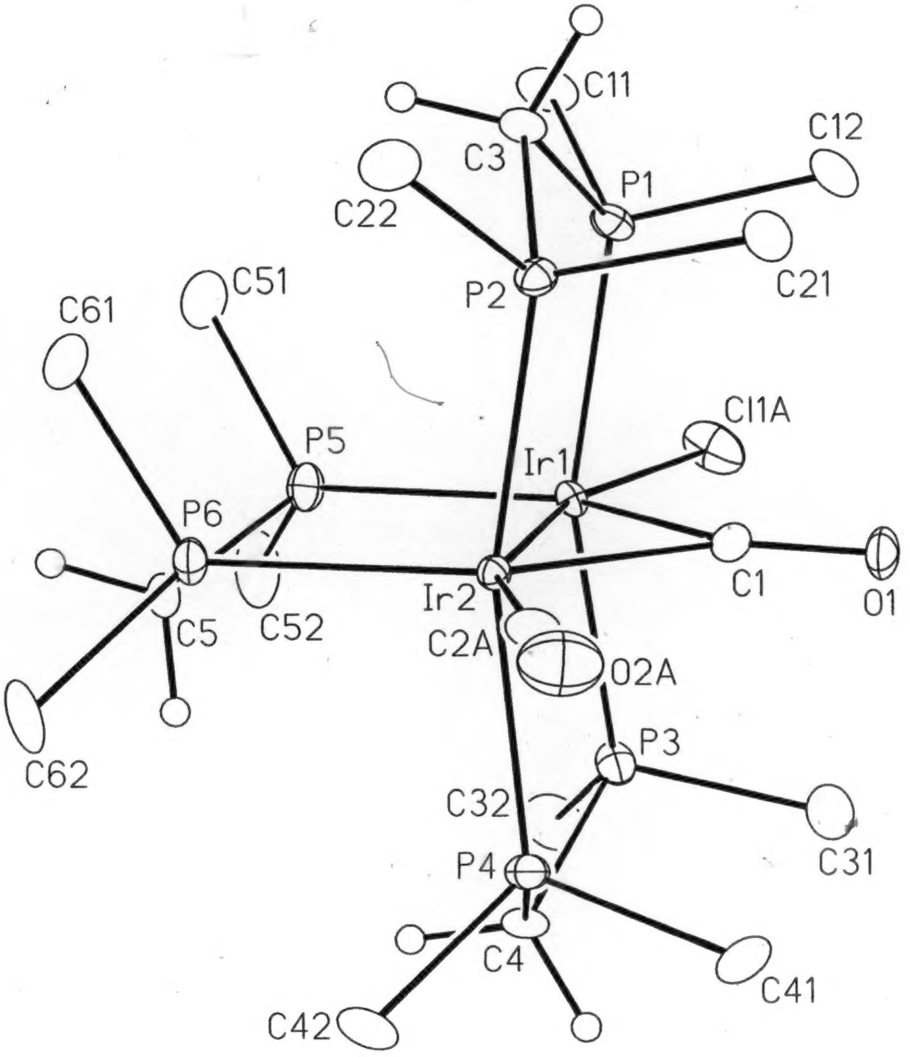
C11
C3
C12
P1
C22
C21
P2
C51
C61
Cl1A
P5
Ir1
P6
C1
O1
Ir2
C5
C52
C2A
O2A
C62
P3
C32
P4
C31
C4
C41
C42

Figure 5.3. Alternate view of the complex cation of **17**.

The $^{31}P\{^1H\}$ NMR spectrum of $[IrCl(dmpm)_2(COD)]$ in CD_2Cl_2 solution at room temperature shows three resonances at -7.20, -50.8 and -86.4 ppm in a 1:1:2 intensity ratio. The high-field resonance is characteristic of a chelating dmpm while the lower field resonances are due to a non-chelated dmpm ligand, one phosphorus of which is bound to iridium, while the other phosphorus is not coordinated. The iridium-bound phosphorus appears as a doublet of triplets at -50.8 ppm; 30 Hz coupling to the low-field ^{31}P signal (the non-coordinated phosphorus of that dmpm ligand), and 14 Hz coupling to the two chelated dmpm nuclei. The chelated phosphorus nuclei appear as a doublet with the above-noted 14 Hz coupling. When the sample is cooled to -100 °C the ^{31}P resonance due to chelating dmpm appears as a broad second order multiplet. The coalescence temperature is approximately -80 °C, indicating a facile fluxional process interconverting the chelated phosphorus atoms. Thus, the geometry of the complex may be described as approximately trigonal bipyramidal, with the chelating dmpm phosphorus atoms occupying one axial and one equatorial position. These positions exchange rapidly at room temperature giving the observed ^{31}P spectrum. The other two phosphorus resonances remained sharp at all temperatures studied, indicating that the dmpm ligands do not exchange with each other. The mass spectrum shows a parent ion corresponding to $[Ir(COD)(dmpm)]^+$ suggesting that the η^1 dmpm ligand is easily lost.

Since the related dppm complex $[Ir(CO)(dppm)_2]Cl$ reacts with $[Rh(\mu\text{-}Cl)(CO)_2]_2$ to form $[RhIrCl_2(CO)_2(dppm)_2]$[16], and since to our knowledge, a heterobimetallic dmpm-bridged complex of Rh and Ir has never been prepared, we investigated the reaction of **4** with $[Rh(\mu\text{-}Cl)(CO)_2]_2$. To our surprise, the only new dmpm-containing species detected was the previously reported *trans*-$[Rh_2Cl_2(CO)_2(dmpm)_2]$. This intriguing result suggests that the dmpm ligand is transferred from the iridium centre to rhodium, presumably because of the electrophilicity of the rhodium in $[Rh(\mu\text{-}Cl)(CO)_2]_2$ due to the presence of the carbonyl ligands. This could proceed via the formation of a trinuclear intermediate (i.e. Rh_2Ir) or via the dissociation of dmpm from the mononuclear complex followed by it being taken up by the Rh complex. One of the dmpm ligands is expected to be somewhat more labile than the other because it is attached by only one phosphorus atom (the other dmpm is chelated). Evidence for lability of the η^1 - dmpm is found in the mass spectrum of $[IrCl(dmpm)_2(COD)]$, as mentioned above. Evidence for higher nuclearity clusters in a related dmpm system, however, is found in the mass spectrum of the reaction mixture in the preparation of $[Ir_2(CH_3)_2(CO)_4(dmpm)_2][CF_3SO_3]_2$ (**16**), particularly when solvents less polar than nitromethane are used, *vide supra*. Given the relatively small steric demands of the dmpm ligand, the close approach of a third metal centre to a dmpm-bridged dimer is feasible.

In an attempt to find alternative routes to iridium-monomethyl complexes, we investigated the possibility of obtaining such products by the reaction of methyl lithium with the reaction mixture reported to contain $[Ir_2Cl(\mu\text{-}CO)(CO)_3(dmpm)_2][Cl]$.[3b] It quickly became clear that the composition of this mixture depended on the concentration, reaction time, temperature and solvent. These mixtures contained varying amounts of the mononuclear product **4**, the tris-bridged product **3** as well other, unidentified species. After unsuccessful attempts to establish reaction conditions that would lead to tractable products, we abandoned this chemistry.

If the reaction of $[IrCl(COD)]_2$ with dmpm, followed by the addition of CO is carried out in CH_2Cl_2, a red solution is obtained. Addition of methyl trifluoromethanesulfonate to this solution causes a rapid colour change to yellow and yields $[Ir_2(CH_3)Cl_2(CO)_2(dmpm)_2][CF_3SO_3]$, (**19**) as shown in Scheme 5.2. The $^{31}P\{^1H\}$ NMR spectrum, obtained in CD_2Cl_2, shows the AA'BB' multiplet pattern expected of trans dmpm ligands at -12.2 and -29.2 ppm. The ^1H NMR spectrum shows an iridium-bound methyl group appearing as a triplet at 1.04 ppm ($^3J_{PH}$ = 8 Hz) due to coupling to two equivalent phosphorus nuclei. This methyl signal is well separated from those of the dmpm methyls, which appear as several multiplets in the range 1.72 to 2.00 ppm. The methylene protons of the dmpm ligands occur as multiplets at 3.08 and 3.24 ppm. The IR spectrum in CH_2Cl_2 shows a single peak at 1967 cm^{-1}. The mass spectrum shows a parent ion at 799 dalton with the correct isotope pattern for the cation $[Ir_2(CH_3)Cl_2(CO)_2(dmpm)_2]^+$.

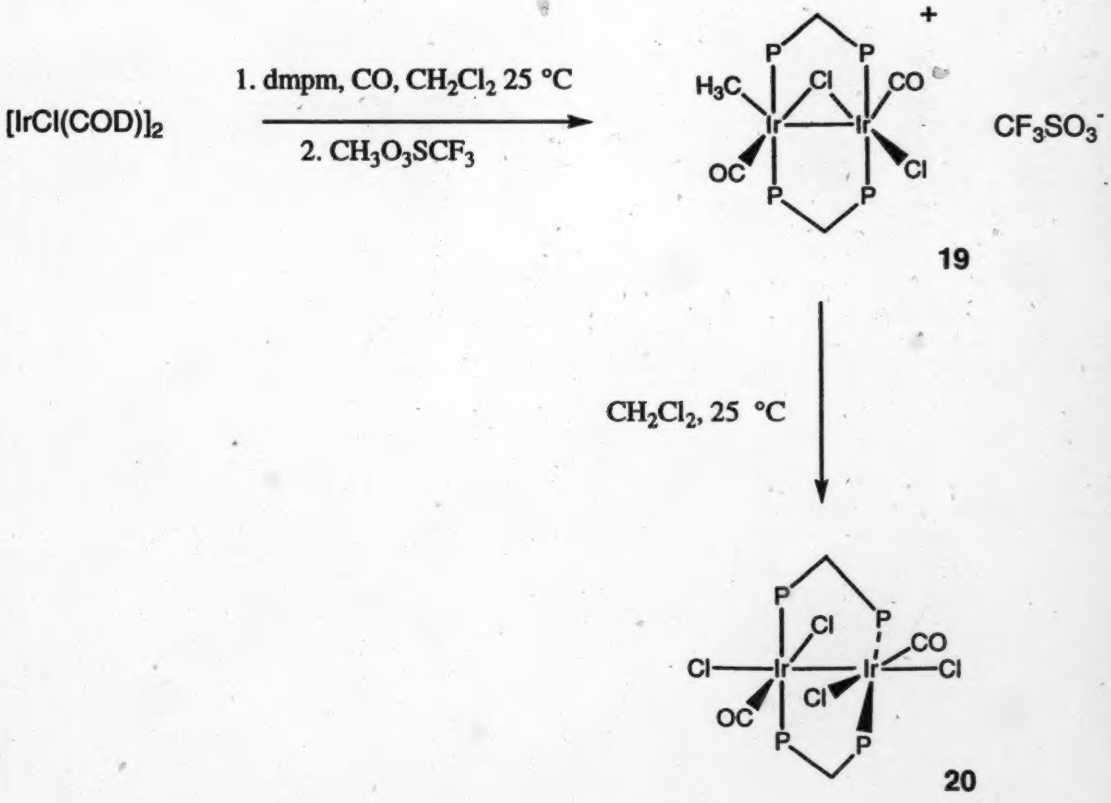

Scheme 5.2. Preparation of $[Ir_2(CH_3)Cl_2(CO)_2(dmpm)_2][CF_3SO_3]$, **19** and its subsequent conversion to $[Ir_2Cl_4(CO)_2(dmpm)_2]$, **20**, upon standing in CH_2Cl_2

Upon standing overnight in CD_2Cl_2, **19** reacts with the solvent to form $[Ir_2Cl_4(CO)_2(dmpm)_2]$, **20**, which has been characterized by X-ray crystallography and NMR spectroscopy. The ^1H NMR spectrum of **20** is similar to that of **19**, but with the absence of an iridium-bound methyl group (this methyl resonance disappears in a few hours from a solution of **19** in CD_2Cl_2). The $^{31}P\{^1H\}$ NMR spectrum shows two multiplets at -27.4 ppm and -31.6 ppm, which are close to the resonance at -29.2 ppm in **19**, suggesting that the ^{31}P nuclei giving rise to these high-field resonances all have similar chemical environments. This suggests that the lower field resonance in **19** (-12.2 ppm) results from the ^{31}P nuclei adjacent to the methyl group. As shown in Scheme 5.2 and as confirmed by an X-ray structure determination (*vide infra*) compound **20** exists in a twisted-trans dmpm-bridged conformation. The analogous Rh complex was also obtained when *trans*-[RhCl(CO)(dmpm)]$_2$ was allowed to stand in chlorinated solvents for extended periods.[5]

The structure of **20** is shown in two alternative views in Figures 5.5 and 5.6, with important structural parameters in Tables 5.6. The structure may be best described as consisting of two iridium octahedra that are bridged by two mutually trans dmpm ligands, but with the iridium octahedra twisted with respect to each other along the metal-metal axis (see Figure 5.6). The degree of twist can be seen in the P(1)-Ir(1)-Ir(2)-P(2), P(3)-Ir(1)-Ir(2)-P(4), C(1)-Ir(1)-Ir(2)-Cl(4) and Cl(2)-Ir(1)-Ir(2)-C(2) torsion angles of 20.90(6)°, 18.62(5)°, 20.02(18)° and 25.0(2)°, respectively, which results in a twist of the two octahedra by approximately 20° with respect to each other. This twist helps alleviate the repulsion between adjacent chloro and carbonyl ligands on the adjacent metals. A comparison of complexes **16** and **20** is enlightening. Both have two octahedrally coordinated iridium(II) centres, yet **16** has an unusually long Ir-Ir separation of 2.9286(2) Å and an almost exactly eclipsed arrangement of ligands whereas **20** has a normal Ir-Ir separation (2.7704(2) Å) and a substantially staggered ligand arrangement. Clearly in **16** the elongation of the metal-metal bond allows the carbonyl ligands to remain eclipsed, whereas the short separation in **20** necessitates a staggering to avoid unusually short interligand contacts. In compound **20**, one chloride ligand on each metal occupies the position approximately collinear with the Ir-Ir bond axis, the angles being Ir(2)-Ir(1)-Cl(1) = 176.92(4)° and Ir(2)-Ir(1)-Cl(3) = 177.88(4)°. The bond lengths from the metal atoms to the chloride ligands coaxial with the Ir-Ir bond are somewhat longer (Ir(1)-Cl(1) = 2.484(1); Ir(1)-Cl(3) = 2.483(2)) than those of the chloride ligands at right angles to these (Ir(1)-Cl(2) = 2.411(2); Ir(1)-Cl(4) = 2.404(2)). This may be explained by the trans influence of the metal-metal bond on the metal-chloride bond.[14]

Table 5.5. Selected interatomic distances (Å) and angles (deg) for compound **20**

(a) Distances (Å)

Atom 1	*Atom 2*	*Distance*	*Atom 1*	*Atom 2*	*Distance*
Ir(1)	Ir(2)	2.7704(3)	P(1)	C(11)	1.814(7)
Ir(1)	Cl(1)	2.4838(14)	P(1)	C(12)	1.815(7)
Ir(1)	Cl(2)	2.4109(15)	P(2)	C(3)	1.818(6)
Ir(1)	P(1)	2.3490(15)	P(2)	C(21)	1.820(7)
Ir(1)	P(3)	2.3366(15)	P(2)	C(22)	1.801(7)
Ir(1)	C(1)	1.859(7)	P(3)	C(4)	1.815(6)
Ir(2)	Cl(3)	2.4833(15)	P(3)	C(31)	1.809(7)
Ir(2)	Cl(4)	2.4035(15)	P(3)	C(32)	1.807(6)
Ir(2)	P(2)	2.3430(16)	P(4)	C(4)	1.820(6)
Ir(2)	P(4)	2.3551(15)	P(4)	C(41)	1.811(6)
Ir(2)	C(2)	1.864(7)	P(4)	C(42)	1.810(6)
P(1)	C(3)	1.821(6)	O(1)	C(1)	1.108(8)
			O(2)	C(2)	1.094(8)

(continued)

(b) Angles (deg)

Atom 1	***Atom 2***	***Atom 3***	***Angle***
Ir(2)	Ir(1)	Cl(1)	176.92(4)
Ir(2)	Ir(1)	Cl(2)	90.78(4)
Ir(2)	Ir(1)	P(1)	93.34(4)
Ir(2)	Ir(1)	P(3)	90.85(4)
Ir(2)	Ir(1)	C(1)	90.96(18)
Cl(1)	Ir(1)	Cl(2)	87.68(5)
Cl(1)	Ir(1)	P(1)	84.03(5)
Cl(1)	Ir(1)	P(3)	91.70(5)
Cl(1)	Ir(1)	C(1)	90.72(18)
Cl(2)	Ir(1)	P(1)	91.45(6)
Cl(2)	Ir(1)	P(3)	85.81(6)
Cl(2)	Ir(1)	C(1)	176.52(19)
P(1)	Ir(1)	P(3)	175.02(5)
P(1)	Ir(1)	C(1)	91.47(18)
P(3)	Ir(1)	C(1)	91.15(18)
Ir(1)	Ir(2)	Cl(3)	177.88(4)
Ir(1)	Ir(2)	Cl(4)	94.15(4)
Ir(1)	Ir(2)	P(2)	89.75(4)
Ir(1)	Ir(2)	P(4)	92.54(4)
Ir(1)	Ir(2)	C(2)	90.90(19)
Cl(3)	Ir(2)	Cl(4)	86.96(5)
Cl(3)	Ir(2)	P(2)	92.04(5)
Cl(3)	Ir(2)	P(4)	85.66(5)
Cl(3)	Ir(2)	C(2)	88.06(19)
Cl(4)	Ir(2)	P(2)	90.66(6)
Cl(4)	Ir(2)	P(4)	89.57(5)
Cl(4)	Ir(2)	C(2)	174.59(19)
P(2)	Ir(2)	P(4)	177.67(5)
P(2)	Ir(2)	C(2)	87.4(2)

Atom1	***Atom2***	***Atom3***	***Angle***
P(4)	Ir(2)	C(2)	92.2(2)
Ir(1)	P(1)	C(3)	114.3(2)
Ir(1)	P(1)	C(11)	116.0(3)
Ir(1)	P(1)	C(12)	112.5(2)
C(3)	P(1)	C(11)	103.2(3)
C(3)	P(1)	C(12)	105.3(3)
C(11)	P(1)	C(12)	104.5(4)
Ir(2)	P(2)	C(3)	111.0(2)
Ir(2)	P(2)	C(21)	118.4(2)
Ir(2)	P(2)	C(22)	114.9(3)
C(3)	P(2)	C(21)	104.7(3)
C(3)	P(2)	C(22)	103.2(3)
C(21)	P(2)	C(22)	103.1(4)
Ir(1)	P(3)	C(4)	111.1(2)
Ir(1)	P(3)	C(31)	113.8(2)
Ir(1)	P(3)	C(32)	116.5(2)
C(4)	P(3)	C(31)	104.4(3)
C(4)	P(3)	C(32)	105.6(3)
C(31)	P(3)	C(32)	104.4(3)
Ir(2)	P(4)	C(4)	115.0(2)
Ir(2)	P(4)	C(41)	115.2(2)
Ir(2)	P(4)	C(42)	113.0(2)
C(4)	P(4)	C(41)	106.0(3)
C(4)	P(4)	C(42)	103.3(3)
C(41)	P(4)	C(42)	102.8(3)
Ir(1)	C(1)	O(1)	176.6(6)
Ir(2)	C(2)	O(2)	171.6(6)
P(1)	C(3)	P(2)	112.2(3)
P(3)	C(4)	P(4)	111.6(3)

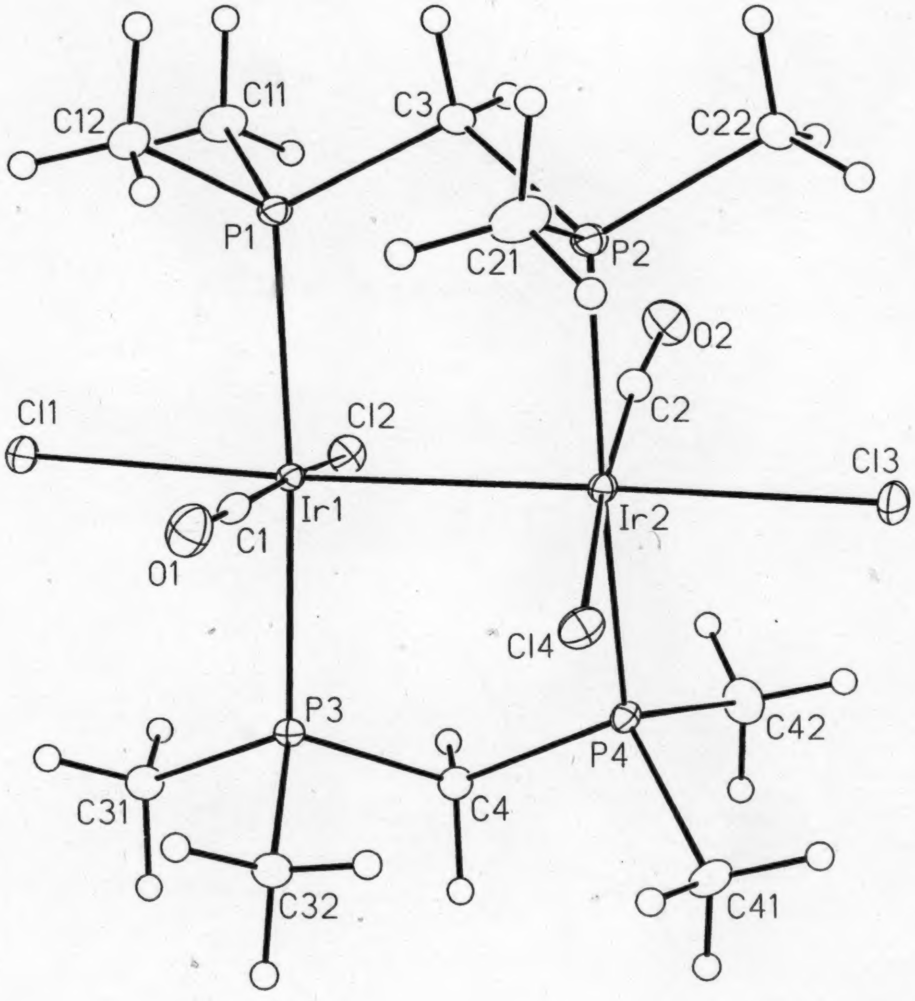
C12
C11
C3
C22
P1
C21
P2
O2
Cl1
Cl2
C2
Cl3
Ir1
Ir2
C1
O1
Cl4
P3
C42
P4
C31
C4
C32
C41

Figure 5.5. Perspective view of $[Ir_2Cl_4(CO)_2(dmpm)_2]$, **20**, showing the atom labeling scheme. Non-hydrogen atoms are represented by Gaussian ellipsoids at the 20% probability level. Hydrogen atoms are shown with arbitrarily small thermal parameters.

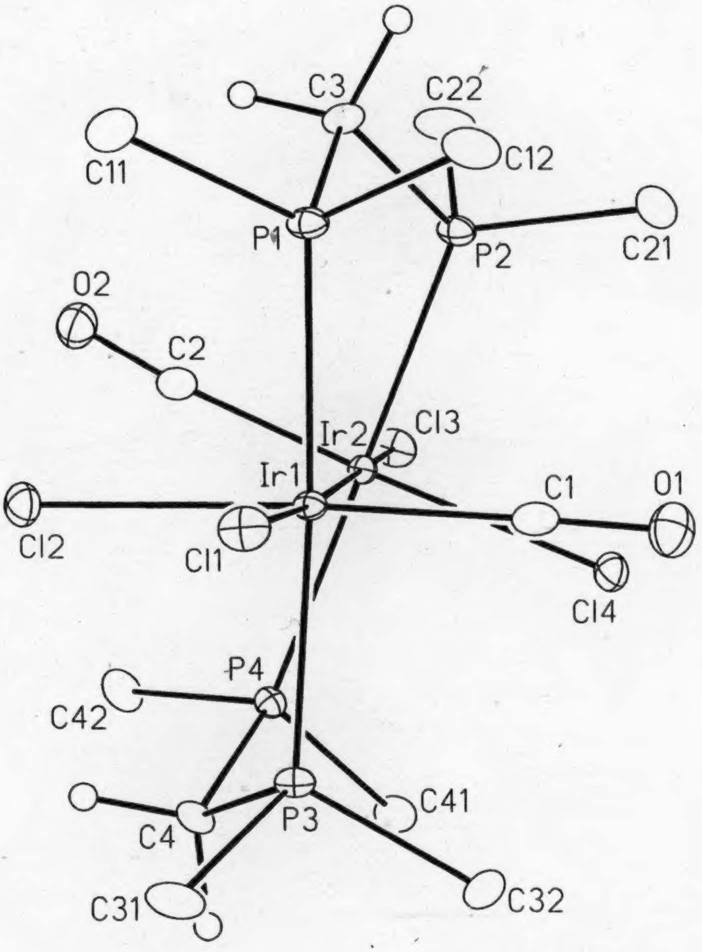
C3
C22
C12
C11
P1
P2
C21
O2
C2
Ir2
Cl3
Ir1
C1
O1
Cl2
Cl1
Cl4
P4
C42
C41
P3
C4
C31
C32

Figure 5.6. Alternate view of the molecule, **20**, illustrating the torsion of the trans biphosphine groups about the Ir(1)-Ir(2) bond. Hydrogen atoms of the dmpm methyl groups have been omitted.

Conclusions

At the outset, the aim of this work was to prepare dmpm analogues of coordinatively unsaturated dppm-bridged complexes of iridium, especially **1-dmpm**, in order to study their reactivity with olefins and other small molecules in the manner of Chapters 2, 3 and 4 of this thesis. This goal was frustrated by the inaccessibility of **1-dmpm** and was further complicated by the extreme air sensitivity and reactivity of the compounds, coupled with their generally reduced solubility compared to their dppm congeners. While the preparation of the compound **1-dmpm** by the route shown in Scheme 5.1 has been previously reported,[3,9] we have been unable to reproduce this synthesis. We have, however, succeeded in preparing several related compounds of interest. These serve to elucidate the chemistry of diiridium dmpm complexes, which is found to display important differences from that of dppm complexes. We have also improved the preparation of the key synthetic intermediate, $[Ir_2(CO)_4(dmpm)_2]$ (**15**) by removing the requirement for the use of Hg, a reagent being increasingly deprecated because of its toxicity and environmental impact.

Fortunately, by optimizing the conditions it was possible to obtain several interesting binuclear products, as well as an unusual mononuclear complex. These serve to highlight the differences between dppm and dmpm, in both the steric requirements and the electronic properties of the resulting diiridium complexes. Thus, whereas $[Ir_2(CO)_3(dppm)_2]$ will only add one equivalent of methyl trifluoromethanesulfonate, the more electron-rich $[Ir_2(CO)_4(dmpm)_2]$ reacts with two equivalents to give a dicationic species, **16**. The compound $[Ir_2Cl(CO)(\mu\text{-}CO)(dmpm)_3][Cl]$ (**17**), shows that the reduced steric requirements of dmpm allow the formation of a triply-bridged complex. The increased propensity of dmpm (over dppm) to form bridging complexes is well known.[17] In common with other known dmpm complexes, there is also a marked tendency towards reaction with chlorinated solvents, and so the only monomethyl complex obtained in this study, **19**, reacts in a few hours with dichloromethane to yield a tetrachloride, **20**, a behaviour also reported for dmpm complexes of rhodium.[5] Unfortunately, many of these dmpm complexes are less soluble than their dppm counterparts and so the choice of good solvents with which they do not react (i.e. no chlorines or ionizable hydrogens) is limited.

The reaction mixtures obtained when $[Ir(COD)Cl]_2$, dmpm and CO are combined are complex and variable depending on the precise conditions. In the course of many attempts, we were never able to resolve this mixture into a single product, or a tractable mixture. It was clear however, that the constituents of these mixtures included mono- and dinuclear species, as well as the triply bridged **17**, which was practically ubiquitous as a contaminant in the products obtained.

References and Footnotes

1. Ristic-Petrovic, D.; Torkelson, J. R.; Hilts, R. W.; McDonald, R.; Cowie, M. *Organometallics* **2000**, *19*, 4432.
2. Torkelson, J.R. Ph. D. Thesis, University of Alberta, 1998.
3. a) Reinking, M. K.; Fanwick, P.E.; Kubiak, C. P. *Angew. Chem. Int. Ed. Engl.* **1989**, *28*, 1377.

   b) Reinking, M. K. Ph. D. Thesis, Purdue University, 1989.
4. The authors of the previously reported preparation (see reference 3b) report variable yields (0 - 80 %) for **1-dmpm**.
5. Jenkins, J. A.; Ennett, J. P.; Cowie, M. *Organometallics* **1988**, *7*, 1845.
6. a) Tolman, C. A. *Chem. Rev.* **1977**, *77*, 313.

   b) Karsch, H. H. *Chem. Ber.* **1984**, *117*, 3123.
7. Vrieze, K.; Collman, J. P.; Sears, C. T.; *Inorg. Syn.* **1968**, *11*, 101.
8. van der Ent, A.; Onderlinden, A. L. *Inorg. Syn.* **1968**, *14*, 92.
9. Reinking, M. K.; Ni, J.; Fanwick, P.E.; Kubiak, C. P. *J. Am. Chem. Soc.* **1989**, *111*, 6459.
10. No data are given in reference 3b to support the formulation of this mixture. The author presumes it to be $[Ir_2Cl(\mu\text{-}CO)(CO)_3(dmpm)]_2[Cl]$ "in analogy to dppm reactions" (page 63).
11. Antwi-Nsiah, F.; Cowie, M. *Organometallics* **1992**, *11*, 3157.
12. Sutherland, B. R.; Cowie, M. *Organometallics* **1985**, *4*, 1637.
13. J.R. Torkelson, F.H. Antwi-Nsiah, R. McDonald, M. Cowie, J.G. Prius, K.J. Jalkanen and R.L. DeKock *J. Am. Chem. Soc.* **1999**, *121*, 3666.
14. a) Sutherland, B.R.; Cowie, M. *Organometallics* **1984**, *3*, 1869.

b) Cowie, M.; Dwight, S.K. *Inorg. Chem.* **1980**, *19*, 209.

c) Cowie, M.; Gibson, J.A.E. *Organometallics* **1984**, *3*, 984.

d) Farr, J.P.; Olmstead, M.M.; Balch, A.L. *Inorg. Chem.* **1983**, *22*, 1229.

15. a) Cowie, M.; Vasapollo, G.; Sutherland, B.R.; Ennett, J.P. Ennett, J.P. *Inorg. Chem.* **1986**, *25*, 2648.

b) Sola, E.; Torres, F.; Jimenez, M.V.; López, J.A.; Ruiz, S.E.; Lahoz, F.J.; Elduque, A.; Oro, L.A. *J. Am. Chem. Soc.* **2001**, *123*, 11925.

c) Rowsell, B.D.; Trepanier, S.J.; Lam, R.; McDonald, R.; Cowie, M. submitted to *Organometallics.*

16. Hutton, A. T.; Pringle, P.G.; Shaw, B.L. *Organometallics* **1983**, *2*, 1889.

17. a) Manojlivic-Muir, L.; Muir, K.W.; Frew, A.A.; Ling, S.S.M.; Thomson, M.A.; Puddephatt, R.J. *Organometallics* **1984**, *3*, 1637.

b) Manojlivic-Muir, L.; Jobe, I.R.; Maya, B.J.; Puddephatt, R.J. *J. Chem. Soc., Dalton Trans.* **1987**, 2117.

Chapter 6

Conclusions

The primary objective of this thesis was to investigate the reactivity of $[Ir_2(CH_3)(CO)_2(dppm)_2][CF_3SO_3]$ (**1**) with a variety of olefins. The secondary goal was to investigate the dmpm analogue (**1-dmpm**) because of its lower steric demands and increased basicity. Prior work on **1** had shown that it reacts with a range of unsaturated compounds, including cumulenes and mono- and di-olefins to give products of five basic types: 1) a simple olefin adduct, such as $[Ir_2(CH_3)(CO)_2(\eta^2\text{-}C_2H_4)(dppm)_2][CF_3SO_3]$ (**2B**) from its reaction with ethene; 2) an olefin-bridged species from tetrafluoroethene, i.e. $[Ir_2(CH_3)(CO)_2(\mu\text{-}C_2F_4)(dppm)_2][CF_3SO_3]$; 3) a product resulting from C-H bond cleavage of the iridium-bound methyl of **1**, i.e. $[Ir_2(H)(CO)_2(L)(\mu\text{-}CH_2)(dppm)_2][CF_3SO_3]$, where L = CO, phosphines, etc.; 4) vinyl-carbene products, which ultimately result from the reaction with allene, i.e. $[Ir_2(H)(CO)_2(\mu\text{-}\eta^1\text{:}\eta^3\text{-}HCC(CH_3)\text{=}CH_2)(dppm)_2][CF_3SO_3]$ (**3F**); and 5) the unusual doubly C-H activated product, $[Ir_2(CH_3)(H)(CO)_2(\mu\text{-}H)(\mu\text{-}CC(H)C(H)CH_2)(dppm)_2][CF_3SO_3]$ (**6B**) from the reaction with 1,3-butadiene.[1-5] Thus, it was hoped that by studying the intimate details of the coordination of these and related substrates at different temperatures some generalizations could be made about the natures and energetics of the different products and intermediates, from which an unified explication of the reaction pathway(s) could be arrived at. These aspects of the reactivity of **1** were explored in Chapters 2, 3 and 4 of this thesis. In Chapter 3, the apparent C-H *and* C-F activation of trifluoroethene (giving the bridged difluorovinylidene complex $[Ir_2CH_3(H)(CO)_2(\mu\text{-}X)(\mu\text{-}C{=}CF_2)(dppm)_2][CF_3SO_3]$ (**11**, X = F or OH) led to the investigation of the reactions of some other halofluoroolefins. Finally, in Chapter 5, the related chemistry of the alternative biphosphine ligand, dmpm, was explored. Initially the goal was to repeat some of the dppm chemistry (particularly the reactions with olefins) with **1-dmpm**,[6-8] but its preparation was problematic. However, some interesting new species were synthesized and helped to shed further light on the steric and electronic factors determining the reaction paths of **1** and related species. Some ancillary data, in the form of DFT calculations of the structures of **1** and **1-dmpm** are presented in Appendix A.

One of the central results from our study of olefin adducts (Chapters 2 and 3) was the appearance of several different product types, the order of stabilities of which was the same irrespective of substrate. Thus, in all the cases in which such a species was observed, the methylene hydride product, containing an η^2-bound olefin was the least stable, being found only at the lowest temperature. This is the first kinetic product, and presumably results from a pathway requiring the least amount of rearrangement of the dppm framework (thus incurring the smallest energy penalty). Thus, the incoming olefin attacks the exposed metal atom in a terminal site, which presumably is least obscured by phenyl groups in the equilibrium geometry. As previously proposed, the cation of **1** is highly fluxional in solution, with the methyl group moving back and forth between terminal positions, via a symmetrical methyl-bridged form. Our calculations (Appendix A) show that there is a minimum in the potential energy surface for this species corresponding to a structure very similar to that found in the crystal (where the methyl group is terminal). In contrast to this, the results for dhpm that were previously reported showed the nearest minimum to be a somewhat different structure, implying a different average solution structure.[2, 9] Clearly the bulk of the phenyl groups alters the geometry in solution, because these groups need to "pack" with each other in a "gear-wheel" arrangement even in the isolated cation. For dhpm it was found that the species containing a bridging methyl group, analogous to the solid-state structure of the dmpm compound,[7, 8] was higher in energy than a terminal form.[2] This must be largely an electronic effect since the dhpm ligand is not very sterically demanding. While we have not been able to calculate a methyl- bridged structure for the dppm complex yet because of the prodigious requirements of computer time, it is likely that even for dppm the methyl- bridged form is somewhat higher in energy than the structure bearing a terminal methyl group. Also, in the dhpm calculations there was a minimum for an agostic intermediate, on the pathway to C-H activation of the methyl group.

Thus, in the formation of the initial olefin adduct, the incoming olefin ligand arrives as the methyl group is undergoing its fluxional transfer from one metal to the other (see Figure 6.1).

Because structure **III** is higher in energy than **I** or **II** which are degenerate with **I'** and **II'**, respectively, the complex spends most of its time in these lower energy forms. We propose that the kinetic product upon olefin coordination captures the iridium-bound methyl group near this bridged agostic geometry,[2] perturbing it slightly to the fully C-H activated methylene hydride (see Scheme 6.1). Interaction of **II** (**II'**) with the ligand forms the methylene-bridged hydride **IV** (**IV'**).

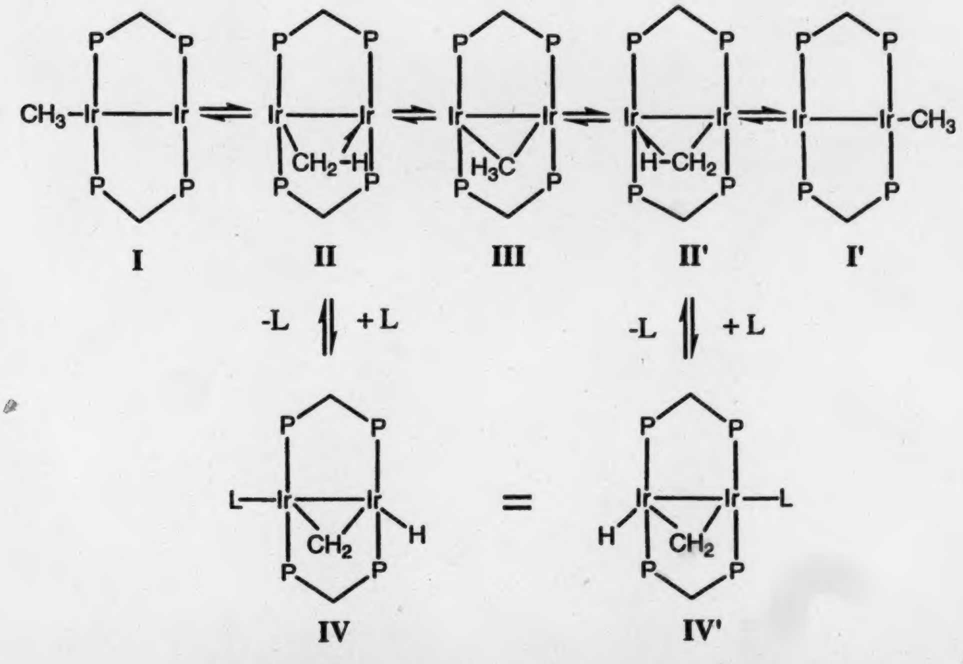

Figure 6.1. Fluxional process connecting the two terminal methyl forms of **1** and the interception of an agostic intermediate by an olefin ligand L to give the observed methylene-hydride product. Phenyls and carbonyl ligands have been omitted for clarity.

As the temperature is raised the methylene hydride reverts to a terminal methyl, as a slightly more stable form. Thus, while the favoured species for attack by the olefin ligand is the methylene hydride, once formed, the adduct is more stable as a terminal methyl complex.

For olefins such as ethene, fluoroethene and Z-1,2-difluoroethene, which do not form an olefin-bridged structure, the final product remains as the η^2-olefin adduct having a terminally bound methyl group (i.e. $[Ir_2(CH_3)(CO)_2(\eta^2\text{-olefin})(dppm)_2][CF_3SO_3]$). However, for olefins that are sufficiently electron withdrawing, a subsequent transformation to a more stable olefin-bridged product occurs. Thus tetrafluoroethene bridges the metals at room temperature,[1] whereas ethene remains terminally bound to one metal.[4] The dividing line between bridging and non-bridging in the fluoroolefin series studied in Chapter 3 appears to lie between Z-1,2-difluoroethene which is terminally bound and 1,1-difluoroethene which forms a bridged product at temperatures at and above where it forms the η^2 product. The bridging site is believed to be more crowded than the terminal site, and requires some rearrangement of the dppm ligands from the terminal η^2-olefin binding mode.

For diolefins, alternate bridging modes are possible in which *both* olefinic moieties interact with the metals. The initial steps in the reaction of the cumulenes with **1** mirror those of the monoolefins. Thus, the first kinetic product is the η^2-olefin, methylene hydride species, the second is the η^2-olefin adduct with a terminally bound iridium-methyl group, and at higher temperatures bridging species are formed (except in the case of 1,1-dimethylallene where the steric requirements of the ligand are such that this does not occur). The subsequent rearrangements that occur presumably result from the interaction of the *two* olefinic bonds with the metals. We have proposed that the alternative bridged forms interconvert between a cis-cis form in which both double bonds of the allene are coordinated to the metals, i.e. diagonally bridged in an η^2:η^2 fashion (see Scheme 2.9). This form relaxes to either of the singly bridged dimetallacyclobutane forms which are less crowded since the dppm ligands are in the trans-trans arrangement. When the temperature is high enough, a bridged geometry, in which the allene is η^1 bound to the central carbon at one metal while interacting with the second in an η^3 allyl binding mode, such as $[Ir_2(CH_3)(CO)_2(\mu\text{-}\eta^1\text{-}\eta^3\text{-}H_2C{=}C{=}CH_2)(dppm)_2][CF_3SO_3]$ (**3E**) forms.[2] In this product the crowding due to the cis/trans coordination is compensated for by the additional bonding interactions over the μ-η^1:η^1 (dimetallacyclobutane) form.

The transformation of the initial methylene hydride product through several species containing intact methyl groups militates against this hydride being involved in the formation of the ultimate vinyl carbene product, such as $[Ir_2(H)(CO)(\mu\text{-}\eta^1\text{:}\eta^3\text{-}HCC(CH_3){=}CH_2)(dppm)_2][CF_3SO_3]$ (**3F**). It had originally been proposed that a methylene hydride intermediate such as **3A** or **3B** could yield **3F** by insertion of the allene into the Ir-H bond, followed by migration of the isopropenyl group to the methylene fragment. However, the previously reported structure of $[Ir_2(CH_3)(CO)_2(\mu\text{-}\eta^1\text{-}\eta^3\text{-}H_2C{=}C{=}CH_2)(dppm)_2][CF_3SO_3]$ **(3E)**[3] shows the iridium-bound methyl poised for direct coupling with the central allylic carbon. As shown in Scheme 2.9, this could occur as a direct methyl transfer, or accompanied by C-H activation in concert with C-C bond formation. These two possibilities, taken together, explain the earlier ^{13}C labeling results which put the label in all possible positions expected of either pathway in the final product.

The conjugated diene, 1,3-butadiene, also forms a bridged species which is present in substantial amounts at low temperature. Again, this diolefin has one olefinic moiety bound to each metal. We have presented chemical (as opposed to kinetic) evidence that suggests that this, or a similar species may be an intermediate in the activation of the two geminal C-H bonds of 1,3-butadiene. This is because: 1) diolefins which do not form such adducts for steric reasons do not go on to undergo C-H activation and 2) substitution at one end of the olefin inhibits C-H activation at the other end. The latter observation points to the need for coordination of both double bonds, since if the C-H activation involved only one of the double bonds there should be no such effect. Convincing arguments for olefin activation *not* involving prior coordination have been made,[10 - 12] but these obtain in the context of *mono*metallic species. Even for monometallic complexes there is a notable exception in the case of $[(\eta^2\text{-}HBPf_3)Ir(CO)(\eta^2\text{-}C_2H_4)]$ ($HBPf_3^-$ = tris(3-(trifluoromethyl)-5-methyl-pyrazol-1-ylborate anion) which isomerizes to the more stable $[(\eta^3\text{-}$

$HBPf_3)Ir(CO)(H)(CH{=}CH_2)]$ upon warming in solution.[13] The accompanying change in hapticity of the pyrazolylborate ligand is not unlike the additional flexibility extant in bimetallic complexes where the local geometry and coordination number at a metal centre can be variable, with little energy difference between the isomers. The intimate details of the cleavage of the olefinic C-H bond may differ in the mono- and bimetallic cases in that, for the bimetallic system studied, the second metal centre may be tethering the olefin at one end, while reaction occurs at the other by essentially the same pathway as in monometallics. In contrast, most monometallic complexes appear to activate the C-H bonds of olefins directly via a short-lived σ-complex,[12] whereas π-olefins lie on a separate pathway not leading to activation (dissociation of the π-olefin is required for C-H activation to occur). Such reactions of monometallic complexes typically require heating or photolytic activation to occur and proceed via production of a highly reactive, coordinatively unsaturated intermediate which then forms the σ-complex, leading to C-H bond cleavage. Notably the reagent **1**, which activates two C-H bonds of 1,3-butadiene, requires no further activation and is itself an indefinitely stable species. The presence of a second metal dramatically lowers the activation energy required for 1,3-butadiene activation, in contrast to the traditional C-H activation process which requires that the metal fragment be generated in a very highly activated state.

The question arises of whether the 1,3-butadiene adduct $[Ir_2(CH_3)(CO)_2(\mu\text{-}\eta^2{:}\eta^2\text{-}H_2C{=}CH\text{-}CH{=}CH_2)(dppm)_2]^+$ (**6A**) is identically the intermediate in the room temperature formation of the doubly activated product $[Ir_2(CH_3)(H)(CO)(\mu\text{-}H)(\mu\text{-}CC(H)C(H)CH_2)(dppm)_2][CF_3SO_3]$ (**6B**) or whether it is some related, but unseen, species which also involves coordination of both double bonds. Apart from the former view satisfying the requirement of Occam's razor, is the observation of rehybridization towards sp^3 of one of the butadiene carbons, as seen in the NMR study. This carbon resembles an alkyl group in **6A**, the adjacent-metal assisted α-elimination of which occurs with facility in these systems. Taking these arguments, together with the chemical evidence, we thus conclude that **6A** is probably an intermediate on the path to C-H activation of 1,3-butadiene.

The observation that trifluoroethene undergoes an apparent C-H and C-F activation led us to investigate the chemistry of fluoroethenyl species which were presumed to be intermediates in such activation processes. We had hoped to be able to remove the bridging halogen ligand from the fluoroethenyl products in order to induce C-H activation in $[Ir_2(C(H)\!=\!CF_2)(CH_3)(CO)_2(\mu\text{-}Br)(dppm)_2][CF_3SO_3]$ (**12**) or C-F activation in $[Ir_2(CF\!=\!CF_2)(CH_3)(CO)_2(\mu\text{-}Cl)(dppm)_2][CF_3SO_3]$ (**11**), but this was unsuccessful. We did, however, succeed in replacing a β-fluorine of the trifluoroethenyl moiety of **11** with a methyl group. Perhaps the most interesting part of that transformation is that there is an apparent migration of the fluoroethenyl group from one metal to the other, suggesting the intermediacy of some type of fluorocarbyl-bridged species.

We had hoped to duplicate the previously reported synthesis of $[Ir_2(CH_3)(CO)_2(dmpm)_2][CF_3SO_3]$ (**1-dmpm**) in order to test its reactivity with the olefins and fluoroolefins that we had investigated with the analogous dppm complex. In the published preparation, the iridium-bound methyl group is obtained first as a bridging methylene in which the C_1 fragment has come from the dichloromethane solvent and then this dicationic tetracarbonyl complex is transformed to methyl-bridged dicarbonyl monocation (i.e. **1-dmpm**) by the reaction with K[HBsec-Bu_3], with the concomitant *loss* of two carbonyl ligands (see Scheme 5.1). We were able to obtain the methylene-bridged dication, but only in conjunction with several other species. The next step, which the authors indicate occurs in quite variable yield (0-80%), was unsuccessful in our hands. Thus, we decided to pursue a rational synthesis of **1-dmpm** by first attempting to characterize the products of the initial reaction of $[IrCl(COD)]_2$ with dmpm followed by the addition of carbon monoxide. The composition of this reaction mixture was highly variable, depending on the solvent, concentrations of reagents and temperature. By manipulating these conditions we were able to obtain the mononuclear species $[Ir(COD)(dmpm)_2]Cl$ (**18**) and the triply dmpm-bridged $[Ir_2Cl(CO)(\mu\text{-}CO)(dmpm)_3][Cl]$ (**17**), but not the compound $[Ir_2Cl(\mu\text{-}CO)(CO)_3(dmpm)]_2[Cl]$ which was presumed by the previous author to have been present in the reaction on the basis of its colour.[8] The binuclear Ir(II)-Ir(II) complex $[Ir_2(CH_3)Cl_2(CO)_2(dmpm)_2][CF_3SO_3]$ (**19**) was obtained from the reaction of methyl trifluoromethanesulfonate with the reaction mixture in CH_2Cl_2. Presumably, the methyl trifluoromethanesulfonate trapped nascent *trans*-[IrCl(CO)(dmpm)]$_2$ which is in equilibrium with other species in the reaction mixture.[14] Not surprisingly, **19** reacted with CH_2Cl_2 solvent to give a tetrachloride, [$Ir_2Cl_4(CO)_2(dmpm)_2$] (**20**).

Unlike the dppm-bridged complexes, the dmpm complexes are, with a single exception, very air sensitive. They are also rather reactive and seem to prefer higher formal oxidation states for the metal atoms, presumably in order to relieve the buildup of electron density due to the electron-rich dmpm ligand. The enhanced basicity of the metal centres is demonstrated by the reaction of [$Ir_2(CO)_4(dmpm)_2$] with two equivalents of methyl trifluoromethanesulfonate to give [$Ir_2(CH_3)_2(CO)_4(dmpm)_2$][$CF_3SO_3$]$_2$ (**16**), whereas the related dppm complexes only react with a single equivalent. As a consequence of the reduced steric requirements of dmpm as compared to dmpm there is a marked tendency to increase the coordination number of the metals, either by oxidative addition, as described above, or by adding a third dmpm bridge, to give the compound [$Ir_2Cl(CO)(\mu$-CO)(dmpm)$_3$][Cl], (**16**). Being coordinatively saturated, **16** is relatively unreactive and is air-stable for brief periods.

The goal of finding a less sterically demanding system with enhanced metal basicity would benefit from the study of some alternative drpm ligands (r = alkyl substituents), other than dmpm. The ligand dmpm suffers from being too small, decreasing the selectivity in reactions, and generally leading to the formation of some triply bridged product (**17**) or higher nuclearity clusters. In choosing a drpm system for bridging a pair of metals consideration should be given the flexibility of the ligand (so that the r groups can move out of the way of incoming substrates, or so that changes in the bonding mode can occur) and to the degree of crowding both in the immediate vicinity of the metal atoms and further away. Thus dppm gives a very crowded environment near the metals so that only narrow molecules like 1,3-butadiene (but not 2-methyl-1,3-butadiene) can occupy the bridging site. Looking at the calculated structure of **1-dmpm** (Appendix A) it can be seen that larger molecules can occupy the bridging site. Indeed, in the tris-bridged complex $[Ir_2Cl(CO)(\mu\text{-}CO)(dmpm)_3][Cl]$ (**17**) the facial dmpm ligand coordinates in a fashion not unlike what is proposed for the 1,3-butadiene ligand in $[Ir_2(CH_3)(CO)_2(\mu\text{-}\eta^2\text{:}\eta^2\text{-}H_2C\text{=}CH\text{-}CH\text{=}CH_2)(dppm)_2][CF_3SO_3]$ (**6A**). Thus a ligand like bis(diethylphosphino)methane (depm) or one with a larger alkyl group might combine the favourable properties of dppm and dmpm.

The need to include the full steric bulk of the ligands in calculations is demonstrated by the difference in the calculated solution structure of **1** compared to **1-dppm**. It would be useful to extend such calculations to the other species discussed in Chapter 2 (i.e. the terminal and bridged olefin complexes). Also, the energy and structures of the methyl-bridged dppm and dmpm complexes should be calculated to see how they differ from the dhpm structure, which was previously reported. While the minimization of the structure of **1** took about six months of computer time, progress in computer speed continues, and as of this writing, desktop machines more than 8X faster than this are available.

Since it has been shown that fluoroolefin-bridged species are accessible at low temperature, and, in some cases are stable at or near room temperature, the reactions of these, such as α-fluorine abstraction by acids, should be explored. The dimetallacyclobutane fragment $M_2(\mu\text{-}F_2CCF_2)$ resembles two linked M-R_f (R_f = perfluoroalkyl) moieties. The latter are known to be susceptible to α C-F cleavage,[15] so the former could be expected to be also. Of related interest would be the reaction of **1** with fluoroallenes (such as the readily prepared 1,1-difluoroallene)[16] which might stabilize the bridged form sufficiently for their isolation and structural characterization.

The reaction of $[Ir_2(CH_3)(CO)_2(dppm)_2][CF_3SO_3]$ (**1**) with olefins involves a variety of kinetic products which can rearrange *via* the involvement of both metals (e.g. the formation of bridging species) or, in the case of diolefins, the involvement of both olefinic bonds with the metals. Although the reaction of olefins with **1** can induce C-H activation of the iridium-bound methyl group, neither the methylene nor the hydride fragments are involved in subsequent chemistry. The subsequent C-C bond-forming reactions of the allenes appear to proceed via the direct coupling of the methyl group (accompanied by C-H activation) with the preformed bridged olefin. In monoolefins the tendency to form bridged complexes appears to be related to the electron-withdrawing ability of the olefin, with the more electron-withdrawing olefins forming bridged complexes because the additional bonding interactions in that position can overcome the unfavourable steric demands of the bridging site. Similarly, where steric requirements permit, diolefins form bridging complexes. In some cases (allene and methylallene) the energetics of the bridging interaction were such that a cis-trans conformation of the "Ir_2dppm_2" framework would be adopted. Clearly the effect of the bulky dppm ligands is both beneficial, in that there is selectivity in the reactions due to the crowding of the "active sites" of the metals, and detrimental in that bulkier substrates cannot approach the metals, and so cannot be activated. The utility of other drpm ligands lies in their potential for allowing the fine-tuning of the balance of steric discrimination and electron richness of the metal centres. This could allow enhanced reactivity towards the activation of unreactive C-H and C-F bonds in a more selective fashion than has been achieved with the dppm-bridged systems that have been the topic of this thesis.

References and Notes

1. Torkelson, J. R. Ph. D. Thesis, University of Alberta, 1998.
2. J.R. Torkelson, F.H. Antwi-Nsiah, R. McDonald, M. Cowie, J.G. Prius, K.J. Jalkanen and R.L. DeKock *J. Am. Chem. Soc.* **1999**, *121*, 3666.
3. Torkelson, J. R.; McDonald, R.; Cowie, M. *J. Am. Chem. Soc.* **1998**, *120*, 4047.
4. Antwi-Nsiah, F. H.; Cowie, M. *Organometallics* **1992**, *11*, 3157.
5. Ristic-Petrovic, D.; Torkelson, J. R.; Hilts, R. W.; McDonald, R.; Cowie, M. *Organometallics* **2000**, *19*, 4432.

6. Reinking, M. K.; Ni, J.; Fanwick, P.E.; Kubiak, C. P. *J. Am. Chem. Soc.* **1989**, *111*, 6459.

7. Reinking, M. K.; Fanwick, P.E.; Kubiak, C. P. *Angew. Chem. Int. Ed. Engl.* **1989**, *28*, 1377.

8. Reinking, M. K. Ph. D. Thesis, Purdue University, 1989.

9. Strictly, this is a gas phase structure, since the calculation is on an isolated molecule. The effect of the solvent on the core geometry of the complex, especially the disposition of the methyl group, is expected to be small. This is supported by the effect of changing the solvent on the methyl resonance in the ^{1}H NMR, which is negligible. If the solvent affected the preferred arrangement of the methyl in solution the chemical shift would change as would the coupling in the virtual quintet that is observed for **1** at room temperature in solution.

10. Stoutland, P. O.; Bergman, R. G. *J. Am. Chem. Soc.* **1985**, *107*, 4581.

11. Silvestre, J.; Calhorda, M. J.; Hoffmann, R.; Stoutland, P. O. Bergman, R. G. *Organometallics* **1986**, *5*, 1841.

12. Stoutland, P. O.; Bergman, R. G. *J. Am. Chem. Soc.* **1988**, *110*, 5732.

13. Ghosh, C. K.; Hoyano, J. K.; Krentz, R.; Graham, W. A. G. *J. Am. Chem. Soc.* **1989**, *111*, 5480.

14. The ^{31}P NMR spectrum of this mixture is complex, and indicates the presence of mono- and dinuclear species, including **17**, and **18**.

15. Richmond, T. G. *Angew. Chem. Int. Ed. Engl.* **2000**, *39*, 3241.

16. Drakesmith, F. G.; Stewart, O. J.; Tarrant, P. *J. Org. Chem.* **1967**, *33*, 280.

Appendix

Calculated Structures of 1 and 1-dmpm

Introduction

A problem of fundamental importance in solution chemistry is the question of the relationship of solid-state structures of compounds as determined using X-ray crystallography and the structures of these in solution. While in many cases there may be a close correspondence between the two, this is not necessarily the case, because different conformations may be adopted in solution where the requirements of crystal packing are not present. Increasingly, the structures of transition metal complexes are being calculated in the gas phase using Density Functional Theoretical (DFT) methods. To make such calculations practical, i.e. so that they may be completed with a reasonable expenditure of computing resources, complex ligands such as dppm are often modeled using simpler systems such as the bis(dihydrogenphosphino)methane (dhpm) ligand. By reducing the number of electrons in the system to be calculated the time required can be reduced substantially.

The structure of the cation $[Ir_2(CH_3)(CO)_2(dppm)_2]^+$ (**1**) has been modeled using dhpm.[1] The resulting geometry of $[Ir_2(CH_3)(CO)_2(dhpm)_2]^+$ (**1-dhpm**) differed in several important respects from that found in the X-ray structure determination of **1**. In order to investigate the effect of the substituents upon the structure, we undertook a DFT calculation of the geometry of the dppm-bridged cation **1**, and of the related dmpm-bridged complex **1-dmpm**.

Theoretical Methods and Software

A series of DFT[2] calculations at the B3LYP level[3] employing the LanL2DZ basis set[4] were carried out, using Gaussian 98,[5, 6] to clarify the relationship between the crystallographically determined geometry of **1** and its structure in solution. Full geometry optimizations were completed on both of the cations for which data are reported. Theoretical vibrational frequencies were calculated for each of these species to characterize them as minima on the potential energy surface or n^{th} order saddle points depending on the presence of n-imaginary frequencies wherein n=0 for a minimum.[6] Also, the stability of the calculated wavefunctions for the optimized geometries was tested using computational protocols contained in Gaussian 98.[6]

Results

The crystal structure of **1** shows that there is an unsymmetrical A-frame structure in which one carbonyl group is bridging, while the other carbonyl and the methyl group occupy terminal positions, on different metals.[1] However, the

DFT-calculated gas phase structure of the model cation $[Ir_2(CH_3)(CO)_2(dhpm)_2]^+$ **(1-dhpm)** shows a different arrangement, with both carbonyl ligands being terminal[1], and the methyl nearly at right angles to the Ir-Ir axis.

To address the issue of the steric effects of substituents, other than hydrogen, on the phosphorus atoms, full geometry optimizations of $[Ir_2(CH_3)(CO)_2(dmpm)_2]^+$ and $[Ir_2(CH_3)(CO)_2(dppm)_2]^+$ were carried out using the same model chemistry as that previously reported for the dhpm model, i.e. B3LYP/LanL2DZ. Figure A.1 compares the core geometries calculated by us for **1**, and **1-dmpm** with the previously reported geometry of **1-dhpm** and the X-ray structure of **1** and of **1-dmpm.**[7] Tables A.1 and A.2 list important distances and angles, respectively, for these species. Figures A.2 and A.3 show the DFT-calculated structure of **1**, and Figures A.4 and A.5 show the calculated structure of **1-dmpm**. As in the dhpm study, we started with the X-ray coordinates of **1**. For **1-dmpm** we replaced the phenyls with methyl groups. Much like the dhpm study, the calculation for **1-dmpm** converged to a structure with the bridging carbonyl moved away from the bridging position and the methyl moved away from the Ir-Ir axis. The calculated structure is intermediate between that for **1-dhpm** and the X-ray structure of **1**. Moreover, the *calculated* structure of **1** is similar to that found in the solid state, suggesting that the retention of phenyls in the calculation is important for determining the structure. The reported X-ray structure for **1-dmpm** is at variance with these results in that it suggests a bridging methyl, which for **1-dhpm** was found to be 25-28 kJ/mol higher energy than the structure with a terminal methyl group.[1] In our calculations, it appears that the effect on the core geometry of a P-methyl is intermediate between that of a P-H and of a P-phenyl, a trend that is in keeping with the steric demands of these groups, but not with the electron donating/withdrawing character, which would have P-methyl as an extreme. Compound **1** is known to be highly fluxional in solution so that the ^{1}H NMR resonance of the iridium-methyl group appears as a quintet at room temperature (with equivalent coupling to all four phosphorus nuclei), but as a triplet below the coalescence temperature for the fluxional process.[1] The reported activation enthalpy for this process is 25.5±0.4 kJ/mol, which is close to the energy difference between a methyl-bridged dhpm and a terminal-methyl dhpm analogue.[1] It is likely that in **1** the methyl moves from one iridium to the other *via* a methyl bridged species, but that the energy minima in solution are similar to the solid state structure, in that they have a terminal methyl and a bridging CO.

The inclusion of bulky phenyl groups in geometry optimization calculations, while extremely costly in computer time, is necessary to adequately model the solution chemistry of the complexes such as **1**. Thus, we have shown that the dichotomy between the solid-state structure of **1** and the calculated structure of **1-dhpm** is not due to crystal packing forces,[1] but is due to the profound influence of the phenyl groups upon the core geometry of the complex. Notwithstanding the influence of the dppm phenyls on the geometry, the compound **1** is highly fluxional. The presence of a lengthwise region of coordinative unsaturation (the bridging site), shielded by phenyl groups, allows for a degree of selectivity of substrates.

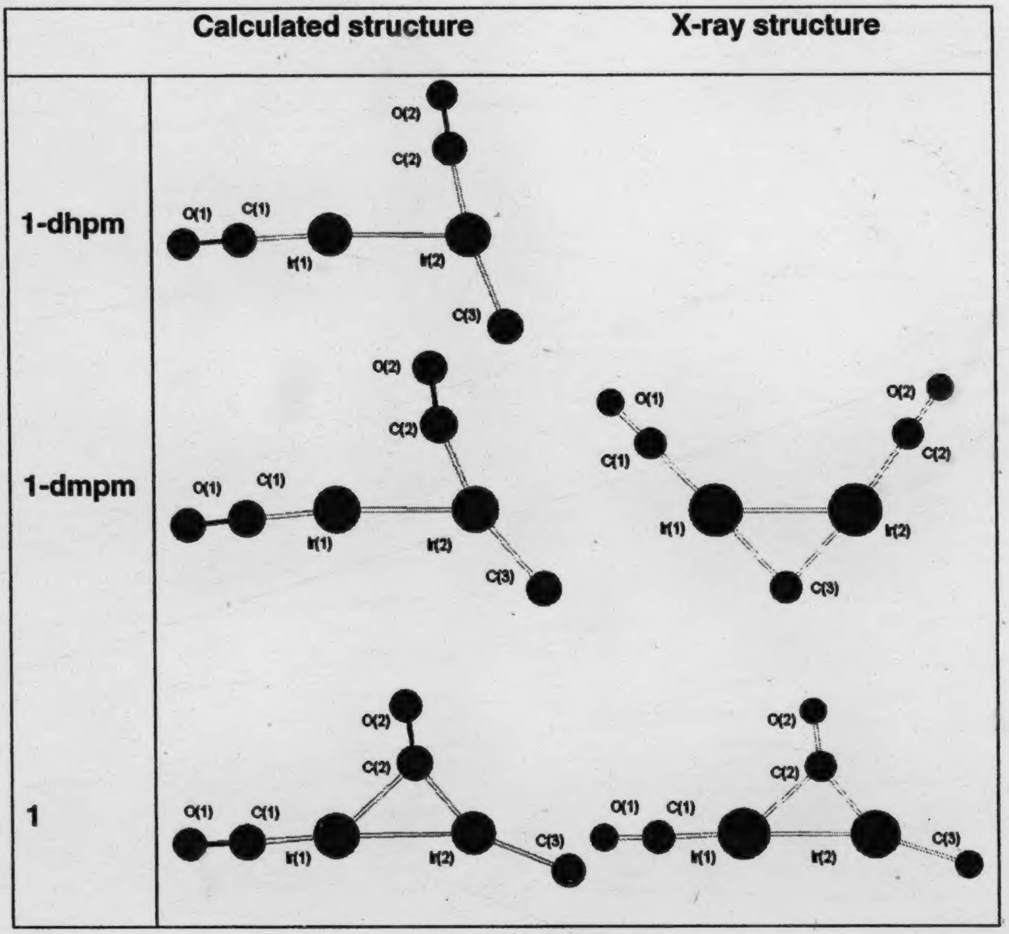
Calculated structure
X-ray structure
1-dhpm
1-dmpm
1
O(1)
C(1)
Ir(1)
Ir(2)
C(2)
O(2)
C(3)

Figure A.1. Comparison of calculated and X-ray core geometries of dhpm, dmpm and dppm analogues of **1**.[1, 7] Only the atoms directly bonded to iridium, other than phosphorus, are shown.

Table A.1. Selected distances for the calculated and experimentally determined structures of **1**

		calculated			X-ray structure	
atom 1	atom 2	**1-dhpm**[a]	**1-dmpm**	**1**	**1**[a]	**1-dmpm**[b]
Ir(1)	Ir(2)	2.94	2.80	2.86	2.7775(5)	2.885(1)
Ir(2)	C(3)	2.14	2.13	2.13	2.15(2)	2.18[c]
Ir	P (avg)	2.34	2.42	2.42	2.311	2.328
Ir(1)	C(1)	1.94	1.83	1.86	1.77(2)	1.95[d]
Ir(2)	C(2)	1.93	1.89	1.92	2.089(9)	

[a] From reference 3; [b] From reference 7; [c] Average of Ir(1)-C(3) and Ir(2)-C(3) for the reported methyl-bridged structure; [d] Average Ir-C bond length for the two terminal CO ligands

Table A.2. Selected angles for the calculated and experimentally determined structures of **1**

			calculated			X-ray structure	
atom 1	atom 2	atom 3	**1-dhpm**[a]	**1-dmpm**	**1**	**1**[a]	**1-dmpm**[b]
Ir(1)	Ir(2)	C(2)	78.60	72.60	42.00	48.9(2)	
Ir(1)	Ir(2)	C(3)	111.60	130.20	157.00	162.4(5)	48.3(6)[c]
P	Ir	P (avg)	174.50	176.60	173.50	172.2	171.4
C(2)	Ir(2)	C(3)	169.80	162.50	151.30	148.5(6)	48.8(6)[c]

[a] From reference 3; [b] From reference 7; [c] In this structure the methyl is approximately symmetrically bridging Ir(1) and Ir(2). See Figure A.1.

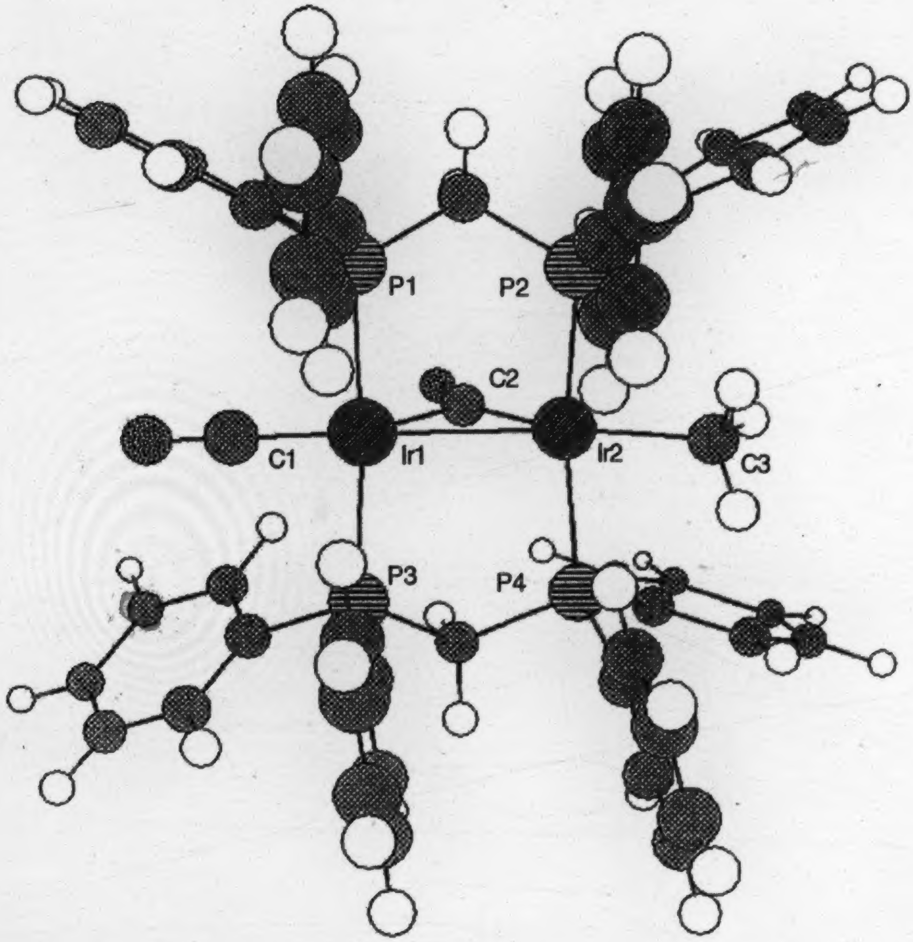
P1
P2
C2
C1
Ir1
Ir2
C3
P3
P4

Figure A.2. DFT-calculated structure of $[Ir_2(CH_3)(CO)_2(dppm)_2]^+$ (**1**).

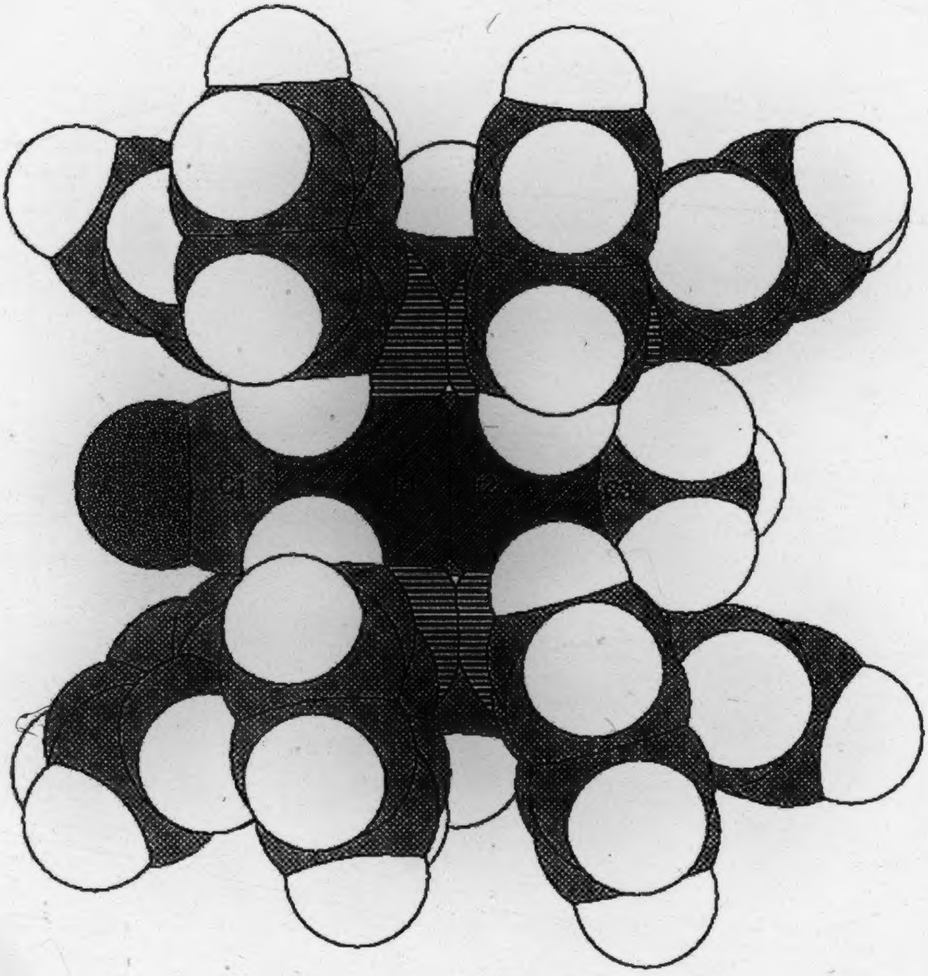

Figure A.3. DFT-calculated structure of $[Ir_2(CH_3)(CO)_2(dppm)_2]^+$ (**1**) shown in a space filling representation.

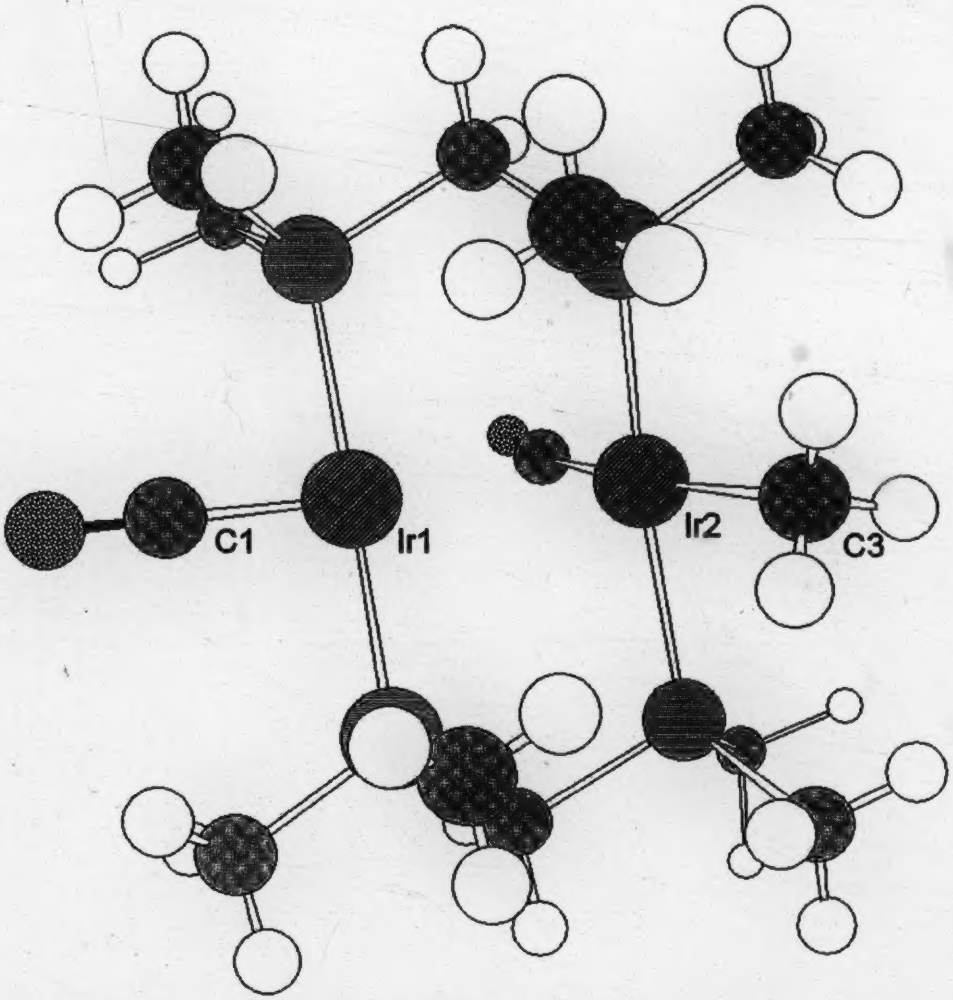
C1
Ir1
Ir2
C3

Figure A.4. DFT-calculated structure of $[Ir_2(CH_3)(CO)_2(dmpm)_2]^+$ **(1-dmpm)**.

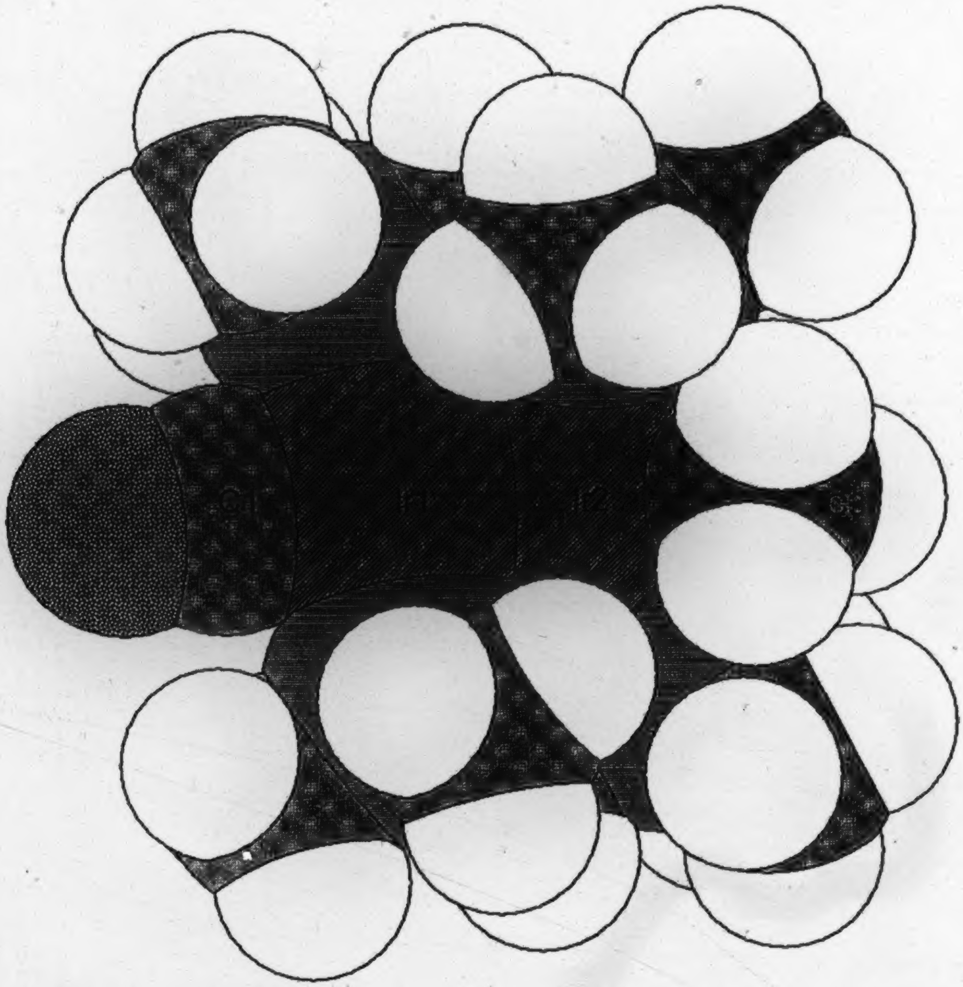
C1
Ir1
Ir2
C3

Figure A.5. DFT-calculated structure of $[Ir_2(CH_3)(CO)_2(dmpm)_2]^+$ **(1-dmpm)** shown in a space filling representation.

References

1. J.R. Torkelson, F.H. Antwi-Nsiah, R. McDonald, M. Cowie, J.G. Prius, K.J. Jalkanen and R.L. DeKock *J. Am. Chem. Soc.* **1999**, *121*, 3666.

2. Ziegler, T. *Chem. Rev.* **1991**, *91*, 651.

3. a) Becke, A. D.; *J. Chem. Phys.* **1993**, *93*, 5648.

   b) Lee, C.; Yang, W.; Parr, R. G. *Phys. Rev. B* **1988**, *37*, 785.

   c) Miehlich, B.; Savin, A.; Stoll, H.; Preuss, H. *Chem. Phys. Lett.* **1989**, *157*, 200.

   d) Stephens, P. J.; Devlin, F. J.; Chabalowski, C. F.; Frisch, M. J. *J. Phys. Chem.* **1994**, *98*, 11623.

4. a) Hay, P J.; Wadt, W. R. *J. Chem. Phys.* **1985**, *82*, 270.

   b) Wadt, W. R. ; Hay, P. J. *J. Chem. Phys.* **1985**, *82*, 284.

   c) Hay, P J.; Wadt, W. R. *J. Chem. Phys.* **1985**, *82*, 299.

5. Gaussian 98, Revision A.7, M. J. Frisch, G. W. Trucks, H. B. Schlegel, G. E. Scuseria, M. A. Robb, J. R. Cheeseman, V. G. Zakrzewski, J. A. Montgomery, Jr., R. E. Stratmann, J. C. Burant, S. Dapprich, J. M. Millam, A. D. Daniels, K. N. Kudin, M. C. Strain, O. Farkas, J. Tomasi, V. Barone, M. Cossi, R. Cammi, B. Mennucci, C. Pomelli, C. Adamo, S. Clifford, J. Ochterski, G. A. Petersson, P. Y. Ayala, Q. Cui, K. Morokuma, D. K. Malick, A. D. Rabuck, K. Raghavachari, J. B. Foresman, J. Cioslowski, J. V. Ortiz, A. G. Baboul, B. B. Stefanov, G. Liu, A. Liashenko, P. Piskorz, I. Komaromi, R. Gomperts, R. L. Martin, D. J. Fox, T. Keith, M. A. Al-Laham, C. Y. Peng, A. Nanayakkara, C. Gonzalez, M. Challacombe, P. M. W. Gill,

B. Johnson, W. Chen, M. W. Wong, J. L. Andres, C. Gonzalez, M. Head-Gordon, E. S. Replogle, and J. A. Pople, Gaussian, Inc., Pittsburgh PA, 1998.

6. Foresman, J. B.; A. Frisch *Exploring Chemistry with Electronic Structure Methods, 2nd Ed.*, Gaussian, Inc., Pittsburgh, 1996.

7. Reinking, M. K.; Fanwick, P. E.; Kubiak, C. F. *Angew. Chem. Int. Ed. Engl.* **1989**, *28*, 1377.